Development of High Strength Hot Rolled Strip Steel Products with Bainitic Microstructures

By

Jinlong Du

A thesis
submitted to The University of Birmingham
for the degree of DOCTOR OF PHILOSOPHY

School of Metallurgy and Materials
College of Engineering and Physical Sciences
University of Birmingham
March 2016

UNIVERSITY OF
BIRMINGHAM

University of Birmingham Research Archive

e-theses repository

This unpublished thesis/dissertation is copyright of the author and/or third parties. The intellectual property rights of the author or third parties in respect of this work are as defined by The Copyright Designs and Patents Act 1988 or as modified by any successor legislation.

Any use made of information contained in this thesis/dissertation must be in accordance with that legislation and must be properly acknowledged. Further distribution or reproduction in any format is prohibited without the permission of the copyright holder.

Preface

This thesis is submitted for the Degree of Doctor of Philosophy at The University of Birmingham. It describes research work carried out in the School of Metallurgy and Materials, University of Birmingham, between November 2011 and October 2014, under the supervision of Professor C.L. Davis and Dr. M. Strangwood. Except where appropriately referenced, this work is entirely original, and contains nothing that is the outcome of collaboration. No part of this dissertation has been, or is concurrently being, submitted for any other degree, diploma or any other qualification. It does not exceed 50,000 words in length.

J. Du

March, 2016

Abstract

High strength, low alloy, hot rolled strip steels with yield stresses in the range 700 to 1300 MPa are required for the Lifting and Excavating product sector, and the hot strip process route is attractive as a low cost approach that can readily produce thin steel products with good flatness and surface quality. The process routes normally include hot rolling, continuous cooling and coiling and result in a complex and multi-phase microstructure. Improved combination of strength and toughness in these high strength steels is desired, requiring a detailed understanding of the relationship between microstructure and mechanical properties (especially toughness). Besides, it is also desired in industry that the cost of steel production to be kept as low as possible, which will have influences on alloying level and process routes. Therefore, it is also required to optimise the chemical composition and processing for steel products to achieve desired microstructure and mechanical properties.

In this work 12 mm thick 700 MPa yield stress strip steels with fully bainitic microstructures, produced using different compositions and / or processing conditions, have been studied. The microstructures of the steels were investigated with both optical microscopy (initially) and SEM (as a following up). Micro-hardness tests and Charpy impact tests (at different temperatures) were carried out to investigate the mechanical properties of the materials, followed up with fracture surface analysis and unit crack path (UCP) analysis.

Three types of bainitic microstructures were identified, including upper bainite, lower bainite and granular bainite. Microstructure quantification (through SEM images) was carried out to calculate the percentage of each type of bainite phases to study the

relationship between the phase balance and mechanical properties. The overall amounts of upper bainite, lower bainite and granular bainite in the investigated materials was as follows: granular bainite in the range of 5 % -15 %, lower bainite of 0 – 15 % and upper bainite 70 – 90 %. The fracture surface and UCP analysis revealed the connection between the microstructure features and mechanical properties, indicating that granular bainite is detrimental to toughness, but cannot necessarily be avoided in the steel compositions and processing conditions investigated; while the presence of a small amount of lower bainite (above 5 %) was found to improve the impact toughness significantly.

Gleeble tests on phase transformation behaviour of investigated steels were carried out, as the dilatometry machines both at University of Birmingham and Tata Steel STC were broken down for a long period. Continuous cooling transformation (CCT) diagrams for steels with different compositions were produced, which allowed investigation of the phase transformation behaviour and then selection of optimum chemical composition / coiling temperature for improved properties. The effects of alloying elements on the transformation behaviour, such as boron, molybdenum and vanadium, have been confirmed through the experiments. An optimised combination of alloying and coiling temperature has been proposed and validated via investigating plant trial products with similar alloying and processing parameters.

Acknowledgements

There are many people who I want to thank for their helping during my time as a PhD student. Firstly I need to thank my supervisors, Professor Claire Davis and Dr. Martin Strangwood, for their constant support, advice and encouragement through the course of this work as well as the genuine prospects for my future career. I have learnt a great deal from both of them not only in academic aspect but also the attitude toward life. And thank you to Dr. Dave Crowther from Tata Steel, my industrial supervisor, for his great support and advice throughout the project. I would also like to thank the departmental staff in the School of Metallurgy and Materials, who are always there to help.

Thanks must go to previous and present co-workers in Phase Transformation group: Drs. Carl Slater, Rachel Punch, John-Paul Tovee, Xi Liu, Lei Zhou, Dayue Zhang, (Mr.) Guowei Zhang, and hopefully soon to be Drs Fei Wang and Mo Ji, for always creating a great and enjoyable office where I am looking forward to coming into everyday. I would like to give my special thanks to Dr. Carl Slater and Dr. Lei Zhou, who are always enthusiastic to discuss the latest results and play badminton.

The financial and technique support of Tata Steel is very much appreciated. Thank you for giving me the opportunity.

I must thank my colleagues in Tata Steel Swinden Technology Centre, especially Drs. Andrew Smith, James Nygaard, Bin Xiao and Chen Zhu, for their support on daily work and coming up with tips on writing up thesis efficiently after work.

Finally, the most importantly, I want to give my greatest thanks to my parents. Thank you for always supporting my decisions and being there for me, I could not have got through all the pressures without you.

TABLE OF CONTENTS

CHAPTER 1 1

INTRODUCTION 1

1.1 Background 1

1.2 Aim and Objectives of Research Project 3

CHAPTER 2 4

LITERATURE REVIEW 4

2.1 Introduction 4

2.2 Bainite in Steels 4

2.2.1 General Description of Bainite 5

2.2.2 Types of Bainite 6

2.2.3 Bainite on TTT diagrams 11

2.2.3.1 Formation of Bainite – Thermodynamics and Kinetics 11

2.2.3.2 The Effects of Alloying Elements on Austenite – Bainite Transformation 13

2.2.4 Characteristics of bainite 23

2.2.5 Mechanical Properties of Bainitic Steels 31

2.2.5.1 Strength of Low Carbon, Low Alloy Bainitic Steels 32

2.2.5.2 Impact Toughness and Fracture Behaviour of Bainitic Steels 35

2.3 High Strength Strip Steels 40

2.3.1 Production of Hot Rolled Strip Steels 42

2.3.2 Project Background on Rolling and Industrial Constraints 48

CHAPTER 3 53

EXPERIMENTAL PROCEDURES 53

3.1 Introduction 53

3.2 Materials Details 53

3.3 Metallography and Image Analysis 59

3.4 Mechanical Testing 59

3.4.1 Micro-hardness 59

3.4.2 Impact toughness tests 60

3.5 Fractography 61

3.6 Dilatometry and Gleeble Tests 62

3.6.1 Principles of the technique and experiment setup 64

3.6.2 Limitations of the technique 72

CHAPTER 4 73

MICROSTRUCTURE CHARACTERISATION 73

4.1 Introduction 73

4.2 Forms of bainite in the high strength strip steels 73

4.3 Phase Quantification 91

4.3.1 Identifying different bainite phases 92

4.3.2 Examples of bainitic phase quantification 97

4.4 Phase Quantification Results and Relationship between Coiling Temperature and Phase Balance 111

4.5 Summary 116

CHAPTER 5 117

MECHANICAL PPROPERTIES INVESTIGATION 117

5.1 Introduction 117

5.2 Strength/Hardness and Toughness Test Results 117

5.2.1 Strength and hardness results 118

5.2.2 Impact toughness 123

5.3 Crack Propagation Mechanism 128

5.4 Effect of Bainite Phase Balance on Hardness and Impact Toughness 139

5.5 Summary 147

CHAPTER 6 149

BAINITE PHASE TRANSFORMATION BEHAVIOUR 149

6.1 Introduction 149

6.2 Modelling of Transformation Time Temperature (TTT) and Continuous Cooling Transformation (CCT) Curves 149

6.3 Gleeble simulation and investigation on transformation behaviour 160

6.4 Development on Optimum Coiling Conditions and Alloying Combination 171

6.5 Validation of suggested combination of chemical composition and coiling process 176

CHAPTER 7 191

CONCLUSIONS AND SUGGESTIONS FOR FUTURE WORK 191

7.1 Summary and Conclusions 191

7.1.1 Summary 191

7.1.2 Conclusions 191

7.2 Suggestions for Future Work 192

References 197

LIST OF FIGURES

Figure 2.1 The transition from austenite to upper and lower bainite (Bhadeshia, 2001).. 8

Figure 2.2 Granular bainite structure found in (a) a welded 2.25Cr-1Mo-0.1C steel by Josefsson and Andren (1988) and (b) continuously cooled low carbon low alloy steel (0.05C-0.5Ni-1Cu-10ppm B) (marked as GB) (Sung et al., 2012). 10

Figure 2.3 The iron-carbon dual phase diagram (Bhadeshia and Honeycombe, 2006).. 15

Figure 2.4 Example Time-Temperature-Transformation (TTT) diagram for: (a) a eutectoid (0.89 wt% C) steel and (b) a hypoeutectoid (0.50 wt% C) steel. Note for both steels it is hard to generate fully bainitic structure without any ferrite (Bhadeshia and Honeycombe, 2006). 17

Figure 2.5 Schematic Continuous Cooling Transformation (CCT) diagram for austenite-ferrite/bainite phase transformation during continuously cooling with cooling curves (representing different cooling rate) (Bhadeshia, 2001). 18

Figure 2.6 A schematic TTT diagram showing the general effect of alloying elements on controlling transformation behaviour of a hypoeutectoid steel (Heller and Nuss, 2005). 22

Figure 2.7 A schematic TTT diagram illustrating the effect of boron on shifting the ferrite transformation curve (Bhadeshia, 2001). 23

Figure 2.8 The sub-unit and sheaf in bainite structure (Bhadeshia, 2001), where T1 and T2 are transformation temperatures, and t1 to t4 are transformation times. 24

Figure 2.9 A TEM (transmission electron microscopy) image of a sheaf in upper bainite in a Fe-0.43C-2Si-3Mn steel (Bhadeshia, 2001). (a) Optical image under low magnification. (b, c, d) High magnification TEM image and bright part represents bainitic ferrite sub-units. (d) Merged images showing the bainite sheaf. 26

Figure 2.10 Relationship between transformation temperature and bainite microstructure features: (a) general relationship; (b) sub-unit width (Bhadeshia, 2001)..... 28

Figure 2.11 Schematic Iron-Carbon phase diagram, stating the thermodynamic condition for cementite to precipitate from residual austenite (Bhadeshia, 2001). 29

Figure 2.12 Left: TEM image of lower bainite isothermally transformed at 435 °C of a Fe-0.3C-4.08Cr wt% steel. Right: TEM image of tempered martensite of an AISI steel. (Bhadeshia, 1980) 30

Figure 2.13 Variation of tensile strength of steels transformed at different temperatures (Irvine and Pickering, 1957). 35

Figure 2.14 Schematic graph for the sensitivity of cleavage stress and plastic flow stress against temperature of bcc metal (Bhadeshia, 2001). 36

Figure 2.15 Impact energy absorption at different temperatures of different materials. (Yang and Qiang, 2009)..... 38

Figure 2.16 Impact behaviour of different bainitic structures (Bhadeshia, 2001). 39

Figure 2.17 (a) Typical continuous casting machine in steel plant. (b) Slab product produced by continuous casting. 43

Figure 2.18 A slab is exiting the reheat furnace..... 45

Figure 2.19 Extended slab (bar) after rough rolling..... 46

Figure 2.20 Coiled rough rolled “bar” to be unwound from the Coil Box for finishing rolling. 46

Figure 2.21 The Finishing Mill in a Tata Steel plant, showing the seven rolling stands and replacement rolls beside each stand waiting for next roll change..... 47

Figure 2.22 The Run-Out Table (ROT) and water sprays above to cool the strip steel to a desired temperature before coiling. 47

Figure 2.23 Schematic diagram of the TMCP process and corresponding microstructure at each stage. (Tanaka, 1995)..... 48

Figure 3.1 Rolling schedules for different trials. (a) Temperature at each pass. (b) Strain at each pass..... 56

Figure 3.2 Direction and dimensions of standard Charpy impact samples with V- shaped notch. (a) The direction that Charpy impact samples were taken from the parent material. (b) The dimension of each Charpy sample. 61

Figure 3.3 Experimental data (black dots) of heat transfer coefficient – temperature relationship during cooling of a 0.42 wt% C steel (Jansson et al., 1991). 63

Figure 3.4 Continuous Cooling Transformation (CCT) diagram (solid curves) of a 0.8 wt% C railway steel. Dashed curves are isothermal transformation (TTT) diagram, and curves 1, 2 represent different cooling rates. (Abbaschian et al., 2009) 65

Figure 3.5 Set up for both TCS and PCS Gleeble simulations. 66

Figure 3.6 Gleeble simulation schedule for TCS initial testing. The peak temperature was 900 °C and 1000 °C for initial testing (on the rail steel) and strip steels, respectively. 68

Figure 3.7 Power-temperature curve during cooling of 0.8C rail steel samples at different cooling rates (the trend lines for each curve were also plotted). 70

Figure 3.8 Comparison of the Gleeble results and the literature CCT diagram of a 0.8C rail steel (Gleeble results are shown as red crosses on the graph). 71

Figure 4.1 Representative optical images of strip steels investigated. All images are taken under the same magnification at rolling direction section..... 85

Figure 4.2 Typical SEM (secondary electron) images of bainitic microstructures in investigated strip steels. 91

Figure 4.3 Typical forms of bainite (upper bainite, UB; lower bainite, LB; and granular bainite, GB) found in the strip materials investigated..... 94

Figure 4.4. Adjacent granular bainite blocks found in Steel T1-1 suggesting several granular bainite regions could be formed at the same time within one prior austenite grain. As the granular bainite blocks grow and finally impinge, carbides can form between them due to the high carbon concentration. 97

Figure 4.5. Microstructure of Steel T1-1 at ¼ thickness. (a) original SEM image of microstructure etched by 2 % nital, (b) prior austenite grains are marked in black, (c) granular bainite regions in this image are outlined in yellow, (d) obvious upper bainite regions are outlined in orange, (e) unclear UB/LB regions are outlined in light green, and (f) higher magnification of unclear regions showing they are upper bainite areas. 103

Figure 4.6. Microstructure of Steel T3-1 at ¼ thickness. (a) original SEM image of microstructure etched by 2 % nital, (b) prior austenite grain boundaries outlined in black, (c) granular bainite regions outlined in yellow, (d) obvious upper bainite regions outlined as orange, (e) obvious lower bainite outlined in red, (f) unclear regions outlined in blue, and (g) – (l) higher magnification of unclear regions, which were identified as being lower bainite for (g)-(k) and being upper bainite for (l). 110

Figure 4.7 The relationship between the area fraction of different types of bainite ((a) granular bainite, (b) upper bainite, and (c) lower bainite) and the number of images used for quantification for Steel T1-4. 113

Figure 4.8 Relationship between coiling temperature and bainite phase balance. (a) granular bainite area fraction; (b) upper bainite area fraction; (c) lower bainite area fraction. 115

Figure 5.1 Through thickness (between 1.5mm to 10.5 mm) hardness profile of investigated steels (corresponding coiling temperatures illustrated in legends as CT). 121

Figure 5.2 Micro-hardness – strength relationship of investigated steels. 122

Figure 5.3 Ductile-brittle transition curves of investigated steels. (a) T1 series, (b) T2 series, and (c) T3 series. 124

Figure 5.4 Examples of fracture surface analysis via SEM, showing transgranular cleavage fractures and the crack initiation sites (marked with black arrow). (a) T1-1, tested at -60 °C, impact energy = 21 J/cm^2; (b) T1-2, tested at -56 °C, impact energy = 25 J/cm^2; (c) T1-3, tested at -85 °C, impact energy = 11 J/cm^2; (d) T1-4, tested at -187 °C, impact energy = 5 J/cm^2; (e) T2-1, tested at -82 °C, impact energy = 11 J/cm^2; (f) T2-2, tested at -80 °C, impact energy = 38 J/cm^2; (g) T2-3, tested at -92 °C, impact energy = 33 J/cm^2; (h) T3-1, tested at -101 °C, impact energy = 37 J/cm^2; (i) T3-2, tested at -99 °C, impact energy = 28 J/cm^2. 133

Figure 5.5 Example SEM images of sectioned fracture surfaces of investigated steels. (a) T1-1; (b) T2-1 and (c) T3-2. All Ni-plated and then sectioned perpendicular to the fracture surface, polished and etched with 2% nital. 137

Figure 5.6 Relationship between bainite packet size (BPS) and unit crack path (UCP). 138

Figure 5.7 Effect of bainite phase balance on micro-hardness. (a) granular bainite effect; (b) upper bainite effect; (c) lower bainite effect. 141

Figure 5.8 Relationship between impact toughness and bainite phase balance. (a) granular bainite; (b) upper bainite; (c) lower bainite. 144

Figure 5.9 Relationship between BPS and bainite phase balance. (a) granular bainite; (b) upper bainite; (c) lower bainite. 146

Figure 6.1 TTT diagrams modelled by JMatPro software for (a) T1 steels, (b) T2 steels, (c) T3 steels, (d) T0 composition (T1 chemical without B) and (d) comparison of the 3 trials and T0..... 153

Figure 6.2 CCT diagrams modelled by JMatPro software for (a) T1 steels, (b) T2 steels, (c) T3 steels, (d) T0 composition (T1 chemical without B) and (d) comparison of the 3 trials and T0.....156

Figure 6.3 TTT / CCT diagrams modelled by EWI online tool (note the temperature is in Kelvin) for T1, T2, T3 and T0 compositions.....157

Figure 6.4 CCT diagrams of T1, T2, and T3 measured by Gleeble power-temperature method (T1 data is almost overlapped with T2 data).....162

Figure 6.5 Comparison between measured CCT data and modelled results from (a) JMatPro (with the Gleeble measured data points highlighted with a yellow background colour), and (b) EWI.. 163

Figure 6.6 Optical images of microstructure achieved at different cooling rates. (a) 2.5 °C/s; (b) 5 °C/s; (c) 7.5 °C/s and (d) 10 °C/s. 165

Figure 6.7 SEM (secondary electron) images of microstructure achieved at different cooling rates. (a) 2.5 °C/s; (b) 5 °C/s; (c) 7.5 °C/s and (d) 10 °C/s. 168

Figure 6.8 Modelling of TTT and CCT diagrams of T4 composition. (a) JMatPro TTT result; (b) JMatPro CCT result; and (c) EWI TTT and CCT results.....178

Figure 6.9 Comparison of TTT and CCT modelling of T4 with previous trials. (a) JMatPro TTT diagrams; (b) JMatPro CCT diagrams; and (c) EWI TTT and CCT diagrams. 180

Figure 6.10 Gleeble simulated CCT results for T4 and comparison between the four compositions (note there is a maximum ±3 °C error for each data point on temperature plots)..... 182

Figure 6.11 Comparison between measured CCT (including Steels T1 – T4 data) and modelled results from (a) JMatPro (with the Gleeble measured data points highlighted with a yellow background colour), and (b) EWI..... 183

Figure 6.12 Optical images of the two trial products in T4. (a) T4-1; (b) T4-2. 185

Figure 6.13 SEM (secondary electron) images of the two trial products in T4. (a) T4-1; (b) T4-2. 186

Figure 6.14 Impact transition curves of T4-1 and T4-2. 188

LIST OF TABLES

Table 3.1 Compositions of trials investigated (in wt %).....54

Table 3.2 Rolling and coiling parameters of each strip steel. 57

Table 3.3 Phase transformation points of the tested 0.8C rail steel. 71

Table 4.1 Measured thicknesses (at normal direction) with 95% confidence interval of the prior austenite grains of Steel T1 – T3 76

Table 4.2. The range of carbide sizes measured in the upper and lower bainite regions observed for the strip steels investigated. 95

Table 4.3 Quantification results for all strip steels. 112

Table 5.1 Strength results for the steels, provided by Tata Steel. 118

Table 5.2 Micro-hardness (HV, load = 300g) data for investigated strip steels. 122

Table 5.3 Comparison of the DBTT values along with coiling temperature (CT) of investigated steels.....126

Table 5.4 Summary of UCP and BPS of the investigated steels.....137

Table 6.1 Comparison of calculated (equations (1) and (2) from Section 2.3.2.1) and modelled Bs and Ms. 158

Table 6.2 Micro-hardness (HV30) results of samples with different cooling rate.....168

Table 6.3 Chemical composition of T4 (all in wt %).....176

Table 6.4 Quantification results of phase balance in T4 steels (highlighted in green), and comparison with previous trials (T1 – T3)..... 187

Table 6.5 Comparison of mechanical properties of all trials. 188

CHAPTER 1

INTRODUCTION

1.1 Background

Low carbon, microalloyed high strength hot rolled strip steels with final thicknesses from 6 mm to 16 mm are currently used widely in all kinds of vehicles in the Lifting and Excavating product sector, including lorries, fork lift trucks, cranes and excavators, the so called “yellow goods”. These vehicles, which play an important role in construction sites, are expected to have good combination of strength and toughness, especially low temperature impact toughness, so that they are safe to use and have good performance in different environments and weather conditions. It is also necessary to take manufacturing costs and the mass of these vehicles into consideration as well, to make the production economical and sustainable.

The steels used in the Lifting and Excavating product sector have been developing and improving over a long period. After the High Strength Low Alloy (HSLA, defined as steels which contains less than 0.1 wt% total content of alloying elements (except manganese and silicon), e.g. aluminium, titanium, niobium, and vanadium, to achieve high mechanical properties) steels and controlled rolling techniques were introduced into the steel industry, the development of high strength products matured during the 1960s (Adamczyk, 2006, Yi et al., 2008, Skobir, 2011, Punch, 2014). Acceptable strength and impact toughness of these steels can be achieved through the effects of grain size refining and precipitation strengthening, by increasing additions of alloying elements and controlling the steel making process (Skobir, 2011, Bhadeshia and

Honeycombe, 2006, Adamczyk, 2006). However, the addition of alloying elements such as Ti is not always good, depending on overall composition (including weight percentage of Ti and N, as well as the Ti:N ratio), large and hard particles, for example TiN, may form during casting process and can act as fracture initiation sites and reduce low temperature impact toughness (Fairchild et al., 2000a, Yan et al., 2007, Du et al., 2012). Besides, the manufacturing cost of the steel will also increase due to the higher alloying level and requirements in controlled rolling process such as low coiling temperature. The development of strength and toughness through the use of more non-equilibrium phases, e.g. bainite, rather than through grain size refinement can be a relatively low-cost process and will reduce the risk of having large inclusions that reduce low-temperature toughness present. Recent developments on hot rolled strip products have suggested that bainitic microstructures, which can be achieved through addition of a very small amount of boron and some other alloying elements (for example niobium and molybdenum) and accelerated cooling processing, have attractive combinations of strength and toughness (Bhadeshia, 2001, Kong and Xie, 2006, Han et al., 2008, Feng et al., 2009, Lis et al., 2011, Mun et al., 2012, Sung et al., 2012, Zhang et al., 2012, Heller and Nuss, 2005). By controlling alloying levels, increasing cooling rates and reducing coiling temperatures, ferrite formation can be avoided, and the yield stress of the materials could reach 700 MPa to 1300 MPa, or even higher.

However, it has been found in 700 MPa level yield stress product that the combination of alloying and rolling conditions may not be optimum. Even though the 700 MPa yield stress grade steels have reasonable strength, the impact toughness varies a lot according to the coiling temperatures, which is possibly due to the different types of bainite present in the microstructure. Also, the transformation behaviour of the hot rolled strips

during cooling and coiling processes has not been fully understood. Although it is quite clear that B, Nb, Al and V additions can have effects on phase transformation, the extent of this and the actual performance of these alloying elements have not been investigated yet. Therefore, it is necessary to establish the microstructure – property relationships between complex bainitic microstructure and especially Charpy impact toughness, to enable an optimum combination of alloying and rolling process to be selected.

1.2 Aim and Objectives of Research Project

The aim of this project is to investigate the relationship between bainitic microstructure and impact toughness at high yield stress levels, and therefore predict the optimum combination of alloying level and rolling process for manufacturing high strength low carbon low alloy strip steels. The methodology adopted involves the following areas:

1) Quantitative image analysis of the volume fraction of phase balance in a series of strip steels.

2) Investigation into the influence of microstructural features, including phase balance, prior austenite grain size and possibly bainite packet size on impact toughness and fracture behaviour.

3) Analysis of phase transformation behaviour of investigated strip steels, as well as investigations on the effect of alloying elements and rolling schedules on phase transformation or CCT / TTT diagrams.

Suggestions and verification of improved alloying levels and rolling process parameters for future products based on current trials, to achieve better combinations of mechanical properties and cost of manufacturing.

CHAPTER 2

LITERATURE REVIEW

2.1 Introduction

This chapter reviews the relevant literature on general background information relating to bainite in steels, and high strength hot rolled strip steel products. Section 2.2 principally reviews the discovery and early research work on bainite in steels, as well as the characteristics of bainite, including the transformation mechanism, morphologies, and general mechanical properties. Section 2.3 covers the development of hot rolled strip steels, for example hot rolling processes in steel-making, transformation behaviour of hot-rolled then coiled steels, and the factors, such as alloying level and temperature, that can affect those phase transformations. Section 2.4 reviews the fracture mechanisms of strip steel products and the role of microstructural features on toughness and fracture behaviour.

2.2 Bainite in Steels

This section covers general knowledge on previous research of bainite in steels, which includes the general description of bainite (Section 2.2.1), different types of bainite and their morphologies under optical microscope and scanning electron microscope (Section 2.2.2), the transformation behaviour from austenite to bainite (Section 2.2.3), the characteristics of bainite such as morphology, crystallography, surface relief, and incomplete reaction (Section 2.2.4), the mechanical properties (i.e. strength and toughness) of bainitic structure (2.2.5).

2.2.1 General Description of Bainite

Bainite was first discovered by Bain and Davenport in the 1930s when transforming austenite isothermally at temperatures above those at which martensite formed but below those where fine pearlite formed (Bhadeshia, 2001, Bhadeshia and Honeycombe, 2006). It was found that this type of microstructure was "tougher for the same hardness than tempered martensite" (Bain, 1939 cited from Bhadeshia, 2001, p4), and since then based on various isothermal experimental methods, Time-Temperature-Transformation (TTT) diagrams have been widely utilised to represent the transformation behaviour. It was not until the 1940s, that the terminology "bainite" was accepted by most metallurgists. The general description of bainite is the phase mixed of fine ferrite plates / laths and discontinuous cementite particles in between ferrite plates which forms between martensite start temperature and about 550 °C (Bhadeshia, 2001).

The definition of bainite has been reached through different ways, however, there is still no unified description. Accordingly, bainite can be defined in three ways, according to the microstructure appearance, the surface relief effect, or the overall transformation kinetics (Aaronson et al., 2002). From the microstructural point of view, bainite is defined as "a nonlamellar eutectoid decomposition product" as it forms with ferrite and carbides / cementite (Aaronson et al., 2002, Fielding, 2013), which suggests the existence of diffusional transformation mechanism. From the surface relief aspect, bainite is described as "a plate shaped product that produces an invariant plane strain surface relief as formed by shear" (Fielding, 2013). And the overall reaction kinetics definition states "the existence of an upper limiting temperature well below the eutectoid temperature Bs", as well as "the incomplete reaction" (Bhadeshia, 2001,

Fielding, 2013). However, it can be seen that none of the three definitions perfectly describes the nature, or basics, of bainite, and some of them are using the transformation mechanisms to define the structure. And furthermore, there is some controversy between these definitions, especially interms of transformation mechanism, for example, the microstructural definition suggests a diffusional (reconstructive) transformation behaviour while the surface relief definition applies a displacive transformation process. Therefore, this is suggesting that bainite shows characteristics of both displacive and diffusional transformations and can be considered to be a "displacive + diffusional" transformation product (Bhadeshia and Edmonds, 1980, Bhadeshia, 2001, Fielding, 2013).

2.2.2 Types of Bainite

The structure of bainite changes slightly according to the temperature or cooling rate of formation. There are generally two main forms of bainite; upper bainite (UB) and lower bainite (LB) (Bhadeshia, 2001, Bhadeshia and Honeycombe, 2006). Figure 2.1 shows the different sub-unit structures of upper and lower bainite, and it can be seen from figure is that the main difference between upper bainite and lower bainite is the carbide precipitation from austenite during transformation. Upper bainite forms at around 400 – 550 °C, with a structure that consists of fine plates of ferrite and cementite particles. The fine ferrite plates are around 0.2 μm thick and 10 μm long which have similar "well-defined" crystallographic orientation and habit planes and grow in clusters (called "sheaves"). The carbides (cementite) then form in between the ferrite plates as at upper bainite transformation temperature, diffusivity of carbon is still high enough to enable all carbon in solution move out of ferrite plates and forms carbon-enriched austenite

(then precipitate cementite) in between the ferrite plates (Bhadeshia, 2001, Hiroshi Matsuda, 2004, Bhadeshia and Honeycombe, 2006), resulting in microstructure consisted of carbide-free ferrite plates and discontinuously cementite particles between the ferrite plates.

Lower bainite forms at lower temperatures, which typically range from about 250 – 400 °C, the basic microstructure and crystallographic features of lower bainite are very similar to upper bainite, although a major difference between lower bainite and upper bainite is that the former also has carbide particles (extremely fine particles, and not necessarily always cementite (Bhadeshia and Honeycombe, 2006)) that precipitate from the supersaturated ferrite, i.e. inside the bainitic ferrite plates (Bhadeshia, 2001, Bhadeshia and Honeycombe, 2006). This is due to the reduced diffusivity of carbon under low transformation temperature, and therefore some carbon is trapped inside the ferrite plates and precipitate carbides (not necessarily cementite in lower bainite) (Bhadeshia, 2001, Bhadeshia, 1980). And according to Bhadeshia (1980) the habit plane of the carbides precipitate inside the ferrite plates usually have a single crystallographic orientation of 60° against the plate axis. It is this difference that results in the significant variation between lower bainite and upper bainite, which will be discussed later in this section.

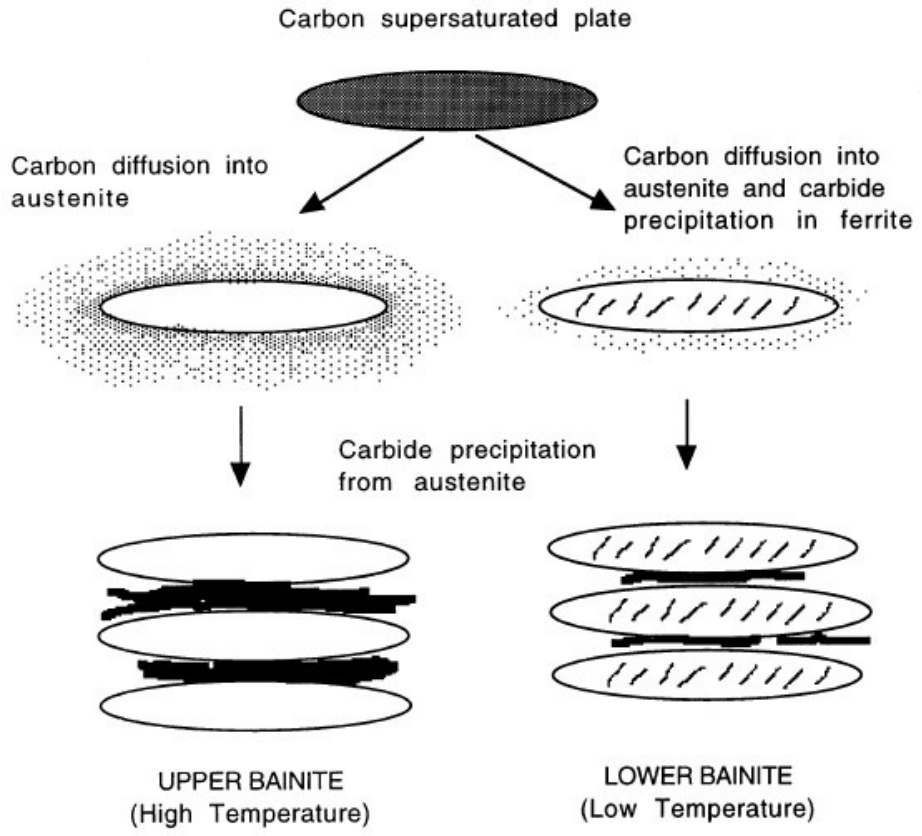
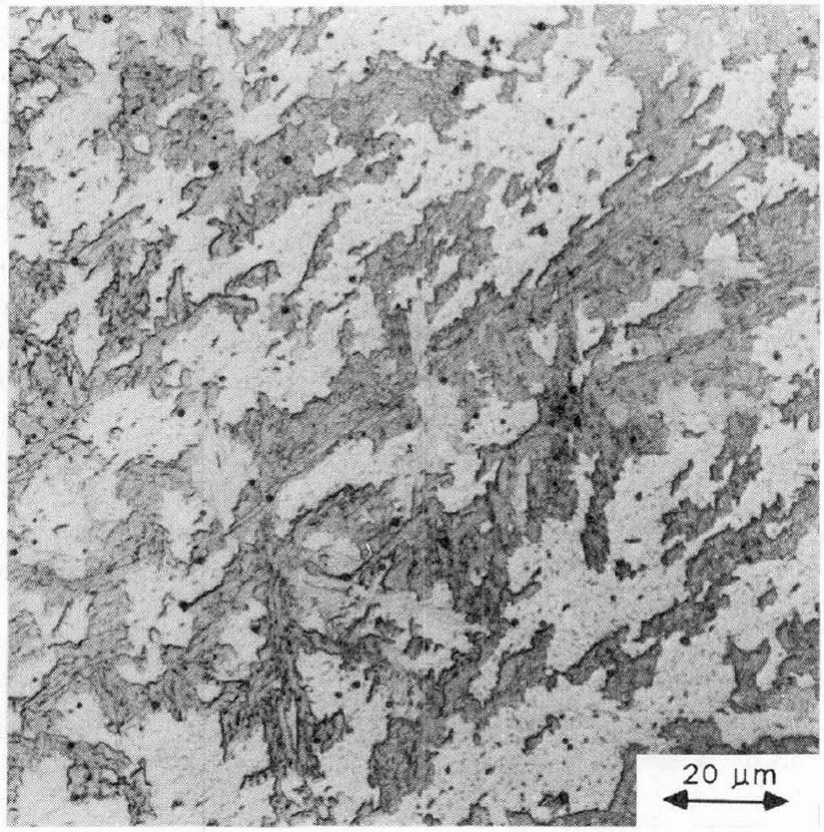


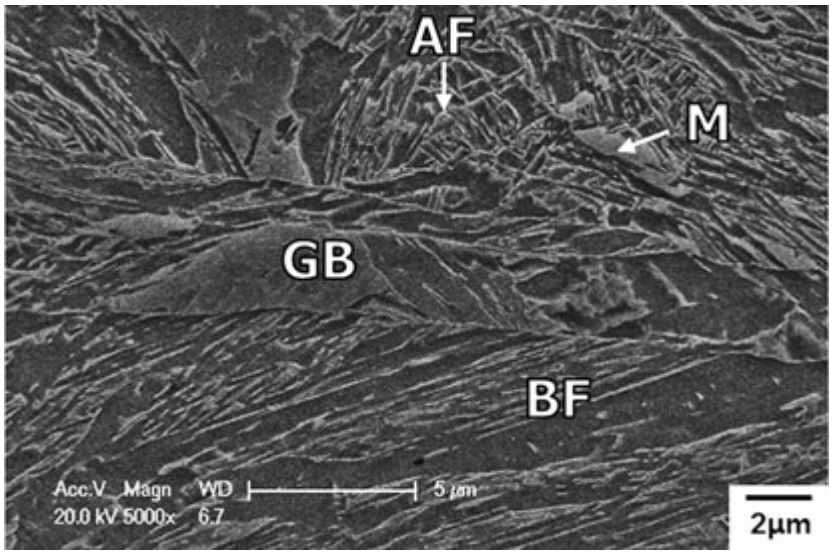
Figure 2.1 The transition from austenite to upper and lower bainite (Bhadeshia, 2001).

In addition to upper bainite or lower bainite, several other types of bainitic microstructures have been found in steels. The most frequently mentioned of these is granular bainite, which was found to form in low carbon steels that cooled continuously in early 1950s, and named by Habraken (Bhadeshia, 2001). The structure of granular bainite consists of coarse granular shaped bainitic ferrite plates and retained austenite (i.e. martensite-austenite island) regions (or carbides if the carbon concentration is low) between the plates (Josefsson and Andren, 1988, Kremnev et al., 1997, Qiao et al., 2009), and in optical microscopy and SEM (Scanning Electron Microscopy) it appears in the form of coarse and blocky plates (Kremnev et al., 1997, Caballero et al., 2012), as shown in Figure 2.2. It has been found that granular bainite tends to form only in steels during continuous cooling. This is because, during continuous cooling, the partitioning

of carbon from bainitic ferrite can stabilise the austenite, and in many cases, results in the formation of high carbon martensite-austenite islands (i.e. M/A islands) between bainitic ferrite platelets.



(a)



(b)

Figure 2.2 Granular bainite structure found in (a) a welded 2.25Cr-1Mo-0.1C steel by Josefsson and Andren (1988) and (b) continuously cooled low carbon low alloy steel (0.05C-0.5Ni-1Cu-10ppm B) (marked as GB) (Sung et al., 2012).

However, as in above literatures, the granular bainite were mostly obtained in low – medium (0.1 – 0.3 wt%) C steels with high amount of Cr (around 1 – 1.5 wt%), Mo (around 0.5 – 1 wt%) and / or Ni (between 0.3 – 3.1 wt%) addition, which tend to enhance stabilisation of supercooled austenite and then form martensite-austenite island, besides, in most cases the microstructure observation was done at re-austenised then cooled condition rather than as rolled condition, which tend to result in the presence of blocky martensite-austenite islands in the microstructure.

2.2.3 Bainite on TTT diagrams

2.2.3.1 Formation of Bainite – Thermodynamics and Kinetics

As mentioned before, the definition of bainite is closely connected with both the transformation mechanisms and the structure morphology. From the definition, the difference in transformation mechanism between bainite and other microstructures such as pearlite and martensite can be easily identified, and this mechanism can be then linked with the morphology, and furthermore, the role of bainite structure in mechanical properties of steels. Although some controversy exists in the bainite transformation mechanisms, some identical features of bainitic microstructures have been well identified, including: the existence of the bainite starting temperature, Bs; the incomplete transformation reaction phenomenon; and bainite has different morphologies for example lower bainite and upper bainite (as reviewed in section 2.2.2) (Fielding, 2013).

Much research work has been carried out on transformation kinetics from supercooled austenite to bainite, however, controversy on austenite-bainite transformation existed

for a long time (Fielding, 2013). Two main theories developed to explain bainite formation are the fully diffusion-controlled mechanism and the "displacive + diffusional" transformation kinetics. Although both theories include the diffusion of carbon to explain the presence of carbides in the microstructure, the fully diffusional theory describes the transformation from austenite to bainite includes the diffusion of carbon and is similar with other reconstructive phase transformations, such as ferrite and pearlite (Borgenstam et al., 2009, Hillert et al., 2010). Whereas the "displacive + diffusional" concept suggests that the bainite formation includes an "autocatalytic nucleation and growth of successive subunits or platelets" (Bhadeshia and Edmonds, 1980, Bhadeshia, 1999, 2001, Fielding, 2013).

However, the competition between the two transformation kinetics will not affect the facts, i.e. the identical features of bainitic transformation, mentioned above. It has been confirmed by lots of researchers in 1940s that the bainite transformation turned out to be an incomplete reaction. This incomplete reaction phenomenon, in detail, was observed as: during isothermal experiments at different transformation temperatures, decomposition of austenite to bainite ceases before the whole sample reach a fully bainitic microstructure, i.e. the austenite reaches its equilibrium composition and therefore bainite transformation completes. Besides, as found by Lyman and Troiano (1946), transformation from austenite to bainite needs to have a large amount of undercooling to start, which leads to the conclusion that a critical temperature for bainite to form, i.e. known as Bs, exists. The transformation behaviour from austenite to bainite both via isothermal and continuously cooling routes, as well as the alloying elements on the phase transformation behaviour are reviewed below.

2.2.3.2 The Effects of Alloying Elements on Austenite – Bainite Transformation

As reviewed in Section 2.2, the transformation from austenite to bainite generally happens between 300 °C and 600 °C for steels, which requires undercooling and possibly isothermal holding during the transformation.

As mentioned previously, the Lifting and Excavating Sector requires steels that have both high strength and good toughness due to the challenging working conditions. While traditional ways of strengthening tend to reduce toughness (Yang and Qiang, 2009), it is well known that strength and toughness can be improved at the same time by refining the grain size (Yu, 2006, Bhadeshia and Honeycombe, 2006). However, grain size refinement can require alloying elements, e.g. Ti and Nb, and more refined hot deformation schedules, which will increase the cost of steel making and processing. In addition, large particles, for example TiN, that sometimes form from those alloying elements (for example Ti) can initiate cleavage cracks at low temperatures reducing toughness (Balart et al., 2000, Fairchild et al., 2000a, Fairchild et al., 2000b, Linaza et al., 1995, Yan et al., 2006, Zhang, 2000, Du et al., 2012). The development of strength and toughness through the use of more non-equilibrium phases, e.g. bainite, rather than through grain size refinement can be a relatively low-cost process and should avoid the risk of large inclusions that reduce low-temperature toughness being present. The factors that affect microstructure can be generally summarised into two categories, i.e. alloying elements and transformation conditions (such as deformation before transformation, cooling rate and isothermal temperature), which will be discussed in more detail in this section.

The use of matrix phase transformations to generate strength and toughness makes it necessary to understand the factors that affect phase transformations in steels before designing the composition and processing route. Under equilibrium conditions (Bhadeshia and Honeycombe, 2006, Yu, 2006), phase transformations in simple steels can be predicted by the Fe-C phase diagram (Figure 2.3); however, in most industrial processes, phase transformations, especially austenite decomposition, will happen under non-equilibrium conditions, therefore the Time-Temperature-Transformation diagram (TTT diagram, Figure 2.4) and Continuous Cooling Transformation diagram (CCT diagram, Figure 2.5) are needed to predict the final microstructure. A change in chemical composition will result in different transformation curves for steels (Bhadeshia and Honeycombe, 2006, Yu, 2006).

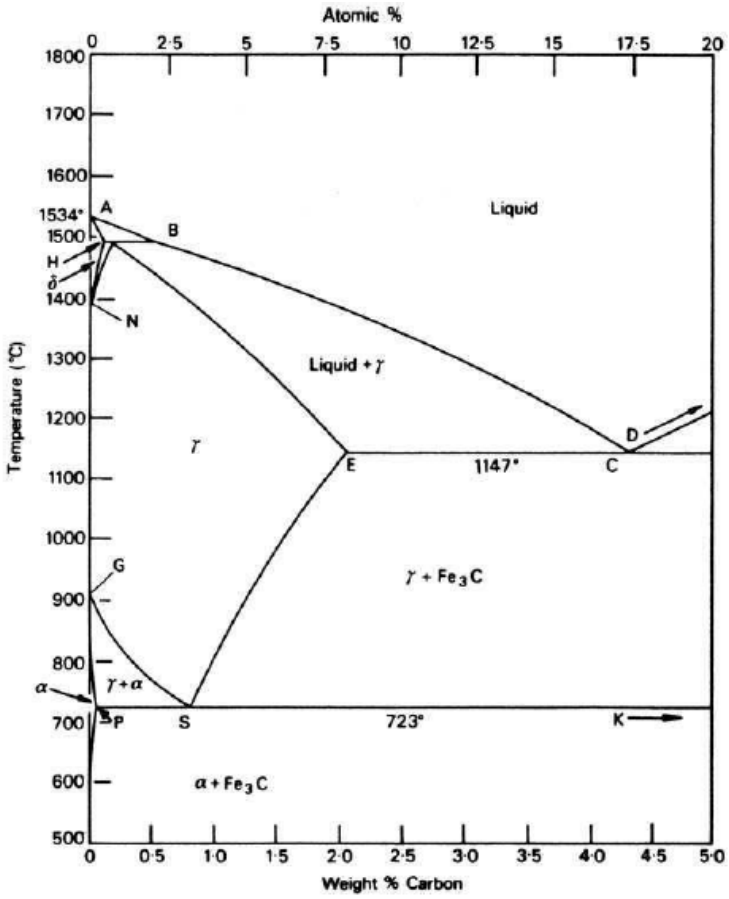
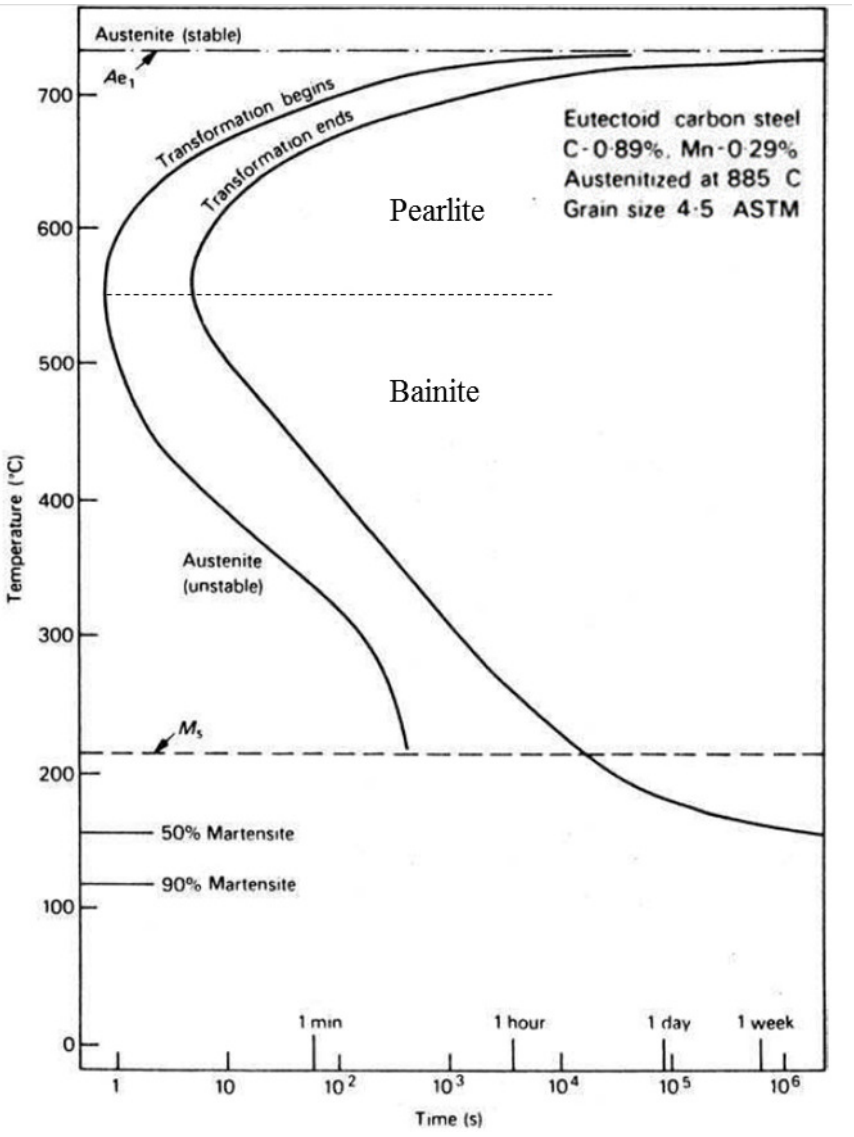
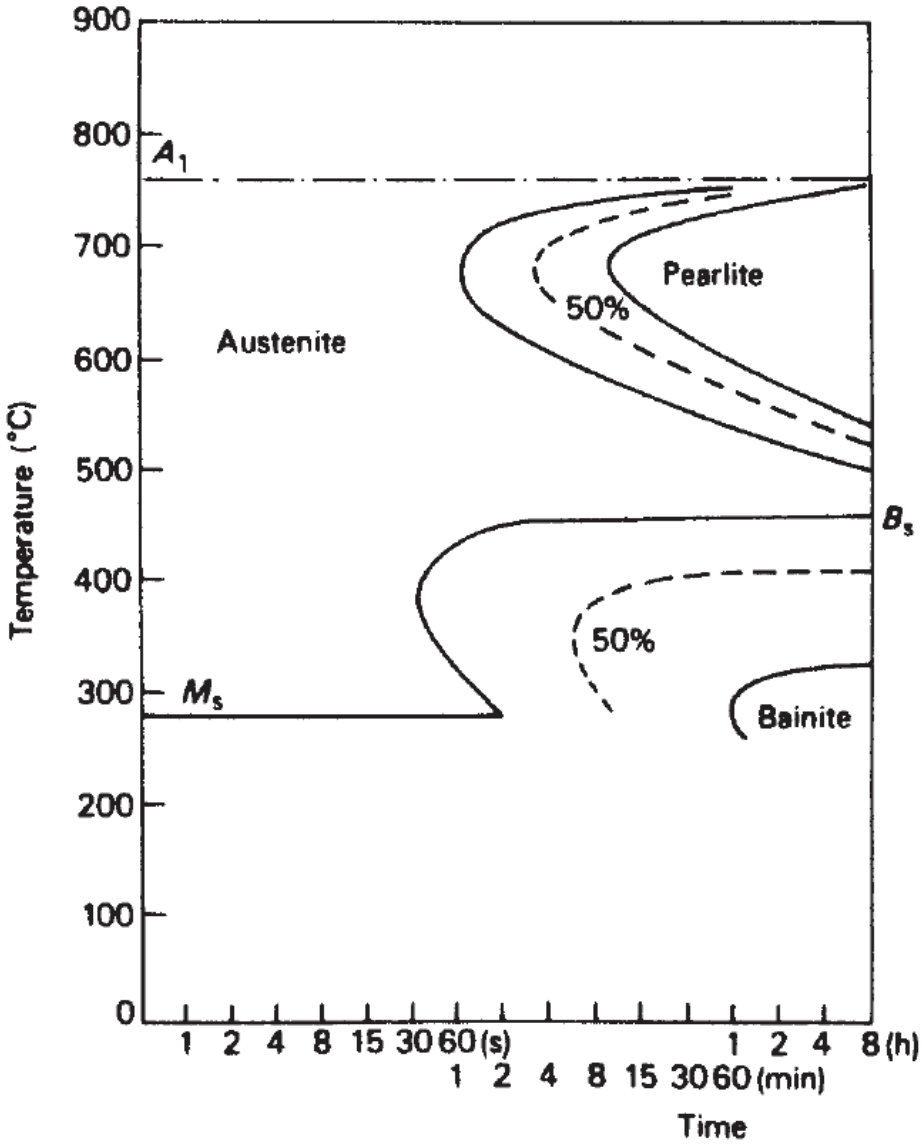


Figure 2.3 The iron-carbon dual phase diagram (Bhadeshia and Honeycombe, 2006).


Austenite (stable)
Ae_1
Transformation begins
Transformation ends
Eutectoid carbon steel
C-0·89%, Mn-0·29%
Austenitized at 885 C
Grain size 4·5 ASTM
Pearlite
Bainite
Austenite
(unstable)
M_s
50% Martensite
90% Martensite
Temperature (°C)
700
600
500
400
300
200
100
0
1 min
1 hour
1 day
1 week
1
10
10^2
10^3
10^4
10^5
10^6
Time (s)

(a)



(b)

Figure 2.4 Example Time-Temperature-Transformation (TTT) diagram for: (a) a eutectoid (0.89 wt% C) steel and (b) a hypoeutectoid (0.50 wt% C) steel. Note for both steels it is hard to generate fully bainitic structure without any ferrite (Bhadeshia and Honeycombe, 2006).

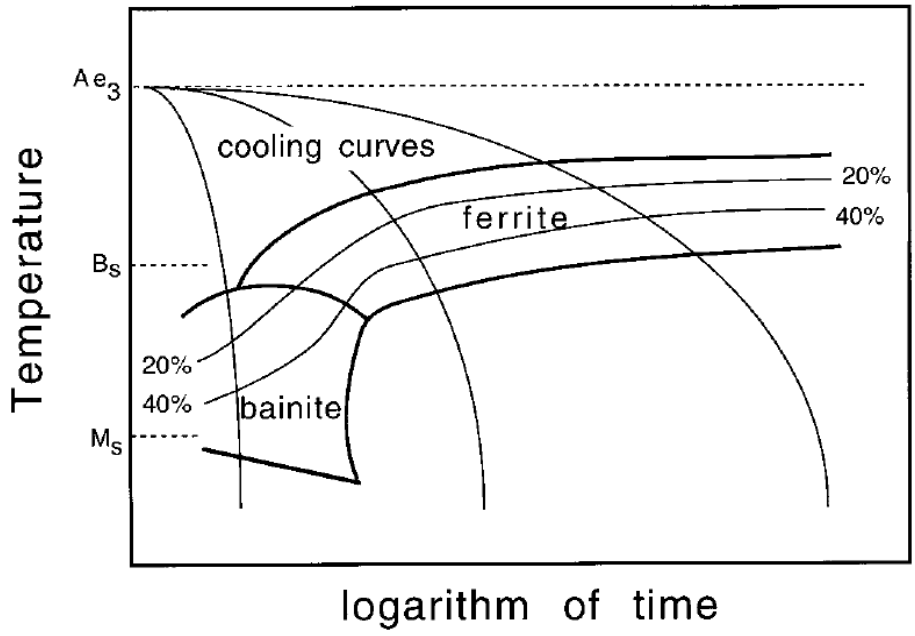


Figure 2.5 Schematic Continuous Cooling Transformation (CCT) diagram for austenite-ferrite/bainite phase transformation during continuously cooling with cooling curves (representing different cooling rate) (Bhadeshia, 2001).

TTT diagrams describe the austenite transformation kinetics for isothermal transformation and present the time needed for given amounts of transformation; while the CCT diagram records the extent of transformation through a range of temperatures and cooling rates. Both of these diagrams are representative for austenite transformations in steels, particularly, in steel processing and heat treatment. Rolling occurs (generally) through a range of temperatures and therefore transformation behaviour during rolling can be presented or predicted by CCT diagrams; cooling after coiling of strip is much slower and so may be approximated more by TTT diagrams.

One of the most important effects of adding alloying elements to steels is to change the shape and position of the TTT and CCT diagrams. As can be seen from Figure 2.5, it is difficult to obtain bainitic or martensitic microstructures for very lean steel compositions, as it will need a very high cooling rate to enable the bainite or martensite

transformation to occur before austenite decomposition into ferrite and pearlite, i.e. these steels have very low hardenability (Bhadeshia and Honeycombe, 2006, Yu, 2006).

Micro-alloying elements, especially strong carbide formers such as vanadium, niobium, titanium, molybdenum, and chromium will have effects on the transformation behaviour of steels, as such elements tend to combine with carbon and increasing the activation energy for carbon to diffuse in austenite, and furthermore, the diffusion of these elements themselves are quite slow in austenite, therefore increase hardenability of steels (Bain and Paxton, 1966, Yu, 2006). However, the content of these elements needs to be carefully optimised when designing the steel chemical composition, as some elements e.g. Ti and N may form large inclusions and reduce the low temperature impact toughness of final products (Zhang, 2000, Du et al., 2012, Punch, 2014). Figure 2.6 shows the general trend of some alloying elements on the TTT diagram, i.e. the transformation behaviour, of a hypoeutectoid steel. It can be seen from the figure that, except for Si, Al and P, most alloying elements tend to delay ferrite and bainite formation (however the ferrite transformation is delayed to a much greater extent than bainite transformation), and increase hardenability of steel (modifying γ-phase region and suppressing the Ac3 temperature), making bainite / martensite reaction easier to happen.

The model for bainite start temperature (Bs) and martensite start temperature (Ms) calculation also reflects the effects of some main elements in altering the requirements for the austenite-bainite and austenite–martensite phase transformation temperatures, shown in Equation (1) and (2), respectively (Bhadeshia, 2001, Bhadeshia and Honeycombe, 2006).

$$Bs = 830 - 270\omega_C - 90\omega_{Mn} - 37\omega_{Ni} - 70\omega_{Cr} - 83\omega_{Mo} \quad (1)$$

$$Ms = 539 - 423\omega_C - 30.4\omega_{Mn} - 17.7\omega_{Ni} - 12.1\omega_{Cr} - 7.5\omega_{Mo} \quad (2)$$

Where Bs and Ms are bainite start temperature and martensite start temperature, respectively, both in Celsius degrees; ω_X is the content of alloying element X, in wt %.

It can be seen from both equations that addition of alloying elements generally reduces Bs and Ms, and among several elements, carbon has the biggest effect on changing bainite / martensite start temperatures. Compared with Ms, the effects of elements such as manganese, nickel, chromium and molybdenum on Bs are more significant. Manganese increases hardenability and strength of steel, however reduces plasticity (Bain and Paxton, 1966). Chromium provides corrosion and oxidation resistance to steel, contributes to hardenability and strength as effectively as manganese, however reduces toughness on its own (Bain and Paxton, 1966). Nickel decreases strength of steel but increases toughness when the content reaches above 0.4 wt%, especially low temperature toughness, in pearlitic-ferritic steels, however is very expensive for low cost steels (Bain and Paxton, 1966). Molybdenum contributes greatly (more effective compared to chromium) to hardenability as dissolved, also raises high temperature strength and creep resistance of steel (Bain and Paxton, 1966, L'ecuyer et al., 1987). Other elements, such as titanium and niobium, can strengthen the steel through precipitation strengthening and grain size strengthening, as the fine precipitates (in nanometre scale, typically smaller than 500 nm) formed in solid state steel can spread evenly and restrict the growth of austenite grains. However, as mentioned before, coarse particles (larger than 5 μm) such as TiN which form in liquid steel can act as fracture initiation sites and result in poor low temperature toughness. Vanadium contributes in

increasing hardenability even with small dissolved amount, and can form V(C, N) precipitates at relatively low temperatures, either at γ/α interface or in ferrite, compared with titanium and niobium (Bain and Paxton, 1966, Shanmugam et al., 2006, Show et al., 2010, Siwecki et al., 2010). As these particles are the last of micro-alloying carbo-nitrides to form, and will be even finer (typically smaller than 10 nm) in size, the functions on restricting austenite grain growth and secondary strengthening are very effective (Hutchinson et al., 2014). Although the size of V(C, N) is small and can provide strengthening effectively, due to the low formation and dissolve temperature it needs extra care when designing the micro-alloying level and processing of the steel.

From the aspect of the effects of micro-alloying elements on phase transformation / final microstructure of steel, it is worth noting that elements include C, Mn, Cr, Mo, V, Ti, and Nb tend to delay bainite transformation at the same time when delaying ferrite formation, though to some different tendencies (depending on the characteristics of the alloying elements). Therefore the effect on promoting austenite-bainite transformation of these elements is not very obvious, especially with small additions in low carbon low alloy steels.

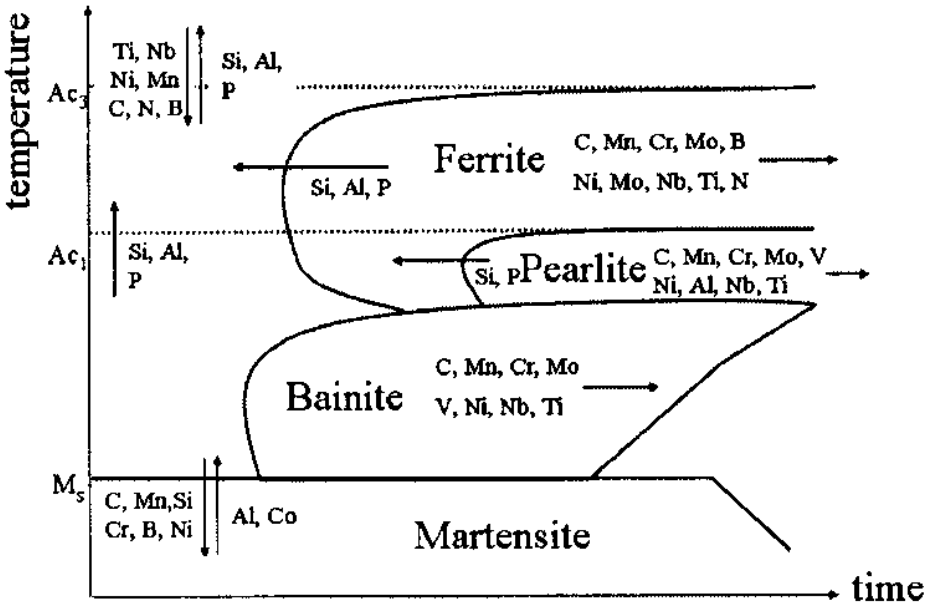


Figure 2.6 A schematic TTT diagram showing the general effect of alloying elements on controlling transformation behaviour of a hypoeutectoid steel (Heller and Nuss, 2005).

It is known that boron can segregate to prior austenite (PA) grain boundaries and retard ferrite nucleation effectively (Bhadeshia, 1992, Datta et al., 2004, Heckmann et al., 2005, Hwang and Lee, 2010, Sung et al., 2012, Zhang et al., 2012), by lowering the PA grain boundary energies. Therefore the addition of a very small amount of B (15-30 ppm) can enable bainite formation at very low cooling rates, from 0.1 °C/s to 10 °C/s (Hyo Kyung Sung, 2011, Bhadeshia, 2012). Recently, some researchers suggested that the addition of boron with Nb and Al could maximise the effect of boron on bainite transformation (and bainite can be obtained at 500 – 600 °C) because Nb and Al will form nitrides allowing boron to remain in solid solution where it can segregate to PA grain boundaries as free boron, rather than boron nitride (P. Cizek, 2002, Anjana Deva, 2011, Kangying Zhu, 2011). As shown in Figure 2.7 (Bhadeshia, 2012), it can be seen from that after addition of boron, the cooling rate requirement for bainite transformation is much lower.

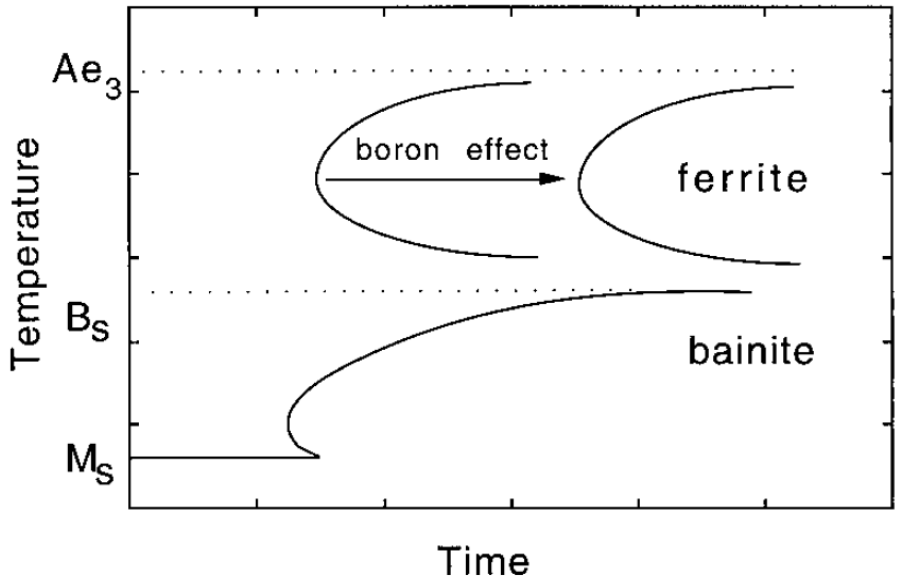


Figure 2.7 A schematic TTT diagram illustrating the effect of boron on shifting the ferrite transformation curve (Bhadeshia, 2001).

2.2.4 Characteristics of bainite

The morphology of bainite can be affected in several ways. For example chemical composition, different processing methods, including continuous cooling and isothermal holding, as well as parameters during processing, such as cooling rate and isothermal holding temperatures. However, the basic structures of bainite would not be affected, and it is these structures form different kinds of bainite in steels.

According to Oblak et al. (1964), as well as Srinivasan and Wayman's (1968) work, bainite consists of aggregates of wedge-shaped plates which are called sheaves (Aaronson and Wells, 1956). The sheaves are formed with bainitic ferrite platelets (sometimes are also called as sub-units individually), and are normally separated by untransformed austenite, martensite or cementite particles because of the increasing carbon concentration of adjacent un-transformed austenite during tranformation (Bhadeshia, 2001). However to be called as "ferrite", "bainitic ferrite" is rather similar

with lath martensite and quite different from the ferrite that forms through equilibrium conditions, both on morphology and crystallography. Therefore, the term "packet", which comes from the description of lath martensite in low carbon, low alloy steels, is also frequently used to describe those clusters of ferrite platelets with parallel habit planes, which usually divide fully transformed austenite grains into "discrete regions" (Bhadeshia, 2001). Figure 2.8 shows a schematic graph presenting the differences in defining sub-unit and sheaf of bainite, as well as the effects of transformation temperature and time on the size of both features.

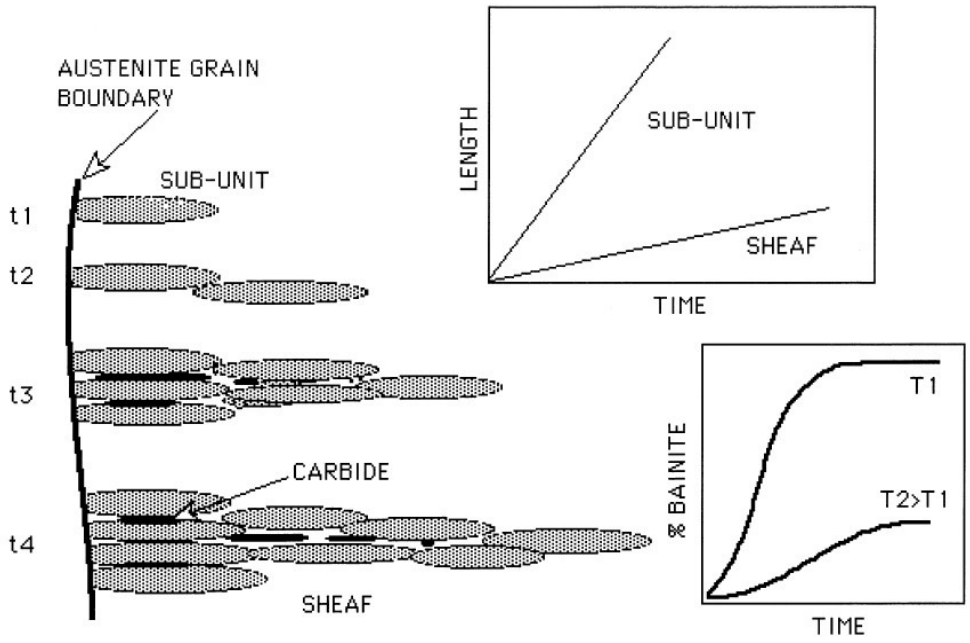


Figure 2.8 The sub-unit and sheaf in bainite structure (Bhadeshia, 2001), where T1 and T2 are transformation temperatures, and t1 to t4 are transformation times.

Analysis work (Bhadeshia and Edmonds, 1980, Oblak et al., 1964, Ohmori, 1971, Srinivasan and Wayman, 1968) have shown that the overall shape of a sheaf is a wedge-shaped plate in three dimensions (3-D), and the "thicker end of the sheaf originates at an austenite grain boundary" (Bhadeshia, 2001). The Transmission Electron Microscopic

(TEM) analysis by Bhadeshia (2001) showing that the sub-units (or platelets) are lenticular or lath-like in morphology, either near the edge/ tip or at the nucleation site of a sheaf so that the impingement effects can be minimised (Figure 2.9). This indicates that the bainite sub-units, or platelets, are limited in size, and in general, their width will not be affected by the parent austenite grain size. Further investigation by Bhadeshia (2001) suggests that the sub-units tend to nucleate close to the tips, rather than sides, of already formed sub-units, which explained the wedge shape (in 3-D) or elongated shape (usually observed in 2 dimensions, Figure 2.9) of a sheaf. Isothermal analysis at different holding temperatures has shown that with the decrease of transformation temperature, the amount of sub-units within a sheaf and the aspect ratio, i.e. the ratio between width (or thickness) and length, of bainitic ferrite sheaves tend to increase, while the sub-unit and sheaf width tend to decrease (Sandvik, 1982, Miihkinen and Edmonds, 1987, Naylor and Krahe, 1974, Hawkins and Barford, 1972), which basically suggests finer bainitic packet and sheaf structures at lower transformation temperatures. Besides, unlike sub-units, bainite packet size tend to change accordingly with the change in transformation temperature and prior austenite grain size.

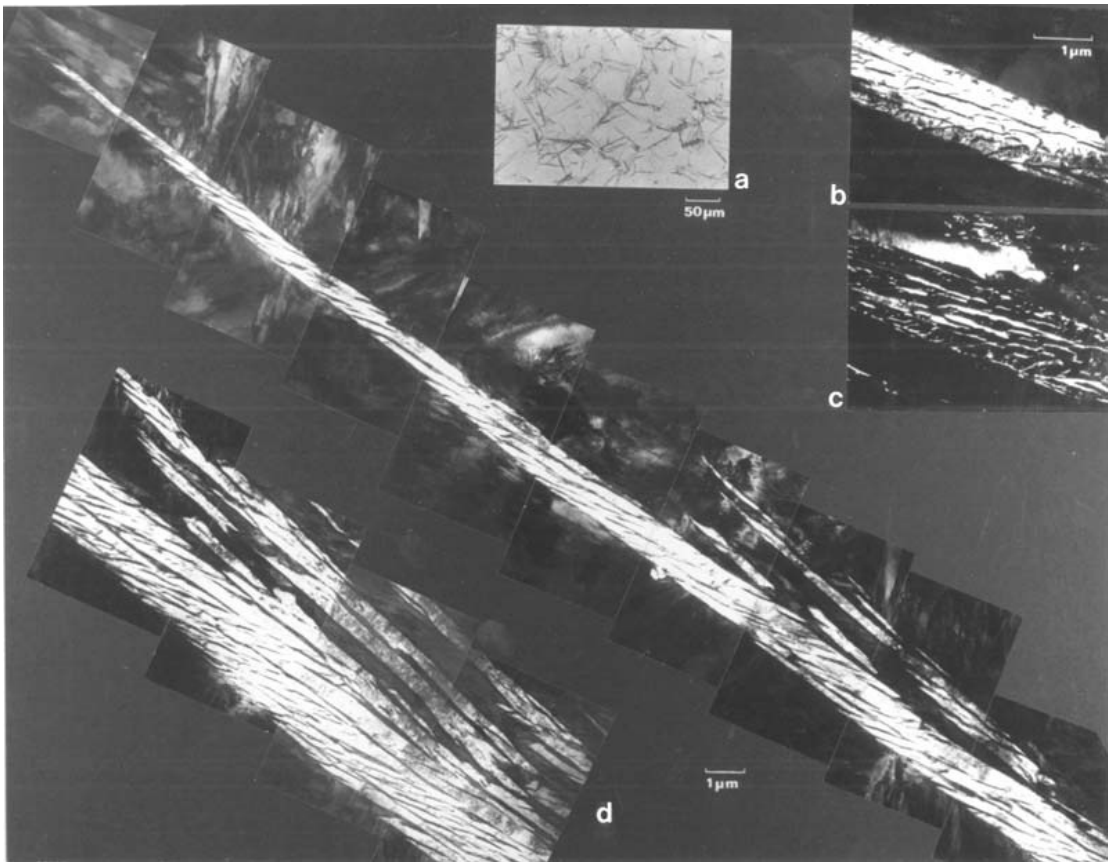
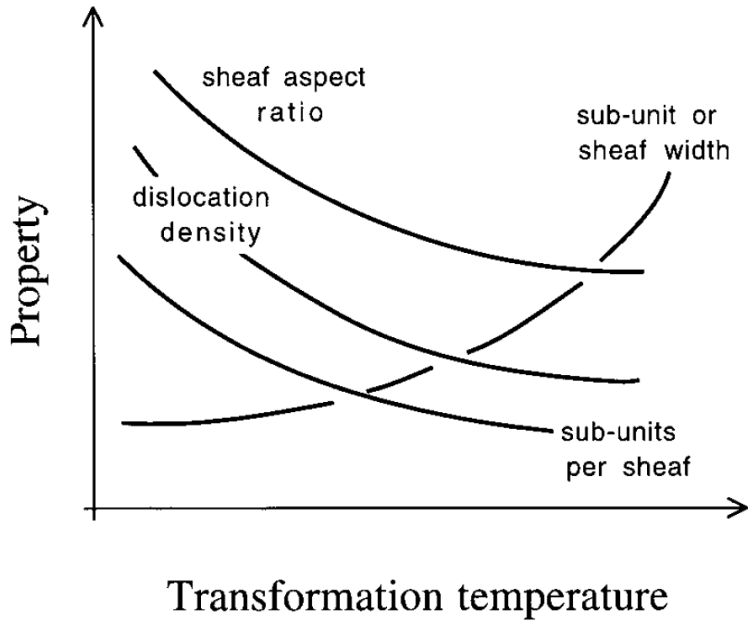


Figure 2.9 A TEM (transmission electron microscopy) image of a sheaf in upper bainite in a Fe-0.43C-2Si-3Mn steel (Bhadeshia, 2001). (a) Optical image under low magnification. (b, c, d) High magnification TEM image and bright part represents bainitic ferrite sub-units. (d) Merged images showing the bainite sheaf.

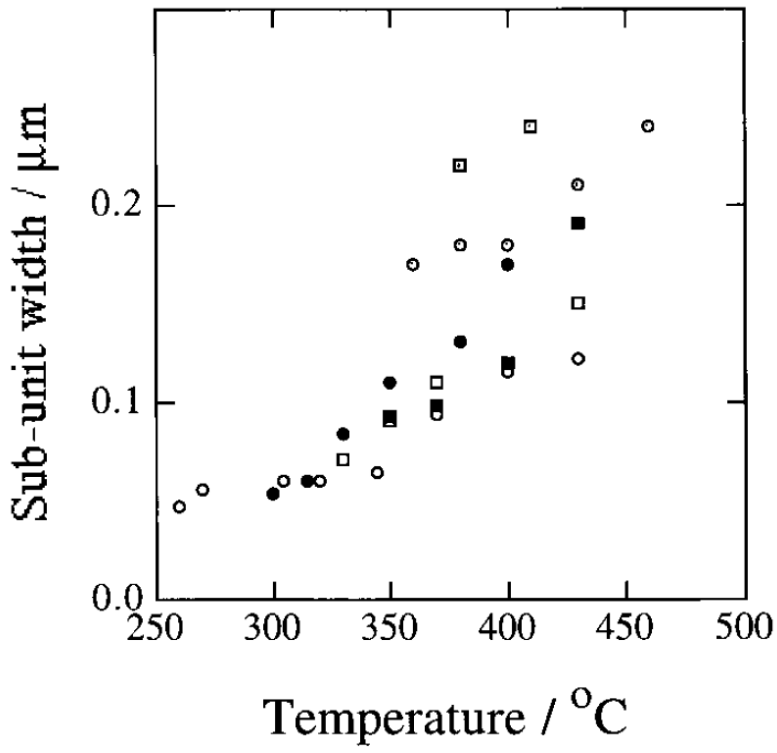
It has been confirmed that bainite has relatively high dislocation density (varies from 10^{14} to 10^{15} m^{-2} depending on transformation temperature, the lower transformation the higher dislocation density will be) than ferrite by many researchers (Oblak and Hehemann, 1967, Smith, 1984, Graf et al., 1985). However, the reason for higher dislocation density in bainite is not simply due to the transformation mechanism from austenite to bainitic ferrite is shearing. According to Bhadeshia (2001), the plastic relaxation accommodated displacive transformation contributes to the formation of dislocations in and around the bainitic ferrite, which has been proved by Transmission

Electron Microscopy (TEM) investigations (Bhadeshia and Edmonds, 1979, Nemoto, 1974). Furthermore, proved by Pickering (1967a) and Fondekar et al (1970), the decrease of isothermal transformation temperature results in the increase of dislocation density in bainite, it is suggested from their work that the dislocation density in bainitic ferrite that formed around 600 °C is about 8×10^{15} m^{-2} while in bainitic ferrite which formed at around 300 °C the dislocation density can reach about 7.5×10^{16} m^{-2}.

The qualitative relationship between isothermal holding temperature (i.e. transformation temperature) and the microstructure features mentioned above is shown in Figure 2.10 (a) and (b).



(a)



(b)

Figure 2.10 Relationship between transformation temperature and bainite microstructure features: (a) general relationship; (b) sub-unit width (Bhadeshia, 2001).

Besides the bainitic ferrite, another very important characteristic of bainite is that of the carbides within the microstructure. The location and morphology of carbide precipitates in bainitic structure is critical to mechanical properties of the material.

In upper bainite, especially low carbon low alloy steels, the carbides always tend to precipitate in the form of cementite (Lyman and Troiano, 1946, Hultgren, 1947, Austin and Schwartz, 1952). This is because, at high transformation temperatures, carbon will diffuse into the untransformed (or adjacent) austenite instead of staying within the bainitic ferrite, which will result in increased carbon concentration of that "residual austenite". As the transformation proceeds, the carbon concentration of those carbon-enriched austenite regions trapped between bainitic ferrite will exceed the value given

by extrapolated γ/(γ+θ) phase boundary (shown in Figure 2.11), and therefore the precipitation of cementite, and probably some more bainitic ferrite as a result of decomposition of the residual austenite (Sandvik, 1982), between bainitic ferrite platelets becomes thermodynamically possible (Kreiesement and Wever, 1956). The precipitated carbides in upper bainite "appear parallel to the traces of habit planes of the bainitic ferrite platelets" (Bhadeshia, 2001). The carbides may also precipitate at the austenite grain boundaries, which will have negative effects on toughness (Bhadeshia, 2001, Fairchild et al., 2000a).

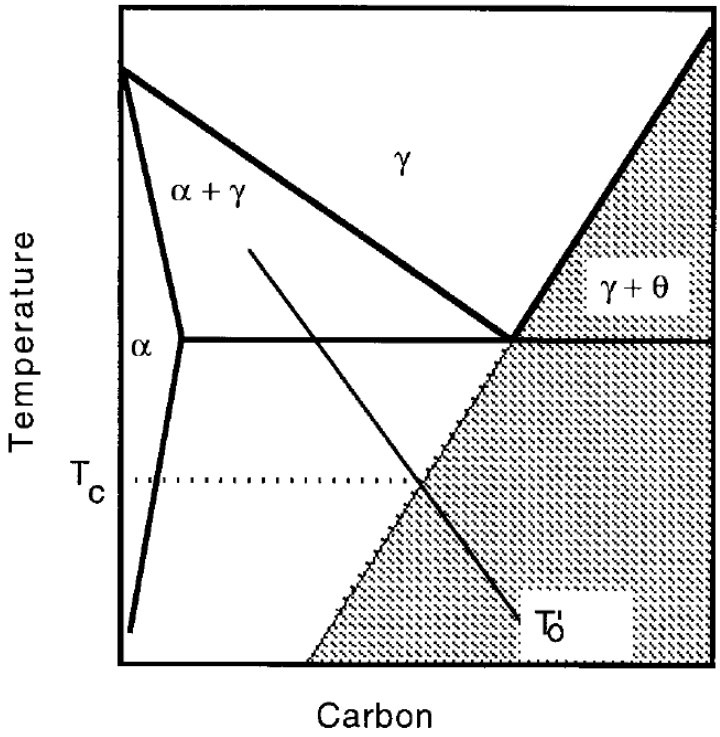


Figure 2.11 Schematic Iron-Carbon phase diagram, stating the thermodynamic condition for cementite to precipitate from residual austenite (Bhadeshia, 2001).

As mentioned previously, the bainitic ferrite sheaves and platelets in lower bainite are much finer compared with upper bainite, due to the lower transformation temperature. However, the form of the carbides appears more complex in lower bainite, also because

of the low transformation temperature. Confirmed by Bhadeshia (1980), the carbides in lower bainite have two forms: (i) those precipitated from carbon-enriched austenite, between bainitic ferrite platelets, which are mainly cementite and very similar with carbides in upper bainite; (ii) in addition, some very fine carbides, usually ε-carbide or cementite, will also form within the ferrite platelets. The latter differ from carbides in tempered martensite, as they will generally form in a single crystallographic variant and therefore become the most identifying feature of lower bainite (shown in Figure 2.12).

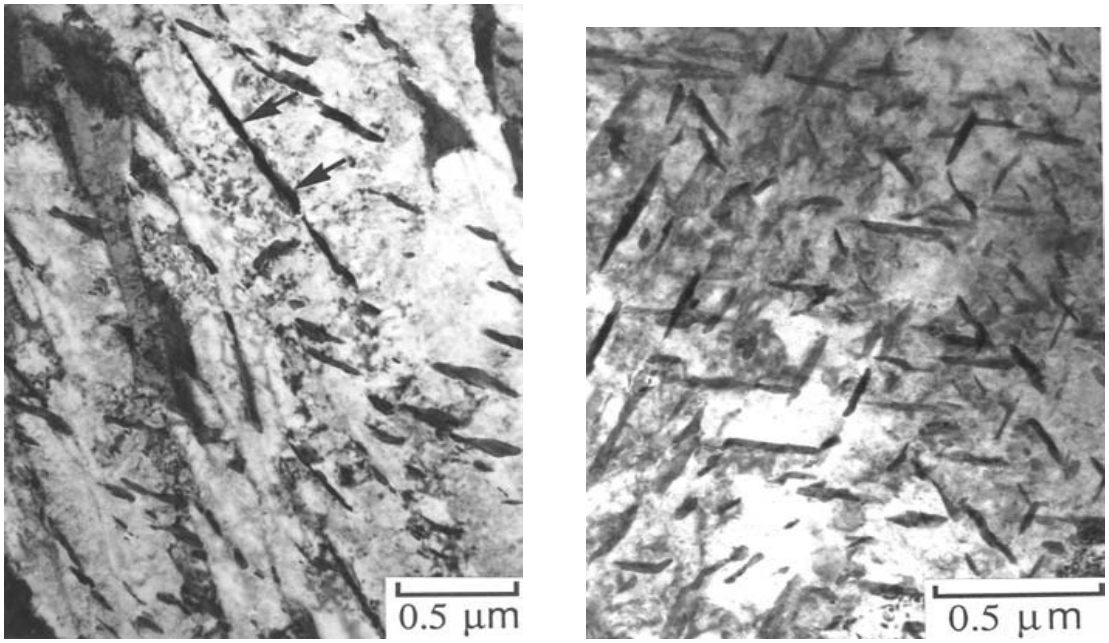


Figure 2.12 Left: TEM image of lower bainite isothermally transformed at 435 °C of a Fe-0.3C-4.08Cr wt% steel. Right: TEM image of tempered martensite of an AISI steel. (Bhadeshia, 1980)

It has been proven that carbide precipitation in both upper and lower bainite will normally occur after the formation and growth of bainitic ferrite, and the atoms in the range of austenite-bainite transformation temperatures have very limited mobility, the precipitation of carbides occurs by a displacive mechanism, and only the interstitial elements will diffuse during the transformation (Bhadeshia, 2001).

One important aspect of bainite is the crystallographic relationship between bainite and the austenite from which it formed. Greninger and Troianos' (1940) initial research found that bainite exhibited an habit plane that is irrational and varies not only with the formation temperature but also the carbon concentration. The habit plane for bainite in that study is different from martensite in the same steel. The result suggested there are fundamental differences between bainite and martensite crystallography. However, formation temperatures between bainite and martensite are different, whilst later experimental work by Smith and Mehl (1942) implied that the orientation relationship between bainite and austenite is considerably different from pearlitic ferrite and austenite, but no significant change was found with change of temperature and carbon content of the steel. This was later confirmed by Bhadeshia (2001), suggesting the crystallographic relationship between bainitic ferrite and its parent austenite are always close to, K-S (Kurdjumov-Sachs) and N-W (Nishiyama-Wasserman) relationships.

2.2.5 Mechanical Properties of Bainitic Steels

The mechanical properties of bainite were not explored right after bainite microstructures were found by Davenport and Bain, as a fully bainitic microstructure could not be readily achieved through normal industrial processes at that time. It was not until low carbon, low alloy steels were developed with the addition of boron and molybdenum that made fully bainitic microstructure achievable, that investigation of mechanical properties of bainite was started (Irvine and Pickering, 1957, Bhadeshia, 2001).

As mentioned in Section 2.2.2, unlike ferrite, pearlite or martensite, bainite is formed of fine bainitic ferrite platelets and contains dislocations and fine carbides (except granular

bainite, which has retained austenite/MA phase between the platelets) in the microstructure. It is the combination of these microstructural features that determines the mechanical properties of bainitic steel, including strength, toughness, ductility, fatigue and creep behaviour. According to different applications, emphasis on optimising the combination of microstructural parameters may vary. In the Lifting and Excavating Sector, the most important mechanical properties of the material include yield/tensile strength and toughness/fracture behaviour. Therefore, this section will mainly focus on the strength and toughness, especially impact toughness, properties of low carbon, low alloy bainitic steels.

2.2.5.1 Strength of Low Carbon, Low Alloy Bainitic Steels

As concluded by Bhadeshia (2001), the strength of bainite can be determined by several components, including strength of pure iron, solid solution strengthening by carbon and substitutional elements, dislocation density and particle and grain size. Therefore the strength of bainite, in principle, can be expressed by the following equation:

$$\sigma = \sigma_{Fe} + \Sigma_i \sigma^i_{SS} + \sigma_C + k_\varepsilon (L_3)^{-1} + k_P \Delta^{-1} + C_{10} \rho_d^{0.5} \quad (3)$$

where

σ_{Fe} – intrinsic strength of pure annealed iron

σ_{SS} – strengthening contribution of substitutional alloying elements in solid solution

σ_C – strengthening contribution of carbon in solid solution

ρ_d – dislocation density

k_ε – constant, approximately 115 MPa/m

L3 – Mean intercept length in stereology

k_P – equals approximately 0.52Vθ, where Vθ is the volume fraction of cementite

Δ – average distance between a cementite particle and its two nearest neighbours

C10 – constant, approximately 7.34 MPa m

ρ_d – dislocation density

It can be concluded from the equation that the strength of bainite is affected by ferrite microstructure, solid solution strengthening, precipitates strengthening, and dislocation density. However, it is very difficult to make quantitative investigations on each parameter separately, as these microstructural features (e.g. grain size and particle spacing) cannot be varied independently (Bhadeshia, 2001). Therefore, the equation provides only a qualitative view on how can the strength of bainite be affected.

Another approach to the strength of steels is through the investigation of hardness. It is well known that the strength of steels is linked closely with hardness (Pavlina and Tyne, 2008). A general conclusion is that with the increase of hardness, the strength of steel will also increase. Irvin and Pickering (1965) discovered that the hardness increase of bainite is approximately linear with carbon concentration, by about 190 HV per weight percentage of carbon, and furthermore, they found that as long as the re-austenitisation temperature is high enough to dissolve all the carbides, hardness of fully bainitic microstructures will not be affected by the re-austenitisation temperature. This finding was later confirmed by research work of Kamada et al. (1976), stating that the hardness

of bainite is independent of the prior austenite grain size. This is because the bainitic ferrite sub-unit/platelet size is limited and will not be affected by the austenite grain size. Similarly, the strength of fully bainitic microstructures seems insensitive to the austenite grain size (which is also linked with bainite "packet size" frequently), as the retained austenite films and carbides between bainitic ferrite sub-units are much more formidable barriers than the low angle boundaries between the sub-units (Bhadeshia, 2001). However, this does not mean that other mechanical properties, for example toughness, will not be affected by factors such as austenite grain size/shape and packet size.

Mentioned by Irvine et al. (Irvine and Pickering, 1957) and Bhadeshia (2001), the tensile strength and hardness of steels with bainitic microstructure tend to vary with the transformation temperature. Higher transformation temperature, under which upper bainite forms, result in lower tensile strength and hardness compared to microstructures (lower bainite) that formed under lower transformation temperatures. Figure 2.13 shows the relationship between transformation temperature and tensile strength after work by Irvine et al. The reason for the increase in strength / hardness with the decrease of transformation is that microstructure forms at low temperature (e.g. lower bainite) contains finer bainitic ferrite plates and finer carbides (which can provide precipitation strengthening), also the dislocation density in lower bainite is higher than upper bainite due to low transformation temperature (as mentioned in Section 2.2.4) (Abbaszadeh et al., 2012). As for granular bainite, as reported by (Sung et al., 2011) the strength of a low carbon (0.05 wt% C) low alloyed steel decreases with the increase of the amount of granular bainite.

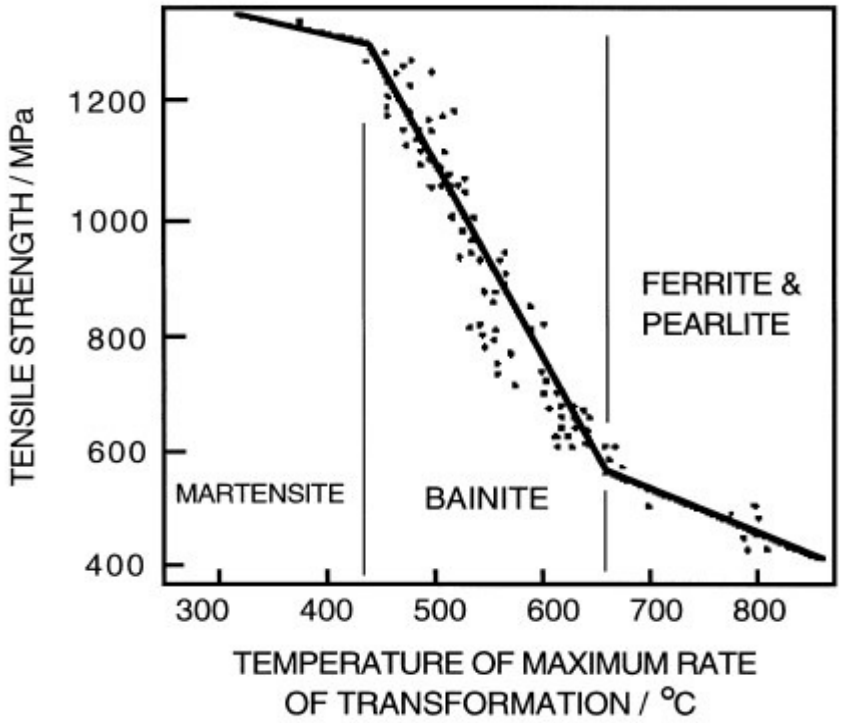


Figure 2.13 Variation of tensile strength of steels transformed at different temperatures (Irvine and Pickering, 1957).

2.2.5.2 Impact Toughness and Fracture Behaviour of Bainitic Steels

Toughness of steels is frequently evaluated by the Ductile-Brittle Transition Temperature (DBTT) via performing impact tests, normally Charpy impact tests. Body-centred cubic (bcc) metals show an obvious ductile to brittle transition as the temperature decreases while face-centred cubic (fcc) metals tend to maintain good ductility at all temperatures. The mechanism of this ductile to brittle transition of bcc metals is based on the different sensitivity of plastic flow stress (or resolved shear stress representing yield stress) and cleavage stress (representing ultimate tensile strength) against temperature. As temperature decreases, the plastic flow stress, i.e. the yield stress, of bcc metals increases rapidly while the cleavage stress of the material does not have change significantly. Below a certain temperature (T_t in Figure 2.14), the plastic

flow stress (i.e. the critical resolved shear stress) exceeds the critical cleavage stress, meaning that deformation before cleavage fracture becomes more and more difficult. This is the consequence of the increasing Peierls-Nabarro barrier to dislocation motion as temperature drops, which is also affected by the presence of interstitial elements in solution in the matrix metal (Bhadeshia, 2001, Fairchild et al., 2000b, Yang and Qiang, 2009). With conditions that raise the plastic flow stress (yield strength) of the material but do not influence the cleavage stress, such as low temperature and existence of notch, there will be much less plastic deformation before the fracture failure of bcc metals, which result in extremely limited absorbed energy and very little warning before cleavage fracture happens. Therefore, low DBTTs become an important objective for safety design, and due to its convenience, the impact test has been applied widely from an industrial aspect, especially in steel industries as many steel products (such as ferrite- and martensite-based steels) have bcc / bct structures.

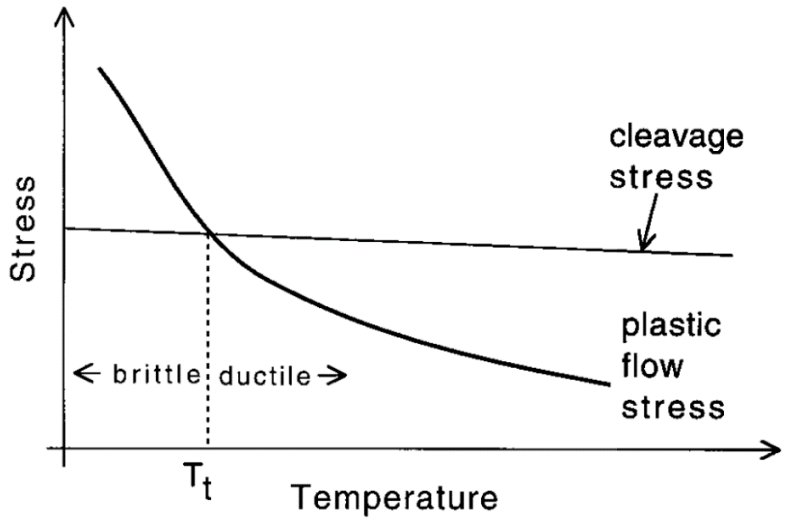


Figure 2.14 Schematic graph for the sensitivity of cleavage stress and plastic flow stress against temperature of bcc metal (Bhadeshia, 2001).

To perform a Charpy impact test, the material is cut into parallelpiped bars with 10×10 mm^2 square section and 55 mm in length, and with a notch which goes through the width/height direction at the centre of one of the rectangular sides. The test pieces will then be tested under given temperature conditions, and the absorbed energy at each test temperature will be recorded to plot an energy-temperature curve. Unlike the tensile test, after which a yield stress or ultimate tensile strength will be given directly, the Charpy impact test provides only the impact energy (absorbed energy) of the material, which does not directly give a toughness value or a "fracture strength" value of the material. A minimum value is normally specified in official standards for different components and the materials will be tested using impact to assess if they fulfil the safety standard. The impact toughness – temperature curve for materials with different lattice structure is presented in Figure 2.15, and the ductile-brittle transition temperature (DBTT) can be taken as the point on the curve corresponding to energy midpoint between upper and lower shelf energies. DBTT is sometimes referred as 50% ITT (impact transition temperature), and other criteria such as 27 J ITT or 34 J/cm^2 ITT are also used widely to suggest the position of the lower shelf of the curve.

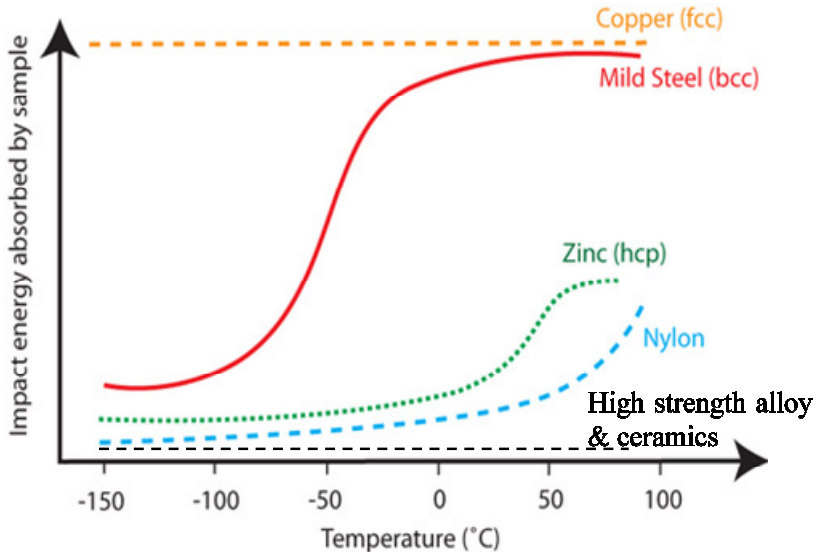


Figure 2.15 Impact energy absorption at different temperatures of different materials.

(Yang and Qiang, 2009)

It can be seen from the figure, as mentioned above, that materials with face-centred-structure (fcc) structures tend to retain a high impact energy (i.e. absorbed energy) across the entire temperature range, representing high toughness; on the contrary, ceramic materials tend to have low impact energy even at high temperatures, suggesting low toughness behaviour for this kind of material. For body-centred-cubic (bcc) materials, the impact energy tends to vary along with temperature.

For steels with bainite microstructure, the impact toughness varies with the different types of bainitic structure (Figure 2.16). According to research work of Bhadeshia (2001) and Irvine and Pickering (1963), for low carbon, low alloy, boron and molybdenum added steels, upper bainite formed at high temperatures was found to have lower strength but better impact performance, compared with the upper bainite that formed at lower temperatures after continuous cooling (however this type of upper bainite has higher strength compared with the previous one, due to the lower extent of

autotempering compared with upper bainite that formed at high temperature and therefore dislocation density remains high to strengthen the steel). Lower bainite, however having higher strength values than upper bainite, was found to present even better impact toughness than the low strength upper bainite. This is due to the much finer cementite precipitates in lower bainite compared to upper bainite and mentioned by Abbaszadeh et al. (2012) both the strength and impact toughness of a medium carbon (0.47 wt% C) steel were improved by increasing lower bainite percentage (rather than upper bainite) in a mixed microstructure with martensite / tempered martensite. As suggested by Curry and Knott (1978), Fairchild et al (2000b), and Yang and Qiang (2009), carbide, especially cementite, in steels is brittle and therefore tends to act as the source of micro-crack under stress, and under certain conditions, these micro-cracks will be able to propagate into the matrix and result in final cleavage crack of the material (Fairchild et al., 2000b, Du et al., 2012).

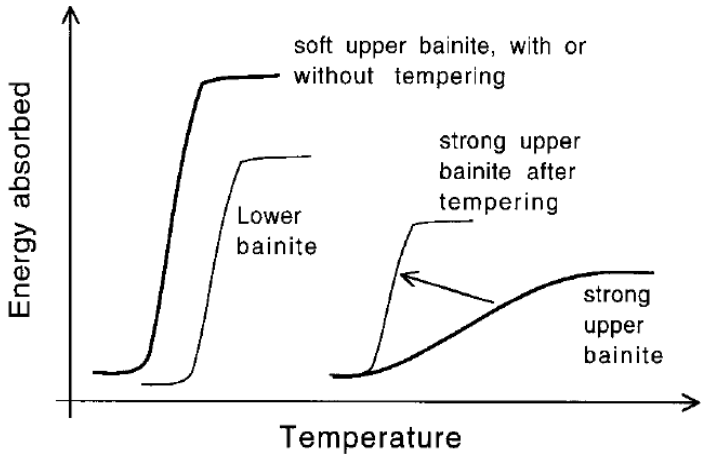


Figure 2.16 Impact behaviour of different bainitic structures (Bhadeshia, 2001).

When a crack propagates in a bainitic microstructure (either upper or lower or other types of bainite, as they are all formed with paralleled bainitic ferrite plates and carbides / retained austenite between the plates, however worth to note the width of bainitic

ferrite plates, dislocation density, and carbide / retained austenite size and distribution is different and therefore result in different toughness in different types of bainite), it has been found that the crack does not deviate when going across individual sheaves of bainitic ferrite in low carbon, low alloy steels (Pickering, 1967a). However, when encountering bainite packet or the prior austenite boundaries, the crack normally tends to change its propagation direction. This is because of the low angle boundaries of bainite platelets and high angle boundaries (larger than 15° misorientation) between different bainite packets (Brozzo et al., 1977, Bhadeshia, 2001, Rancel et al., 2011, Medina et al., 2014). Some research work suggested that the Unit Crack Path (UCP), which is defined as the region within which a crack propagates in a nearly straight fashion (Matsuda et al., 1968, Matsuda et al., 1972), is approximately 1.5 times of the bainite packet size, as the packets transformed from austenite via K-S relationship may present "a continuity of their (100) cleavage planes within a misorientation of 10°" (Brozzo et al., 1977), hence the length of unit crack path has become an important factor on fracture behaviour of bainitic steels. Furthermore, reported by Caballero et al. (2012), in the low carbon (< 0.15 wt% C) steels investigated, granular bainite tend to result in larger bainite packet size due to its coarse crystallographic structure, also the retained austenite and / or coarse carbides that formed during transformation tend to contribute to crack nucleation and therefore reduces the resistance for cleavage crack propagation.

2.3 High Strength Strip Steels

Hot rolled, high strength strip steels have been applied widely in building construction, automotive applications, as well as Lifting and Excavating sectors, due to their good mix of mechanical properties and cost effective characteristics (Morris et al., 2004). To

deliver good mechanical properties, including high strength and toughness, to the steel products, carbon content is controlled at a low level (between 0.05 and 0.25 wt %), small amounts of alloying elements such as Nb, V, Mo and Ti are added, and hot rolling process is applied during steel making. Several types of product include TRIP (Transformation Induced Plasticity) steel, HSLA (High Strength Low Alloy) steel and TWIP (Twinning Induced Plasticity) steel have been applied in Lifting and Excavating Sector (Punch, 2014). However, as the customers are requiring better steels for application, traditional materials, for example ferritic strip products, will not be able to fulfil customers' requirements, and new products with higher mechanical property combinations are needed, which has led to the innovation of bainitic strip products (Morris et al., 2004, Morris et al., 2012, Morris et al., 2013).

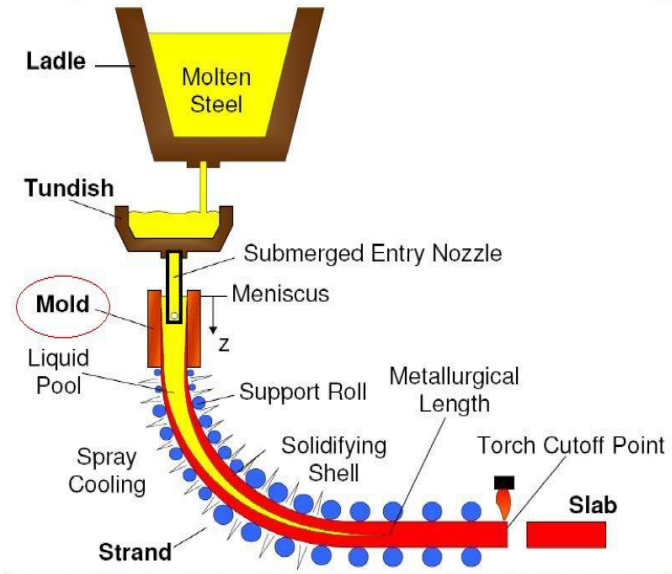
Although bainite has been discovered at early 1940s, quenched and tempered (Q&T) martensitic steels were still preferred by manufacturers and the market, especially the high strength steel sector. Because, in the early stages, bainite contained coarse carbides / cementite particles in the microstructure, and due to the continuous cooling process applied in most industries, a fully bainitic microstructure could not be produced in industrial practice at that time. Till late 1950s, Irvine and Pickering (1957) introduced low carbon low alloy steel, with addition of boron and molybdenum, and made the manufacturing of fully bainite steel became commercially possible. Furthermore, laminar water jet systems were developed to provide faster cooling rates so that partially or fully bainitic microstructure can be achieved. More research work has been carried out on developing accelerated cooling systems during the past twenty years, leading to the design and production of various low carbon low alloy steels with continuously

improved properties and decreased manufacturing cost (Morris et al., 2004, Crowther et al., 2005, Kern et al., 2005, Morris et al., 2012, Li et al., 2013).

2.3.1 Production of Hot Rolled Strip Steels

Hot rolled strip steels are produced through several steps in steel plant, including iron making, steel making, casting, hot rolling and coiling. In this section, the general process applied in steel plants, especially in Tata Steel Port Talbot site, will be reviewed, focusing on the hot rolling procedures.

Compared with traditional casting technology, i.e. ingots and moulds casting, continuous casting is much more efficiency and is able to produce shapes such as billets, blooms or slabs, as the technology eliminates the need for a "slabbing mill", soaking pits, and storage for large amount of ingots and moulds, yet besides the cost saving benefits, the quality of finished steel products is better. The continuous casting machine / process is shown in Figure 2.17 (a), and Figure 2.17 (b) shows the solidified steel slab (before cutting) produced through the process, note the good surface finishing and uniformity of the shape. When entering the water-cooled copper mould, the outer shell of molten steel is cooled and solidified, while the centre is still in liquid status. The partially solidified steel is then drawn very slowly into a curved arrangement of guides, support rollers and water coolers until it emerges horizontally as solid slab from discharge end of the caster, by which time the slab is fully solid. The slab is then cut into desired length by automatic gas cutting equipment, marked with unique identity for traceability and transferred to stockyards, waiting for further processing in the hot rolling mill.



(a)



(b)

Figure 2.17 (a) Typical continuous casting machine in steel plant. (b) Slab product produced by continuous casting.

The slabs produced by continuous casting are then transported to the reheat furnaces to be heated to an optimum temperature, normally between 1180 °C and 1250 °C, before hot rolling (Figure 2.18). The slabs are loaded into reheating furnace continuously, as the heated slab exiting the furnace, another cold slab enters the furnace for reheating.

After reheating, a continuous series of motor-driven rollers guides the red hot slab into two sets of descale rollers, with help of additional high pressure water jets, scale or oxidation on the surface of the slab is removed to reduce the surface inclusions and laminations. The slab then enters the rough rolling mill to start the rolling process. At the beginning of this stage, the thickness of slab is 234 mm, and the slab is then passed forwards and backwards through the reversing roughing mill, for up to 5 times to reduce the thickness into 38 mm. The temperature of the slab during rough rolling is monitored by a set of pyrometers, as the rolling progresses, the slab becomes thinner and the temperature of the slab drops from 1180 °C to about 1100 °C. By the end of rough rolling, the slab has been elongated up to 70 metres long (Figure 2.19), which becomes too long to convey between different rolling stands, therefore a kit called "Coil Box", which winds the rough rolled slab, is normally placed between Roughing Mill and Finishing Stand (especially for mills constructed into a limited size) to enable the extended bar to be handled with a much short space (Figure 2.20). The Coil Box also helps the extended slab (now can be referred as "bar") stabilise heat loss and equalise temperature across the whole length. The coil is then moved to Finishing Mill for further reduction of thickness. The coil remains temperature about 1000 °C when entering the Finishing Mill, Crop Shears before the Finishing Mill is used for slicing the "tail end" and "nose end", which refers to the front and back of the "bar" after rough rolling respectively, of the coil to provide a straight edge to the entry rolls. The Finishing Mill comprises seven consecutive roll stands of rolls, with each geared to steady reducing the coil thickness from 38 mm to a gauge ranged from 1.5 mm to 15 mm, depending on customer's requirements (Figure 2.21). The coil is rolled and passed to the next roller very quickly, the time gap between two rolling stands is approximately

2 seconds. Water sprays are constantly running to reduce heat generated due to the quick rolling. There are also pyrometers between each stands to monitor the temperature of the coil, by the time the coil has passed all seven rolling stands, the temperature has fallen to about 800 °C, and the length of the coil can stretch to as long as 1.5 kilometres. The hot rolled steel is then enters the Run-Out Table (ROT), which is equipped with water sprays both above and under the guides, to help to cool the strip down to desired temperature before coiling (Figure 2.22). The temperature of the strip can be adjusted by amending the amount and pressure of water spray, therefore different types of microstructure can be achieved combining with coiling. Another Coil Box is setup at the end of Finishing Mill to wind the hot rolled steel tightly and the coil is then moved to a designated area to cool. After cooling, the hot rolled coil products can then be send to cold rolling mill, other business sectors, or external customers for further processing into different applications.



Figure 2.18 A slab is exiting the reheat furnace.



Figure 2.19 Extended slab (bar) after rough rolling.



Figure 2.20 Coiled rough rolled "bar" to be unwound from the Coil Box for finishing rolling.



Figure 2.21 The Finishing Mill in a Tata Steel plant, showing the seven rolling stands and replacement rolls beside each stand waiting for next roll change.



Figure 2.22 The Run-Out Table (ROT) and water sprays above to cool the strip steel to a desired temperature before coiling.

2.3.2 Project Background on Rolling and Industrial Constraints

Thermo-mechanical controlled processing (TMCP, or TMP) is widely used in steel industries at present, as through this process the microstructure of a product can be controlled by inducing the formation of fine grained structures or desired microstructures in combination with precipitation (Tanaka, 1995, Porter, 2011). A schematic graph of the process of TMCP is shown in Figure 2.23.

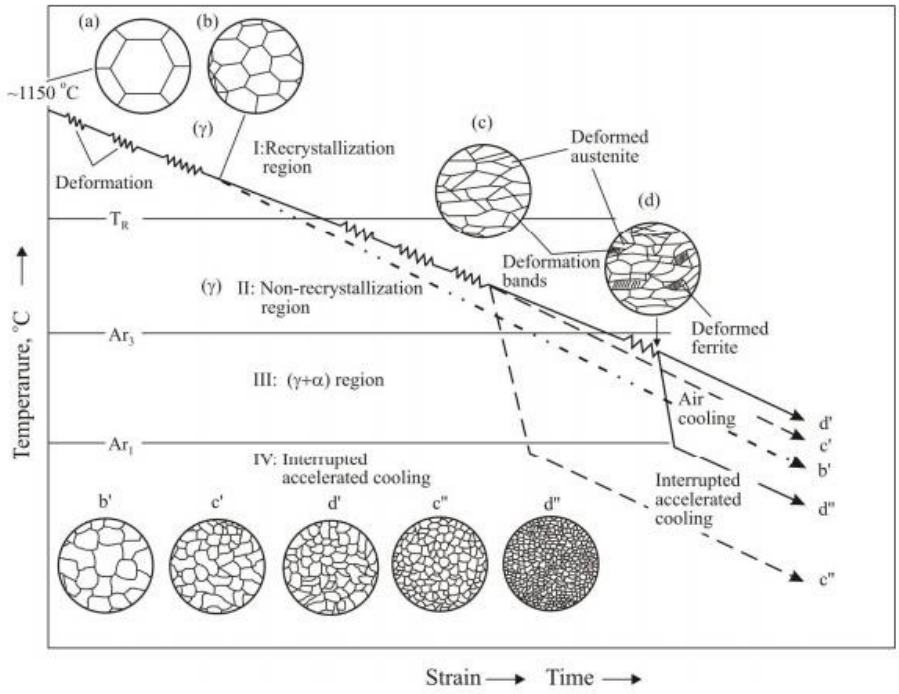


Figure 2.23 Schematic diagram of the TMCP process and corresponding microstructure at each stage. (Tanaka, 1995)

Through controlling the temperature and the deformation of rolling process, TMCP is able to produce elongated (pancake-shaped) austenite grains in the non-recrystallised region and achieve fine grain size / structure after phase transformation, and with the help of accelerated cooling, the final microstructure such as ferrite, bainite or martensite can be achieved. In industrial processes, roughing rolling starts at temperatures between

1180 °C to 1200 °C and the finishing rolling starts at about 1050 °C, the coiling process can be carried out in the range of 600 °C to 300 °C depending on the final microstructure required. Therefore, it is necessary to consider the optimum processing temperatures, which are beneficial to the microstructure and mechanical properties.

As required by customers from the Lifting and Excavating sector, the yield strength of steel products above 700 MPa, combined with toughness requirements of DBTT lower than -40 °C (Crowther, 2012). Although currently most products with ferritic structures, produced through TMCP, have yield strength ranging from 680 to 800 MPa, however this is often accompanied by large variation in DBTT with different gauge thicknesses, ranging from -50 °C to +30 °C (Punch, 2014). Reported by Punch (Punch, 2014), steels with ferritic structure can achieve about 700 MPa yield strength and DBTT lower than -40 °C in steels gauged from 8 to 10 mm or thinner, whilst higher gauges from 10 to 16.8 mm still show worse strength – toughness combination (normally with 650 to 690 MPa yield strength and 0 to 30 °C DBTT) than thinner gauge products, due to presence of higher amount of coarse grains and coarse TiN particles. However, according to private communication with Dr. D. Crowther (Crowther, 2012), steels with thick gauges between 12 to 16 mm are currently required by customers to have above 700 MPa yield strength and DBTT below -40 °C or even lower (-60 °C), for different applications in the Lifting and Excavating sector. Currently, Tata Steel is developing steels with bainitic microstructure at high gauges between 10 to 16 mm, as such bainitic structure is potentially able to achieve a good strength – toughness combination due to its different characteristics from ferrite (i.e. fine lath structure, fine carbide precipitations, and high dislocation density, as mentioned in Sections 2.2.4 and 2.2.5). However, constraints in industrial production may cause difficulties in achieving a beneficial bainitic

microstructure and therefore mechanical properties. Therefore, further investigation is required on the relationship between bainitic microstructures and mechanical properties, especially impact toughness, and the factors (such as alloying level and rolling / coiling parameters) that can be adjusted to achieve a beneficial microstructure.

There are several constraints in industrial production of steel. Due to the limitation in production cost for commercial steels, the content of expensive micro-alloying elements, such as Ni, Mo and Ti needs to be controlled (and preferably reduced to low level), to make the products cost efficient. In addition there are other constraints in industrial production that need to be taken into account when designing new steels, for example for rolling / coiling parameter control - although the starting rolling and finishing rolling temperatures are carefully designed, control of these temperatures during production is not easy, and there will usually be some differences in these temperatures from one strip to another. During production of high strength strip steels the finishing rolling temperature can vary by about ± 10 to 20 °C from the pre-set values and it is not desired for them to be lowered much (normally the finishing rolling temperature is set as 880 – 920 °C or higher, depending on the grade of steel according to private communication with Dr. D. Crowther) (Crowther, 2012). In addition, controlling of coiling temperature, which is another important factor that affects the final microstructure and therefore the mechanical properties of products, also has constraints. In general, the coiling temperature is achieved by controlled water quenching (on the run-out table, the cooling rate varies from 10 °C/s to 40 °C/s depending on the different setup / layout of water spray sections and the thickness of the strip) after hot rolling, therefore in order to save energy and cut cost, high coiling temperatures (e.g. 500 – 600 °C) are desired. However, the high coiling temperatures may not achieve the desired microstructures to give the

optimum combination of strength and toughness. Additionally, there are some variations between the designed coiling temperature and actual values, as well as the temperature distribution along the length of a strip; these variations depend on the aim coiling temperature, where low coiling temperatures (below 350 °C) usually have larger variations compared with high coiling temperatures (above 500 °C). Due to the required final microstructure for some steel grades (normally for bainitic / martensitic products), the coiling temperature has to be set below 500 °C or even lower. It is difficult to accurately achieve low coiling temperatures such as 250 or 300 °C and for coiling temperatures below 350 °C a variation of ± 50 °C along the length of a coil can occur with inaccuracies in the measured temperature due to optical pyrometer error from the large amount of residual water on the strip surface) (Crowther, 2012).

Based on above literature review, the industrial constraints associated with the production of high strength strip steels and the customer requirement in the Lifting and Excavating sector then a bainitic microstructure is suggested to achieve the hot rolled steel product with a good combination of strength (around 700 MPa) and impact toughness (lower than -40 °C ductile-brittle transition temperature). Optimisation of the bainitic microstructural components and the chemistry-processing combination to achieve the desired microstructure and hence properties is required. Therefore, the aim of this work is to study the relationship between the complex bainitic microstructure (mixture of different types of bainite) and the mechanical properties (strength and impact toughness) of S700 grade steels, and to propose a desired microstructure to fulfil the customer requirements on strength and toughness; then, through investigating the austenite – bainite transformation behaviour during cooling and coiling, while taking industrial constrains of steel production into consideration, to propose an optimised

alloying level and processing route to achieve the desired microstructure and therefore mechanical properties.

CHAPTER 3

EXPERIMENTAL PROCEDURES

3.1 Introduction

This chapter includes the experimental techniques, microstructure characterisation methods, and mechanical tests employed in the project. The chemical compositions of the high strength strip steels provided by Tata Steel (UK) plc have been given in section 3.2. Section 3.3 includes the microstructure characterisation and image analysis methods. Section 3.4 describes the techniques used for mechanical testing, and section 3.5 describes the fracture analysis methods. Section 3.6 covers the simulation techniques used for obtaining phase transformation behaviour, include dilatometry testing and Gleeble thermomechanical simulations.

3.2 Materials Details

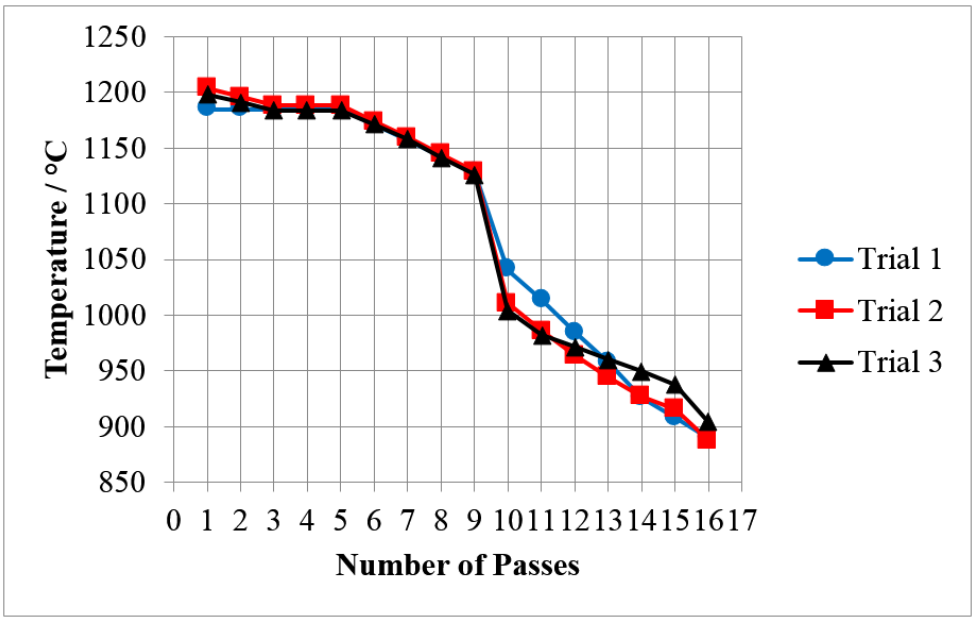
A number of low carbon, low alloy high strength strip steels produced during three full scale commerical trials, where coils were produced at different coiling temperatures, were supplied by Tata Steel (UK) plc for this study. The steels are graded as "S700" class, and as stated in British Standard BS EN 10149-2:2013, for S700 grade steels, the yield strength in the longitudinal direction (i.e. rolling direction) should be no lower than 680 MPa for products with thickness 8 mm and above, where the longitudinal tensile strength should be between 750 – 950 MPa, and the elongation (A80) should be higher than 12 %. Steels from the same trial have identical composition, however the chemical compositions of these three trials were slightly different, as shown in Table

3.1. All the trials have around 20 ppm B addition, which is used to increase the steel hardenability to ensure bainitic microstructures are produced. Trial 1 has the lowest V (less than 0.01 wt %) content and highest Mo (0.255 wt %) and Nb (0.04 wt %) content among the three trials, while trial 2 is very similar with trial 1 but with increased V (0.051 wt %) and slightly decreased Mo (0.239 wt %) content (which might be caused by the casting variation between one trial product and another), where the V was added to increase strength, and trial 3 has the highest C (0.071 wt %) content (which is also possibly because of variability between casts) but the lowest Si, Mo (0.198 wt %) and Nb (0.031 wt %) compared with the other trials. In summary, design changes falls on decreased Mo, Si and Nb in Trial 3 compare to Trials 1 and 2, as well as the increased V in Trials 2 and 3 compare to Trial 1, are designed changes in these products.

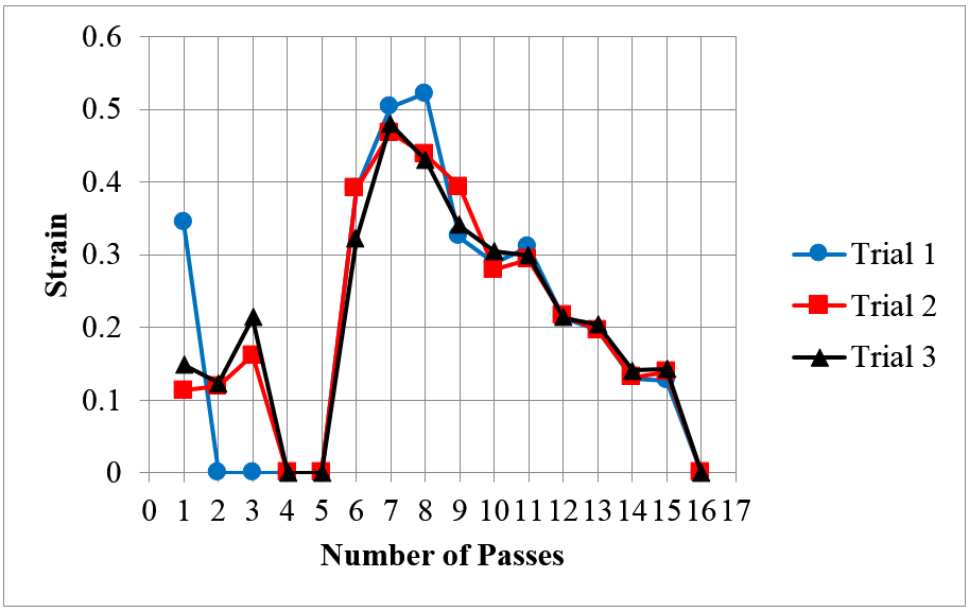
Table 3.1 Compositions of trials investigated (in wt %)

Trial 1	*C*	*Si*	*Mn*	*P*	*S*	*Ni*	*Mo*	*Cr*
	0.065	*0.1*	*1.50*	*0.01*	*0.005*	*<0.1*	*0.255*	*0.5*
	Cu	*Al*	*Nb*	*V*	*Ti*	*N*	*B*	-
	<0.06	*0.075*	*0.04*	*<0.01*	*<0.01*	*0.002*	*0.002*	
Trial 2	*C*	*Si*	*Mn*	*P*	*S*	*Ni*	*Mo*	*Cr*
	0.066	*0.1*	*1.56*	*0.01*	*0.003*	*0.024*	*0.239*	*0.5*
	Cu	*Al*	*Nb*	*V*	*Ti*	*N*	*B*	-
	0.012	*0.075*	*0.04*	*0.051*	*0.002*	*0.005*	*0.002*	
Trial 3	*C*	*Si*	*Mn*	*P*	*S*	*Ni*	*Mo*	*Cr*
	0.071	*0.06*	*1.50*	*0.01*	*0.001*	*0.018*	*0.198*	*0.5*
	Cu	*Al*	*Nb*	*V*	*Ti*	*N*	*B*	-
	0.013	*0.076*	*0.031*	*0.046*	*0.002*	*0.0045*	*0.0024*	

Samples, measuring approximately 600 x 400 mm, were provided from the central part (as in mid-length) of each hot rolled coil. All of the strip steels were hot rolled to 12 mm thick from an initial slab thickness of 225 mm, with the Finishing Rolling Temperature (FRT) between 890 °C and 920 °C, then coiled at different Coiling Temperatures (CT) between 250 °C and 460 °C. The above temperatures were monitored by pyrometers, however, the coiling temperature, particularly at low coiling temperatures, is affected by water spray and may not be 100 % accurate, and can also vary along the length of the strip product. Therefore, the average rolling / coiling temperature along the whole length of the strip (which has a standard deviation of approximately ± 10 to ± 30 °C from position to position according to information via private communication from Dr. D. Crowther, Tata Steel (Crowther, 2012) was used as the rolling / coiling temperature. It is known that coiling temperatures lower than 350 °C tend to show more inaccuracy in the measured average temperature compared with measurements made for strips with higher coiling temperatures (Crowther, 2012). The rolling parameters (temperatures and strain) for the different trials are shown in Figure 3.1 (a) and (b), in which the first 9 passes represents rough rolling and the last 7 passes represent finishing rolling, the strain and temperature values are all provided by Tata Steel via private communication from Dr. D. Crowther (2012). In rough rolling, the data of first 5 passes come from the reverse rolling stand and depending on the requirement of final product gauge sometimes the steel will not go through all the 5 passes in reversing mill. However, for the convenience of comparing different trials all the passes are plotted on the graphs, whether the steel went through or not. Table 3.2 shows the thickness, FRT and CT for the coils within each trial, where ascending numbers relate to a decrease of coiling temperature.



(a)



(b)

Figure 3.1 Rolling schedules for different trials. (a) Temperature at each pass. (b) Strain at each pass.

Table 3.2 Rolling and coiling parameters of each strip steel.

Trial	*Trial 1*				*Trial 2*			*Trial 3*	
Sample ID	*T1-1*	*T1-2*	*T1-3*	*T1-4*	*T2-1*	*T2-2*	*T2-3*	*T3-1*	*T3-2*
Thickness / mm	*12*	*12*	*12*	*12*	*12*	*12*	*12*	*12*	*12*
CT / °C	*453*	*411*	*393*	*290*	*347*	*314*	*253*	*400*	*390*
FRT / °C	*881*	*890*	*893*	*892*	*860*	*880*	*870*	*880*	*895*

As can be seen from Figure 3.1 (a), there were 16 passes during the whole rolling process, the first 9 passes were roughing rolling, which were performed at temperatures between 1200 °C and 1125 °C; and the last 7 passes were finishing rolling, the temperature ranged from 1050 °C down to around 900 °C. Figure 3.1 (b) shows the strain at each rolling pass. As indicated in Figure 3.1, the rolling schedules for the three trials are different from each other, especially in terms of the strain during the rough rolling stage and the rolling temperature during the finish rolling stage. For rough rolling, larger strain (0.35) has been applied on the first pass (reverse rolling) of rough rolling for T1 steels (compared to the other trials), and the following several zero strain roughing passes are reversing passes that were not applied to the plate (as the strain at first pass was enough to reduce the plate thickness to the second roughing stand requirement), while for T2 and T3 steels smaller strains (0.1 – 0.2) were introduced during the first rough rolling pass (but reversing rolled for 3 times) and followed by another two zero strain reverse rolling passes before the second roughing stand. The reason for this change is not clear, however is possibly due to a different setting on the production line between the times the different trial were rolled. However, this difference in rolling schedule may affect the final austenite grain size and grain shape after deformation. As reported by Abad et al. (2001), Xiao (2013) and Rehman (2014)

in low carbon Nb alloyed steels the recrystallized austenite grain size during rough rolling can be affected by strain. Equation (4) shows the relationship between the recrystallised grain size, initial grain size and strain during hot rolling (Abad et al., 2001, Xiao, 2013):

$$d_{rex} = 1.4 d_0^{0.56} \varepsilon_{eff}^{-1} \quad (4)$$

where

d_{rex} – statistical recrystallised austenite grain size

d_0 – initial austenite grain size

ε_{eff} – effective strain for statistical recrytallisation

It can be seen from equation (4) that larger strain during rough rolling (above non-recrystallisation temperature) will result in a smaller recrystallised austenite grain. For this reason, it is very likely that T1 steels will have a smaller austenite grain size than T2 and T3, due to the large strain in the first rough rolling pass.

For finishing rolling, T1 has higher starting finishing rolling temperature (approximately 35 – 40 °C higher) for the first 3 – 4 passes than the other trials, while T3 shows smaller temperature gradient for finishing passes compare with T1 and T2 (similar starting temperature with T2 but higher from pass No. 12, i.e. the 3rd pass of finishing mill). The temperatures of finishing rolling passes are critical in prior austenite grain shape, i.e. the more rolling passes below recrystallisation temperature, the more austenite grains will be deformed.

3.3 Metallography and Image Analysis

Samples measuring 10 × 10 × 12 mm^3 were cut from the centreline of each steel strip and the longitudinal section (transverse-normal plane) was investigated for microstructure features. The samples were mounted in conductive Bakelite, then ground and polished to an OPS finish before being chemically etched using 2 % nital. Microstructures were observed by a Carl Zeiss optical microscope initially and then a Jeol 7000 Scanning Electron Microscope (SEM). The SEM images were used for microstructure analysis and quantification, as well as carbide size measurements. ImageJ software was used to analyse the images for bainitic phase quantification and bainite packet size measurements, and around 20 high magnification (1200x – 1400x) SEM images, randomly taken at positions 3 – 4 mm deep below the surfaces for each sample, covering approximately 0.15 mm^2, were used for each sample. The detailed method used for recognizing different forms of bainite and the quantification results are discussed in Chapter 4.

3.4 Mechanical Testing

3.4.1 Micro-hardness

Tensile tests for all the strips investigated were carried out at Tata Steel (UK) plc, according to BS EN ISO 6892-1:2009 in both the Longitudinal (L) direction and Transverse (T) direction. The Yield Strength (YS) and Ultimate Tensile Strength (UTS) were given as the average value of at least 3 repeat tests. Vicker's hardness tests were carried out on the strip materials, and the relationship between yield strength and Vicker's micro-hardness value assessed(Pavlina and Tyne, 2008):

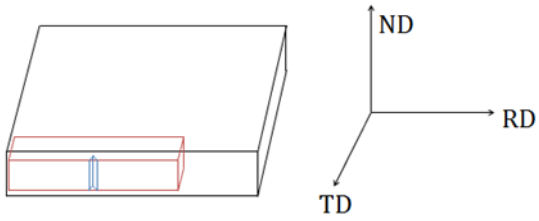
$$\sigma_{ys} = a_0 + a_1 \times H_v \quad (5)$$

where σ_{ys} is yield strength, H_v is hardness value, a_0 and a_1 are a regression constant and regression coefficient, respectively, which can vary (from -270 to 60 for a_0 and from 2.1 to 4.5 for a_1) for different steels.

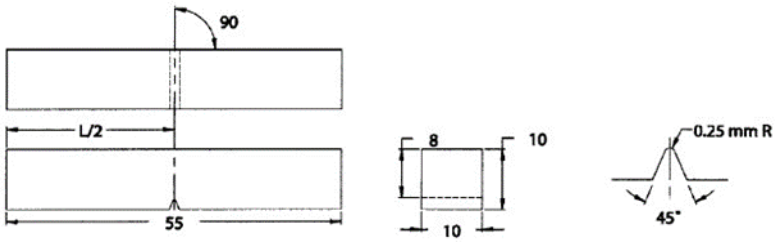
Vicker's micro-hardness (HV) tests were performed with a load of 300 g (the diamond indenter was held for 10 s) at room temperature on etched samples, at positions about 3 to 4 mm below the surface, close to areas where the SEM images used for phase quantification were taken. At least 5 readings were used to determine an average hardness value. Furthermore, through thickness Vicker's hardness tests were also carried out for all samples, to provide the hardness profile of each strip steel. The through thickness HV tests were performed from 1.5 mm below one surface to 1.5 mm below another, and each position was 0.5 mm away from another. Again, 5 readings were taken at each position.

3.4.2 Impact toughness tests

Charpy impact tests were performed in accordance with ASTM A370 and ASTM E23 standards. Standard longitudinal Charpy impact specimens (10 × 10 × 55 mm, long axis parallel with rolling direction) were used for impact toughness testing. A through thickness notch (long axis of the notch parallel with the normal direction of the original material) was made on each specimen, with 45° angle and 2 mm depth, as shown in Figure 3.2. Test temperatures were in the range of -196 °C (liquid nitrogen) to 50 °C (hot water), and mixture of ethanol and liquid nitrogen was used to achieve temperatures between -120 °C and 15 °C.



(a)



(b)

Figure 3.2 Direction and dimensions of standard Charpy impact samples with V-shaped notch. (a) The direction that Charpy impact samples were taken from the parent material. (b) The dimension of each Charpy sample.

3.5 Fractography

A Philips XL-30 SEM was used for fracture surface analysis, operated under 20 kV accelerating voltage and 5.5 – 6 spot size. The fracture surfaces were then Ni plated and sectioned, mounted in Bakelite, polished to an OPS finish and etched in 2 % nital for fracture path investigation, to determine the correlation between microstructure and crack propagation behaviour. A Joel 7000 SEM was used for Unit Crack Path (UCP) analysis on sectioned samples. The UCP is defined as "the region in which the cleavage crack propagates in a nearly straight line" (Mazancová et al., 2007, Yang and Qiang, 2009, Medina et al., 2014, Punch, 2014).

3.6 Dilatometry and Gleeble Tests

In order to investigate the phase transformation behaviour of these low C low alloy steels, and the effects of parameters, such as alloying level and deformation, on the bainite phase transformation, dilatometry and Gleeble simulation tests were carried out. Initially dilatometry tests were carried out at Tata Steel Swinden Technology Centre (UK), however, due to the long-term unavailability of the test machine after the initial tests (equipment failure), a Gleeble 3500 thermo-mechanical simulator was used for further investigations.

It is well known that phase transformation is normally accompanied with heat absorption or release due to the difference in specific heat capacity (C_p) of the two (or more) phases. Through investigation on the change of enthalpy (ΔH) during $\gamma - \alpha$ phase transformation, researchers have found that during cooling, the phase transformation from austenite to a ferritic / pearlitic microstructure tends to release heat, and the transformation temperature range is comparable with dilatation measurements (Hagel et al., 1956, Krielaart and Zwaag, 1998, Li et al., 2002, Liu et al., 2003). In addition, reported by Jansson et al. (1991), the heat transfer coefficient is able to indicate phase transformation in steels. The change of heat transfer coefficient of a medium carbon steel (0.42C-0.86Mn-1.09Cr-0.18Mo-0.18Ni-0.24Cu) with temperature during cooling is shown in Figure 3.3. It can be seen from the figure that the measured heat transfer coefficient differs significantly from calculated data (assuming no phase transformation) between 560 and 400 °C, which is due to the heat release by the austenite – bainite transformation during cooling. As heat transfer coefficient is a measure of heat transfer between two different phases, and it reveals phase transformation, it is then reasonable

to use the actual heat absorption or release between two phases as a measure of phase transformation process, which leads to the development of the following method by using a Gleeble thermo-mechanical simulator.

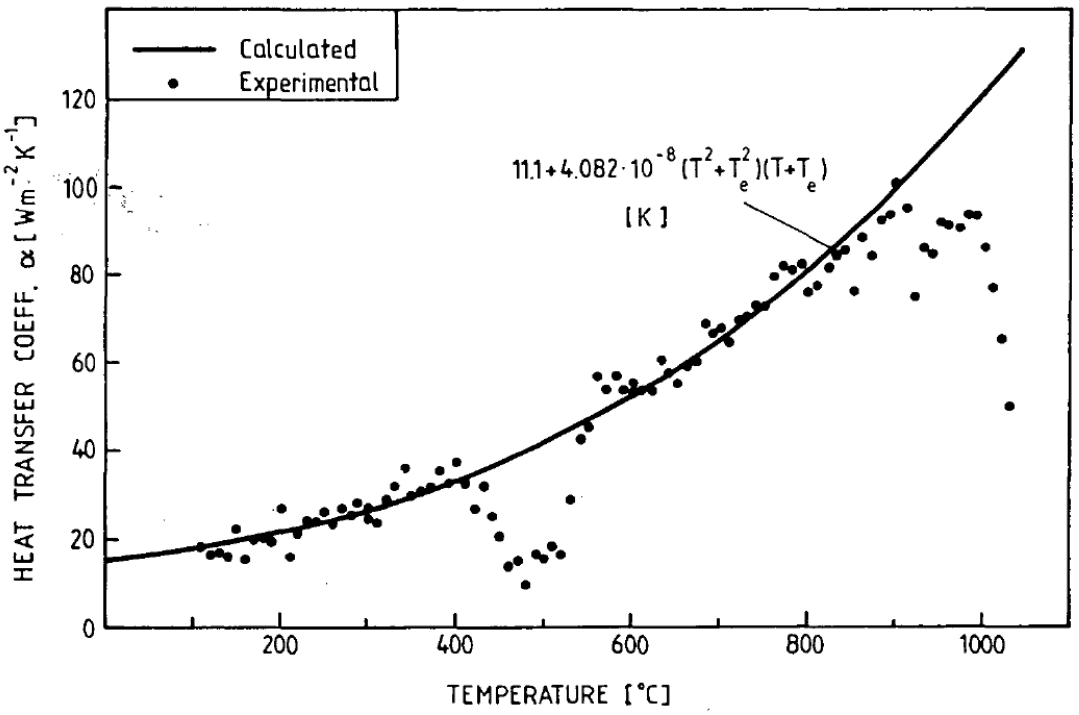


Figure 3.3 Experimental data (black dots) of heat transfer coefficient – temperature relationship during cooling of a 0.42 wt% C steel (Jansson et al., 1991).

As indicated above, it is possible to determine the temperature range of phase transformation using test equipment such as a Gleeble thermo-mechanical simulator instead of a dilatometer machine, through monitoring the test time and heat absorption / release during the thermal cycle. A Gleeble 3500 machine, fitted with an additional power module which can monitor the power (in "Watts") that the equipment uses to heat or maintain the required temperature of the specimen, was used heat and cool a standard Charpy sized sample (10 × 10 × 55 mm, without notch) at prescribed rates with the cooling curve used to determine the temperature range of the phase transformation,

which was used to plot the CCT diagram for the steels. The detail of the testing procedure is explained below:

3.6.1 Principles of the technique and experiment setup

During the Gleeble 3500 thermo-mechanical simulator tests, the machine measured the specimen's temperature via K-type thermocouples welded on the mid-point of the sample, and used this to control the temperature of the sample by adjusting the current flow through the specimen. If phase transformation happens during a programmed thermal cycle, the heat release/absorption will affect the specimen's temperature and the machine will need to modify the power applied on the sample to maintain the programmed schedule according to the feedback from the thermocouple. Therefore, it should be possible to detect the phase transformation start and finish points by monitoring the power that the Gleeble 3500 machine applies to the sample during the programmed temperature – time schedule (referred to as "Temperature – Control Scheme", TCS). At the end of the test, the transformation start and finish points can be determined from the temperature – power curves. However, as this testing method have not been used for phase transformation before, some pre-tests were carried out to make sure this method gives accurate phase transformation temperatures. A 0.8 wt% C rail steel, with known transformation behaviour (the CCT curve is shown in Figure 3.4), was tested before the formal experiments on the strip steels. Also, comparison between results from dilatometry tests done by Tata Steel and Gleeble 3500 tests were also carried out. Detailed discussion on the phase transformation behaviour of the investigated steels is provided in Chapter 6.

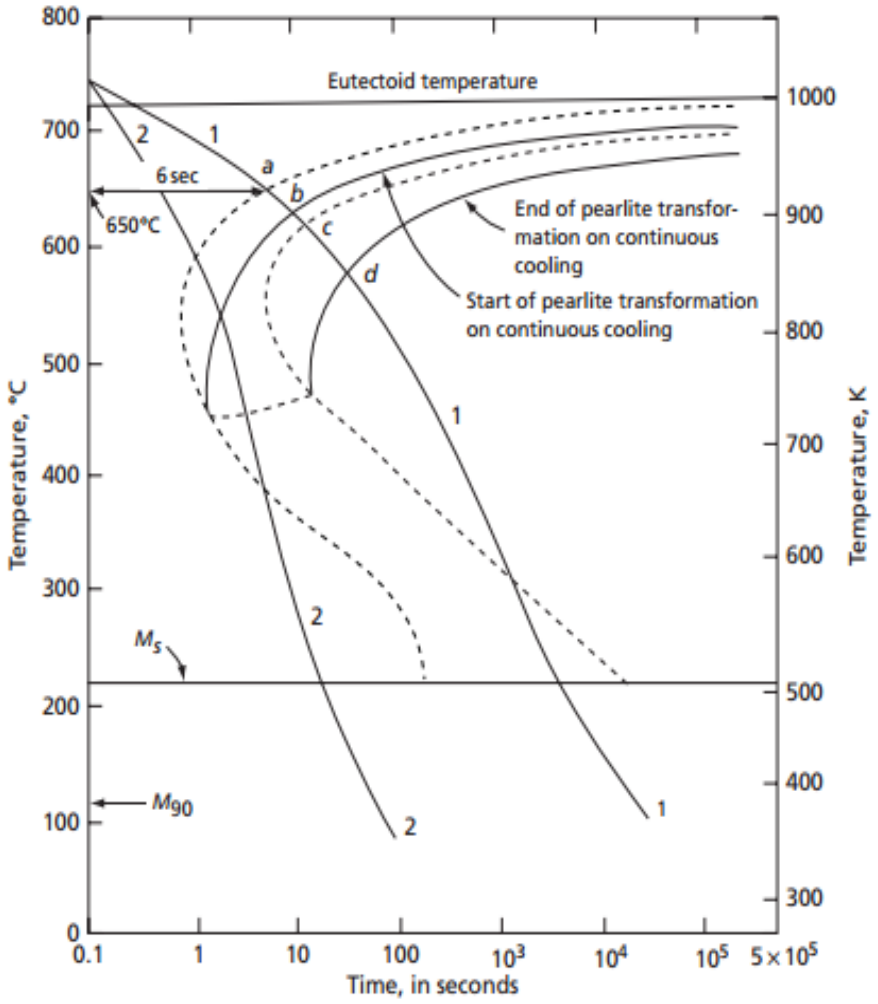


Figure 3.4 Continuous Cooling Transformation (CCT) diagram (solid curves) of a 0.8 wt% C railway steel. Dashed curves are isothermal transformation (TTT) diagram, and curves 1, 2 represent different cooling rates. (Abbaschian et al., 2009)

For all Gleeble testing experiments test pieces measuring 10 × 10 × 55 mm were used. Two copper grips were used to hold the samples, and according to Gleeble handbook (1996-1998), a standard tension setup was used to provide enough contact area (10 mm) between the grips and sample to give the cooling rates required. The experimental set up is shown in Figure 3.5.

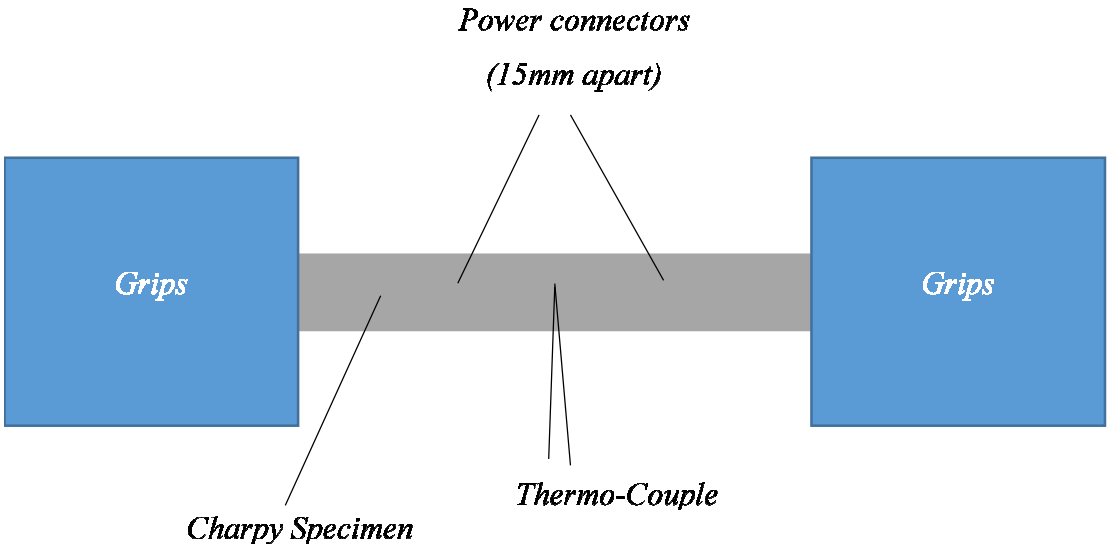


Figure 3.5 Set up for both TCS and PCS Gleeble simulations.

A pair of K-type thermocouples was spot welded close together at the centre line of one side of the specimen, to control/monitor the temperature. Another pair of thermocouples was spot welded on another side of the specimen, each wire is 7.5 mm away from the central line of the specimen, and connected to the power module terminals to measure the voltage between the two points, and therefore the power that the Gleeble 3500 uses to heat the specimen can be calculated and displayed. The distance between the thermocouples that go into the power module needs to be carefully controlled for two reasons: 1. The measured voltage increases as the two connectors separate from each other, and higher measured voltage gives larger calculated power and less noise, therefore for better resolution the two connectors should be as far away from each other as possible; 2. The central part of the specimen has the highest temperature, and the temperature drops significantly towards the sample ends in the copper grips; to make sure the measured part of sample is heated above the austenisation temperature, the two power connectors should be as close as possible. According to the Gleeble handbook

and application notes (2014), the temperature varies less than 5 °C in the central part of sample (within 10 mm from where thermocouples are welded) and drops significantly near the grips. Before the strip steel tests samples with the same size and similar composition with the test pieces were used for dummy testing to double check the optimum separation between the power connection thermocouples.

The testing process for the 0.8 wt% C rail steel was to use a continuous cooling schedule after austenitisation; initially the temperature was programmed to rise 10 °C/s to 900 °C from room temperature, then held at 900 °C for 5 min to make sure the sample was fully austenised, following by continuous cooling from 900 °C to room temperature at different cooling rates (1 °C/s, 5 °C/s and 10 °C/s), as shown in Figure 3.6 The power change against test temperature was recorded, analysed and compared with the literature CCT data (Abbaschian et al., 2009).

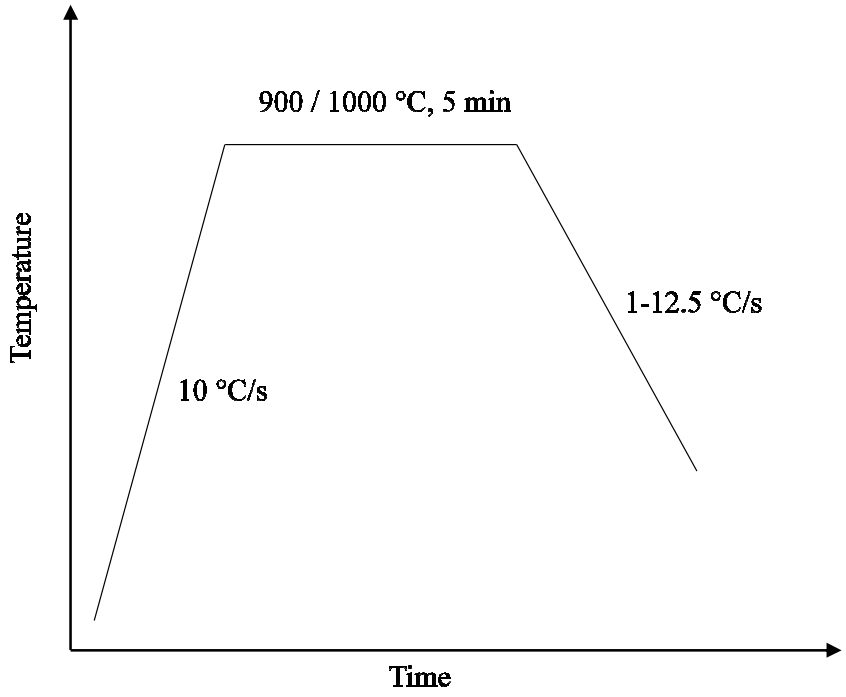


Figure 3.6 Gleeble simulation schedule for TCS initial testing. The peak temperature was 900 °C and 1000 °C for initial testing (on the rail steel) and strip steels, respectively.

Results of the Gleeble simulation on 0.8 C wt% rail steel samples are given in Figure 3.7, which shows the power that Gleeble machine put into the sample during the cooling process, to maintain the required cooling profile, plotted against the temperature of the specimen. In total three different cooling rates were used, 1 °C/s, 5 °C/s and 10 °C/s (two repeat tests for 1 °C/s and 5 °C/s and three repeat tests were carried out for 10 °C/s cooling rate). In Figure 3.7 the change in the gradient of the power-temperature curves show when phase transformation from austenite to pearlite occurs (confirmed via optical microscopy after the tests). According to the Gleeble hand book (1996-1998), the power that the Gleeble machine puts into the sample for linear heat up/cool down schedules should be proportional to the temperature of the specimen, however, if phase transformation happens, heat will be absorbed or released from the specimen, which

will result in a change in the power (either increase or decrease) that the Gleeble puts into the sample to keep up with the pre-set temperature schedule. In this case, when the temperature reached the austenite-pearlite transformation point, due to the heat release from the sample and registered by the thermocouple feedback, the Gleeble machine reduced the current flow through the specimen, therefore the power input to the specimen dropped gradually. As the transformation process completes (or the rate reduces to a very low level) the latent heat released reduces and the Gleeble machine increases power to the specimen to maintain the temperature to the pre-set value, resulting in the presence of the trough in the power-temperature curve. Therefore, the start of the power drop and the finish of power increase are the transformation start and finish points, respectively. To determine the phase transformation starting points, for each curve, the data points between 800 °C and 700 °C were used to give an extended trend line for the power values that Gleeble machine would put to the sample if no phase transformation happens during cooling; then comparing the data points (power values) of experimental results and the ones given by the extended trend line, when the difference between the two becomes consistently larger than 5W in a 10 °C temperature range (therefore avoiding the normal power floating of the machine during a thermal cycle, according to Gleeble hand book (1996-1998)), the phase transformation starting temperature and time can then be defined. The same data generating process also applied on T1 to T4 steel samples. It can be seen from Table 3.3 that the difference of phase transformation starting temperatures given by at least two repeat tests for all samples was less than 3 °C, therefore the repeatability of such test is quite good when taking a maximum error of ±3 °C into consideration.

However, as can be seen from Figure 3.7, when the cooling rate reached 10 °C/s, the power input to the sample from the Gleeble machine becomes 0 approximately between 580 °C and 525 °C, resulting in an incomplete trough in the power-temperature curve. This is because when the required cooling rate is high enough, due to the large heat release during phase transformation no input power to the specimen is needed from the machine to maintain the required cooling rate and temperature in that temperature range, and the phase transformation start and finish points could be missed out, which is a drawback of using this technique for high cooling rates (generally higher than 20 °C/s).

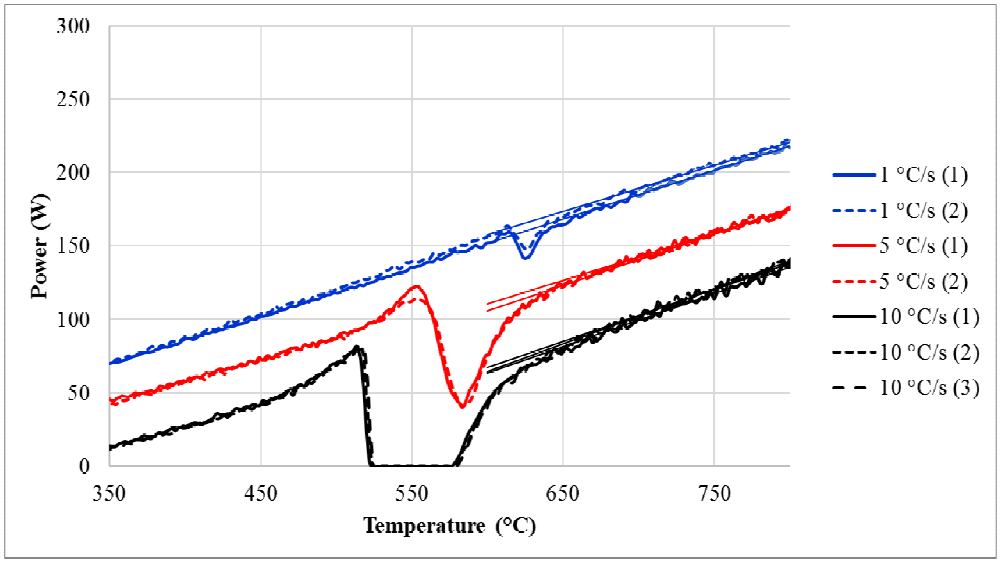


Figure 3.7 Power-temperature curve during cooling of 0.8C rail steel samples at different cooling rates (the trend lines for each curve were also plotted).

Table 3.3 below summarises the austenite-pearlite transformation temperatures and the times from eutectoid temperature (727 °C) to transformation start / finish points of the tested samples, and these phase transformation points are plotted on the same CCT diagram from literature for comparison (Figure 3.8) for comparison. It can be seen that the Gleeble test results matches quite well with the literature CCT diagrams.

Table 3.3 Phase transformation points of the tested 0.8C rail steel.

Cooling rate	Test number	Start temperature	Time to start temperature	Finish temperature	Time to finish temperature
1 °C/s	1	650 °C	83 s	620 °C	110 s
	2	653 °C	84 s	620 °C	110 s
5 °C/s	1	651 °C	15 s	570 °C	33 s
	2	650 °C	16 s	563 °C	32 s
10 °C/s	1	640 °C	9 s	520 °C	21 s
	2	642 °C	9 s	520 °C	21 s
	3	640 °C	9 s	520 °C	21 s

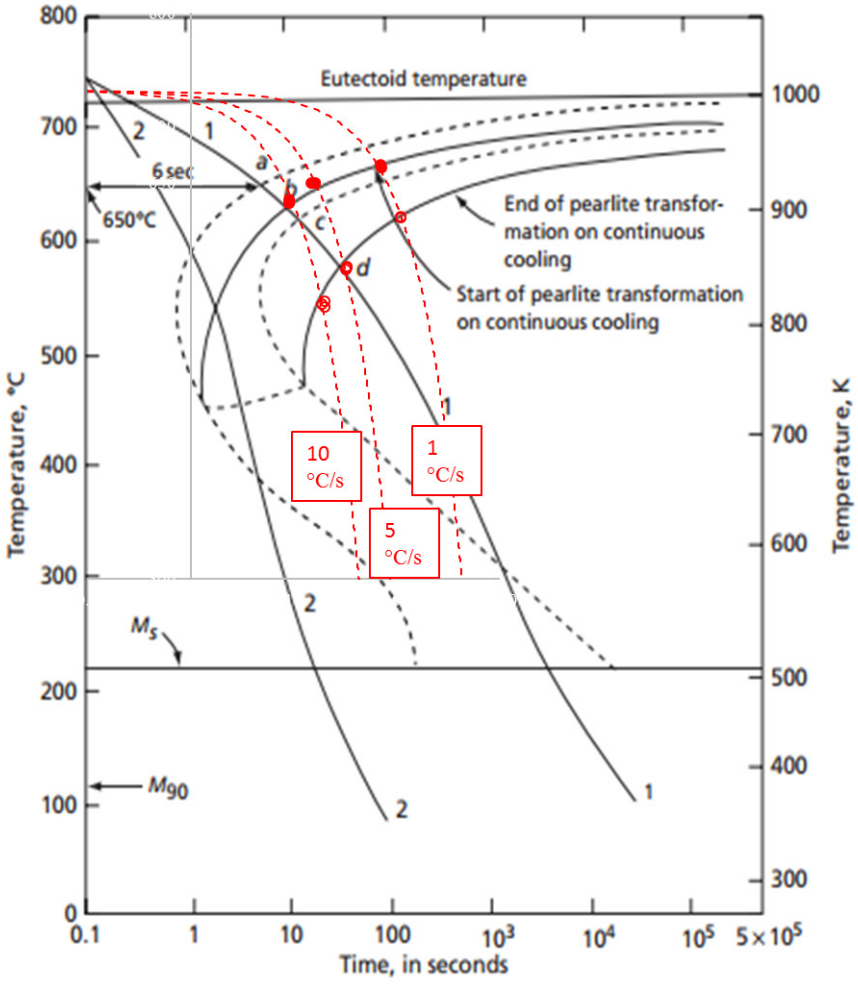


Figure 3.8 Comparison of the Gleeble results and the literature CCT diagram of a 0.8C rail steel (Gleeble results are shown as red crosses on the graph).

After the initial testing to confirm the potential for investigating phase transformation behaviour using the Gleeble 3500 thermo-mechanical simulator, tests on the strip steel samples used in this project were carried out. The same set up (i.e. TCS program, tension mode) was applied using the strip steel specimens (also 10 × 10 × 55 mm specimens). However, due to the chemical composition differences, the simulation schedules were slightly modified for the HSLA steel, to make sure the samples were fully austenized before cooling. The peak and holding temperature was raised to 1000 °C, and cooling rates from 2.5 °C/s to 12.5 °C/s were applied, as previously shown in Figure 3.6.

3.6.2 Limitations of the technique

As the Gleeble 3500 thermo-mechanical simulator controls the temperature of the specimen through applying current/voltage at the end of the sample, the cooling rate that the Gleeble 3500 can achieve without additional cooling methods (such as water quench or air quench) was found to be 15 °C/s maximum (air cool in the specimen chamber). Besides, due to the heat release during the γ-α phase transformation, the Gleeble 3500 machine sometimes has to turn the heating power off to achieve the required cooling rate, which will result in no power input in the phase transformation temperature range, and therefore the phase transformation could not be distinguished, as stated in the last section. For the tests completed cooling rates above about 20 °C/s meant the finish point of phase transformation could not be identified from the temperature-power curve.

CHAPTER 4

MICROSTRUCTURE CHARACTERISATION

4.1 Introduction

This chapter describes the investigation of microstructure and phase balance for the current production trials. The three trials (composition and rolling parameters provided in Chapter 3) consisting of nine strip steel samples in total have been investigated. Section 4.2 describes the typical bainitic microstructures of the materials. Section 4.3 provides details about the method used for phase quantification and an analysis of the results obtained. The results for phase quantification are shown in Section 4.4, and the relationship between coiling temperature and phase balance is investigated and discussed.

4.2 Forms of bainite in the high strength strip steels

Through optical and SEM image analysis, all strip materials were found to have fully bainitic microstructures, which consisted of a number of different types of bainite. As reviewed in Chapter 2, the mechanical properties of bainitic microstructures vary with the bainite structure (lath, carbide and packet sizes), therefore identification and quantification of each type/form of bainite is necessary. This section includes representative optical and SEM images from each steel, as well as higher magnification SEM images used to distinguish the different types of bainite (such as upper, lower and granular bainite) found in the steels.

Figure 4.1 shows through thickness optical images from the longitudinal section of all strip steels; the images clearly show the deformed prior austenite grains, carbides, and bainitic microstructure of the investigated materials. According to initial optical imaging, the microstructure is distributed quite homogenously across the sample, i.e. no bands of upper bainite, granular baintie or lower bainite was observed, which is indicating no significant chemical inhomogeneity from micro segregation.

Due to the hot rolling processes applied to the materials (especially several finishing rolling passes below the austenite recrystallisation temperature), the prior austenite grains are deformed, i.e. in pancaked shapes. The non-recrystallization temperature, T_{NR}, can be defined as "the temperature below which static recrystallization can no longer go to completion in the interpass interval or during cooling" (Vervynckt et al., 2012), therefore any amount of strain induced below T_{NR} will result in elongated austenite grains and possibly deformation bands. To estimate T_{NR}, Boratto et al. (1988) gave an equation which links the T_{NR} with alloying level, as shown below:

$$T_{NR} = 887 + 464C + [6445Nb - 644(Nb)^{1/2}] + [732V - 230(V)^{1/2}] + 890Ti + 363Al - 357Si \quad (6)$$

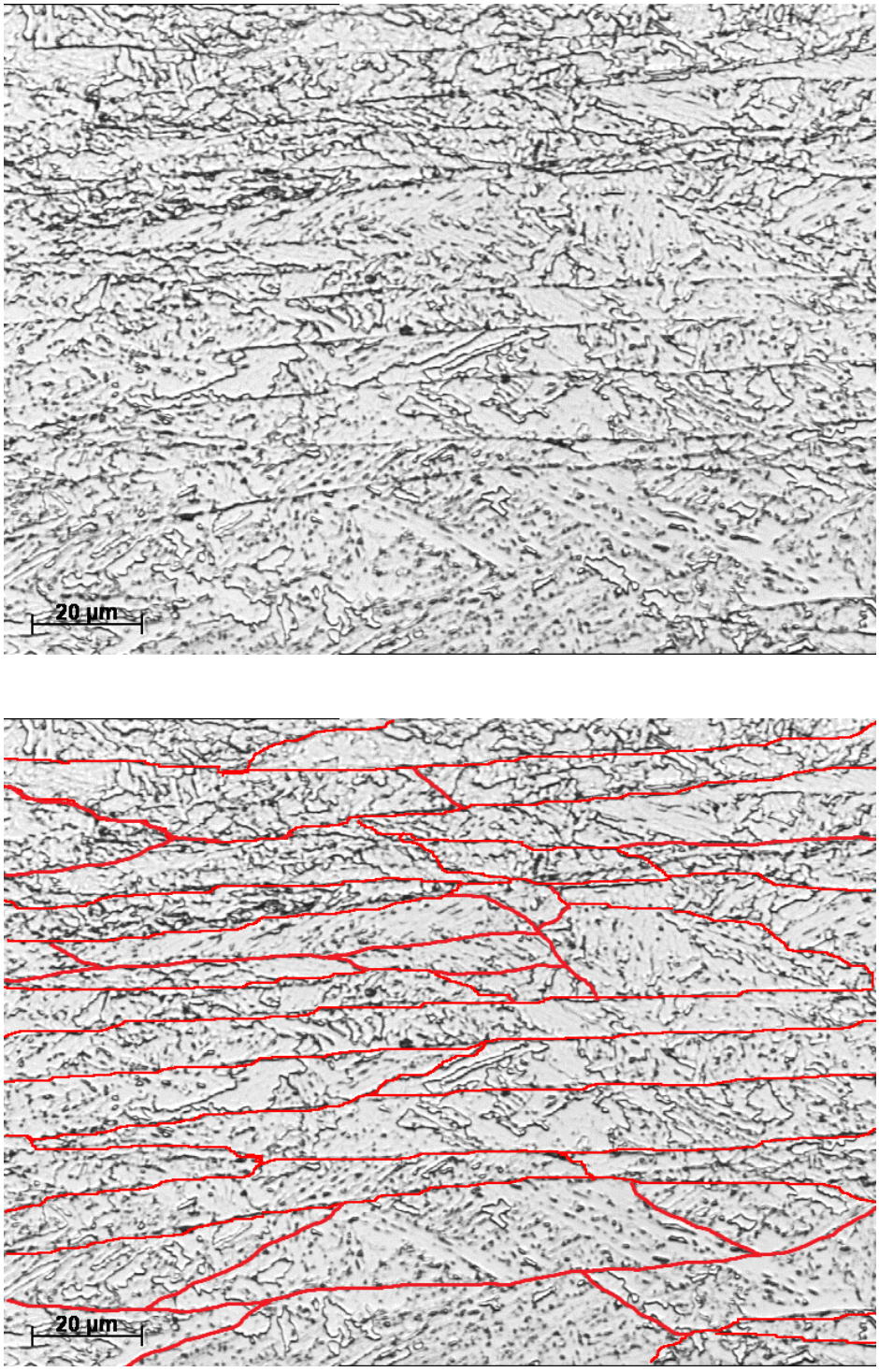
According to equation (6), the calculated T_{NR} of the three trials are 1032 °C for T1, 1023 °C for T2 and 999 °C for T3. Comparing the rolling data of the three trials (Figure 3.1), it can be seen that according to the T_{NR} estimation, there are 6 rolling passes for T1 products below T_{NR}, 7 for T2, and 6 for T3, therefore the corresponding strain below T_{NR} for these trials are 0.571 for T1, 0.662 for T2 and 0.579 for T3, suggesting T2 will have the most pancaked structure among the three, while prior austenite grain shape of T1 and T3 should be similar. In Figure 4.1, it is indicated by both optical and SEM

graphs that T1 steels have more deformed austenite grains than T2 and T3 as under the same magnification the “thickness” of prior austenite grains in T1 steels seems smaller than both T2 and T3 steels, while prior austenite grains of T3 seems the least deformed among the three. This could be because that T1 has a different rough rolling history than T2 and T3. As mentioned in Section 3.2, T1 steels experienced larger strain in the first rough rolling pass than T2 and T3 steels, which may result in a smaller austenite grain size after recrystallisation for the following finishing rolling passes (Abad et al., 2001, Xiao, 2013, Rehman, 2014). The austenite grains in T1 steels are thinner in the normal direction than those in T2 and T3 steels for a similar strain during the subsequent (non-recrystallisation) rolling passes, due to the smaller expected initial austenite grains in T1 steels compared to T2 or T3 steels. Thicknesses of the grains were measured at normal direction using a series of optical microstructure images. According to ASTM E112-13 Lineal Intercept Procedure, 20 images randomly taken at quarter thickness of each specimen were used, resulting in at least 200 intercepts. The results are showing in Table 4.1, along with 95 % confidence intervals. The difference in the deformed austenite grain shape between T2 and T3 is consistent with the TNR predictions, as T2 and T3 steels have similar rough rolling history (and hence expected austenite grain size), and T3 steels has smaller strain below the non-recrystallisation temperature than T2 steels, therefore less deformed austenite grains in T3 than T2 steels.

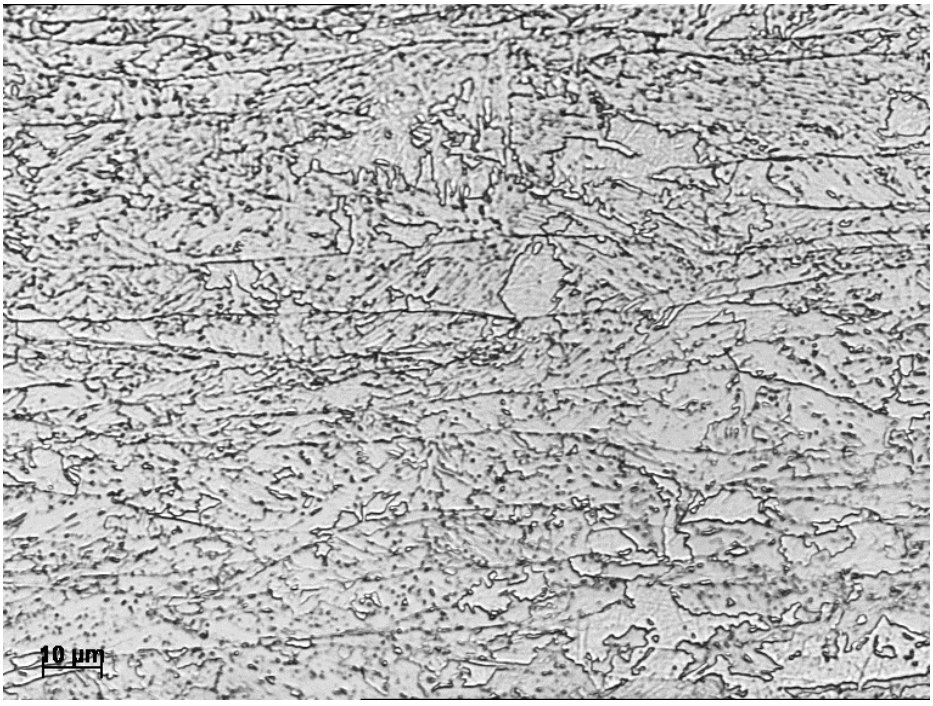
Table 4.1 Measured thicknesses (at normal direction) with 95% confidence interval of the prior austenite grains of Steel T1 – T3

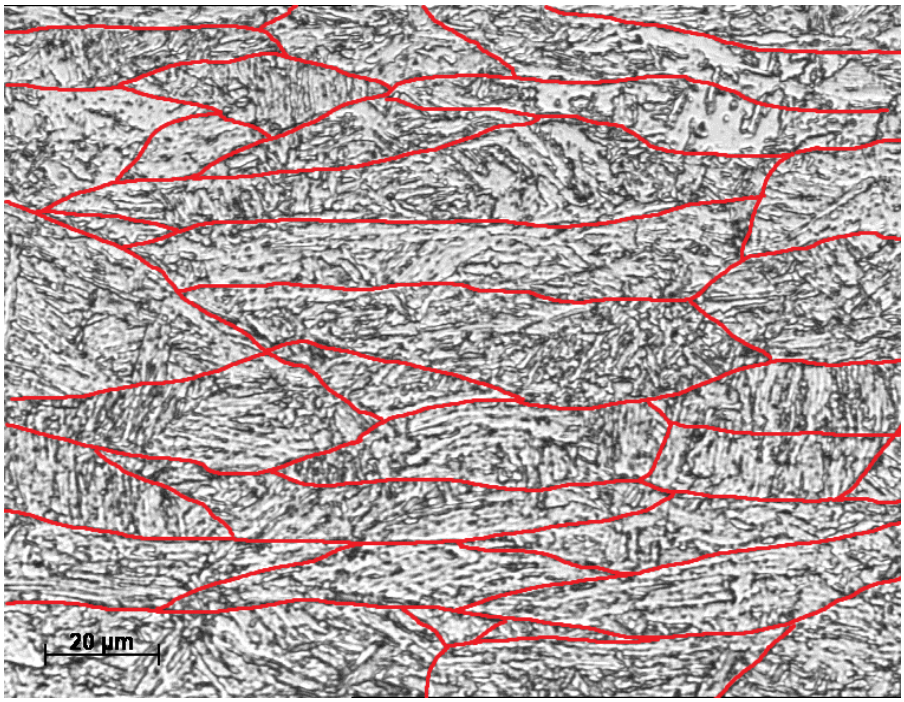
Trial	*Trial 1*				*Trial 2*			*Trial 3*	
Sample ID	*T1-1*	*T1-2*	*T1-3*	*T1-4*	*T2-1*	*T2-2*	*T2-3*	*T3-1*	*T3-2*
Austenite grain thickness / μm	*13 ± 2*	*12 ± 2*	*16 ± 3*	*15 ± 2*	*20 ± 3*	*22 ± 3*	*21 ± 2*	*22 ± 4*	*21 ± 3*

Nevertheless, as shown in Figure 4.1, the prior austenite grains were heavily deformed and elongated after rolling, and most of the grains extended beyond the size of a single optical image using an objective magnification of 50X (and at lower magnification it was hard to identify the austenite grains clearly in the etched images), therefore it was difficult to measure the grain size and aspect ratio accurately. Although the prior austenite grain size was hard to measure due to its elongated shape, the grain boundaries can still be picked up quite clearly under 500X in the optical images, and bainitic structures that formed as packets, which developed from prior austenite grain boundaries, and grew all the way through these austenite grains can therefore be identified. The blocky microstructures that grew through the prior austenite grains were identified as granular bainite, according to the literature descriptions as reviewed in Chapter 2.

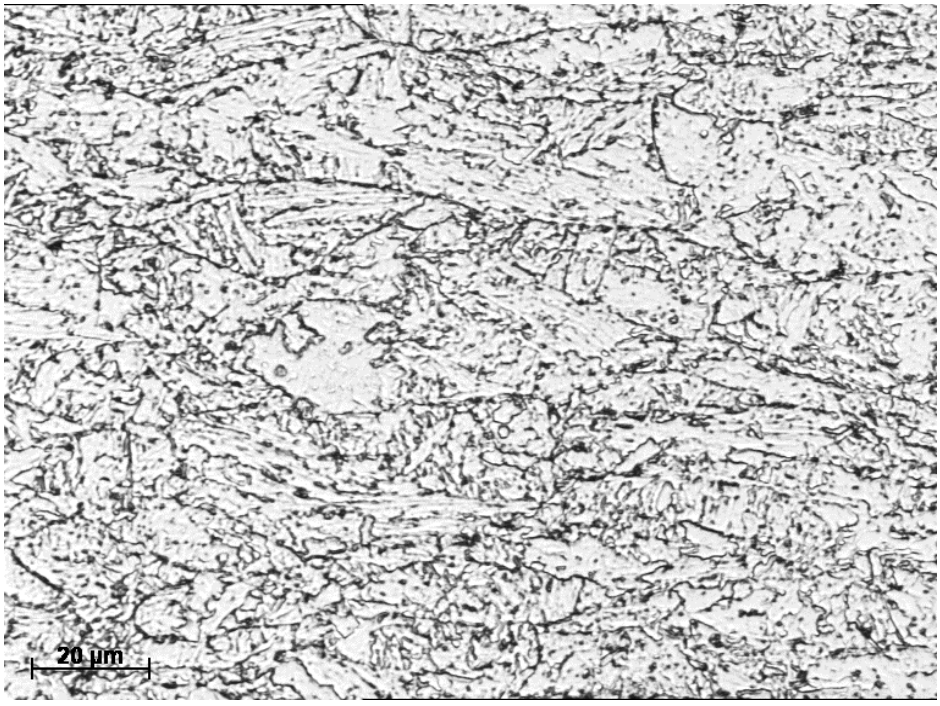


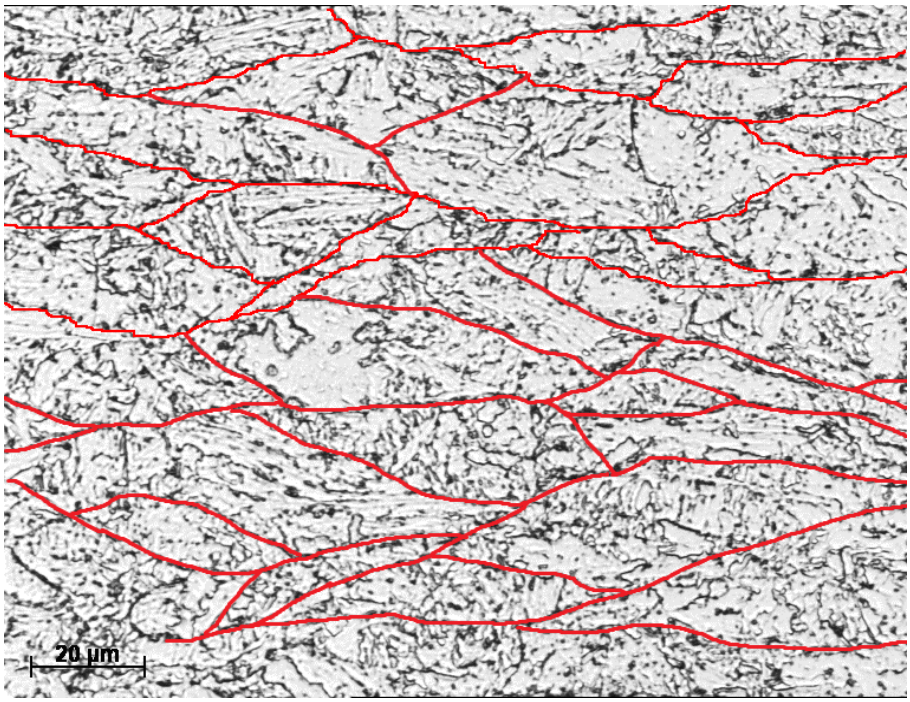
(a) T1-1 (coiling temperature = 453 °C). Top: original optical image; bottom: image with prior austenite grain boundaries marked in red



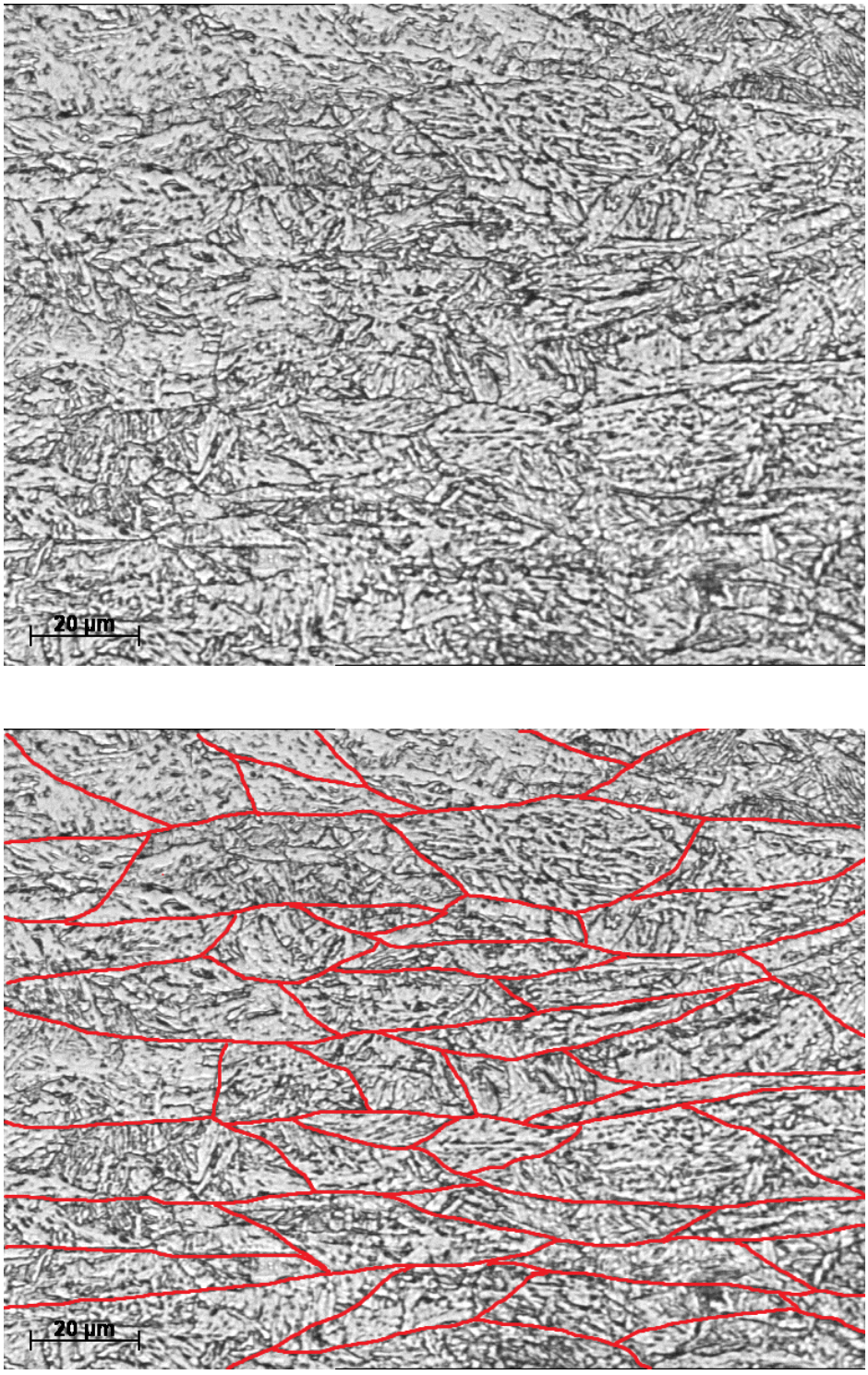


(b) T1-2 (coiling temperature = 411 °C). Top: original optical image; bottom: image with prior austenite grain boundaries marked in red

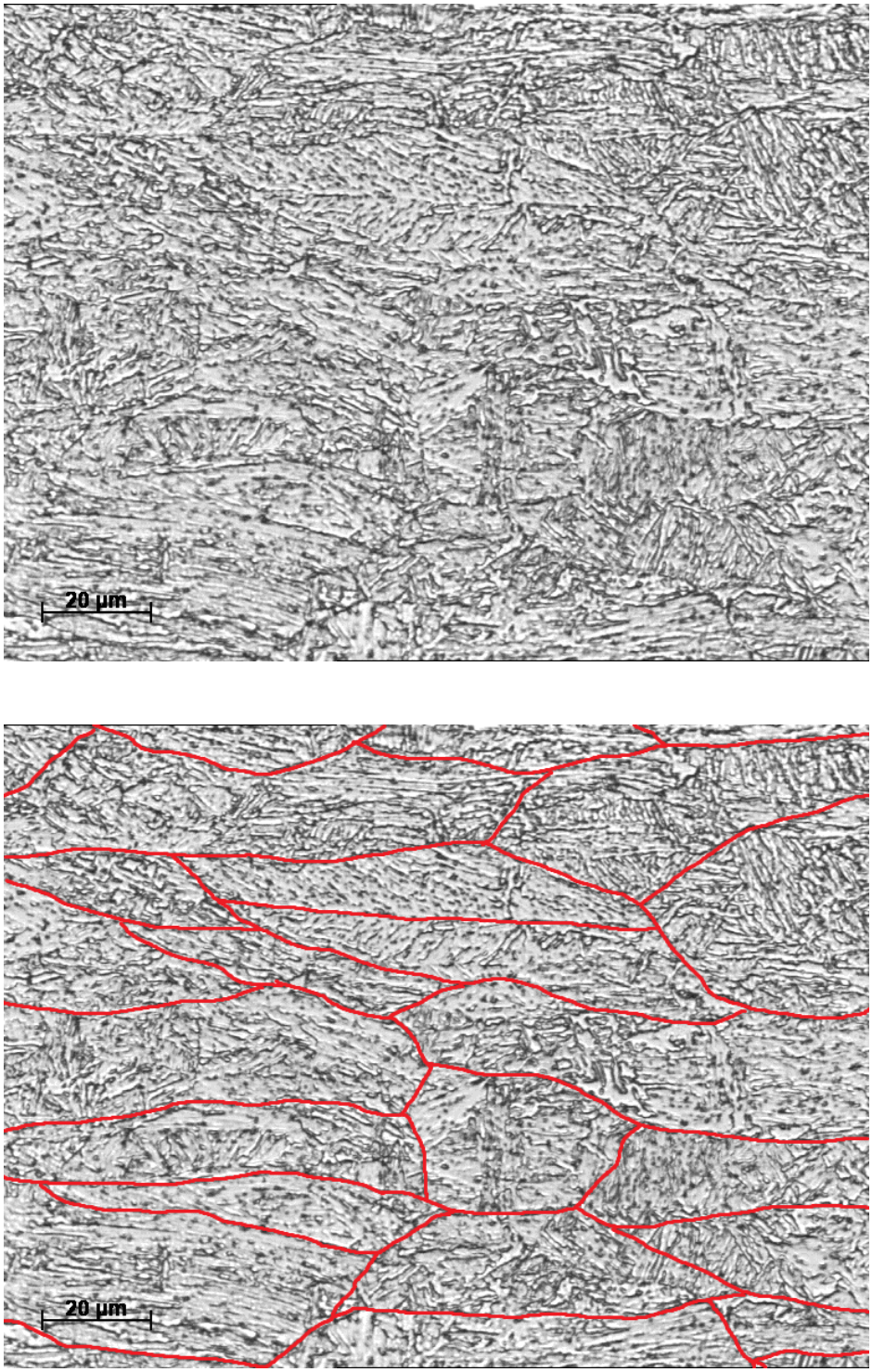




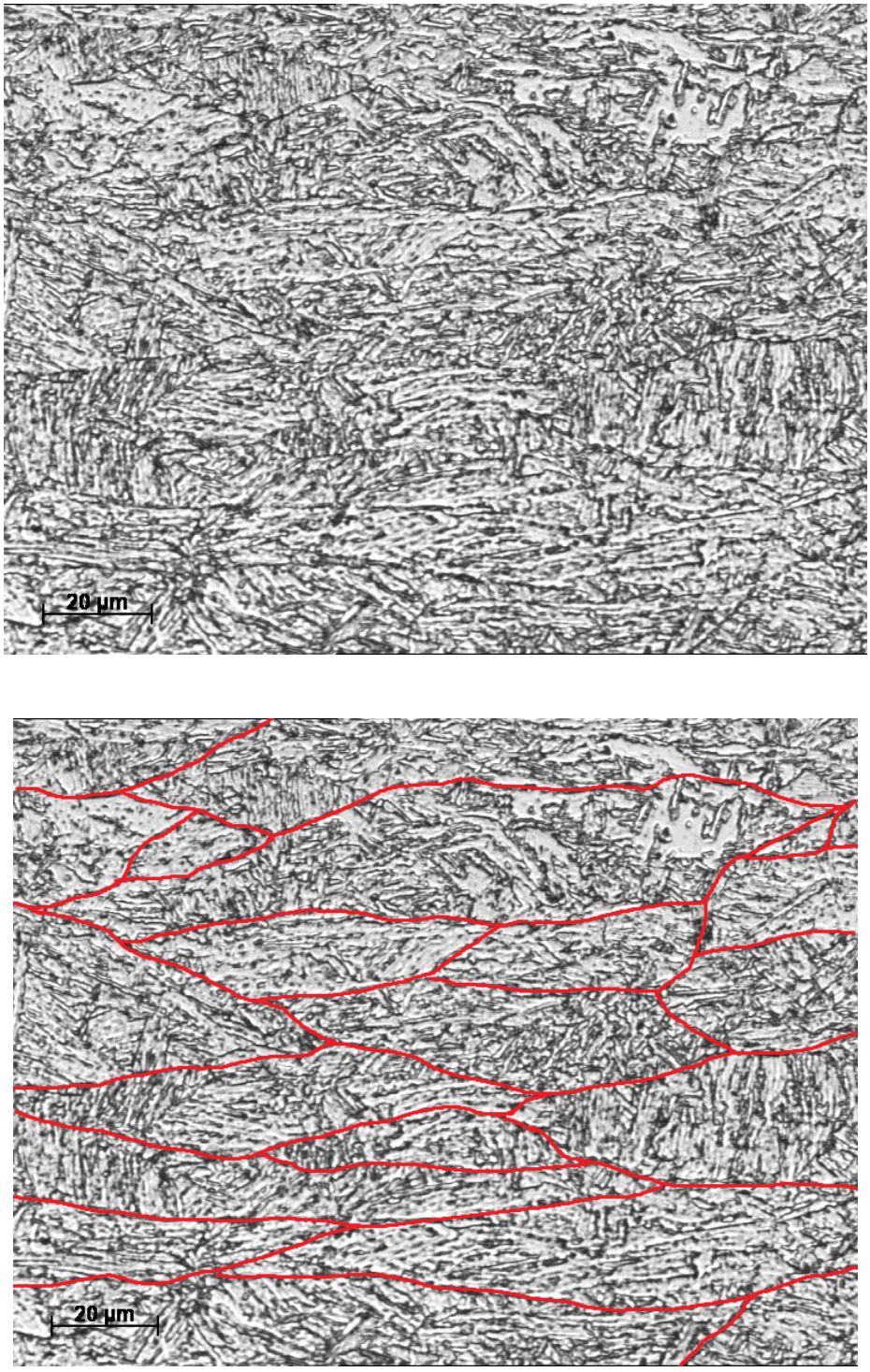
(c) T1-3 (coiling temperature = 393 °C). Top: original optical image; bottom: image with prior austenite grain boundaries marked in red



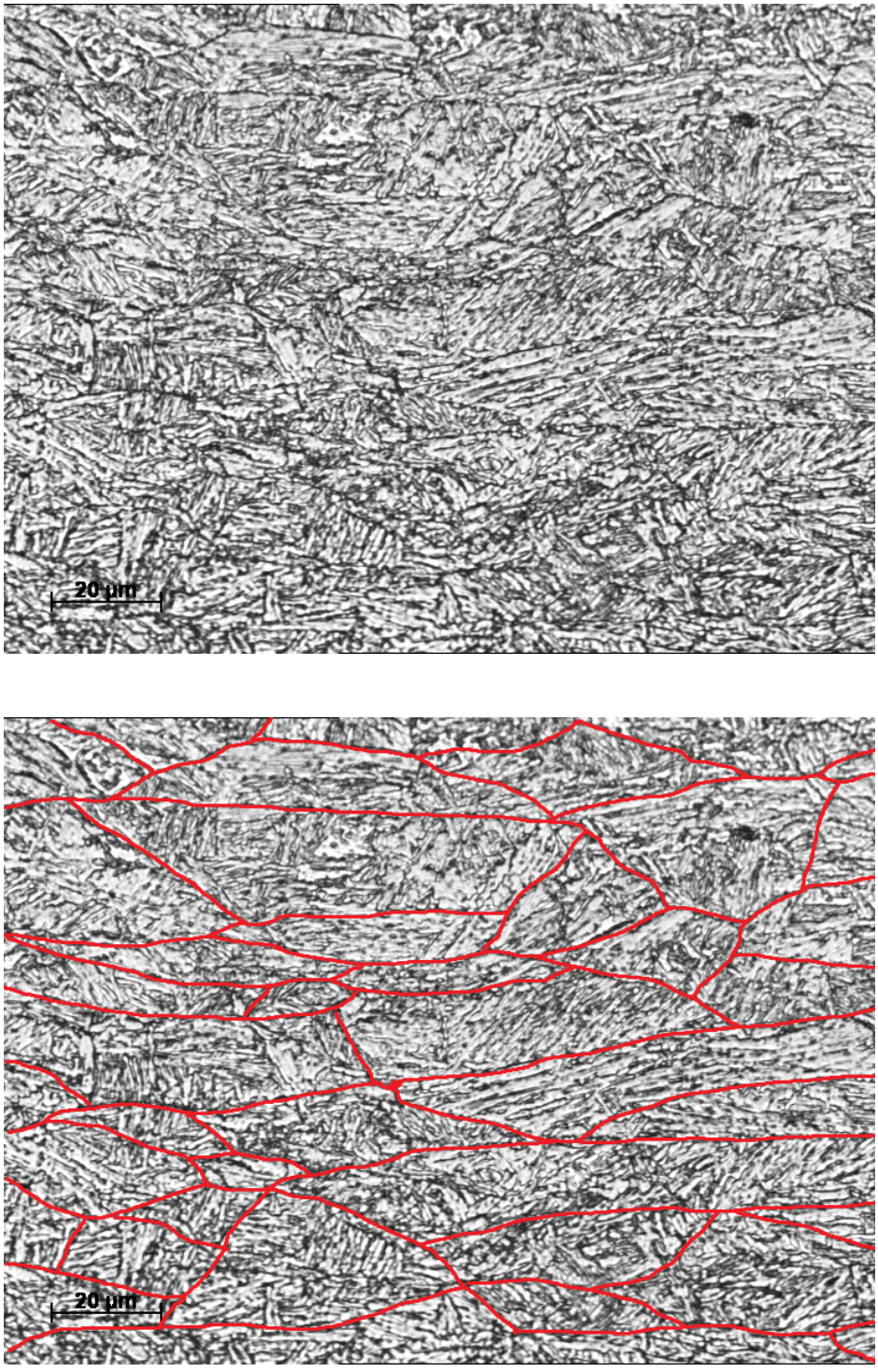
(d) T1-4 (coiling temperature = 290 °C). Top: original optical image; bottom: image with prior austenite grain boundaries marked in red



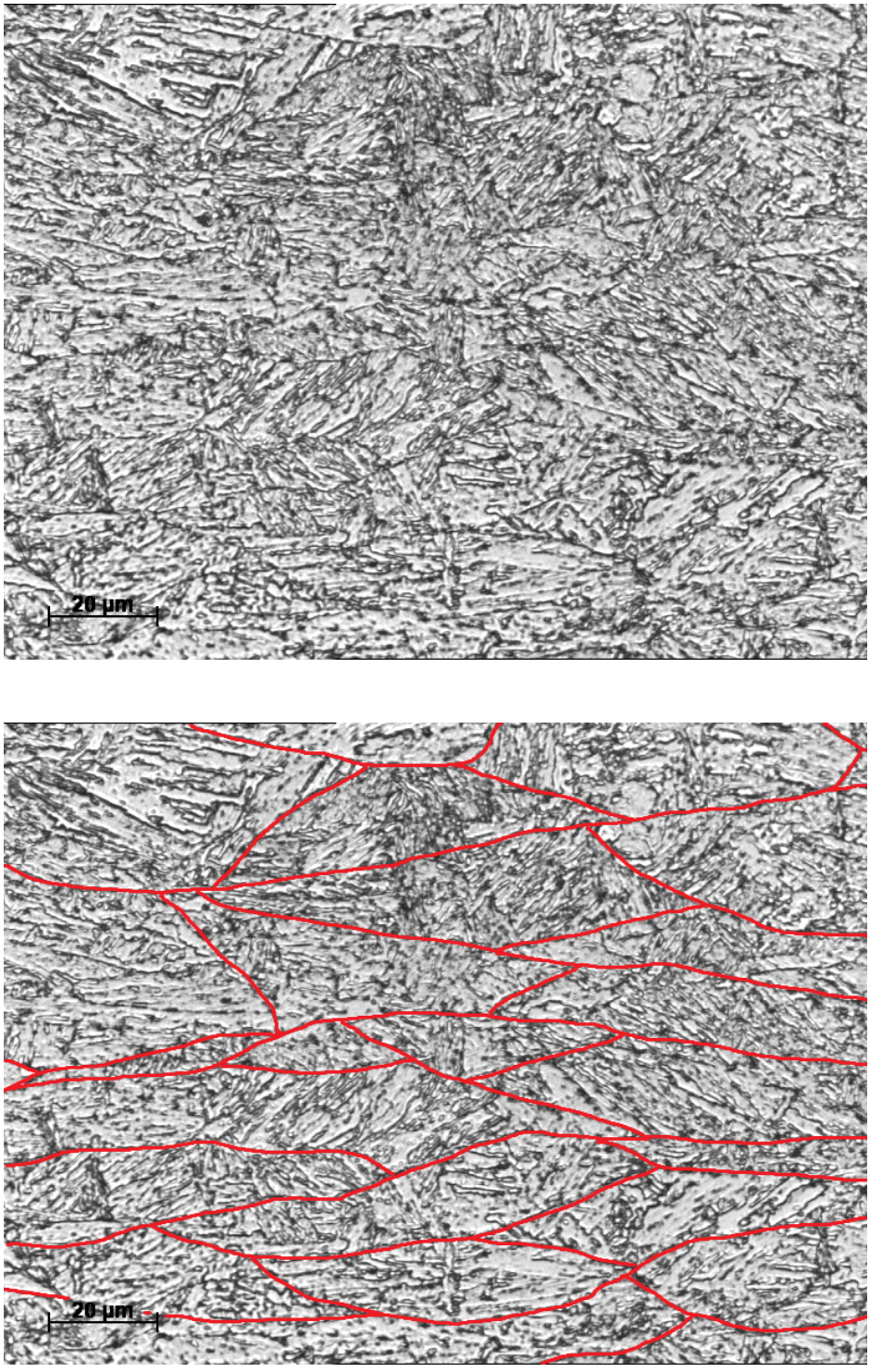
(e) T2-1 (coiling temperature = 347 °C). Top: original optical image; bottom: image with prior austenite grain boundaries marked in red



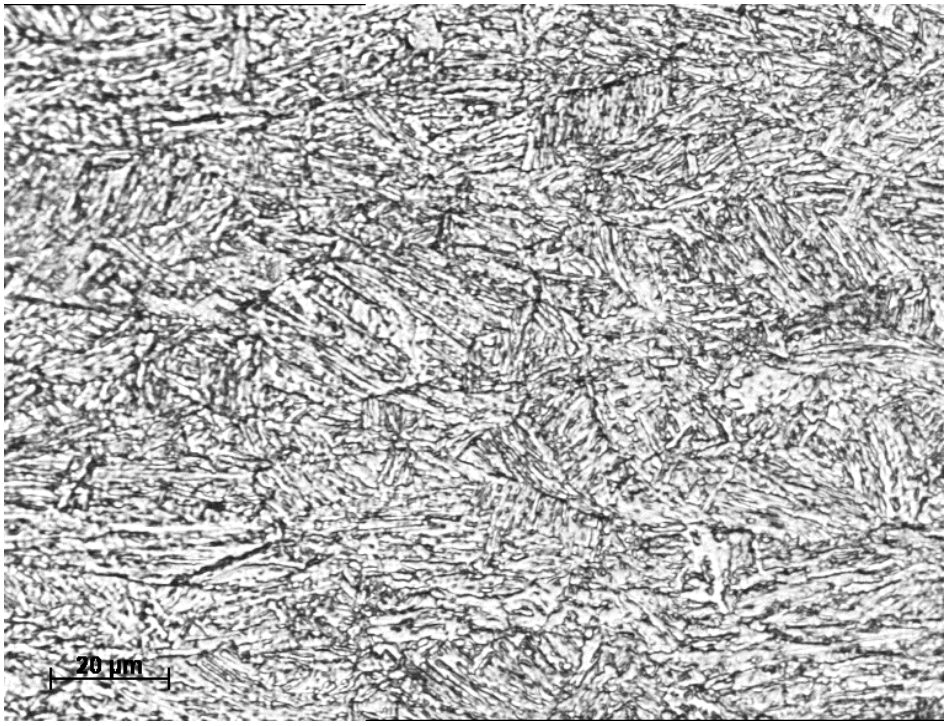
(f) T2-2 (coiling temperature = 314 °C). Top: original optical image; bottom: image with prior austenite grain boundaries marked in red

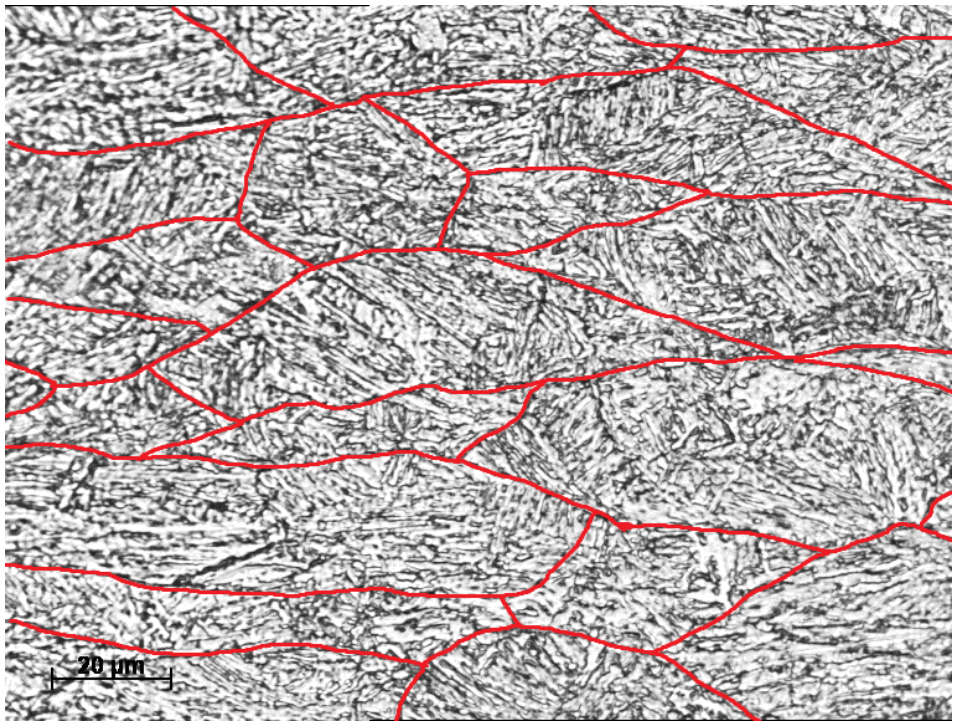


(g) T2-3 (coiling temperature = 253 °C). Top: original optical image; bottom: image with prior austenite grain boundaries marked in red



(h) T3-1 (coiling temperature = 400 °C). Top: original optical image; bottom: image with prior austenite grain boundaries marked in red



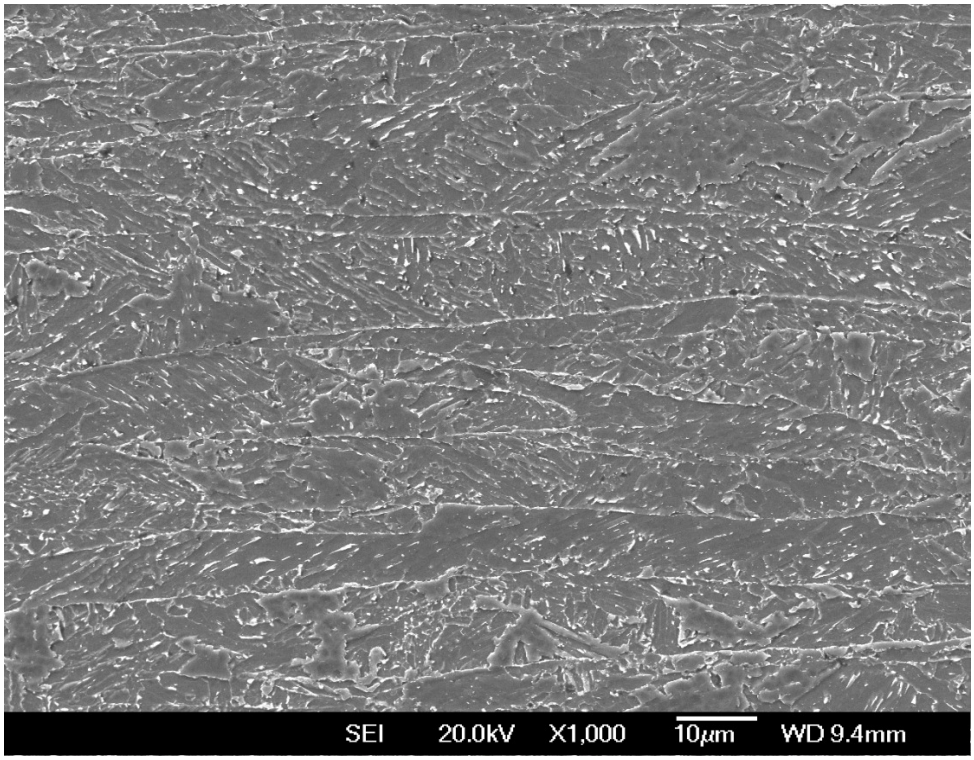


(i) T3-2 (coiling temperature = 390 °C), with prior austenite grain boundaries marked in red

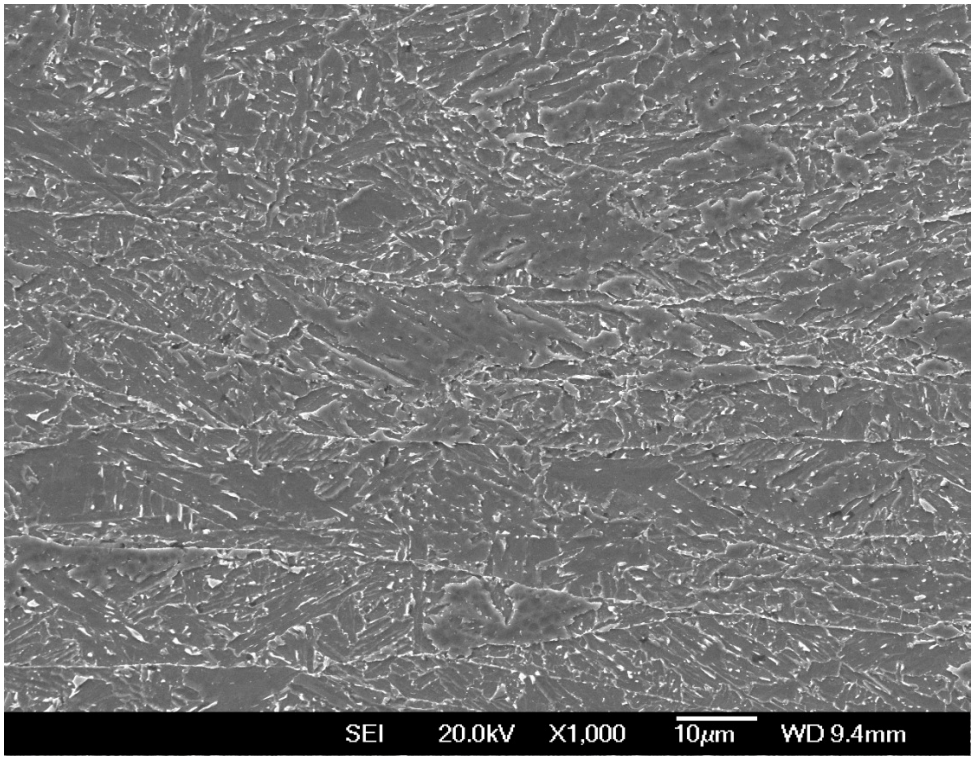
Figure 4.1 Representative optical images of strip steels investigated. All images are taken under the same magnification at rolling direction section.

As reviewed in Chapter 2, according to the structure and distribution of carbides / cementite within the bainitic structure, bainite can be divided into several types, including upper bainite, lower bainite and granular bainite; each of these forms of bainite has different mechanical properties. Therefore, to investigate the effect of different bainitic microstructures on strength, hardness and toughness, it is necessary to make quantitative measurements of the phase balance. However, due to the limited resolution of optical microscopy, the images are not clear enough to carry out quantification for these steels, especially for strips that coiled at relatively low temperatures (normally below 400 °C), as the lower bainite cannot be easily differentiated from upper bainite as both structures can have fine ferritic bainite platelets. Therefore, a JOEL 7000 Scanning Electron Microscope (SEM) fitted with a Field Emission Gun was used to acquire images with higher magnification.

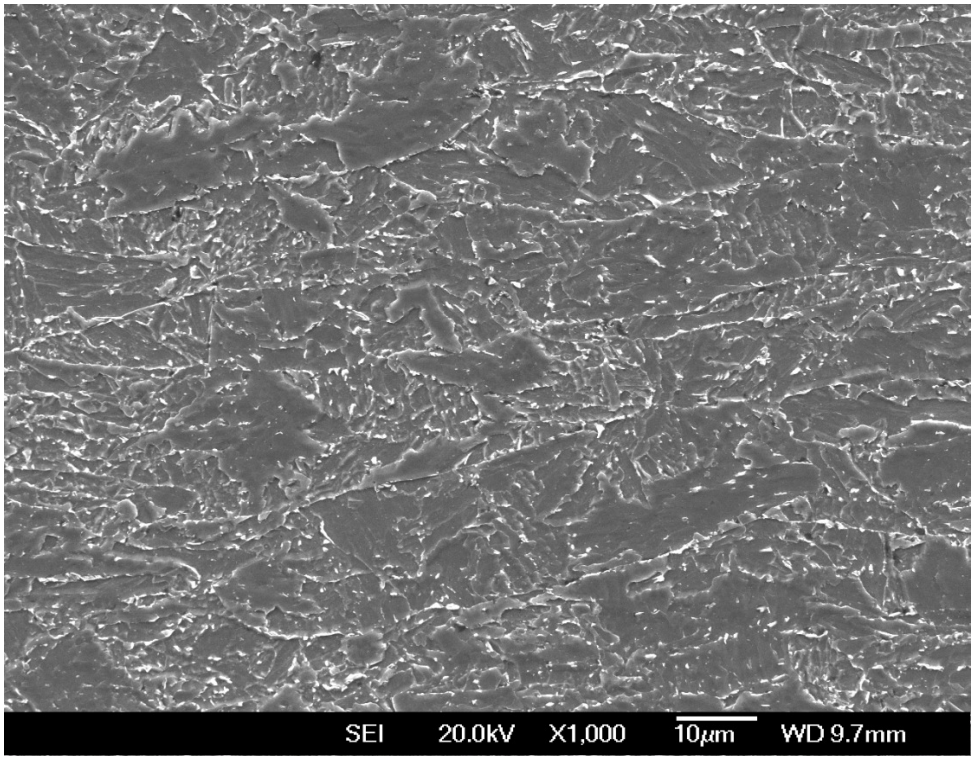
For the T1 series strip steels, as the microstructure were much coarser than for the other trials, about 1000X magnified images were used. For other trials, due to the presence of finer structures such as lower bainite, higher magnified images, about 1200X to 1400X were needed to allow lower bainite to be differentiated from fine upper bainite. Furthermore, higher magnification up to 6000X was used to double-check the finer microstructures. The low magnification (1000X to 1400X) SEM images of the steels are presented in Figure 4.2, bright particles are carbides / cementite, and dark region represents the bainitic ferrite matrix.



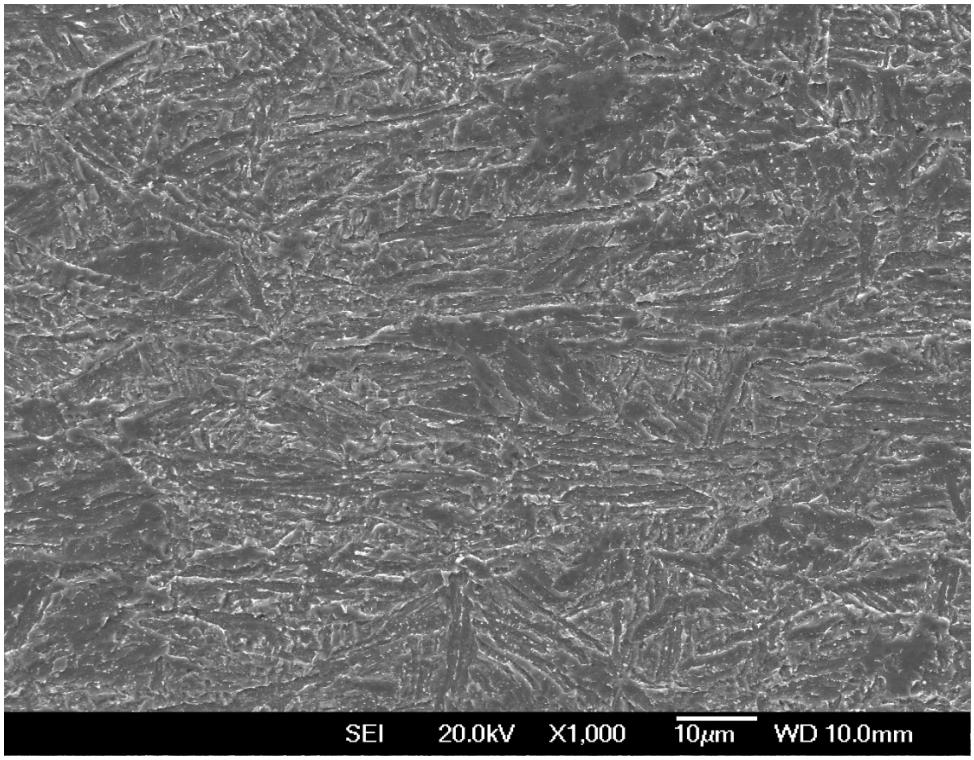
(a) T1-1 (coiling temperature = 453 °C)



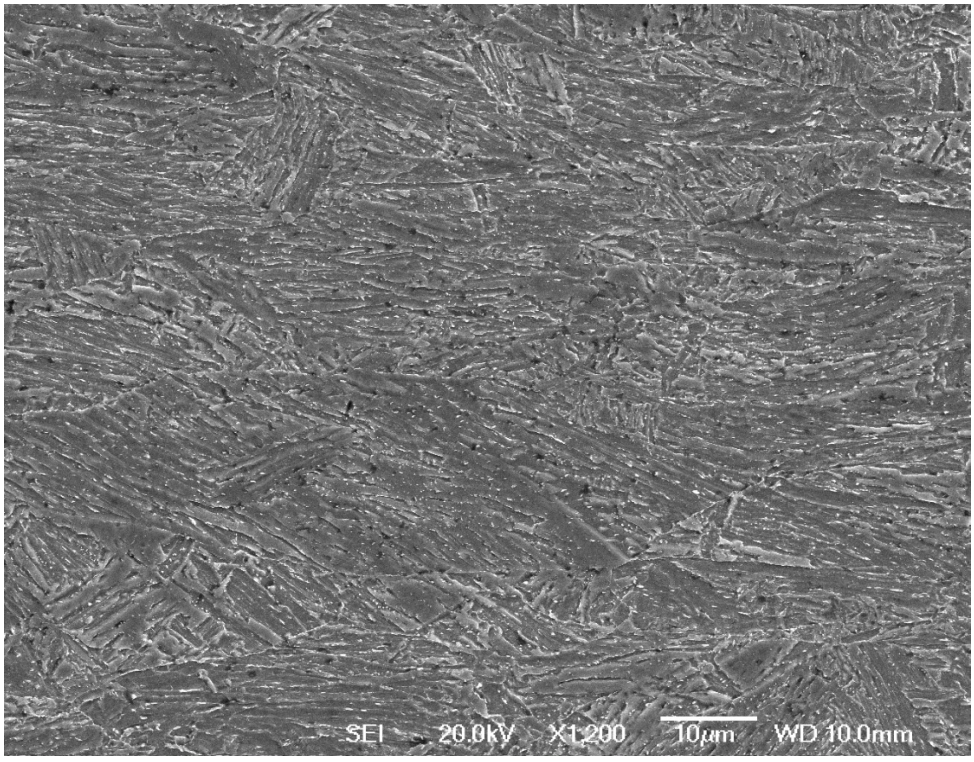
(b) T1-2 (coiling temperature = 411 °C)



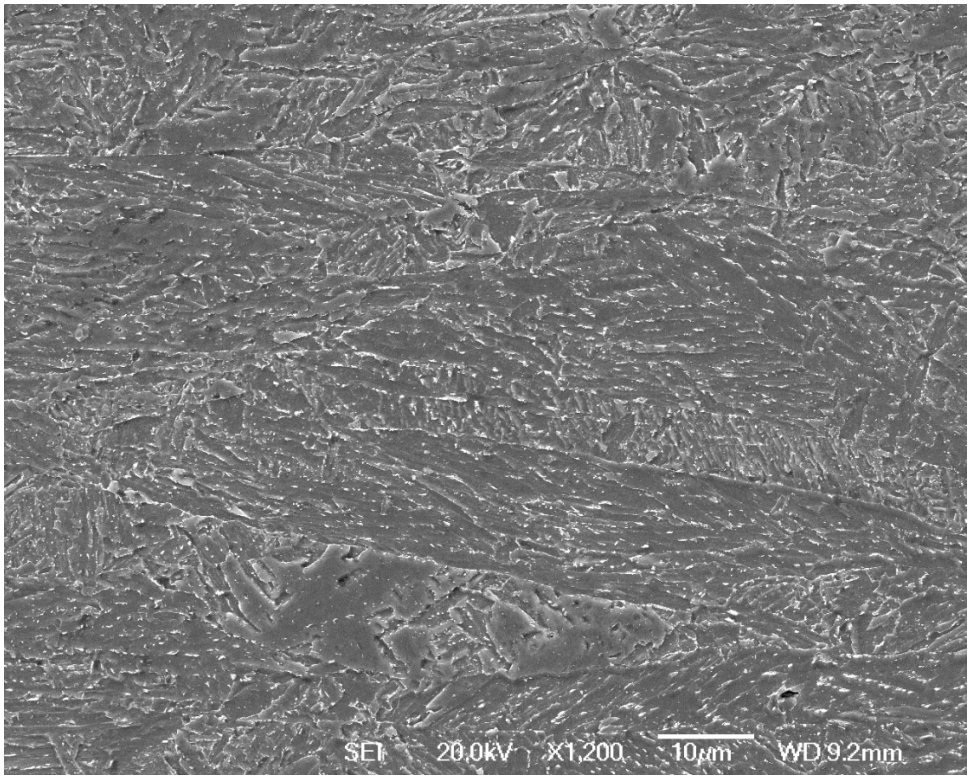
(c) T1-3 (coiling temperature = 393 °C)



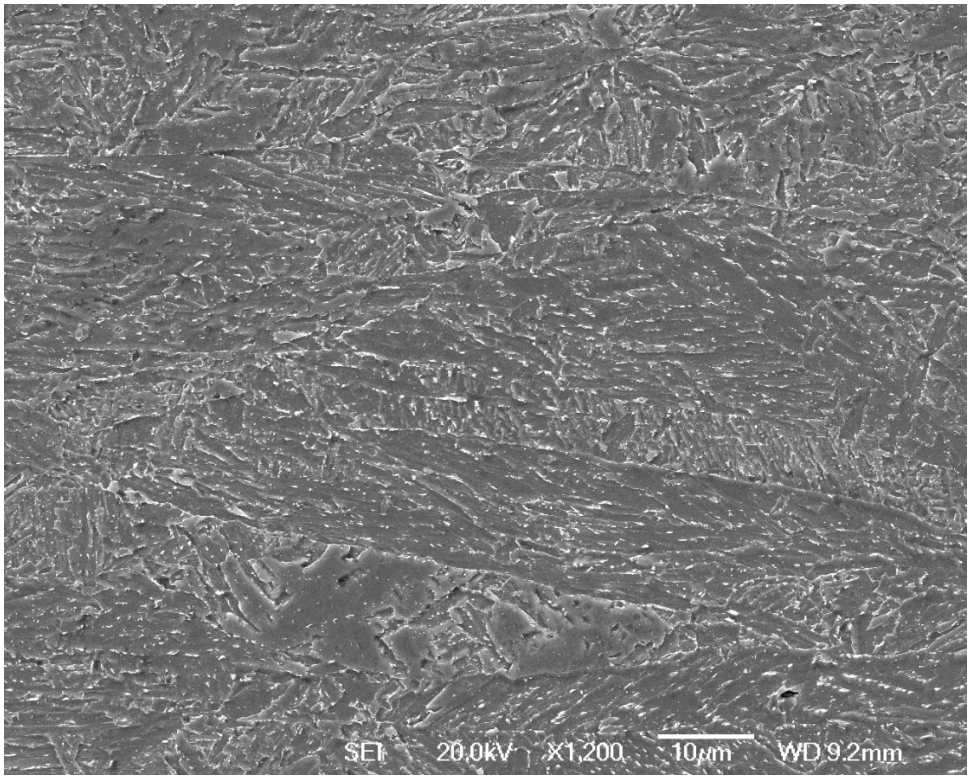
(d) T1-4 (coiling temperature = 290 °C)



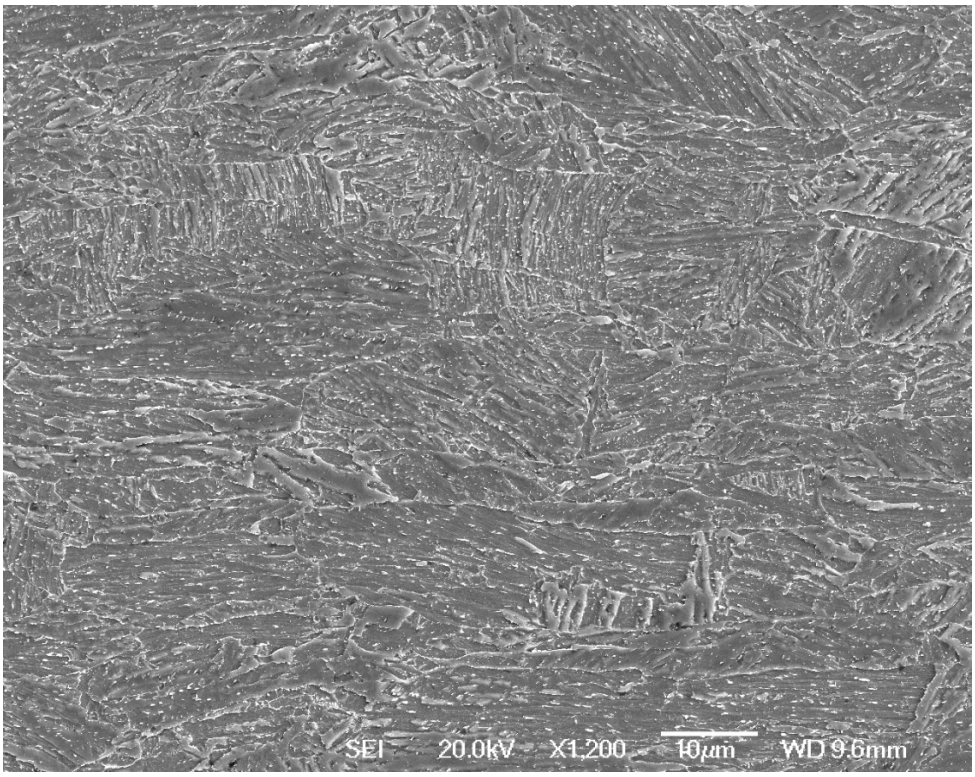
(e) T2-1 (coiling temperature = 347 °C)



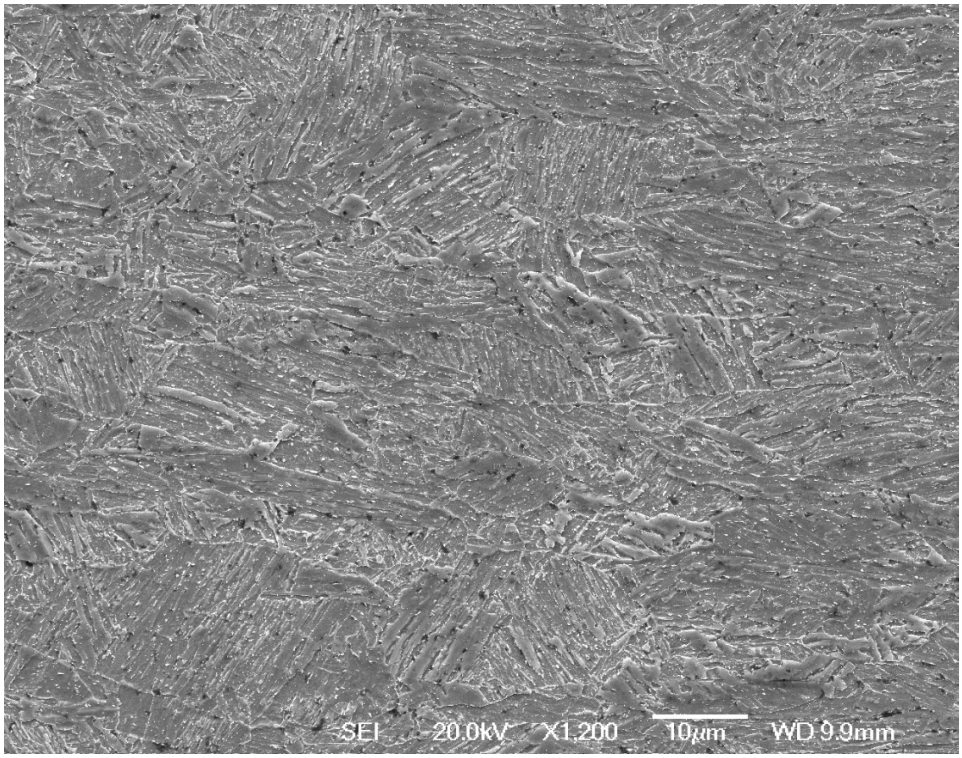
(f) T2-2 (coiling temperature = 314 °C)



(g) T2-3 (coiling temperature = 253 °C)



(h) T3-1 (coiling temperature = 400 °C)



(i) T3-2 (coiling temperature = 390 °C)

Figure 4.2 Typical SEM (secondary electron) images of bainitic microstructures in investigated strip steels.

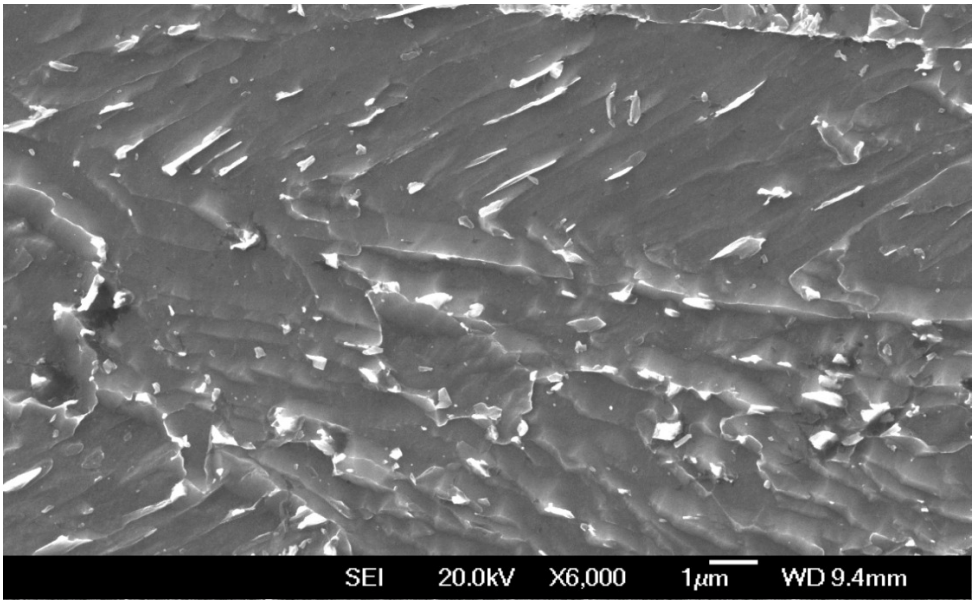
4.3 Phase Quantification

In this section, a method for quantifying the different types of bainitic microstructures (including upper bainite, lower bainite and granular bainite) in low carbon high strength strip steels is summarized. The identification of the various types of bainite is based on the definition and morphology of all kinds of bainitic microstructures; in addition the bainitic carbide size ranges were measured to aid identification. The aim is to describe the way of quantifying bainitic microstructure particularly in this type of low carbon low alloy steels clearly.

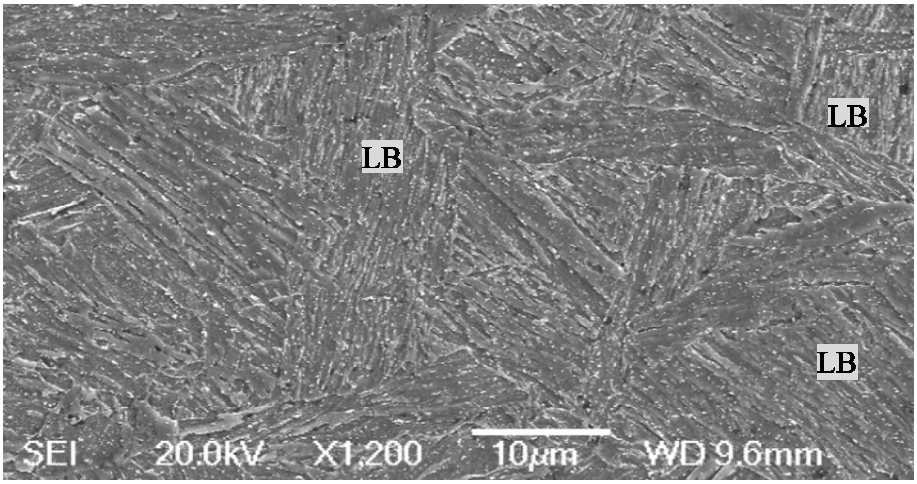
4.3.1 Identifying different bainite phases

The phase quantification method used in this project is based on the morphology of the different types of bainite (including lower bainite, upper bainite and granular bainite).

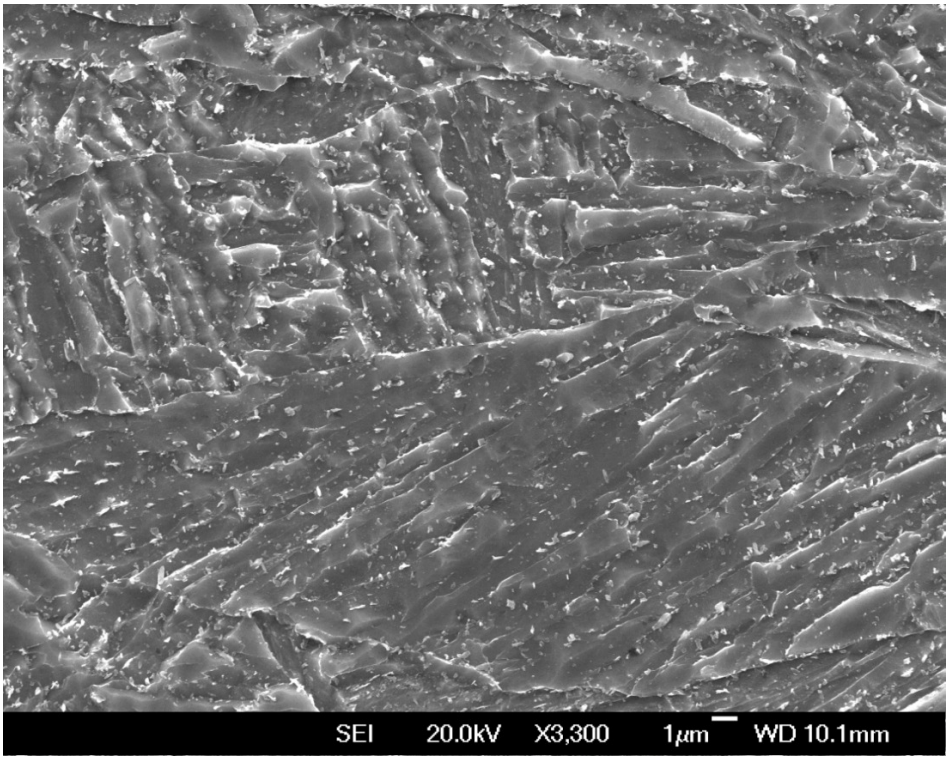
Typical images of the different types of bainite are shown in Figure 4.3:



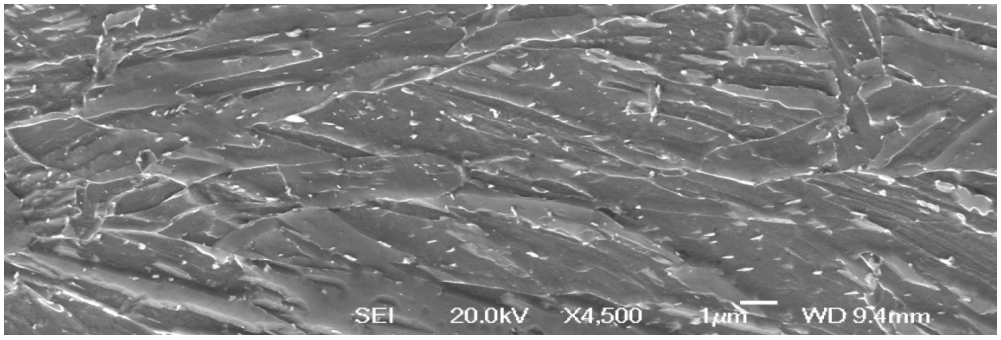
(a) Upper bainite, with interlath carbides, (top of image) found in steel T1-1.



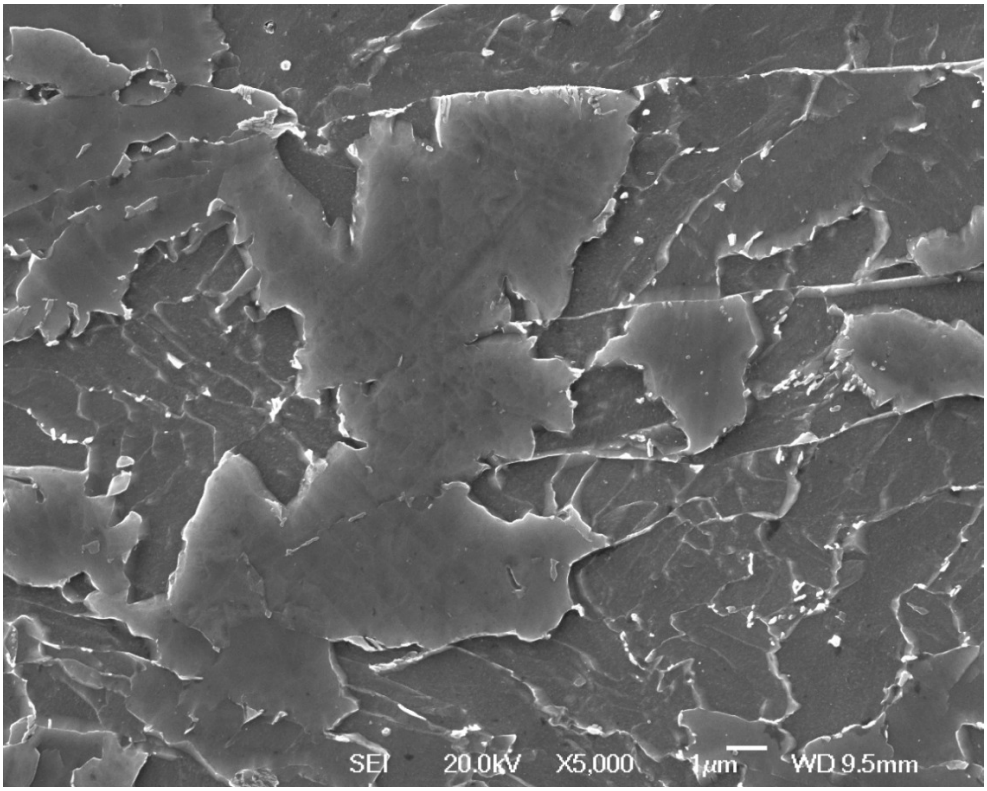
(b) Lower bainite (LB), with intralath carbides, found in steel T1-4.



(c) Higher magnification image of lower bainite found in steel T1-4.



(d) Lower bainite found in steel T4-1.



(e) Granular bainite, blocky morphology growing across the prior austenite grains, with no internal carbides, found in steel T1-2.

Figure 4.3 Typical forms of bainite (upper bainite, UB; lower bainite, LB; and granular bainite, GB) found in the strip materials investigated.

The differences in the microstructural features of upper bainite (UB), lower bainite (LB) and granular bainite (GB) can be used to distinguish between them. General features are described below with specific examples for the strip steels investigated given later. As mentioned in Chapter 2, although in general lower bainite has a finer structure than upper bainite and granular bainite due to it forming at relatively lower temperatures, the main difference between the two is the presence of fine carbides in the bainitic ferrite platelets for lower bainite and the absence of these in upper bainite. Table 4.2 summaries the carbide sizes in the investigated steels, and from the table it can be seen that though there are some overlap between carbide sizes, carbides formed in lower bainite (both intra- and inter-laths) are finer than those in upper bainite.

Table 4.2. The range of carbide sizes measured in the upper and lower bainite regions observed for the strip steels investigated.

Carbide size / µm	UB inter-lath	LB inter-lath	LB intra-lath
Minimum value	0.036	0.028	0.013
Maximum value	0.304	0.187	0.125
Average value	0.131 ± 0.060	0.087 ± 0.036	0.035 ± 0.019

(a) Upper bainite

The typical morphology of upper bainite is that of bainitic ferrite laths with carbides (or retained austenite) present between them. As the formation temperature of upper bainite is higher than that of lower bainite, the carbon has a higher diffusion rate and is able to diffuse further to form carbides, which is why there are no carbides within the bainite laths. In addition the bainite lath size, as well as carbide size, in upper bainite will typically be coarser compared with lower bainite (carbide size ranges shown in Table 4.2 for the strip steels investigated). However, the size of the carbides will show significant variation depending on the steel composition and the transformation temperature.

(b) Lower bainite

As lower bainite tends to form at lower temperatures than upper bainite, the carbon diffusion rate is lower leading to incomplete removal of carbon from the ferrite laths. Therefore, carbides will form within the bainite laths and any carbides present between the bainite laths will be finer than in upper bainite (however, it should be noted that there is no step change in carbide size between lower bainite and upper bainite due to the range of temperatures over which the phases form, therefore there is an overlap in carbide size between lower bainite and upper bainite, as shown in Table 4.2). It is

expected that intra-lath carbides are only seen for lower bainite and that the carbide number density in lower bainite is much higher than in upper bainite.

(c) Granular bainite

Granular bainite forms during continuous cooling, and has a similar growth behaviour to upper bainite, i.e. granular bainite also consists of parallel bainite laths and tends to grow through the austenite grain from one prior austenite grain boundary to the opposite one (this is unlike pro-eutectoid ferrite which will tend to grow along the prior austenite grain boundary resulting in a different morphology – no pro-eutectoid ferrite has been observed in these strip steels). However, as the formation of granular bainite takes place at higher temperatures than upper bainite the carbon is more mobile, but the driving force for bainite formation is less. This means that the interfacial energy needs to be minimised so that a blocky form of bainite can grow at a relatively slow rate such that carbon is rejected ahead of the growing interface. This means that normally carbides are not present within the laths or at lath boundaries to separate bainitic ferrite laths/sheaves, and therefore a granular morphology of granular bainite appears under low magnification SEM and optical microscopy. Carbides can sometimes be observed at the edge of the blocky granular bainite regions. The distinctive blocky shape of the granular bainite with a general absence of carbides, in these strip steels, makes it relatively easy to distinguish.

However, it should be noted that isolated carbides in the blocky regions can sometimes be observed (as shown in Figure 4.4) between adjacent blocks. These carbides will be more isolated and less aligned than expected for upper bainite or lower bainite. The reason for this would be that several blocks of granular bainite may be forming at the

same time within one prior austenite grain, and carbon will diffuse towards the region between the adjacent granular bainite blocks and form carbides there. Therefore, at lower magnification it is possible to find some carbides "within" granular bainite.

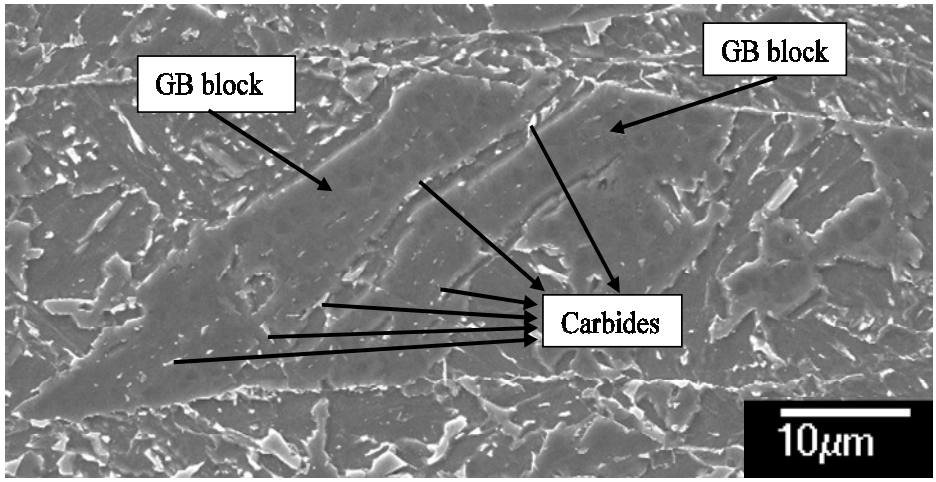


Figure 4.4. Adjacent granular bainite blocks found in Steel T1-1 suggesting several granular bainite regions could be formed at the same time within one prior austenite grain. As the granular bainite blocks grow and finally impinge, carbides can form between them due to the high carbon concentration.

4.3.2 Examples of bainitic phase quantification

As mentioned above, the main difference between lower bainite and upper bainite is the presence of carbides within the bainite laths in lower bainite, which can generally be observed using SEM imaging. It is difficult to identify the different types of bainite by comparing the size of carbides or bainite laths only, as variations in alloy levels and/or processing conditions will result in a range of carbide sizes and bainite lath sizes. Therefore, it has been found that it is only relevant to consider carbide size in trying to identify the different forms of bainite when comparing the same (or similar composition) steels using high magnification SEM imaging.

Discussed below are examples of SEM images used to identify, and quantify, the different forms of bainite in the hot rolled strip steels studied in this project. The strips were hot rolled at temperature between 1140 °C and 890 °C, then water quenched down to different holding temperatures (below 500 °C) for coiling. The combined effects of the alloying elements and coiling temperatures gives rise to microstructures comprised of different types and amounts of upper bainite, lower bainite and granular bainite.

1) Steel T1-1, ¼ thickness.

0.06 wt % C, 1.5 wt % Mn, 0.1 wt % Si, 0.5 wt % Cr, 0.26 wt % Mo, 0.04 wt % Nb, <0.01 wt % V and 20 ppm B.

Coiled at 435 °C.

Figure 4.5 gives a series of SEM images from the quarter thickness position of Steel T1-1, showing the microstructure of the steel in the as-received (hot rolled and coiled) condition. Figure 4.5 (a) shows the general microstructure then the subsequent images show how the bainite types were identified:

In Figure 4.5 (b), the austenite grain boundaries are marked as black lines. The figure clearly shows that the austenite grains were heavily deformed (into 'pancake' shapes) due to rolling below the recrystallization temperature.

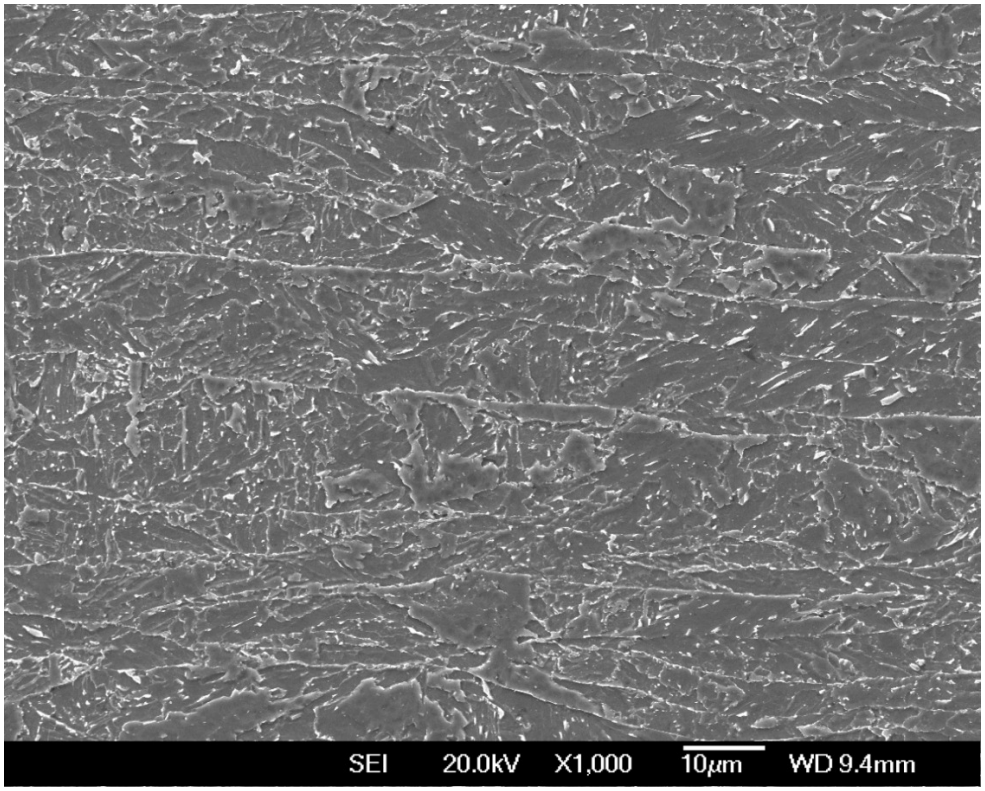
In Figure 4.5 (c), granular bainite regions are outlined in yellow. It can be seen that the granular bainite tends to form on the prior austenite grain boundaries and grow into the austenite grain, and generally has a blocky shape. Examples of granular bainite with isolated (non-aligned) carbides can be seen; these are believed to be where several

granular bainite regions formed together with the carbides occurring between the regions.

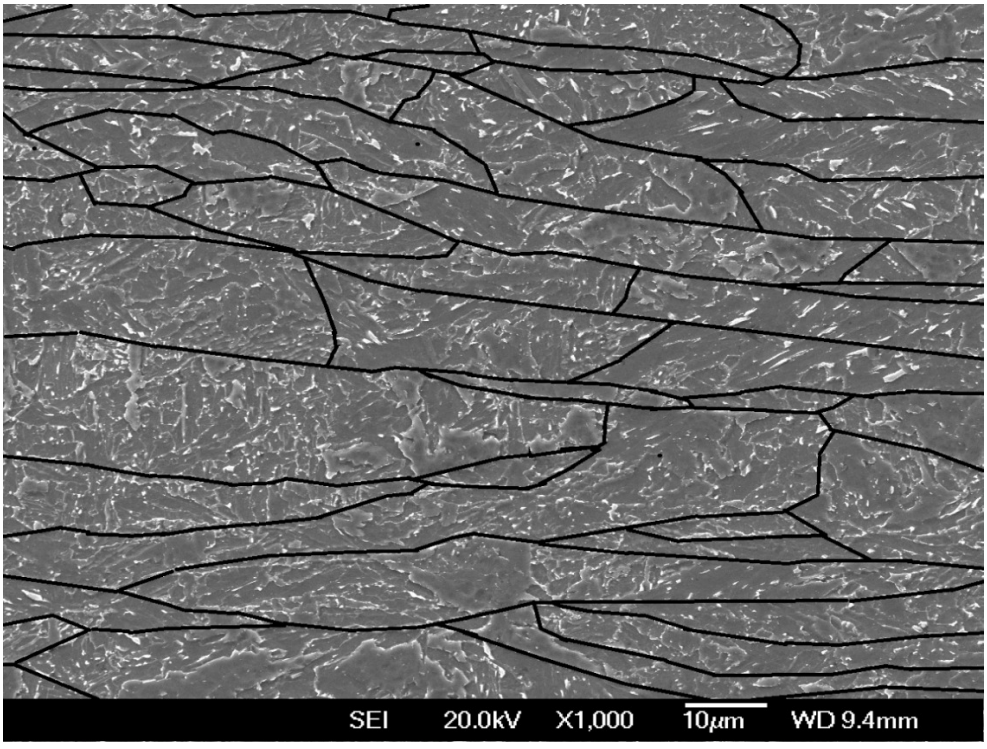
In Figure 4.5 (d), the upper bainite regions that were clearly differentiated from the other bainite structures are outlined in orange. These bainitic regions are formed of bainitic ferrite laths and coarse carbides with thickness ranged from 0.1 μm to 0.3 μm (± 0.04 μm) aligned between the bainite laths.

Figure 4.5 (e) shows the outline (light green) of bainitic regions that were not clearly identified initially in the low magnification image. Higher magnification images were therefore used to determine the bainitic type (Figure 4.5 (f)), from which it is obvious that there are no carbides within the bainitic ferrite laths and the thickness of carbides between the laths are in the range of 0.04 μm to 0.1 μm (± 0.02 μm), which is consistent with upper bainite. Therefore, these regions were classified as fine upper bainite in this steel.

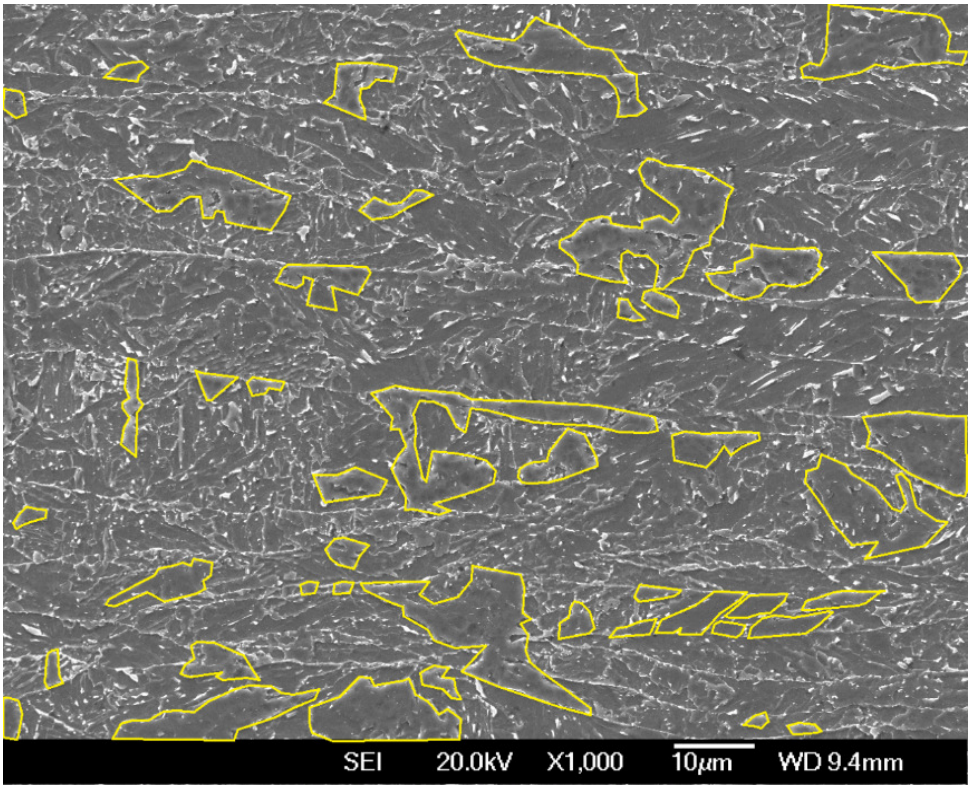
Therefore this steel microstructure consists of 15.8 % granular bainite and 84.2 % upper bainite according to this image. With larger amount of quantification (more than 15 images with the same size as Figure 4.5 (a)), the final result is 13.4 % granular bainite and 86.6 % upper bainite.



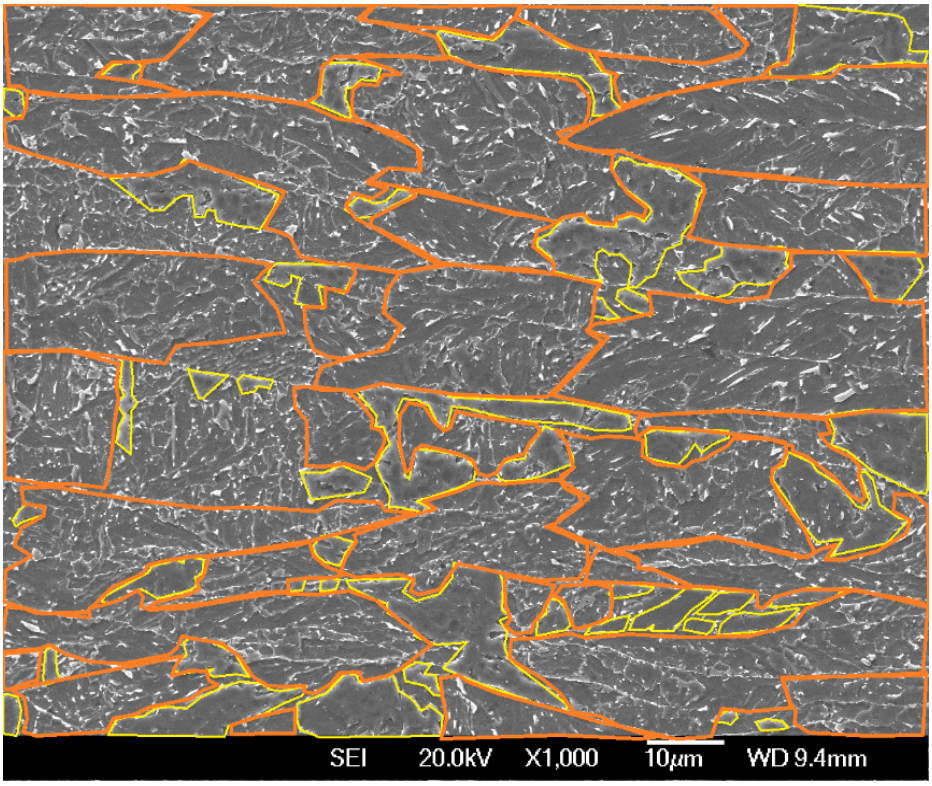
(a)



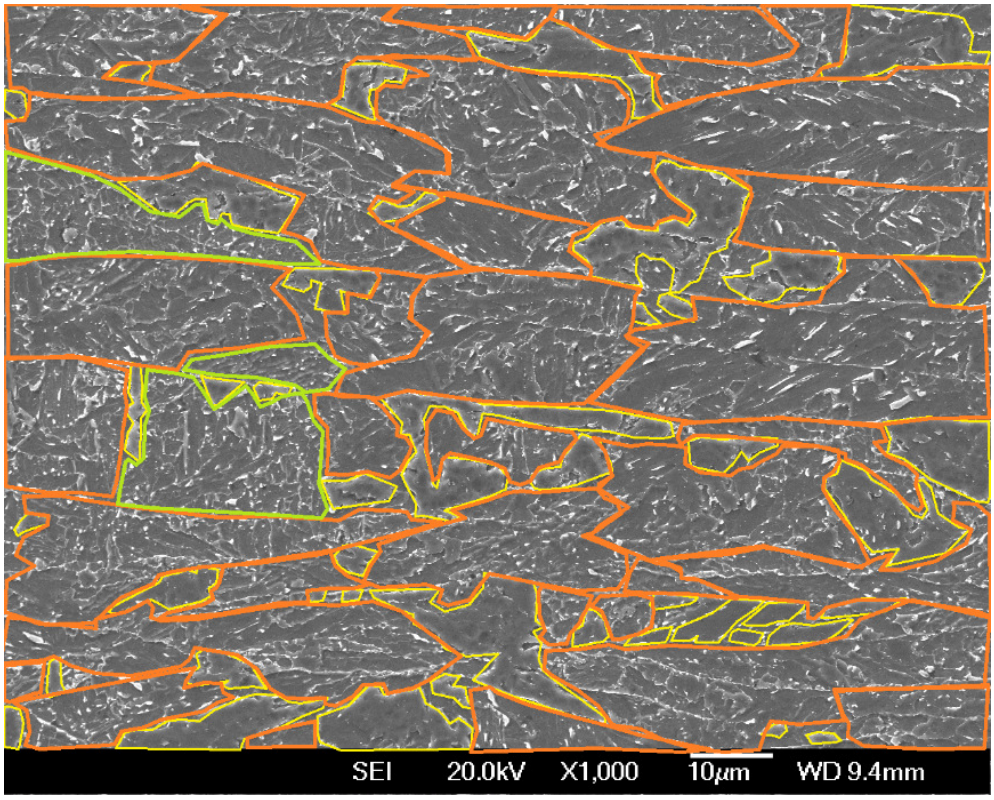
(b)



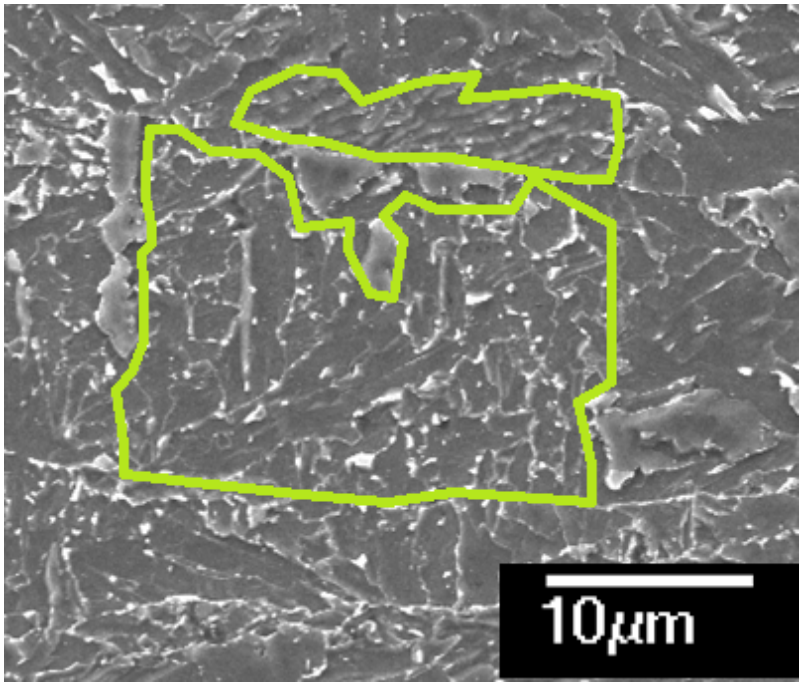
(c)



(d)



(e)



(f)

Figure 4.5. Microstructure of Steel T1-1 at ¼ thickness. (a) original SEM image of microstructure etched by 2 % nital, (b) prior austenite grains are marked in black, (c) granular bainite regions in this image are outlined in yellow, (d) obvious upper bainite regions are outlined in orange, (e) unclear UB/LB regions are outlined in light green, and (f) higher magnification of unclear regions showing they are upper bainite areas.

2) Steel T3-1, ¼ thickness.

0.07 wt % C, 1.5 wt % Mn, 0.06 wt % Si, 0.5 wt % Cr, 0.2 wt % Mo, 0.03 wt % Nb, 0.05 wt % V and 20 ppm B.

Coiled at 400 °C.

This strip contains increased C and V content (giving increased hardenability) and was processed to a similar finish rolling temperature (880 °C compared to 881 °C for the previous example of Steel T1-1). A fully bainitic microstructure was obtained.

Figure 4.6 gives a series of SEM images for this strip, showing the microstructure of the steel in the as-received (hot rolled and coiled) condition, with Figure 4.6 (a) showing the general microstructure and the subsequent images showing how the bainitic regions were identified.

In Figure 4.6 (b), the austenite grain boundaries are marked as black lines. The figure clearly shows that the austenite grains were heavily deformed (into 'pancake' shapes) due to rolling below the recrystallization temperature.

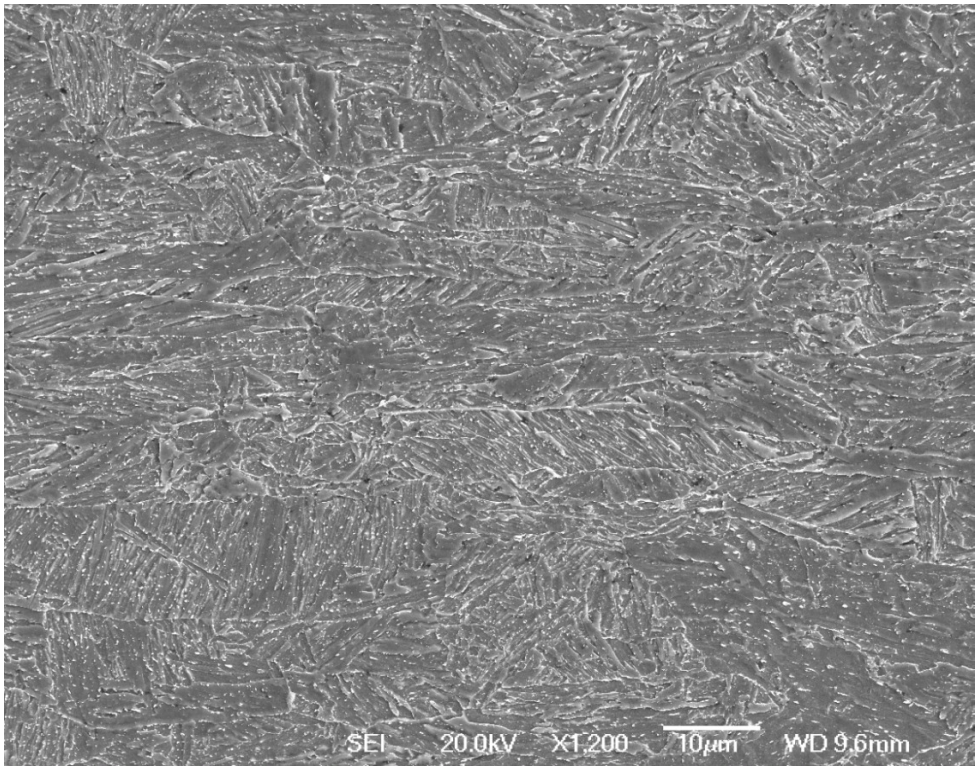
In Figure 4.6 (c), the granular bainite regions are outlined in yellow. As can be seen the granular bainite in this strip also forms at austenite grain boundaries and tends to grow into the austenite grain.

Figure 4.6 (d) shows the outlined obvious upper bainite regions in orange colour. It can be seen that the carbides in this strip are much finer (around 0.06 µm to 0.11 µm ± 0.02 µm) than those in Steel T1-1. This is possibly due to slightly decreased coiling temperature (around 30 – 50 °C lower than Steel T1-1) of this steel.

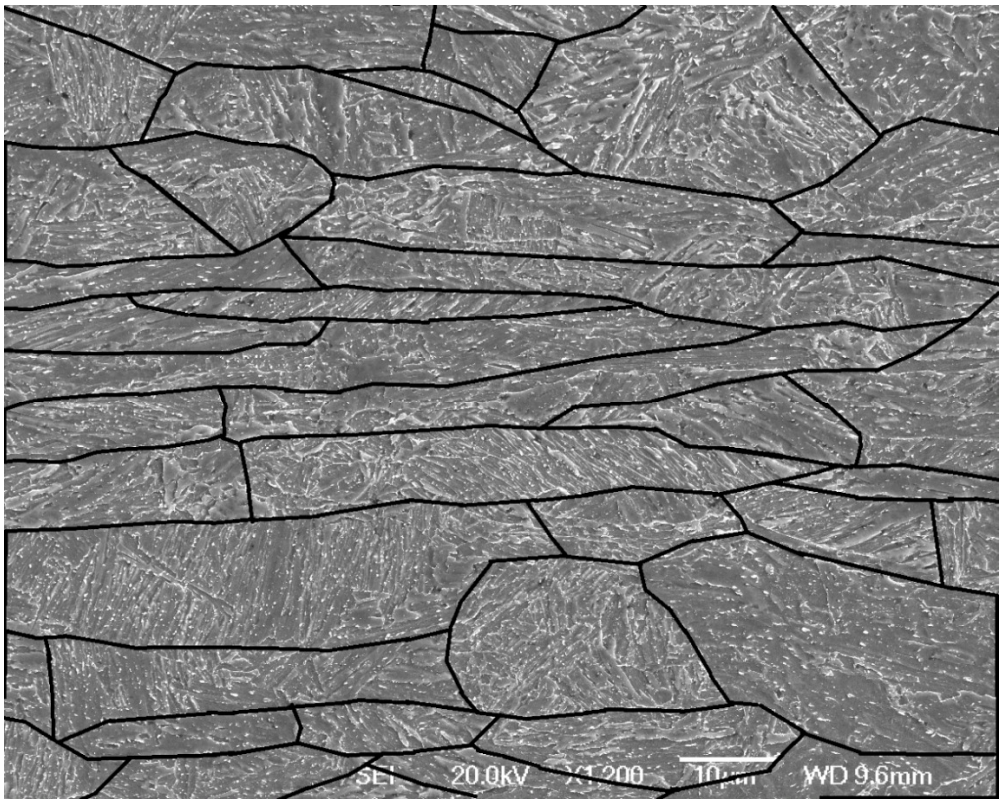
In Figure 4.6 (e), obvious lower bainite regions were outlined in red. In these regions, fine carbides (with sizes ranging from 0.02 μm up to 0.1 μm ± 0.01 μm) present both between and within the bainitic ferrite laths can be found even under low magnification (as shown in the figure) on careful examination.

Figure 4.6 (f) shows some bainitic regions which were hard to identify as upper bainite or lower bainite at this magnification. However, under higher magnifications (Figure 4.6 (g)-(k)), it is possible to identify the carbide size and position in the microstructures. In Figure 4.6 (g), it was measured that the carbides are around 0.06 ± 0.01 μm thick and randomly distributed both between and within bainitic ferrite laths, therefore the feature should be identified as a lower bainite region (the same as Figure 4.5 (h), (j) and (k)). However, in Figure 4.6 (l), the carbides are only distributed between the bainitic ferrite laths, and the sizes are in the range of 0.09 ± 0.03 μm, hence this is upper bainite.

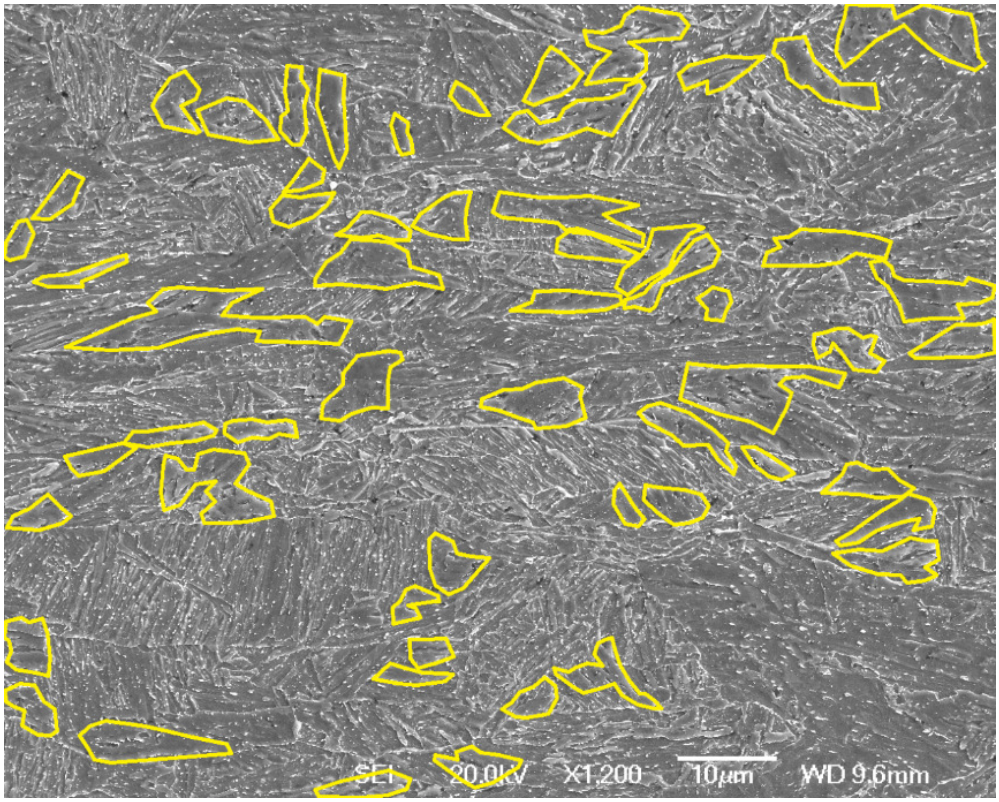
Overall this sample consists of 18.4 % granular bainite, 67.5 % upper bainite and 14.1 % lower bainite. With larger amount of quantification, the final result is 12.7 % granular bainite, 76.7 % upper bainite and 10.6 % lower bainite.



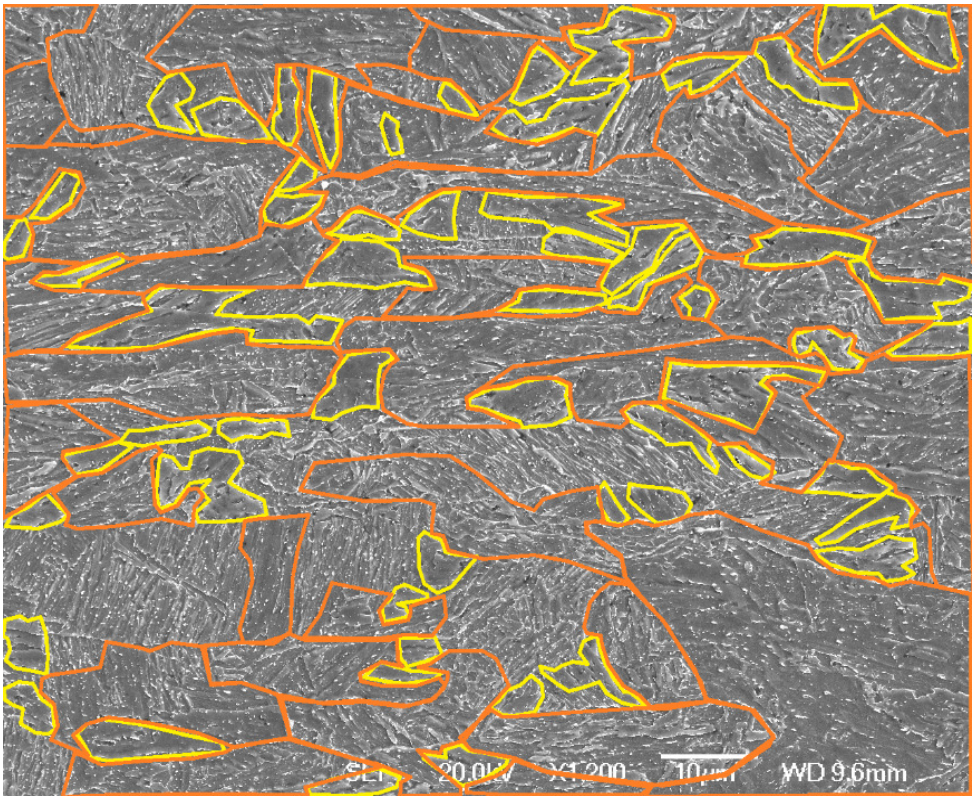
(a)



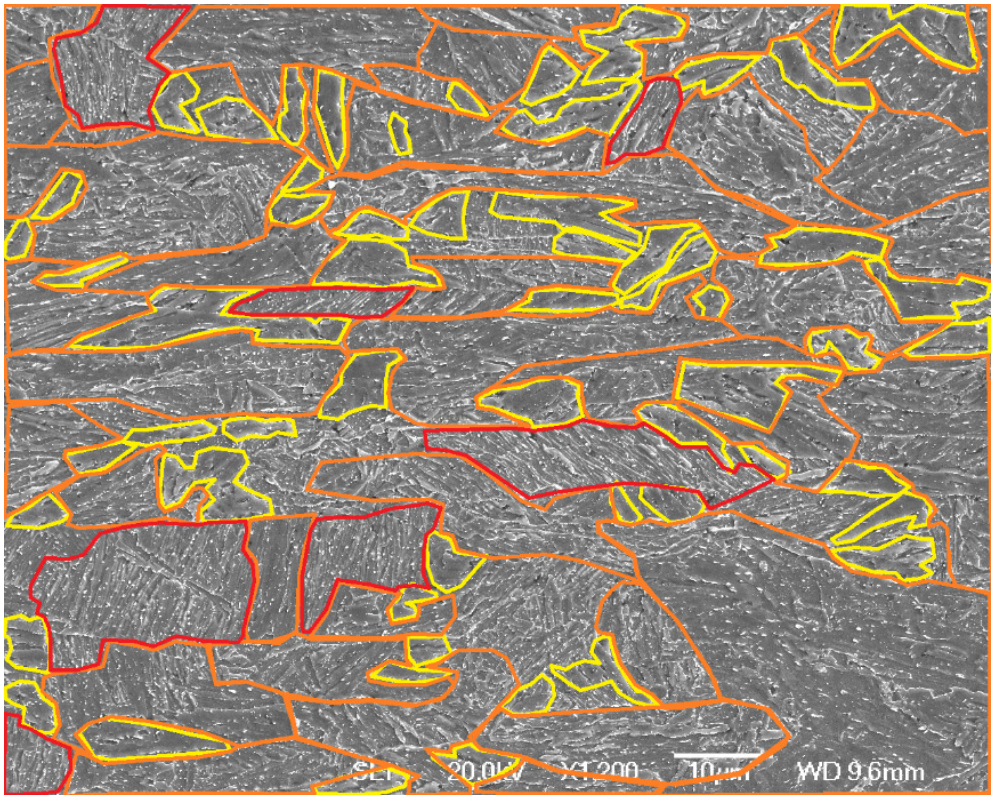
(b)



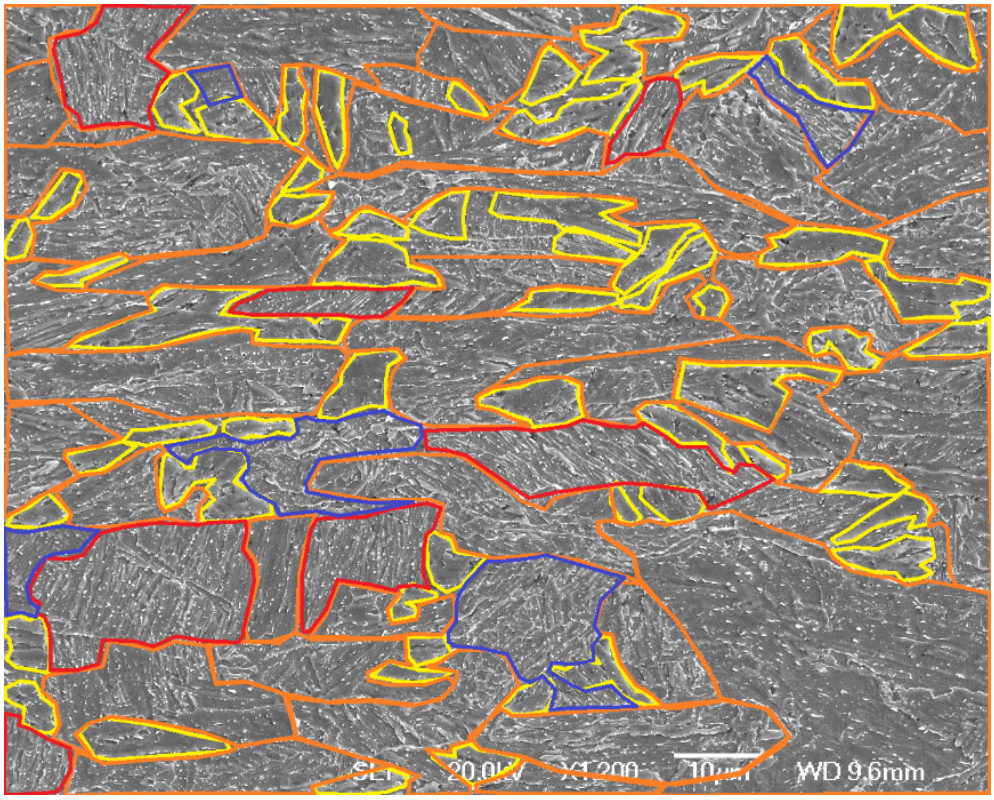
(c)



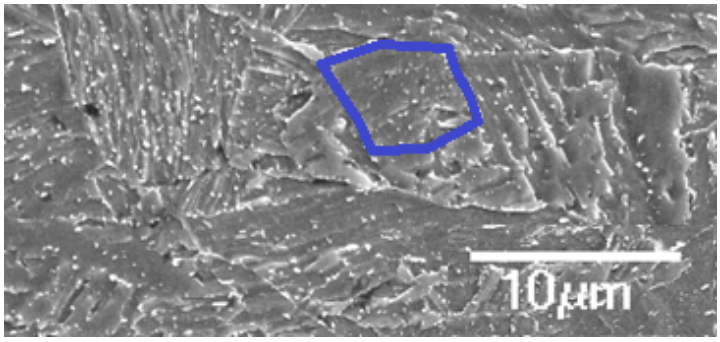
(d)



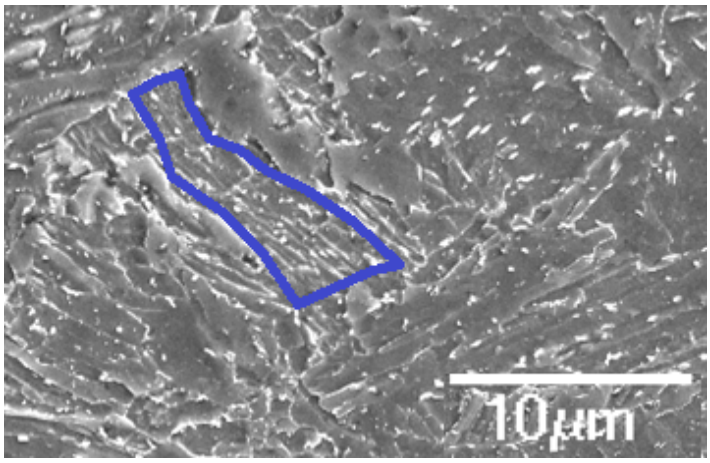
(e)



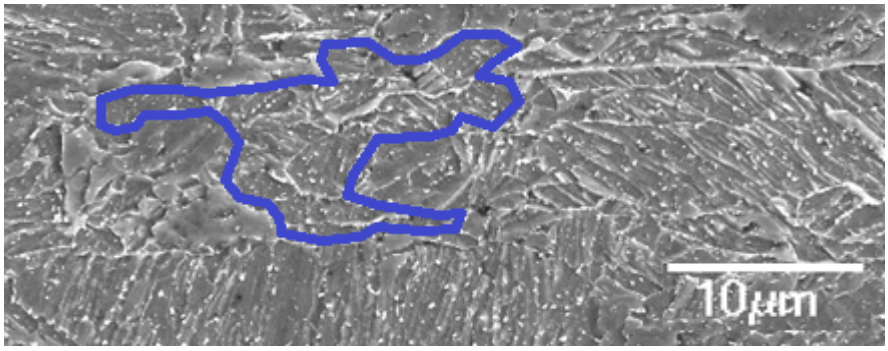
(f)



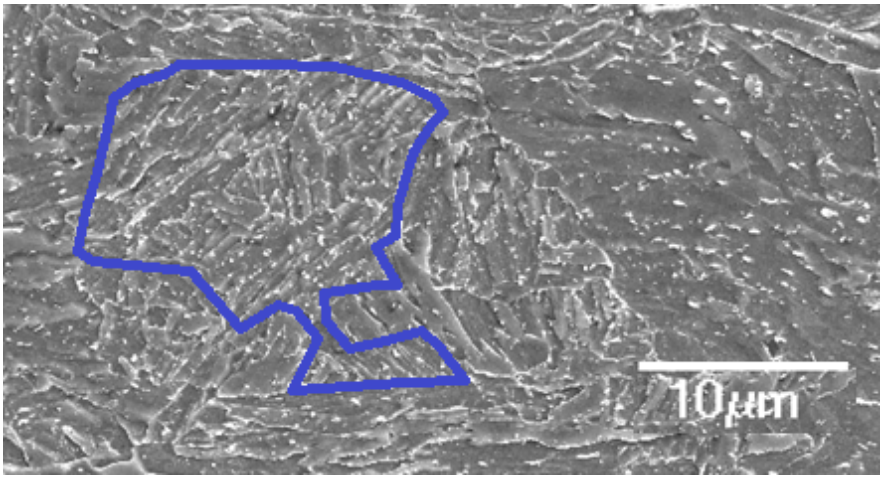
(g)



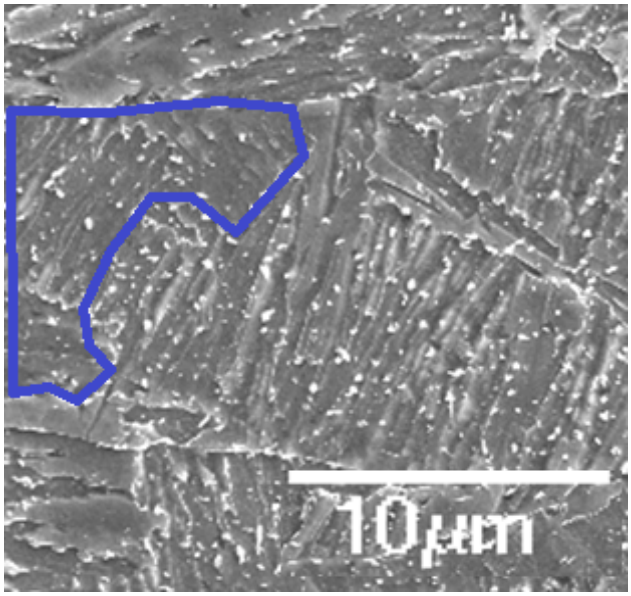
(h)



(j)



(k)



(l)

Figure 4.6. Microstructure of Steel T3-1 at ¼ thickness. (a) original SEM image of microstructure etched by 2 % nital, (b) prior austenite grain boundaries outlined in black, (c) granular bainite regions outlined in yellow, (d) obvious upper bainite regions outlined as orange, (e) obvious lower bainite outlined in red, (f) unclear regions outlined in blue, and (g) – (l) higher magnification of unclear regions, which were identified as being lower bainite for (g)-(k) and being upper bainite for (l).

4.4 Phase Quantification Results and Relationship between Coiling Temperature and Phase Balance

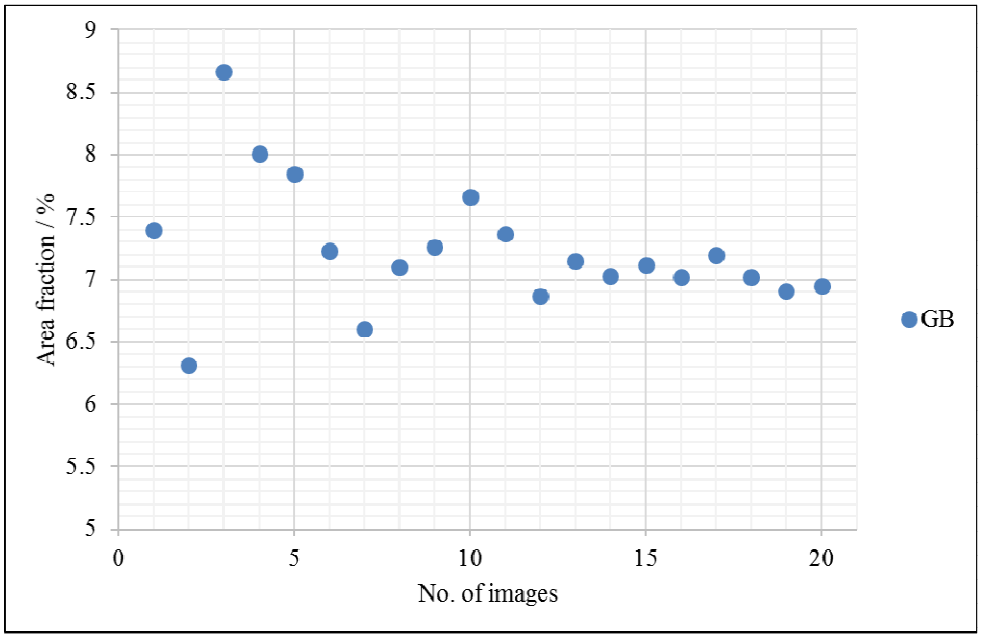
The quantification result is listed in Table 4.3, where CT stands for coiling temperature, UB stands for upper bainite, LB stands for lower bainite and GB stands for granular bainite. As mentioned in Chapter 3, the images used for phase quantification were taken at about quarter thickness beneath the surface, as this area is free of any central line segregation or surface decarburisation and can therefore be considered as representative of the bulk material. Besides, the investigated area is roughly where a Charpy notch will be located in impact samples, and therefore the quantification results will also be representative of microstructure where fracture will occur.

In Table 4.3, the error of microstructure quantification was presented with the standard deviation calculated from the results of 20 images for each steel. Figure 4.7 shows an example (Steel T1-4) of the relationship between the area fraction of each type of bainite and the number of images used for quantification. It can be seen from the figure that when using larger than 12 images, the area fraction results become more reliable (less than 0.5% difference from the average results of 20 images), suggesting the results shown in Table 4.3 are reasonably good estimations of the bulk materials.

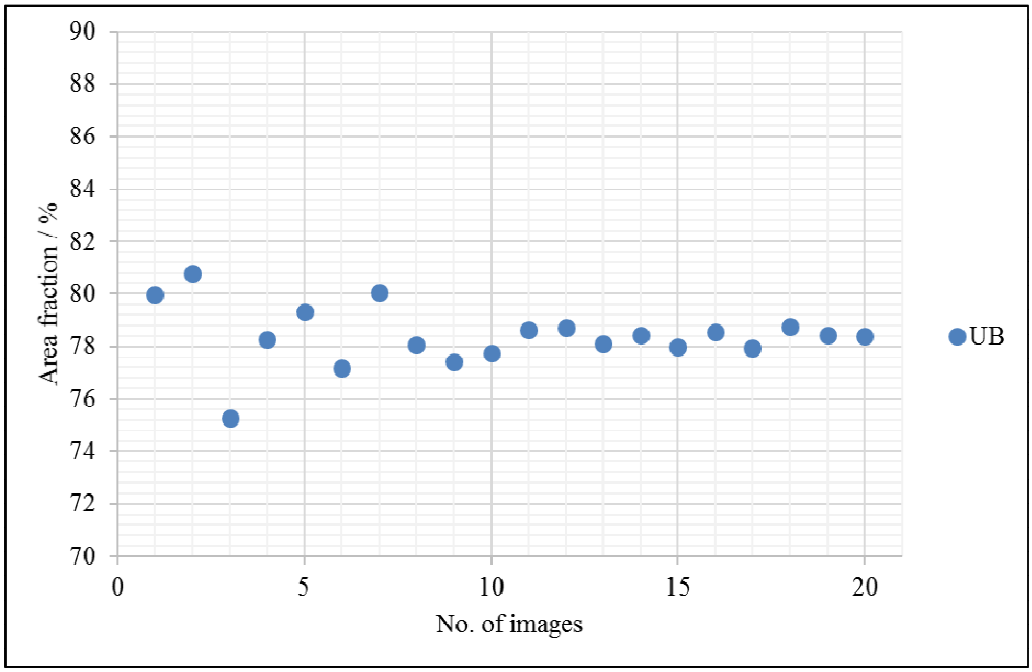
Figure 4.8 shows the relationship between the coiling temperatures and microstructure composition (i.e. area fraction of different types of bainite). As mentioned in Section 3.2, the coiling temperature may have variation due to the steels were processed industrially, from ±10 °C to ±30 °C depending on the aimed temperature for coiling, the error bars were added on the graph to suggest the possible range of the coiling temperature. The standard deviation of phase quantification results were also plotted on the graph.

Table 4.3 Quantification results for all strip steels.

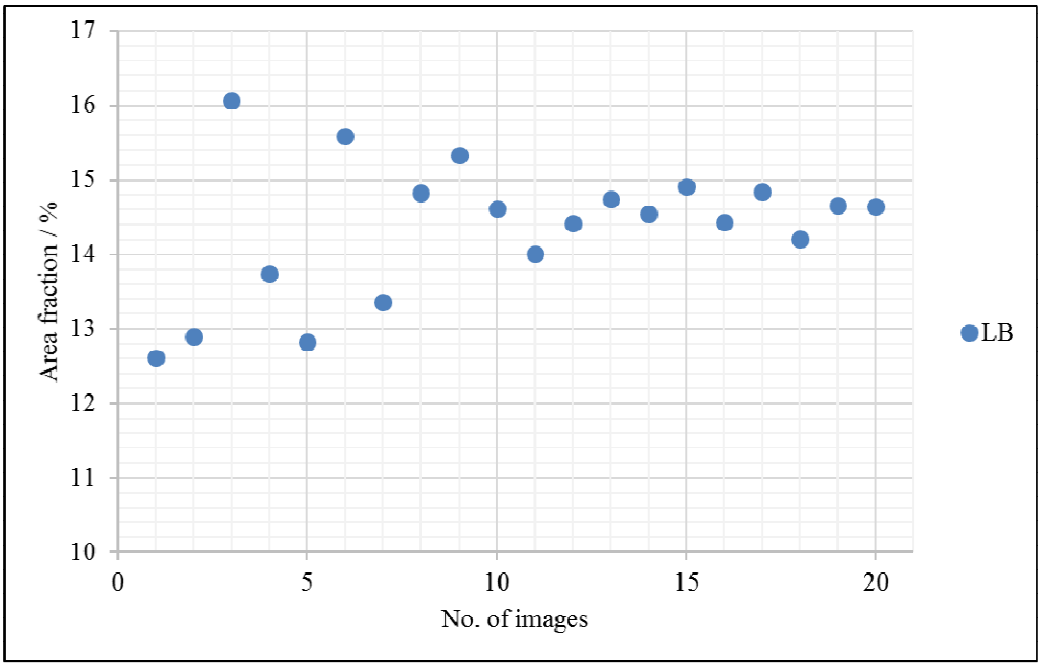
	CT / °C	UB	LB	GB
T1-1	453	86.6±0.8%	0.0%	13.4±0.6%
T1-2	411	87.4±0.4%	0.0%	12.6±0.5%
T1-3	393	84.5±0.7%	0.0%	15.5±0.5%
T1-4	290	78.4±1.0%	14.6±0.9%	7.0±0.5%
T2-1	347	88.0±0.5%	8.0±0.5%	4.0±0.3%
T2-2	314	85.0±0.7%	9.0±0.6%	6.0±0.4%
T2-3	253	87.1±0.9%	10.9±0.9%	2.0±0.2%
T3-1	400	76.7±0.8%	10.6±0.6%	12.7±0.6%
T3-2	390	75.0±0.7%	12.5±0.6%	12.5±0.3%



(a)

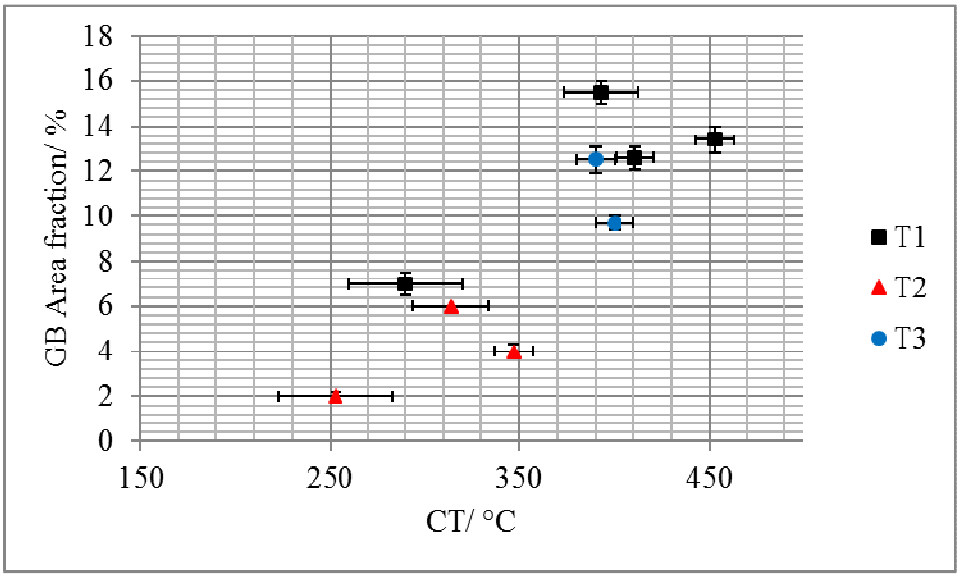


(b)

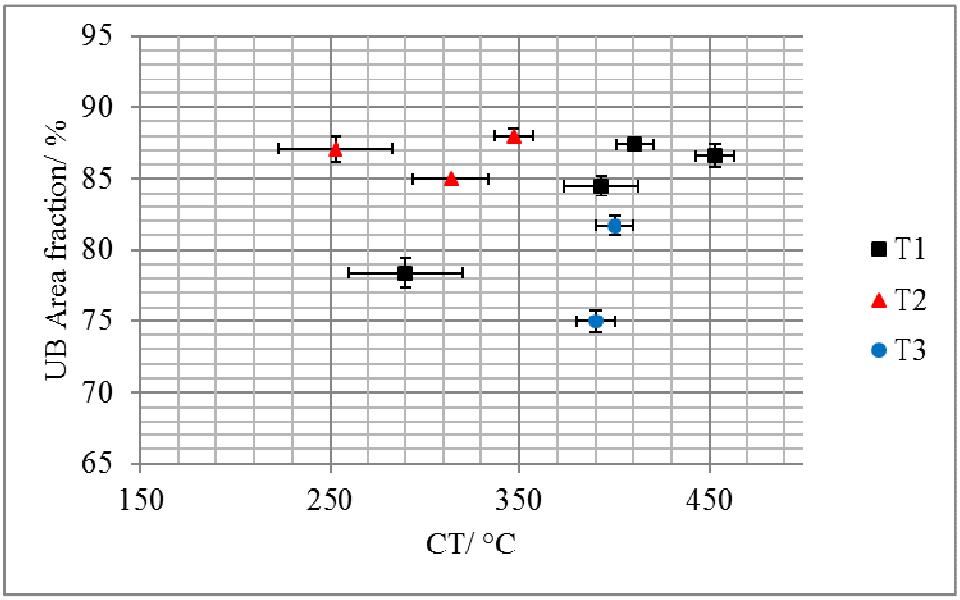


(c)

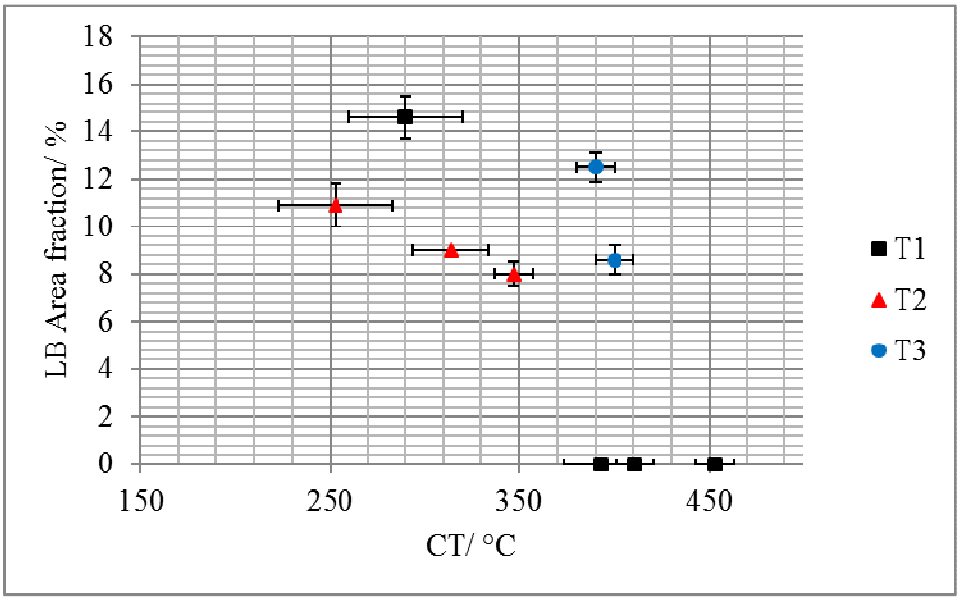
Figure 4.7 The relationship between the area fraction of different types of bainite ((a) granular bainite, (b) upper bainite, and (c) lower bainite) and the number of images used for quantification for Steel T1-4.


GB Area fraction/ %
18
16
14
12
10
8
6
4
2
0
150
250
350
450
CT/ °C
T1
T2
T3

(a)


UB Area fraction/ %
95
90
85
80
75
70
65
150
250
350
450
CT/ °C
T1
T2
T3

(b)



(c)

Figure 4.8 Relationship between coiling temperature and bainite phase balance. (a) granular bainite area fraction; (b) upper bainite area fraction; (c) lower bainite area fraction.

It can be seen from Table 4.3, and from the plots in Figure 4.8 of phase fraction against coiling temperature (although there are some variations), that in general, upper bainite is the dominating phase in all of the investigated samples, and the amount of lower bainite increases with the decrease in coiling temperature (CT), while granular bainite shows the opposite trend. It can be seen that in the T1 series steels, when the coiling temperature is close to and above 400 °C, no lower bainite will form and the amount of granular bainite in the steels all exceed 12%; T2 series all have coiling temperatures below 350 °C, and therefore show a higher amount of lower bainite and less granular bainite compared to T1 steels; T3 series have high coiling temperature around 400 °C, the amount of granular bainite in the steels are higher than 12%, similar with some of T1 steels, but the amount of lower bainite in the T3 steels is much higher considering their high coiling temperature, this is probably due to the effects of different alloying

levels (higher C and V content increasing hardenability). It is also interesting that Steel T1-4 was found to have the largest amount of lower bainite although its coiling temperature was not the lowest. This is probably due to the variation of coiling temperature along the length of a hot rolled coil (as mentioned before in Section 3.2) and the sample taken for analysis may not necessarily have come from the area where coiling temperature was determined, in general the coiling temperature is the average value of the whole coil and shows the most inaccuracy at low values e.g. for Steel T1-4 (coiled at 290 °C) and T2-3 (coiled at 253 °C).

4.5 Summary

According to the microstructure characterisation and discussions above, it can be concluded that, depending on the coiling temperature, the steels investigated may consist of two or three different types of bainitic structures, including upper bainite, lower bainite and granular bainite. Quantification results suggested that coiling temperatures below 400 °C is helpful for lower bainite formation, the area fraction of lower bainite found in the current products are between 0 and 15 %; while both granular bainite and upper bainite were found in all steels, and the amount of granular bainite increases with the increase of coiling temperature, from 2 % to 15.5 %.

CHAPTER 5

MECHANICAL PPROPERTIES INVESTIGATION

5.1 Introduction

This chapter includes the mechanical test results and analysis of the fracture mechanism operating in the strip steels. Together with the microstructure quantification work mentioned in Chapter 4, the relationship between microstructure and mechanical properties is investigated. In section 5.2, results of micro-hardness and impact tests are presented, compared and discussed. Section 5.3 provides analyses of the fracture behaviour of these bainitic steels. Section 5.4 links the mechanical properties with microstructure quantitatively, and suggests an optimum microstructure for a balanced strength and toughness with the current composition ranges. Section 5.5 gives a summary of the main observations and therefore leads to Chapter 6 which will discuss the possible ways to achieve the desired microstructure.

5.2 Strength/Hardness and Toughness Test Results

Both yield strength (YS) and ultimate tensile strength (UTS) of samples from each steel coil were tested by Tata Steel, the tests were carried out according to the BS EN 10002-1 standard on A50 plate tensile samples. Micro-hardness tests have been carried out on samples from each coil, and through thickness hardness profiles of all received samples have been determined (Section 4.2.1). The Charpy impact tests were performed by Tata Steel on each coil, however repeat tests were performed at the University of

Birmingham to provide specimens for fracture surface and crack propagation analysis (Section 5.2.2).

5.2.1 Strength and hardness results

The strength, YS and UTS, and elongation values are presented in Table 5.1. Tensile samples from longitudinal and transverse directions have been tested by Tata Steel UK Plc. In Table 5.1, "L" refers to the longitudinal direction, i.e. the length of the tensile sample is parallel with the rolling direction of the hot rolled coil; while "T" means the length of the test piece is parallel with transverse direction of the coil.

Table 5.1 Strength results for the steels, provided by Tata Steel.

Steel	Coiling temperature /°C	YS / MPa		UTS / MPa		Elongation / %	
		L	T	L	T	L	T
T1-1	453	680	764	748	786	17.9	14.1
T1-2	411	678	754	738	773	16.6	13.5
T1-3	393	708	754	761	771	16	13.3
T1-4	290	755	813	807	836	14.8	12.1
T2-1	347	816	876	918	952	13.1	10.6
T2-2	314	757	826	843	890	14	11
T2-3	253	838	909	951	1001	13	10.9
T3-1	400	862	982	907	996	13.6	11
T3-2	390	861	895	906	906	14.0	11

As can be seen from Table 5.1, the yield strengths of most of the steels are above 700 MPa level (except Steels T1-1 and T1-2 in the longitudinal direction), suggesting these steels have fulfilled the minimum strength requirement of the Grade 700 strip steels. However, according to the British Standard (as mentioned in Section 3.2), the elongation requirement for this steel grade is 12 % minimum in the rolling direction,(L) therefore T2 and T3 steels have elongation values in the L orientation only just above this lower limit and further development is necessary to increase the elongation of the

products. Although the rolling history of the three trials were slightly different, which resulted in a difference between the prior austenite grain shapes, as mentioned in Sections 3.2 and 4.2, the results indicate that the factors affecting the strength and elongation properties are predominantly the coiling temperature and compositional changes, which links to the final microstructure developed, i.e. phase balance according to discussions in Chapter 4 (as the T1 steels, which have the most pancaked austenite grains and presumably smallest austenite grain size among all three trials does not show the best mechanical properties). It can be seen that although coiled at around 400 °C (a relatively high temperature compared with T2 products and T1-4), T3 products have higher strength compared with the previous trials (T1 and T2), which may be due to the carbon and vanadium addition in this trial (where T1 has slightly lower carbon and no vanadium and T2 also has slightly lower carbon but similar vanadium levels) giving more dislocation pinning effect and precipitate strengthening from fine V(C, N), which is consistent with literature findings on V(C, N) precipitation in similar low carbon vanadium microalloyed steels during coiling (Misra et al., 2005, Siwecki et al., 2010, Hutchinson et al., 2014), although no V(C, N) has been observed in this work as this would require TEM. Also, Table 5.1 shows the strength of steels within the same trial tend to change with coiling temperature, i.e. steels coiled at lower temperature tend to perform better (higher strength) than those coiled at higher temperatures.

Through thickness hardness profiles are shown in Figure 5.1, the hardness values were measured from 1.5 mm below one surface to 1.5 mm below the other surface. In order to make the graph clear and easy to read, the standard deviation of each point was not plotted in the figure, but in general, the standard deviation of the hardness measurement varies from ± 10 to ± 20 HV, and varies with the position and sample (steels with higher

hardness have larger standard deviation than those with lower hardness). As indicated in the figure, steel T2-3 showed higher hardness at the half thickness position possibly due to rolling segregation, as similar behaviour, i.e. higher centreline hardness has been reported (Morrison and Abernethy, 1990, Reger et al., 2010) due to the concentration of carbon, manganese etc. at the centreline in a segregation band. However, an increase of hardness at centreline were not found (or not obvious) for other products, this is probably due to the segregation band in these steels being narrow and not have been sampled. Nevertheless, take the standard deviation of each hardness value in to consideration, in general the variations of hardness through sample thickness are not great for the steels investigated, suggesting relatively homogenously distributed microstructure. To simplify the future investigation work, for each steel, an average of 5 micro-hardness measurements at quarter thickness (¼ thickness, or ¾ thickness, i.e. around 4 mm below surfaces) positions were taken as representative (results presented later in Table 5.2), and the corresponding microstructures were investigated for quantification (results presented in Chapter 4).

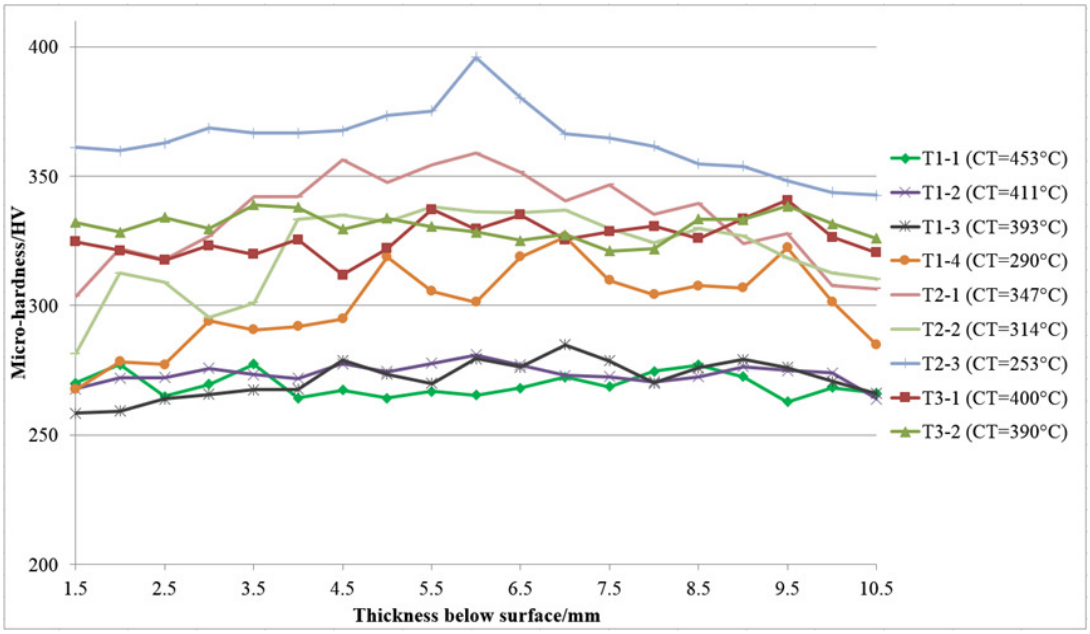


Figure 5.1 Through thickness (between 1.5mm to 10.5 mm) hardness profile of investigated steels (corresponding coiling temperatures illustrated in legends as CT).

The micro-hardness data at ¼ thickness positions for as-received materials are given in Table 5.2, together with the coiling temperatures of each steel, and the ratio between longitudinal yield strength (YS) as well as the ultimate tensile strength (UTS). As shown in the table the YS/Hardness ratio varies from 2.33 to 2.63, whilst the variation of UTS/HV ratio is less, i.e. between 2.65 and 2.81. The relationship between measured micro-hardness and strength (including both yield strength and ultimate tensile strength) is plotted in Figure 5.2, and indicated by trend lines and R^2 values (0.8332 and 0.9637 for YS-HV and UTS-HV, respectively); although there are some variations in the strength / hardness ratio, it is still reasonable to represent strength with the measured hardness data. It can be seen from the table that the hardness tends to increase with the decrease of coiling temperature for each trial, and possibly due to the differences in micro-alloying level (i.e. vanadium addition in T2 and T3 steels to provide precipitation hardening (Zajac et al., 1998, Siwecki et al., 2010, Hutchinson et al., 2014)) between

the three trials, the steels coiled at similar temperature (e.g. T1-3 and T3-2) show different hardness values.

Table 5.2 Micro-hardness (HV, load = 300g) data for investigated strip steels.

Trial	Trial 1				Trial 2			Trial 3	
Sample ID	T1-1	T1-2	T1-3	T1-4	T2-1	T2-2	T2-3	T3-1	T3-2
Hardness / HV	271 ± 6	274 ± 2	271 ± 6	300 ± 14	330 ± 9	313 ± 13	359 ± 7	331 ± 8	327 ± 2
YS/HV ratio	2.51	2.47	2.61	2.52	2.47	2.42	2.33	2.63	2.60
UTS/HV ratio	2.76	2.69	2.81	2.69	2.78	2.69	2.65	2.74	2.77
CT / °C	453	411	393	290	347	314	253	400	390

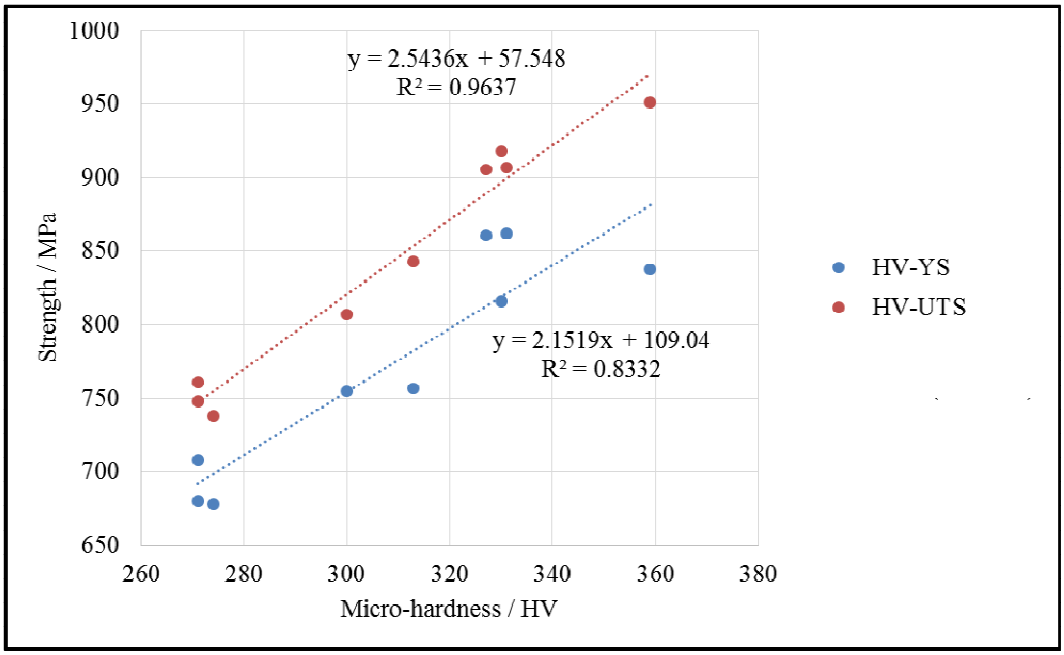
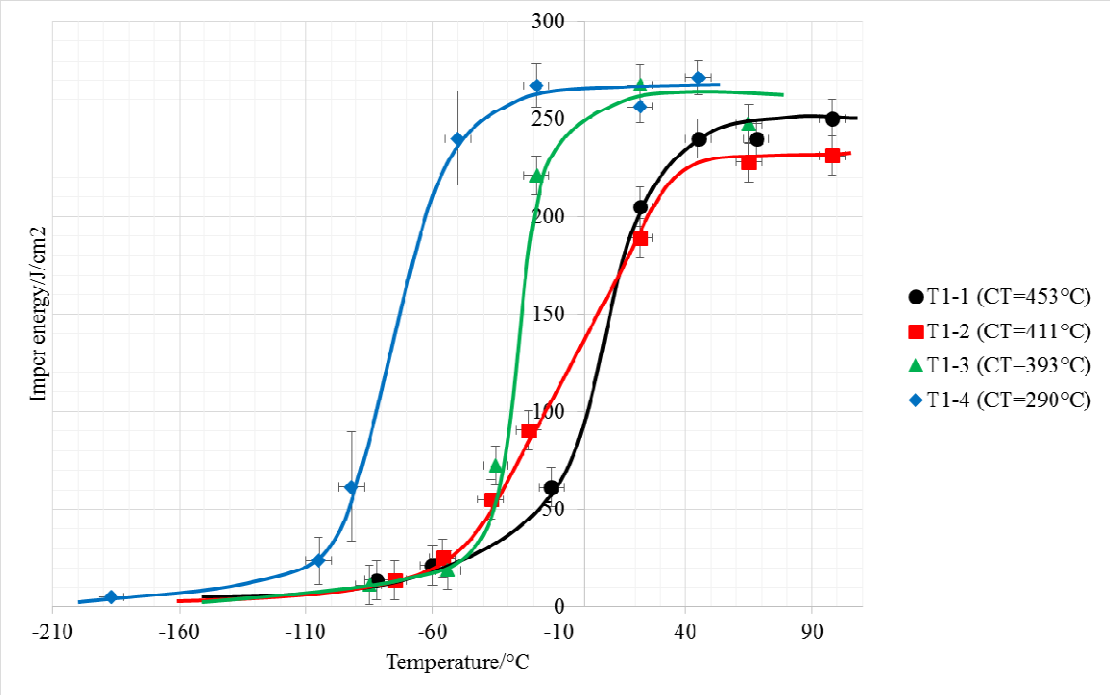


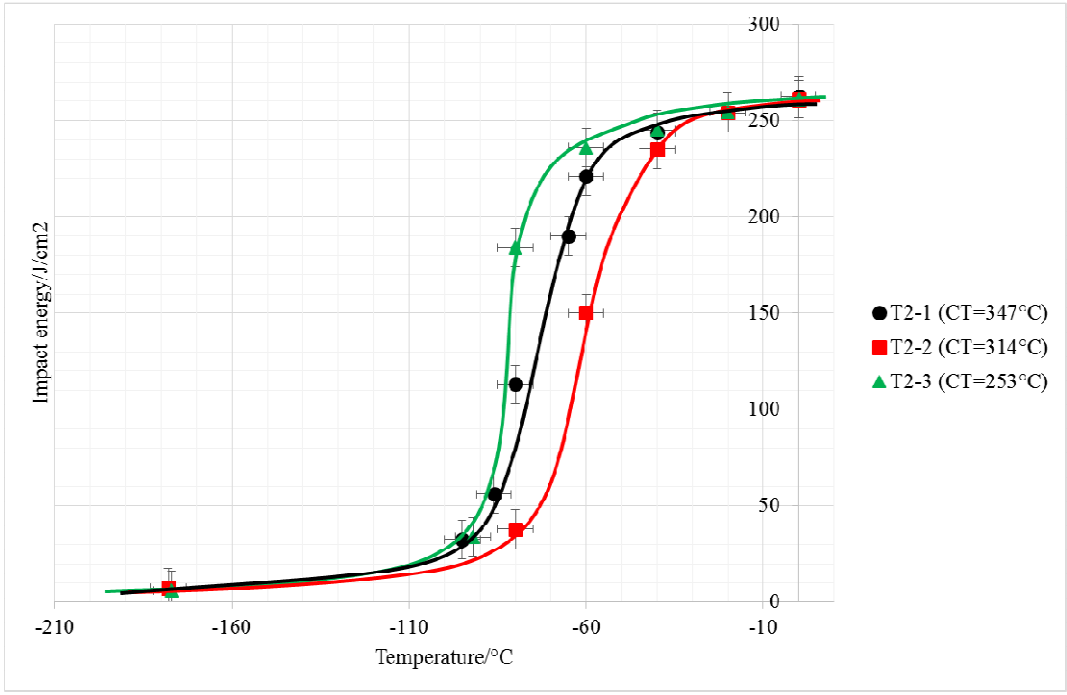
Figure 5.2 Micro-hardness – strength relationship of investigated steels.

5.2.2 Impact toughness

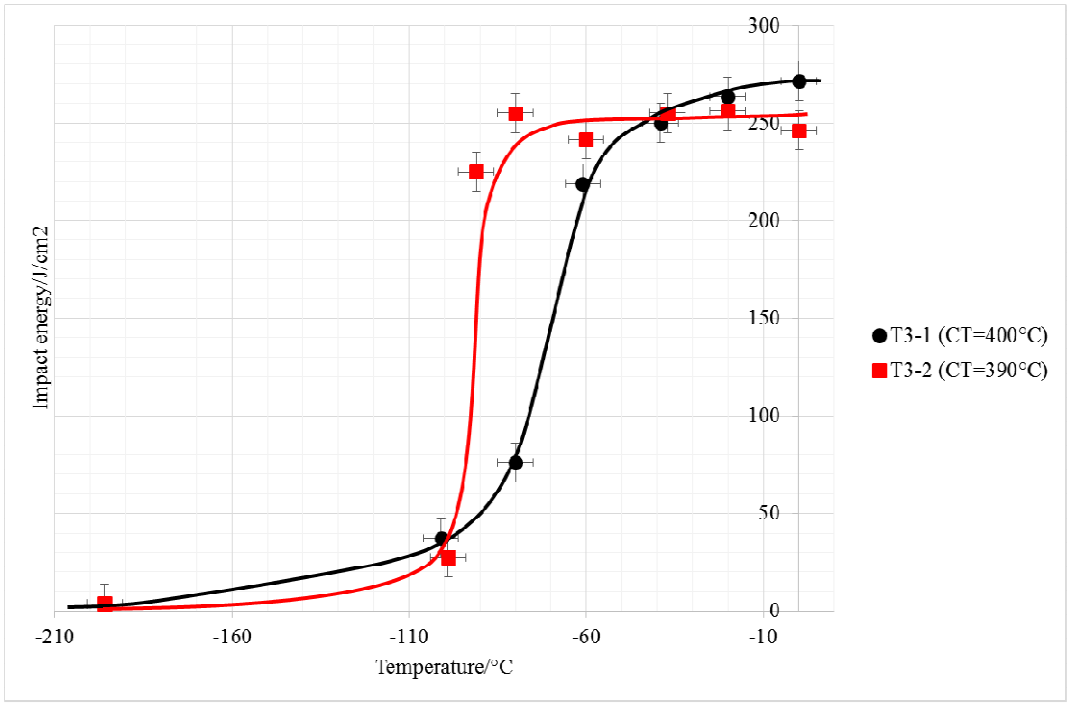
Figure 5.3 summarises the impact test results as ductile-brittle transition curves for the different trials and coiling temperatures.



(a)



(b)



(c)

Figure 5.3 Ductile-brittle transition curves of investigated steels. (a) T1 series, (b) T2 series, and (c) T3 series.

As can be seen from Figure 5.3, each data point on the curve tend to have some variation especially at ductile-brittle transition region, this is caused by the nature of Charpyy impact test (Lont, 2000, Tóth et al., 2002, Yang and Qiang, 2009). Therefore, it is necessary to consider the uncertainty of the test results so that good estimations of DBTT (Ductile-Brittle Transition Temperature), 34 J/cm^2 ITT (Impact Transition Temperature), and -40 °C impact energy values can be made. According to Lont (2000), the uncertainty caused by the test piece can be estimated with the use of confidence interval, which can generally be expressed as below (Chatfield, 1978, Lont, 2000):

$$\bar{x} \pm t_{\frac{1}{2}\alpha, n-1} \frac{s}{\sqrt{n}}$$

where x is the population mean (i.e. average value of the test results), s is the population standard deviation (i.e. standard deviation of the test results), n is the number of results, t is the random variable of a t-distribution, α represents the confidence level of 100(1 – α). Therefore, as each data point was an average of 3 test results, considering a 95% confidence interval, t0.25, 2 will be 3.182 according to t-distribution (Chatfield, 1978), the confidence interval can be calculated, the results are shown in Table 5.3.

From the figures above the impact transition behaviour of the investigated steels are clear, Table 5.3 below lists the coiling temperatures and DBTT (Ductile-Brittle Transition Temperature), impact energy at -40 °C, as well as 34 J/cm^2 ITT (Impact Transition Temperature) values of each steel (all three measured of impact toughness are considered as they are all frequently used in the steel industry, and customers will often ask for these values when purchasing a steel product). The DBTT is measured as the temperature of the mid-point energy between the upper shelf and lower shelf on the

impact transition curve. The impact energy at -40 °C is normally required to be located at the upper shelf of the impact transition curve by customers (Crowther, 2012), i.e. higher than 130 J/cm^2; and 34 J/cm^2 Impact Transition Temperature (ITT) is often considered as a lower limit of the temperature which the steel can be used, and is required to be as low as possible for safety reasons. In general, it is desired to have DBTT and 34 J/cm^2 ITT as low as possible, and -40 °C impact energy as high as possible for a steel with good toughness.

Table 5.3 Comparison of the DBTT values along with coiling temperature (CT) of investigated steels.

Steel code	T1-1	T1-2	T1-3	T1-4	T2-1	T2-2	T2-3	T3-1	T3-2
CT / °C	453	411	393	290	347	314	253	400	390
DBTT / °C	+7 ±5	-10 ±7	-28 ±3	-78 ±11	-73 ±13	-60 ±8	-82 ±8	-70 ±5	-90 ±12
-40 °C IE / J	25 ±7	40 ±13	43 ±16	250 ±22	245 ±12	235 ±21	253 ±11	253 ±11	256 ±6
34 J/cm^2 ITT / °C	-30 ±5	-40 ±7	-45 ±3	-98 ±11	-90 ±13	-80 ±8	-95 ±8	-105 ±5	-100 ±12

From Table 5.3, it can be concluded that within a trial, the DBTT decreases with the decrease of coiling temperature, representing, for a certain chemical composition, that a lower coiling temperature will result in better impact toughness. The -40 °C impact energy and 34 J/cm^2 ITT show a similar trend as DBTT with the change of coiling temperature, i.e. increased coiling temperature in a trial results in decreased -40 °C impact energy and increased 34 J/cm^2 ITT. However, it worth noting that when comparing Steel T2-1 and T2-2, the one with the higher coiling temperature (T2-1) performs better (higher DBTT and 34 J/cm^2 ITT but lower decreased -40 °C impact energy) in terms of toughness than the lower coiling temperature one (T2-2). Besides,

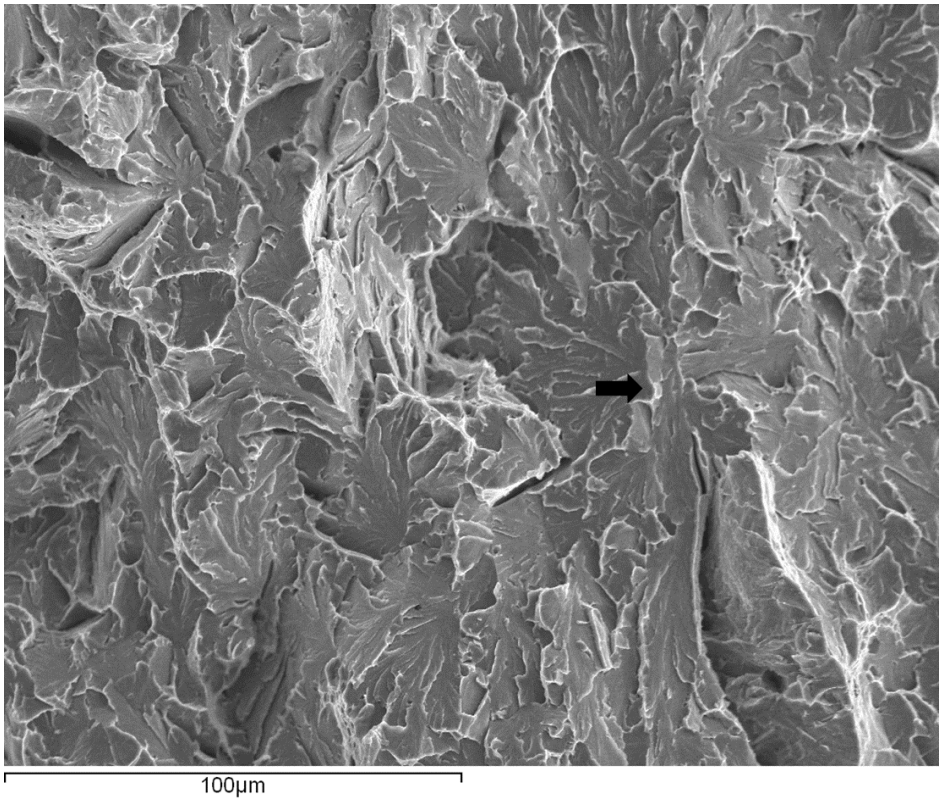
when looking at strength / hardness of these two steels, it can be noted that T2-2 also performs better than T2-1. This can then be linked back to the microstructure characterisation results, i.e. the phase balance of the two steels is different: T2-2 has a larger lower bainite content (9.0 %) than T2-1 (8.0 %). Whilst it is not clear the reasons for this difference, the relationship between the microstructure and toughness is consistent, but not with coiling temperature. This may be due to the coiling temperature being incorrectly measured or being inconsistent along the strip product, however unfortunately the variation of coiling temperature along the coil length was not available). It is known that the coiling temperature can be 20 to 30 °C higher or lower than the average recorded value and lower coiling temperatures (below 300 °C) tend to be even less accurately measured (Crowther, 2012), therefore the sampling area may actually have higher or lower coiling temperature than the average value (which is the one presented in Table 3.2 and in other parts of this thesis).

Between different trials, even if the steels were coiled at similar temperatures, the DBTT tends to vary from one trial to another, for example Steel T1-2 (-10 °C) and T3-1 (-70 °C), the same for T1-3 (-28 °C), T2-1 (-73 °C) and T3-2 (-90 °C). Compared with strength / hardness results, it can be seen that while T3 steels show higher strength / hardness levels than T1 steels, the impact toughness of T3 steels are better than those coiled at a similar temperature in T1, which is normally not expected for steels with similar microstructures (Bhadeshia and Honeycombe, 2006, Yu, 2006, Yang and Qiang, 2009). This observation may be caused by the slightly different chemical composition and different coiling conditions between the trials, which then link back to the microstructure differences in the final products – As shown in Table 4.3, the T3 series contains a larger amount of lower bainite than the ones coiled at similar temperature for

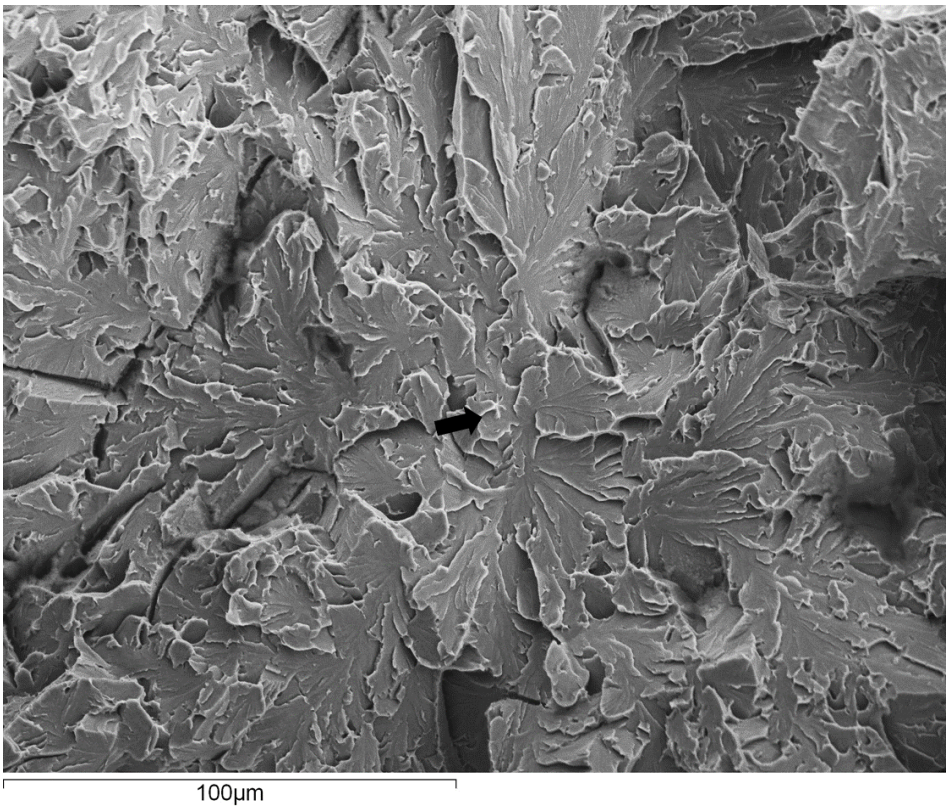
the T1 series, also, compared with T1 steels, T3 steels have higher V content (which will provide precipitation strengthening effect as mentioned in Section 5.2.1), resulting in higher strength whilst still giving lower DBTT (better toughness) for T3 than T1 steels.

5.3 Crack Propagation Mechanism

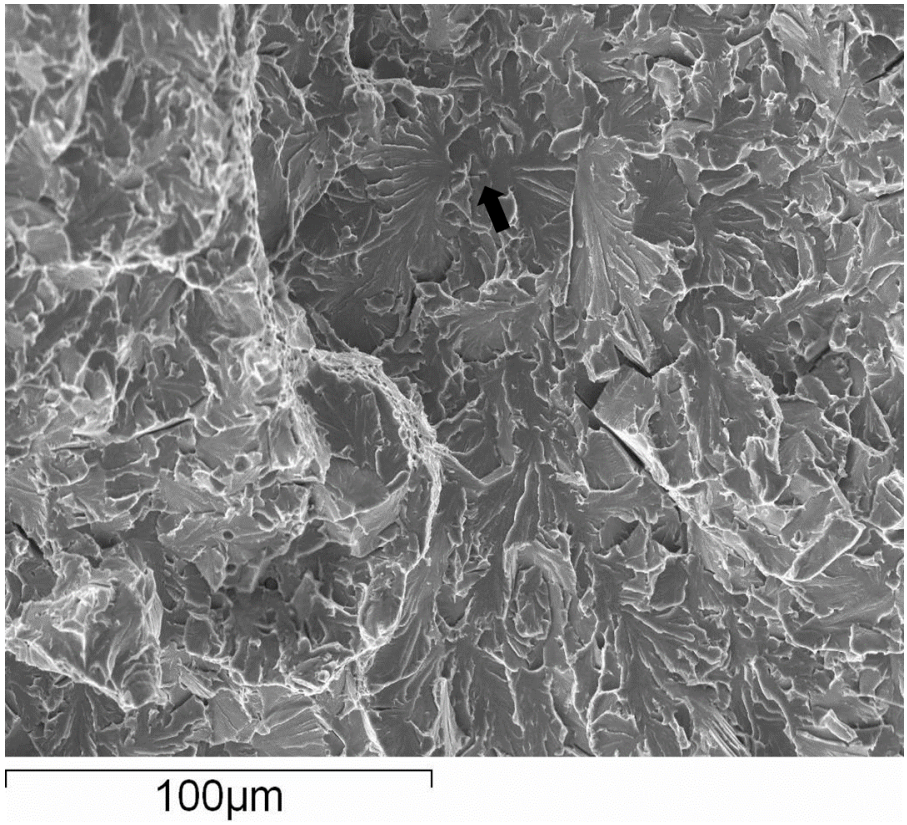
The fracture surfaces and cross-section microstructures have been analysed under SEM, where the brittle fractured samples with low impact energy (located on the lower shelf of the impact transition curve) were investigated. All fracture surfaces were found to be transgranular cleavage fracture, and via tracing the river pattern multiple crack initiation sites have been identified on each sample, located around 150 to 400 μm below the notch. However, no obvious features, such as large particles, were found at the crack initiation site to cause the cleavage fracture. Fracture surface analysis results are shown in Figure 5.4.



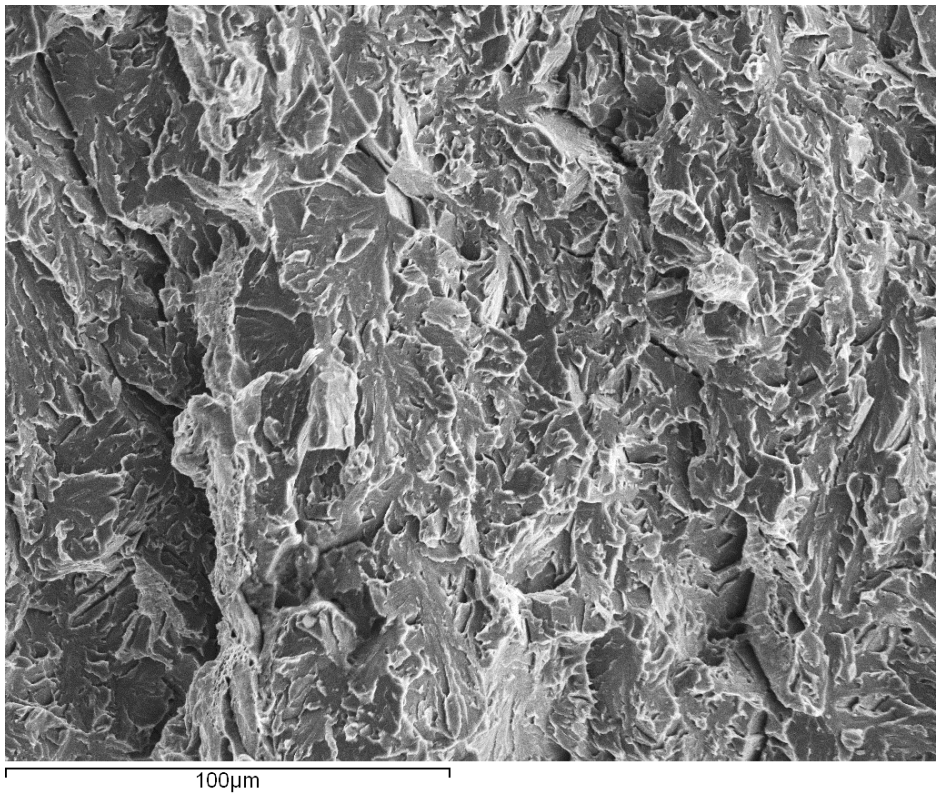
(a)



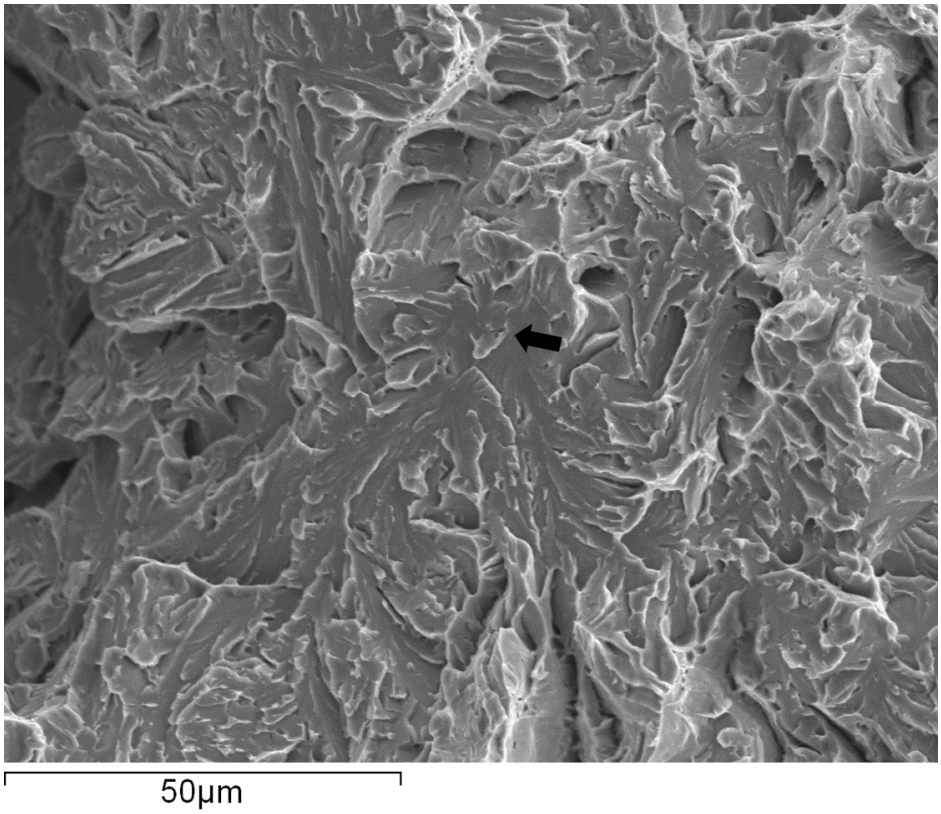
(b)



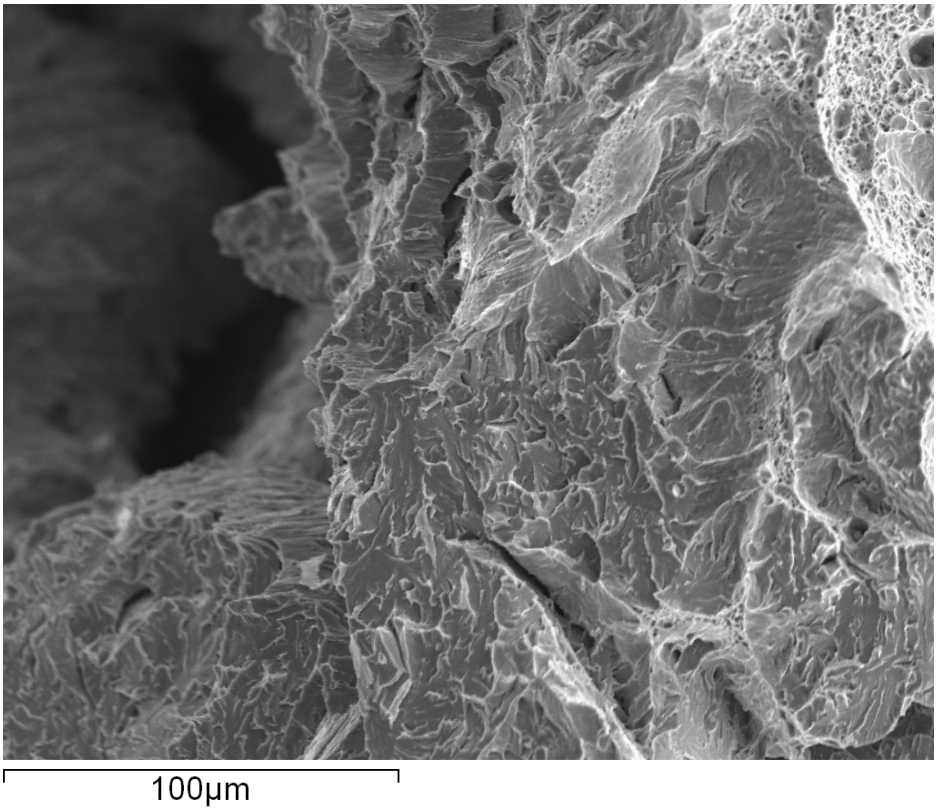
(c)



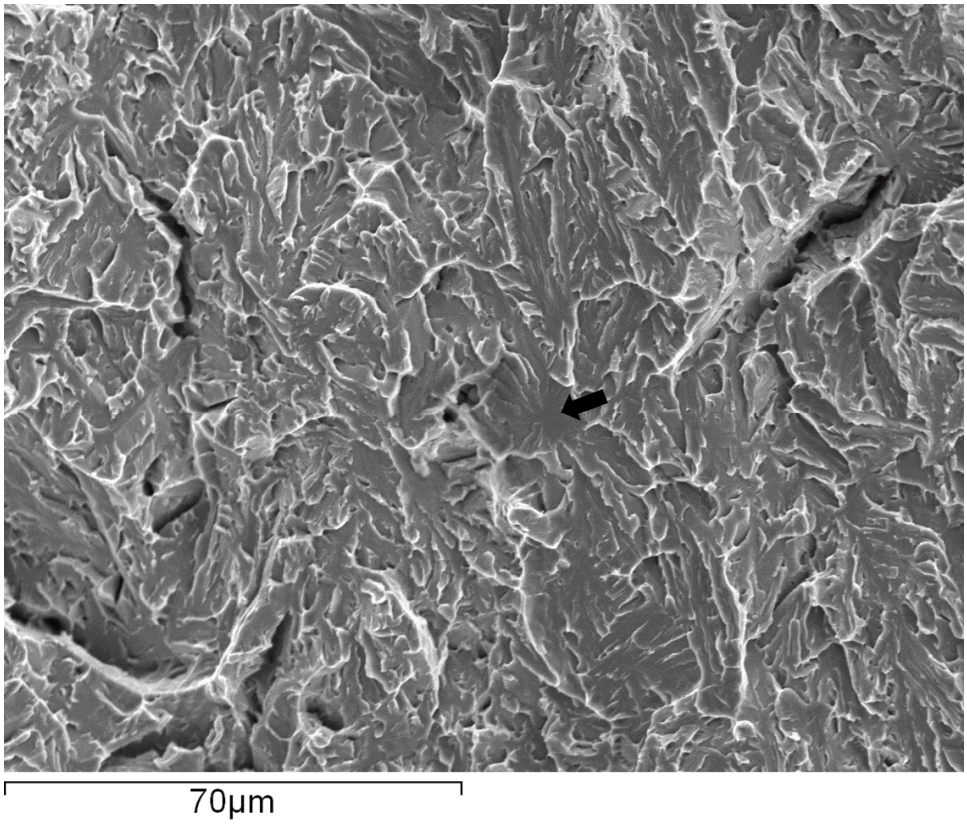
(d)



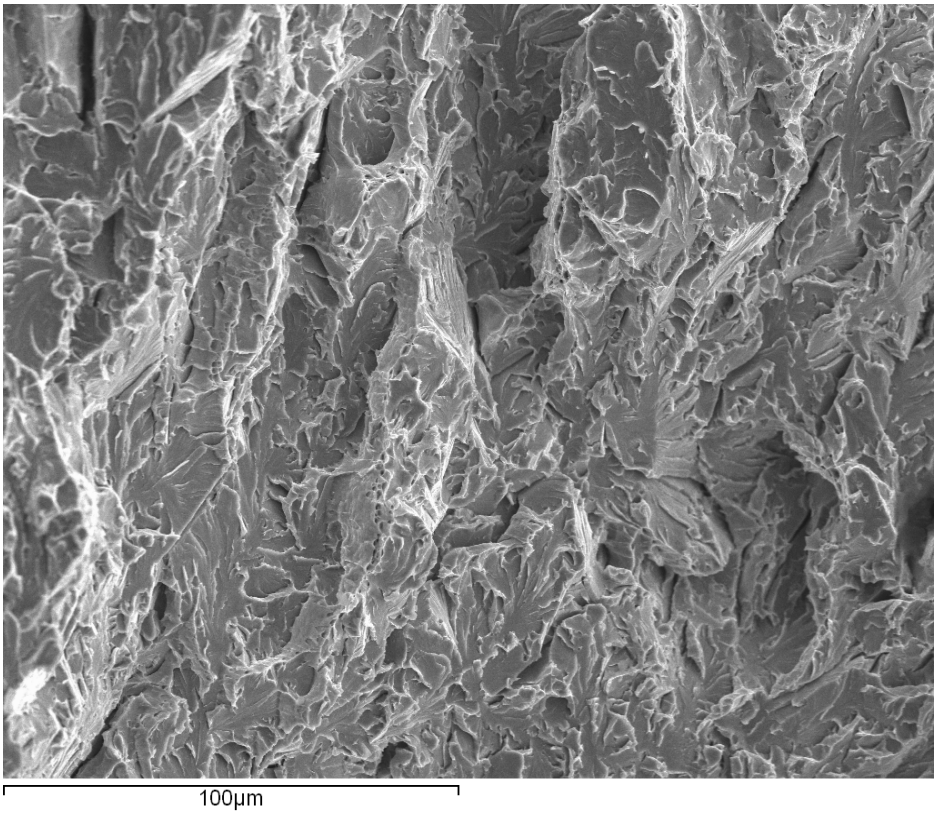
(e)



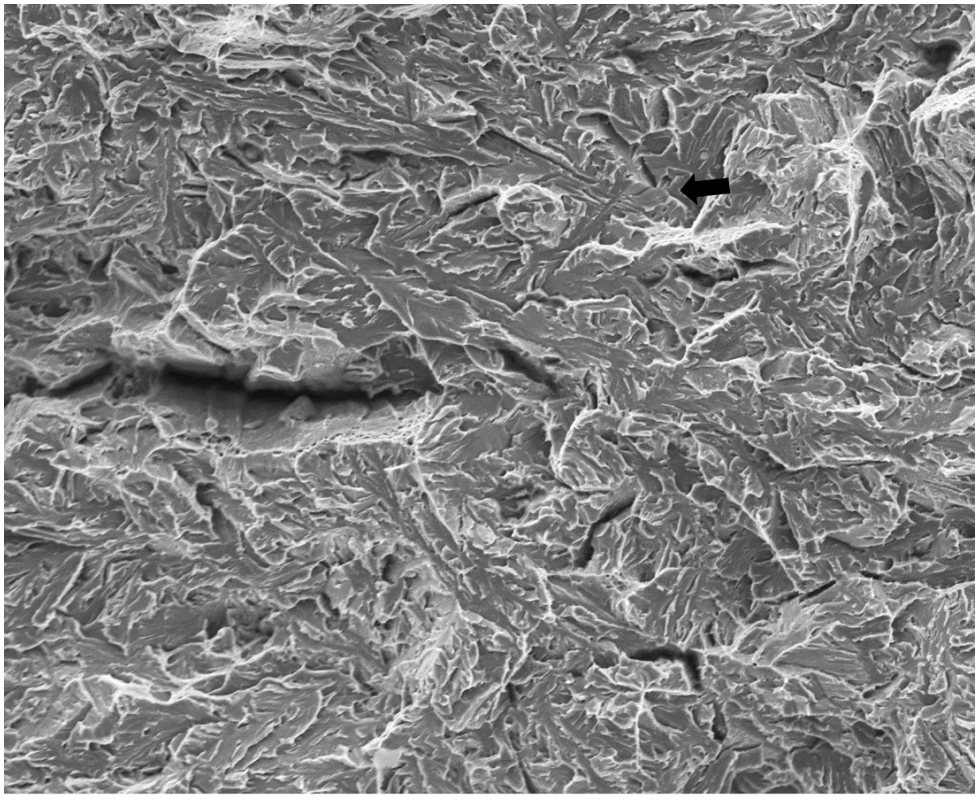
(f)



(g)



(h)

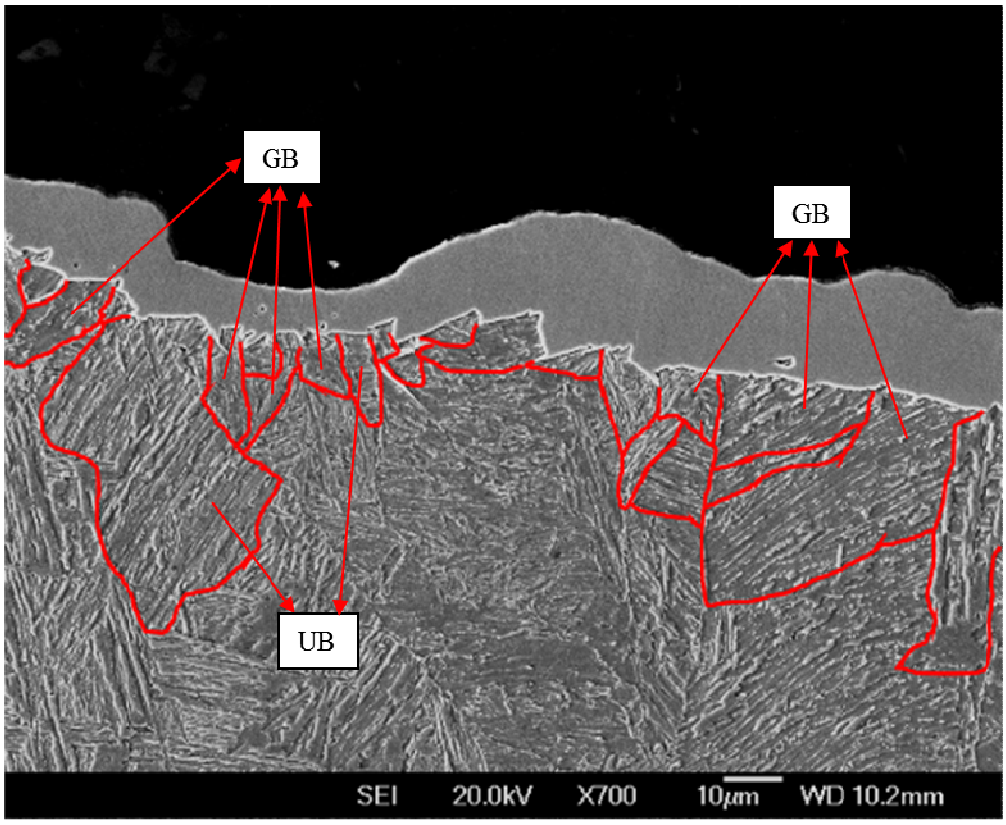


(i)

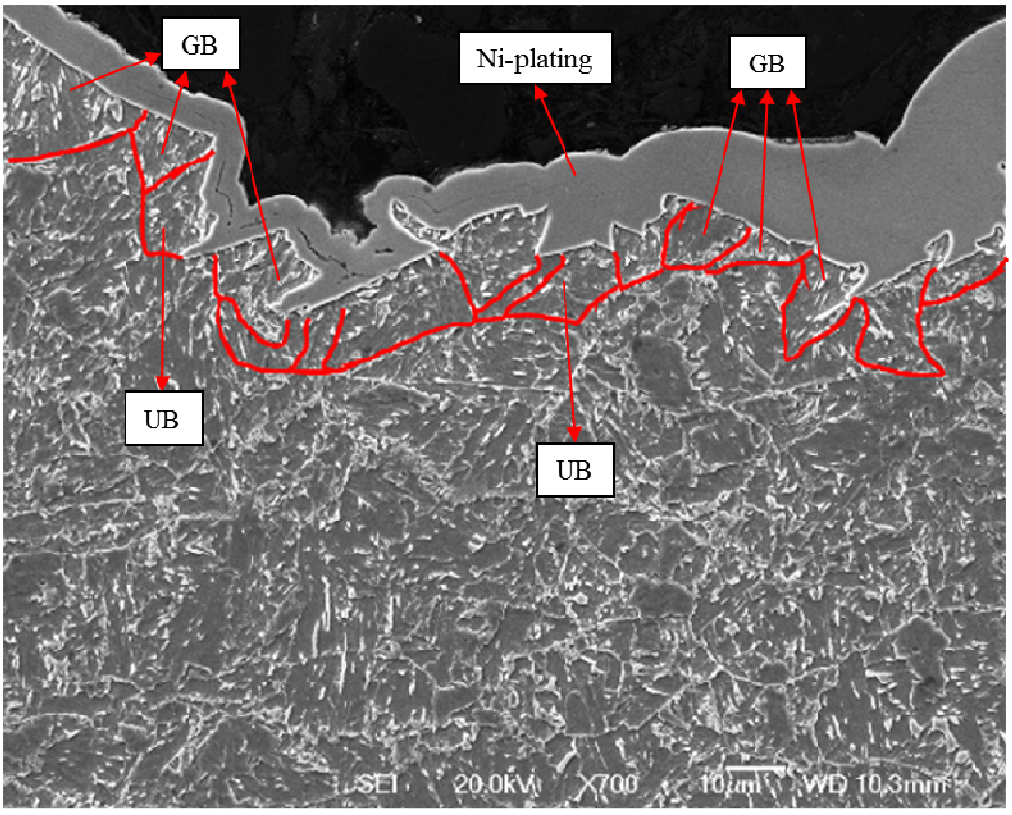
Figure 5.4 Examples of fracture surface analysis via SEM, showing transgranular cleavage fractures and the crack initiation sites (marked with black arrow). (a) T1-1, tested at -60 °C, impact energy = 21 J/cm^2; (b) T1-2, tested at -56 °C, impact energy = 25 J/cm^2; (c) T1-3, tested at -85 °C, impact energy = 11 J/cm^2; (d) T1-4, tested at -187 °C, impact energy = 5 J/cm^2; (e) T2-1, tested at -82 °C, impact energy = 11 J/cm^2; (f) T2-2, tested at -80 °C, impact energy = 38 J/cm^2; (g) T2-3, tested at -92 °C, impact energy = 33 J/cm^2; (h) T3-1, tested at -101 °C, impact energy = 37 J/cm^2; (i) T3-2, tested at -99 °C, impact energy = 28 J/cm^2.

It can be seen from Figure 5.4 that the shape of cleavage facets are generally elongated, which is consistent with pancake shaped prior austenite grains due to deformation below the recrystallization temperature (as suggested in Section 4.2). Unfortunately, the cleavage facet size is not easy to quantify because of its complexity. Therefore, instead of facet size quantification, the Unit Crack Path (UCP) through sectioned fracture surface was measured, covering a total length of fracture surface with no less than 1.5 mm, and the sizes of the UCP were then compared with the Bainite Packet Size (BPS), since it has been reported in literature that the bainite packet size is linked with cleavage resistance, especially with unit crack path in low carbon bainitic steels (Brozzo et al., 1977, Gao et al., 2012, Medina et al., 2014), as mentioned in Section 2.2.5.2. Figure 5.5 shows examples of the sectioned fracture surface of investigated steels, and the UCP length was measured using ImageJ software, the different types of bainite along a crack were identified and marked on the graphs. It can be seen from the figure that the cracks tend to propagate through several packets of granular bainite without any significant / obvious deviation (or plastic deformation), indicating that the granular bainite has larger crystallographic packet size and is not effective on resisting crack propagation, which is consistent with findings by Caballero et al. (2012). Table 5.4 shows the results of UCP and BPS quantification, the bainite packet size is determined as a cluster where bainitic ferrite laths are aligning in the same orientation / direction (Bhadeshia, 2001, Wang et al., 2006). It has been found that the average UCP / BPS ratio varies from 1.33 to 1.59 in the different samples, indicating that the fracture behaviour is connected with the microstructure features, especially the bainite packet size, which is consistent with findings reported in the literature that the UCP / BPS ratio tend to between 1.3 to 1.5 depending on the different types of bainitic structures (Ohmori et al., 1974, Brozzo et al.,

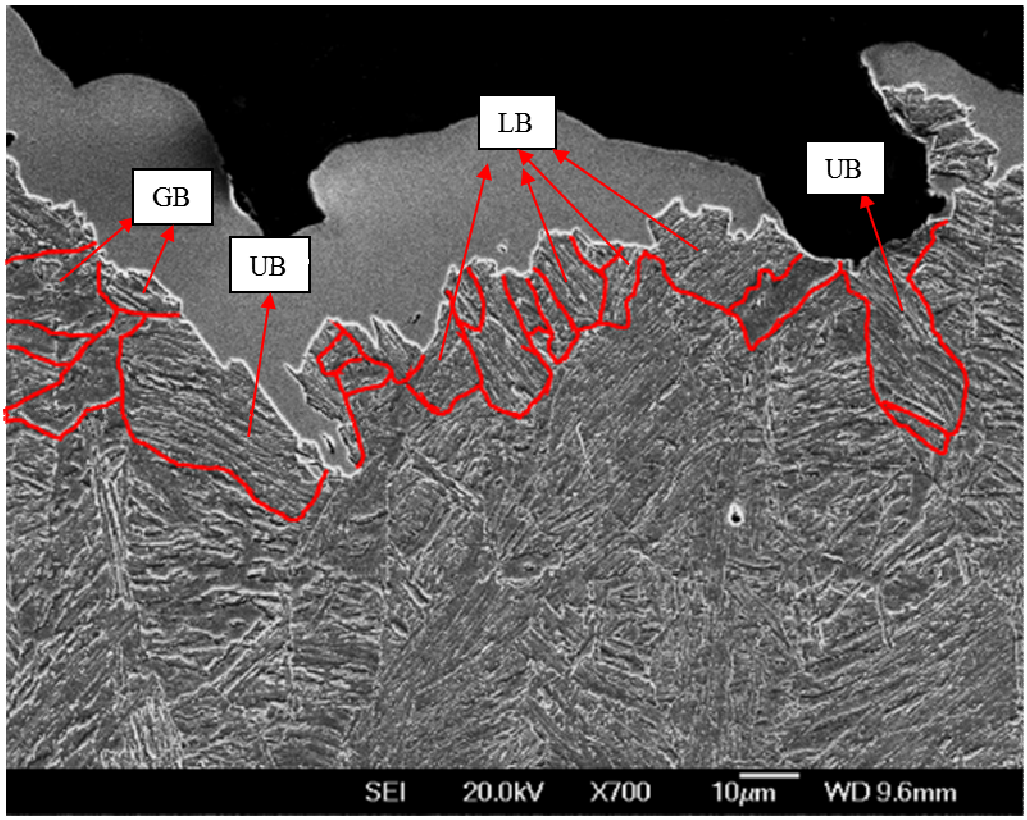
1977, Medina et al., 2014). Table 5.4 indicates that for steels with DBTT below -60 °C, the average UCP tends to be smaller than 13.5 μm and the average BPS smaller than 9 μm, while for those steels having higher DBTT (above -30 °C), the average UCP and BPS are larger than 14 μm and 9 μm, respectively. It can therefore be concluded that smaller BPS will result in better impact toughness for the investigated banitic steel products, although the role of the type of bainite (upper, lower or granular) that forms has not yet been considered. In Figure 5.6, the relationship between BPS and UCP is also plotted, although there are some variations on BPS and UCP measurement results, the general tendency that large UCP size corresponds with large BPS is still obvious.


GB
GB
UB
SEI 20.0kV X700 10μm WD 10.2mm

(a)


GB
Ni-plating
GB
UB
UB
SEI 20.0kV X700 10μm WD 10.3mm

(b)



(c)

Figure 5.5 Example SEM images of sectioned fracture surfaces of investigated steels. (a) T1-1; (b) T2-1 and (c) T3-2. All Ni-plated and then sectioned perpendicular to the fracture surface, polished and etched with 2% nital.

Table 5.4 Summary of UCP and BPS of the investigated steels.

Trial	T1				T2			T3	
Strip	T1-1	T1-2	T1-3	T1-4	T2-1	T2-2	T2-3	T3-1	T3-2
CT / °C	453	411	393	290	347	314	253	400	390
UCP / μm	16.5 ± 3.1	15 ± 2.9	14 ± 2.1	13.5 ± 2.3	12.6 ± 2	13.5 ± 2.6	11 ± 1.4	11 ± 1.6	10.5 ± 2.1
BPS / μm	12.1 ± 2.8	11.3 ± 1.9	10 ± 2.1	8.7 ± 1.1	8.1 ± 2	8.8 ± 1.5	6.9 ± 1.1	7.2 ± 1.3	7 ± 1.1
UCP/BPS	1.36 ± 0.4	1.33 ± 0.3	1.4 ± 0.4	1.55 ± 0.3	1.56 ± 0.5	1.53 ± 0.4	1.59 ± 0.3	1.53 ± 0.4	1.5 ± 0.4

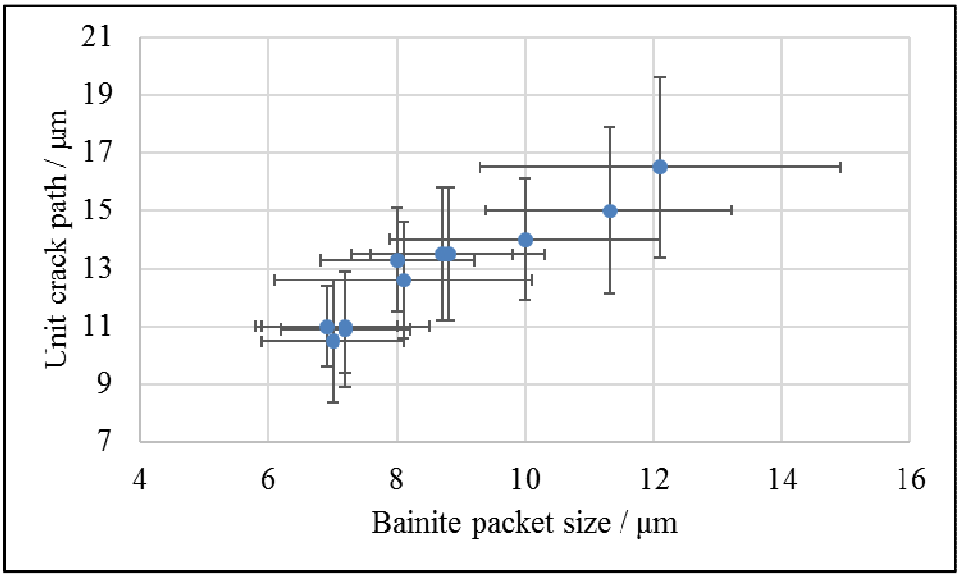


Figure 5.6 Relationship between bainite packet size (BPS) and unit crack path (UCP).

Suggested by the relationship between the UCP and BPS, the bainite packet size (BPS) can be regarded as one unit where the crack does not need to deviate when propagating through. Therefore, it is possible to present the fracture stress for a cleavage crack propagating through the material as:

$$\sigma_F = [4E\gamma_m / \pi(1 - \upsilon^2)D]^{0.5} \quad (7)$$

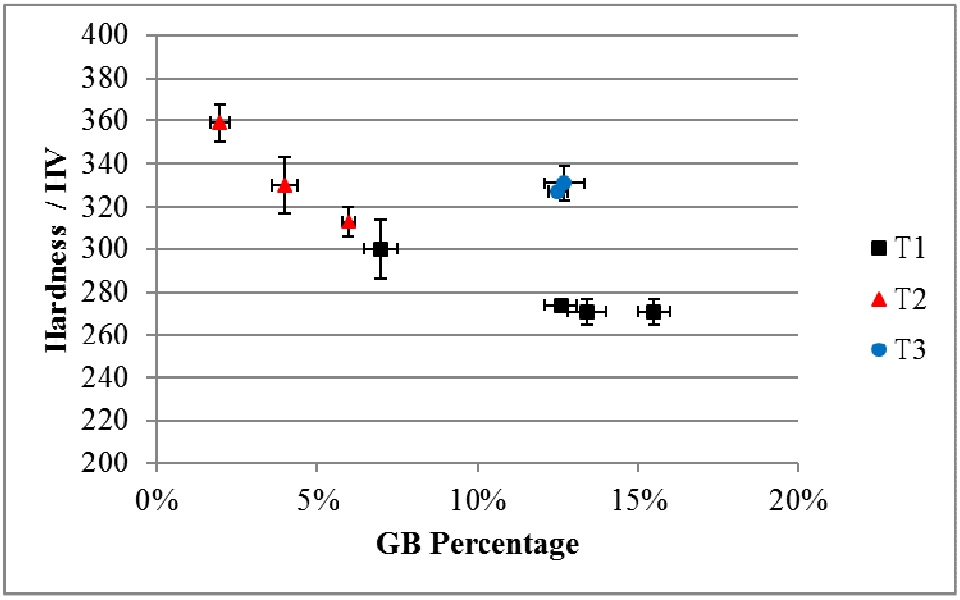
where E is Young's Modulus for ferrite, υ is Poisson's ratio for ferrite and γ_m is the effective surface energy of creating new surfaces inside the matrix, and D is the grain size (i.e. bainite packet size in this case) (Fairchild et al., 2000a, Fairchild et al., 2000b, Du et al., 2012). It can be seen from equation (7) that, with other parameters (E, γ_m and υ) fixed, smaller packet size will result in higher fracture stress, and therefore more energy can be absorbed before fracture, indicating good impact toughness of the material.

5.4 Effect of Bainite Phase Balance on Hardness and Impact Toughness

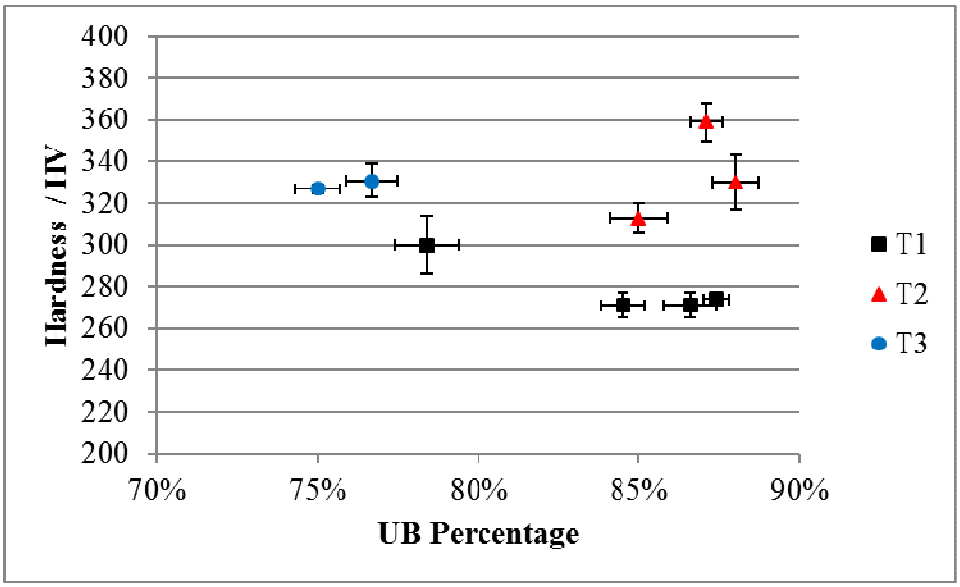
As reviewed in Chapter 2 and from the fracture surface analysis in Section 4.3, the toughness of steel, especially the UCP (Unit Crack Path) length, is closely connected with the BPS (Bainite Packet Size). This section discusses the relationship between the BPS and bainite phase balance, as well as the effect of different bainite phases on both hardness and impact toughness.

Figure 5.7 presents the relationship between micro-hardness and bainite phase amount. It can be seen from the figure that the micro-hardness varies slightly with different amount of lower bainite and granular bainite in the steel, within each trial products the difference in micro-hardness is between 30 HV and 50 HV, however no obvious trend of micro-hardness with upper bainite amount was found. With the increase of granular bainite percentage, the hardness of the steel decreases; while the appearance of lower bainite amount helps increase hardness (and therefore strength) of the steels compared with those without lower bainite. However, it worth to note that although Steel T1-4 has slightly larger lower bainite amount, the hardness of this steel is still lower than T2 and T3 steels, this is probably due to the lack of V in T1 steels to provide precipitation strengthening; and hardness of T3 steels are also slightly lower than T2 steels, which could be caused by the higher coiling temperature of T3 steels (around 400 °C) than T2 steels (below 350 °C). This is because the lower bainite forms at lower temperature compared to granular bainite and has finer sheaves and the precipitate of fine carbides within the ferritic laths in lower bainite helps increase the hardness; also, due to the addition of V in T2 and T3 series steels, the hardness of the steels can be further

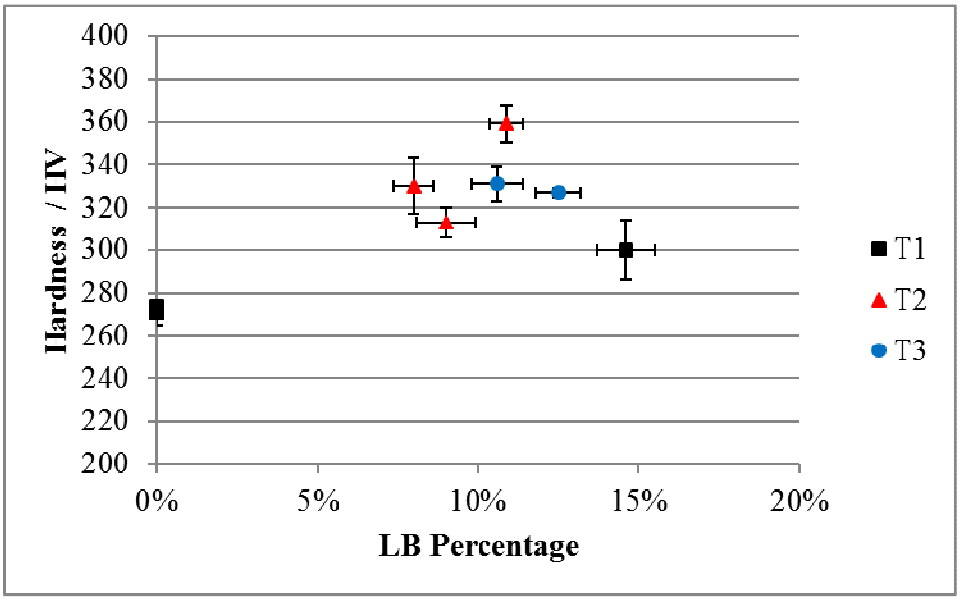
increased (Bhadeshia, 2001, Bhadeshia and Honeycombe, 2006, Yu, 2006, Yi et al., 2008).



(a)



(b)



(c)

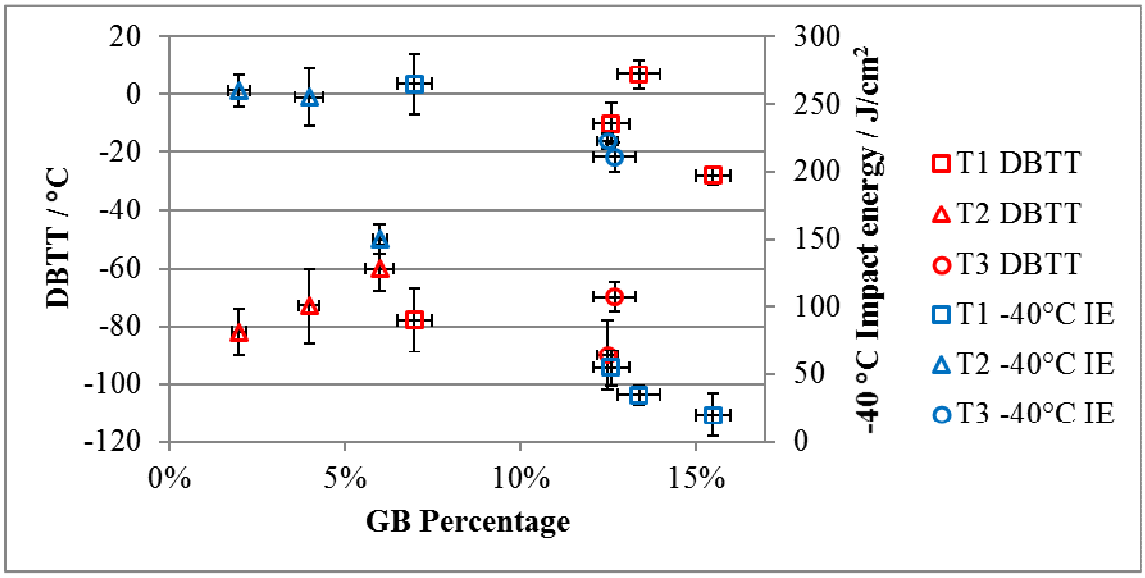
Figure 5.7 Effect of bainite phase balance on micro-hardness. (a) granular bainite effect; (b) upper bainite effect; (c) lower bainite effect.

Figure 5.8 shows the relationship between DBTT / Impact Energy (IE) at -40 °C and the amount of bainitic phases in the steels (as the -40 °C impact energy is a toughness criterion for industrial design). Again it seems that there is no clear relationship between impact toughness and upper bainite amount from Figure 5.8, however, it can be seen that impact toughness decreases with the increasing granular bainite percentage, while with the increase of lower bainite the DBTT decreases and the -40 °C impact energy increases significantly, indicating good impact toughness of the steels. This is consistent with literature findings (Bhadeshia, 2001) that the change in toughness is due to the fact that carbides formed in lower bainite will be much finer than those formed between bainite sheaves in upper bainite. It is well known that during a fracture process, brittle particles, such as cementite (or other kinds of carbide) will crack through its thickness direction and if the stress is large enough the crack will then propagate into the matrix and eventually result in final cleavage fracture (Fairchild et al., 2000a). The fracture

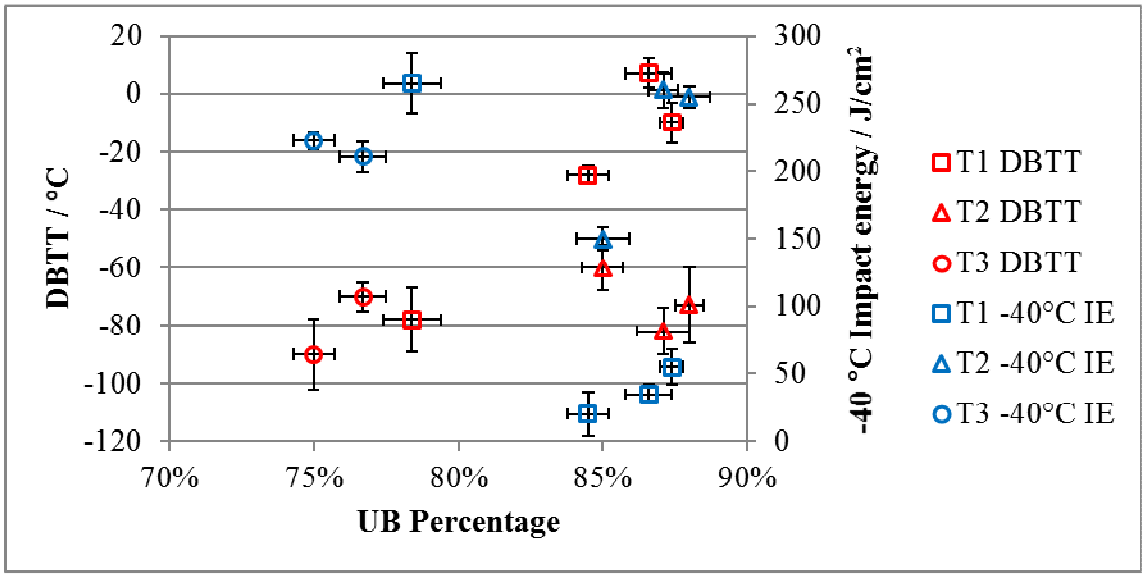
stress for cleavage fracture propagation is given by the equation below (Bhadeshia, 2001, Yang and Qiang, 2009, Du et al., 2012):

$$\sigma_F = [4E\gamma_p / \pi(1 - \upsilon^2)c]^{0.5} \quad (8)$$

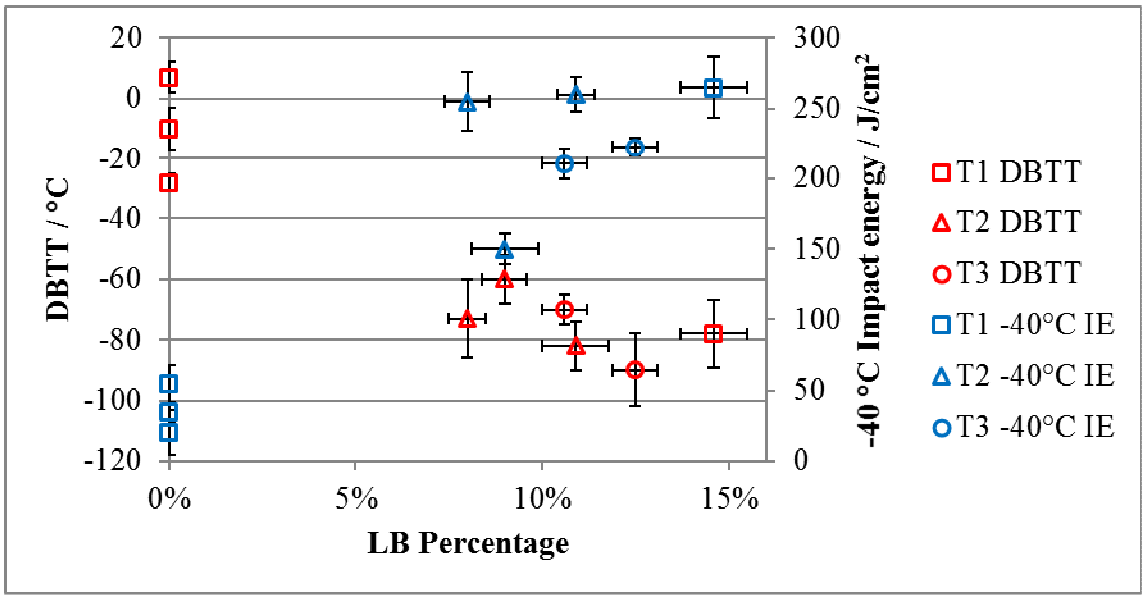
where E is Young's Modulus for ferrite, υ is Poisson's ratio for ferrite and γ_p is the effective surface energy of creating new surfaces between the particle and matrix, and c is the thickness of the cementite or carbide which produces a micro-crack at its thickness direction (i.e. the length of an initial micro-crack). As indicated by equation (8), the fracture stress is affected by the cementite / carbide thickness, c, therefore when for fracture to occur, the micro-cracks in these fine carbides in lower bainite (as summarised in Table 4.2) need higher fracture stress to propagate into the matrix and result in cleavage fracturing, which means more energy will be absorbed before cleavage fracture occurs and therefore better toughness is seen for lower bainite compared to upper bainite. Although the investigated samples did not have fully lower bainite microstructure, in accordance with literature findings (Brozzo et al., 1977, Rancel et al., 2011, Abbaszadeh et al., 2012, Caballero et al., 2012), the presence of lower bainite appears to help improve the impact toughness of these steels while granular bainite is thought detrimental to impact toughness (as mentioned above).


20
0
-20
-40
-60
-80
-100
-120
DBTT / °C
300
250
200
150
100
50
0
-40 °C Impact energy / J/cm²
0%
5%
10%
15%
GB Percentage
T1 DBTT
T2 DBTT
T3 DBTT
T1 -40°C IE
T2 -40°C IE
T3 -40°C IE

(a)


20
0
-20
-40
-60
-80
-100
-120
DBTT / °C
300
250
200
150
100
50
0
-40 °C Impact energy / J/cm²
70%
75%
80%
85%
90%
UB Percentage
T1 DBTT
T2 DBTT
T3 DBTT
T1 -40°C IE
T2 -40°C IE
T3 -40°C IE

(b)

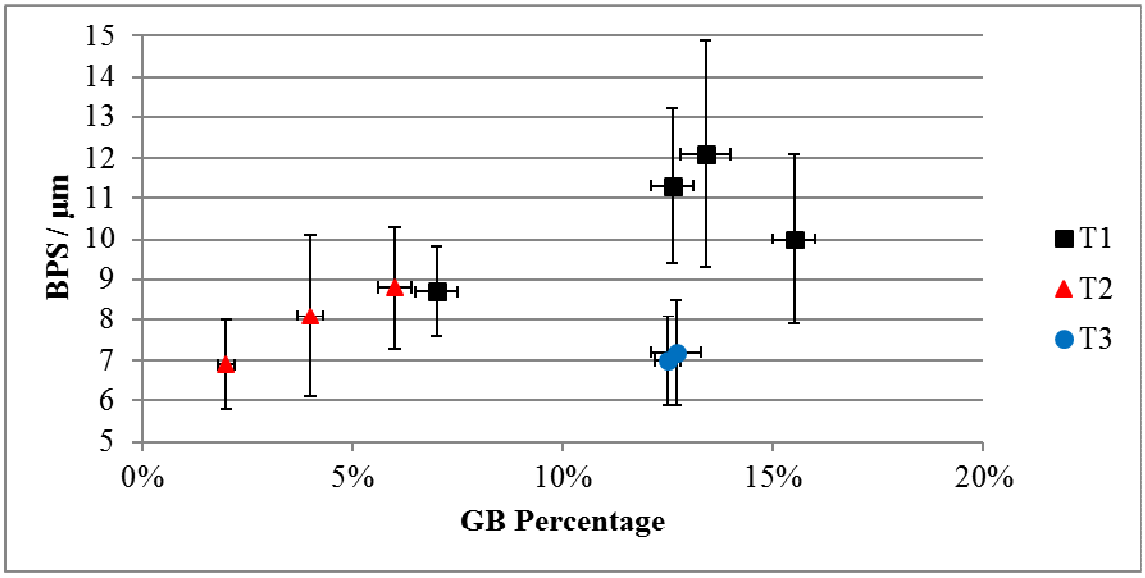


(c)

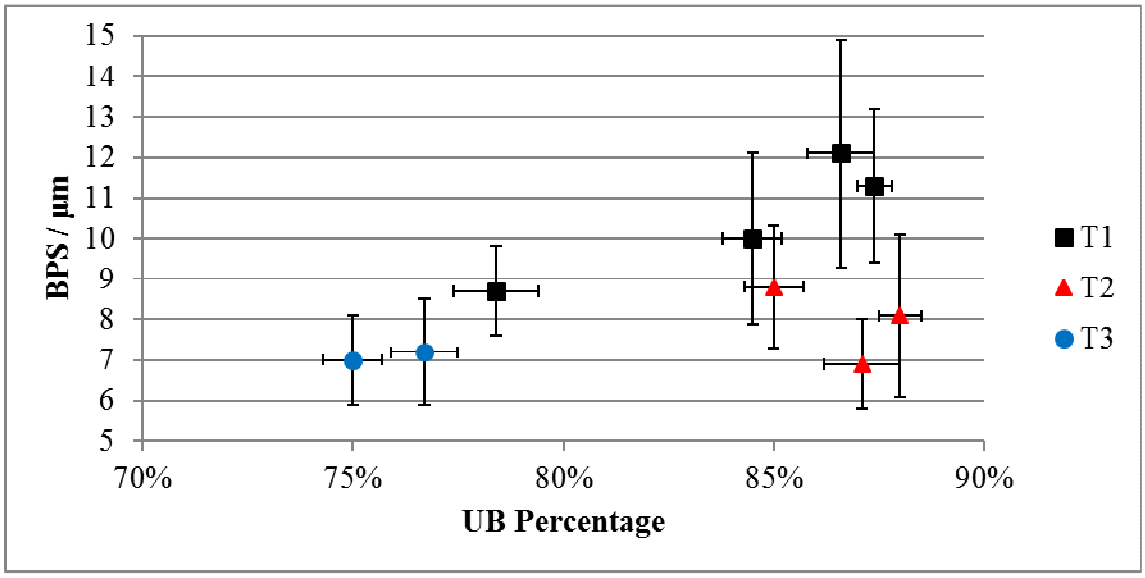
Figure 5.8 Relationship between impact toughness and bainite phase balance. (a) granular bainite; (b) upper bainite; (c) lower bainite.

Figure 5.9 plots the bainite packet size (BPS) against the amount of granular bainite, upper bainite and lower bainite in the investigated steels. Although the bainite packet size measurements have shown some variations, it can still be seen from the figure that with increased granular bainite and upper bainite amount the bainite packet size has a trend to increase, however, the correlations do vary from one trial to another, e.g. T3 samples have an "offset" on granular bainite amount – bainite packet size relationship from T1 and T2, but still show same trend – i.e. the bainite packet size increases with increased amount of granular bainite. While with the presence of lower bainite the bainite packet size generally tends to become smaller, which is probably because within prior austenite grains of similar size, the grain contains multiple bainite phases (granular bainite, upper bainite and lower bainite in this case) and will be divided into more clusters with different bainitic ferrite lath orientation, and therefore has smaller bainite packet size, compared to prior austenite grains containing just upper bainite / granular

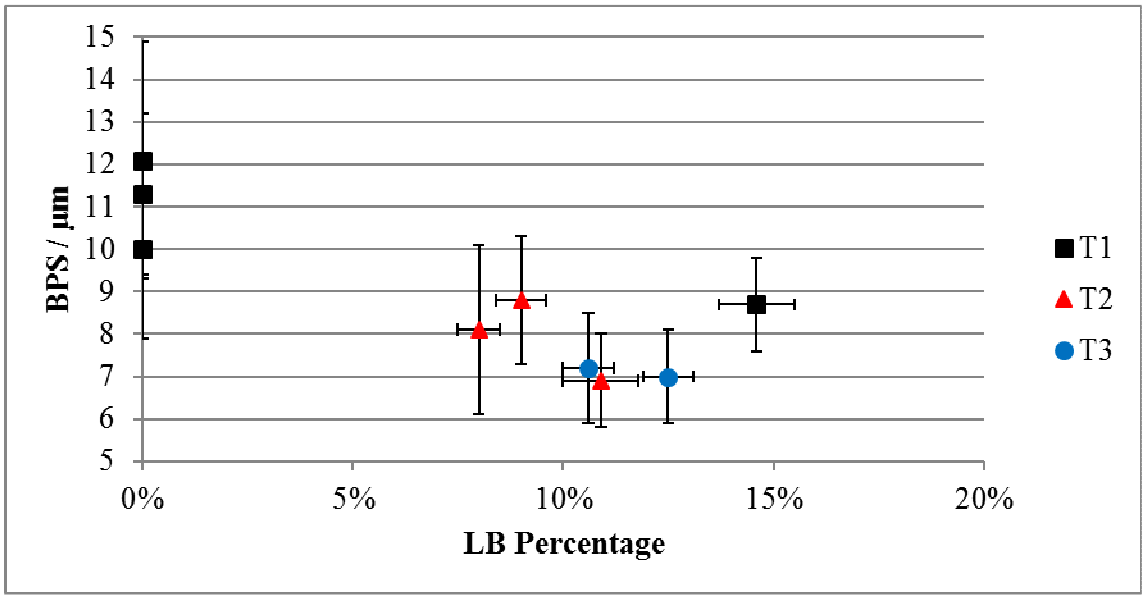
bainite. This links with the unit crack path (UCP) length and therefore fracture toughness (Section 4.3). It can then be deduced that the effect of lower bainite in improving toughness in these steels products consists of two factors: 1. due to the presence of lower bainite, the bainite packet size becomes smaller, resulting in the fracture stress that is required for crack propagation between packets to increase as well (equation (7)); 2. the lower bainite itself can improve impact toughness due to the finer cementite / carbides formed inside the microstructure, therefore the fracture stress for an initiating micro-crack to propagate into the matrix increases (equation (8)).



(a)



(b)



(c)

Figure 5.9 Relationship between BPS and bainite phase balance. (a) granular bainite; (b) upper bainite; (c) lower bainite.

5.5 Summary

From the above analysis on micro-hardness and impact toughness, it has been found that the mechanical properties, include hardness and impact toughness of the current products are linked closely with the coiling temperatures, and therefore are expected to be related to microstructures. Generally, both micro-hardness and impact toughness increases with the decrease of coiling temperature. As indicated by the fracture analysis above, the fracture behaviour of the investigated steels can be related with the phase composition and bainite packet size. And the link between mechanical properties and quantitative microstructure characterisation indicated that presence of up to 15 % lower bainite is beneficial to achieve good combination of strength (hardness) and impact toughness in these steels, therefore an investigation of the transformation behaviour during cooling and coiling process is also necessary to allow optimisation for steel production.

Although it has been found that increasing the amount of lower bainite (up to 15 %) in these strip steels, in the range investigated, is beneficial in terms of improving micro-hardness and impact toughness at the same time, while increasing the amount of granular bainite is detrimental for both mechanical properties. Therefore, it is desired to achieve a microstructure with high lower bainite amount but no granular bainite, however, taking industrial constraints (such as limitations in hot rolling, cooling and coiling processes, and the cost control in using alloying elements) into consideration, it may not be possible to obtain a fully lower bainitic microstructure, therefore a mixed microstructure of lower bainite (aiming for 15 %), upper bainite and small amount of granular bainite is desired for current steel grade. The next Chapter will analysis the

transformation behaviour based on the current products and make recommendations on how to optimise the phase balance and mechanical properties combination.

CHAPTER 6

BAINITE PHASE TRANSFORMATION BEHAVIOUR

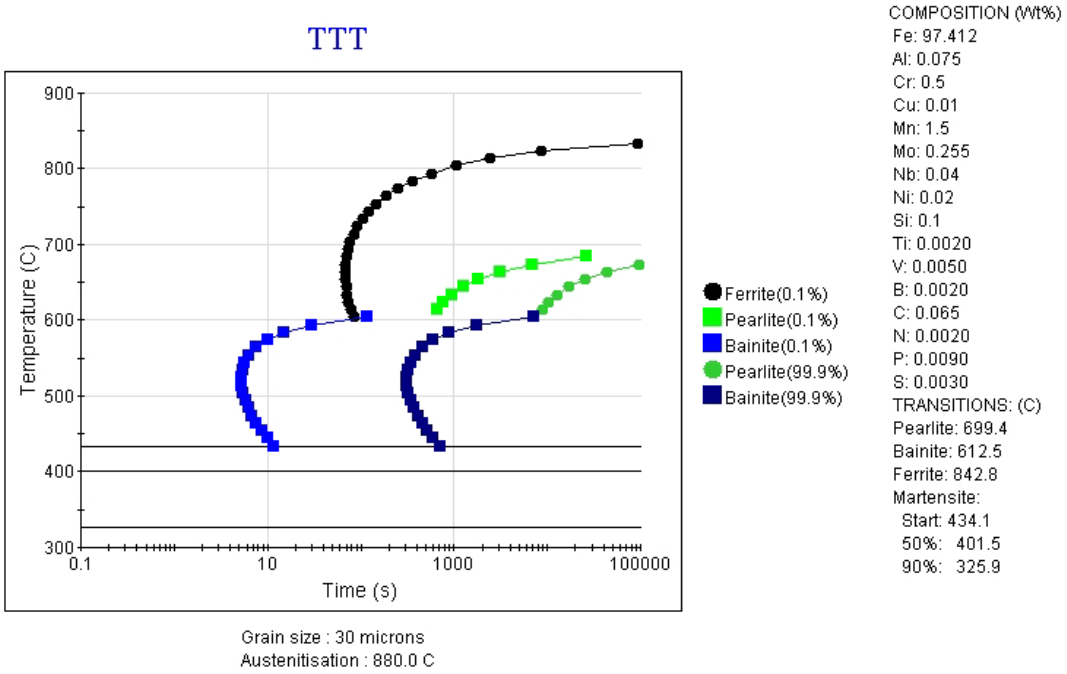
6.1 Introduction

This chapter discusses the formation of the different bainite phases during the cooling and coiling process after hot rolling. In Section 6.2, the predicted TTT / CCT curves for each steel composition are given; Section 6.3 summarises the dilatometry / Gleeble simulations used to investigate the transformation behaviour of the strip steels, and the comparison between simulation results and predicted curves is given; Section 6.4 discusses the effects of the different alloying elements and coiling processes on the low carbon hot rolled strip steel products, and then a suggested chemical composition, together with processing route, to obtain the best combination of strength and impact toughness, considering industrial constraints is discussed; in Section 6.5, the phase balance and mechanical properties of a trial strip, with chemical composition and processing route close to the suggestions is assessed.

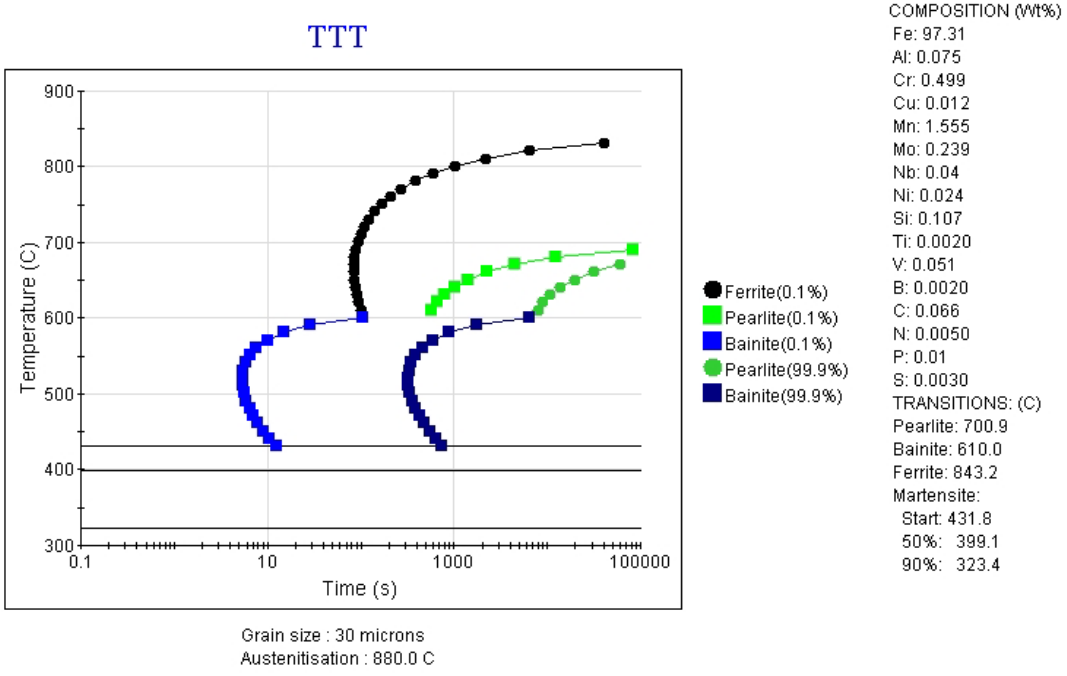
6.2 Modelling of Transformation Time Temperature (TTT) and Continuous Cooling Transformation (CCT) Curves

To determine the phase transformation behaviour of the investigated steels, two modelling tools; thermodynamic modelling software – JMatPro (version 6.0) and the online TTT / CCT diagram modelling program developed by EWI (with Professor Bhadeshia), were used to simulate the TTT and CCT curves of the investigated steels (T1, T2 and T3). In order to investigate the effect of free B on the transformation

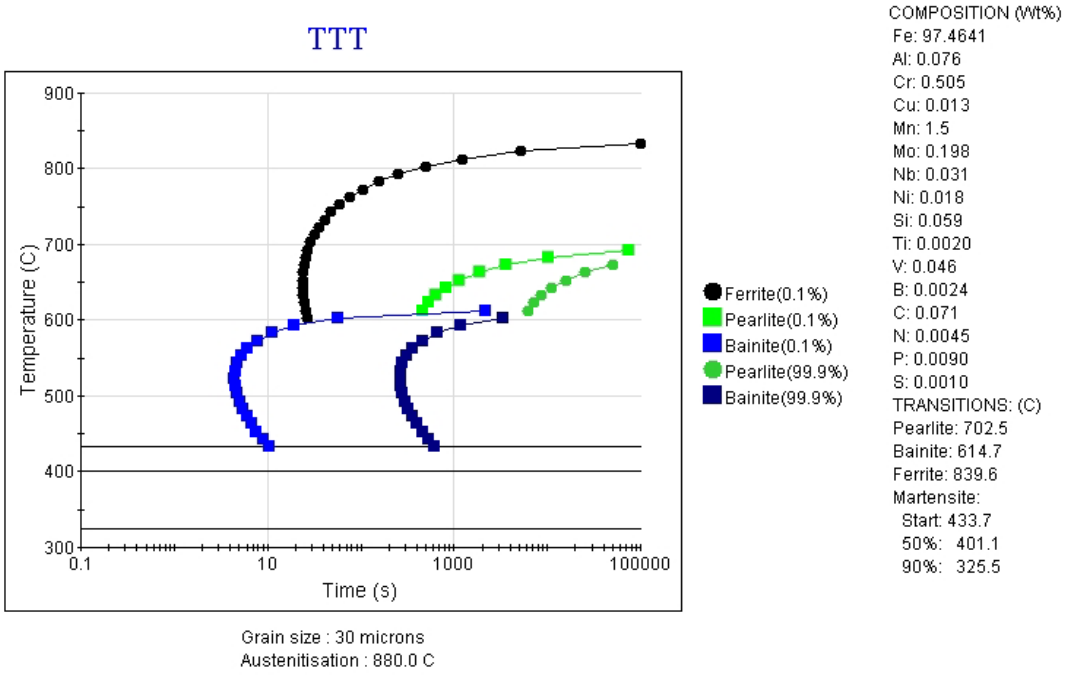
behaviour, another chemical composition (marked as T0), which contains exactly the same alloying levels as T1 but without boron, was also modelled. The results given by the two models are shown below (Figures 6.1 – 6.3), the austenising temperature was set as 880 °C, which is consistent with the finishing rolling temperature in the production line, and the prior austenite grain size was set as 30 μm, determined from the etched microstructure of the samples. However, it worth noting that both models have their limitations and may not perfectly predict the transformation behaviours of the investigated steels. For example, JMatPro assumes the prior austenite grains to be equiaxed (while in real products the austenite grains will be deformed into pancake shape after hot rolling), and the EWI model does not take prior austenite grain size in to consideration. Neither models take into account the deformed / elongated austenite grains having retained strain in them, which will also affect the transformation behaviour.


TTT
Temperature (C)
900
800
700
600
500
400
300
0.1
10
1000
100000
Time (s)
Ferrite(0.1%)
Pearlite(0.1%)
Bainite(0.1%)
Pearlite(99.9%)
Bainite(99.9%)
COMPOSITION (Wt%)
Fe: 97.412
Al: 0.075
Cr: 0.5
Cu: 0.01
Mn: 1.5
Mo: 0.255
Nb: 0.04
Ni: 0.02
Si: 0.1
Ti: 0.0020
V: 0.0050
B: 0.0020
C: 0.065
N: 0.0020
P: 0.0090
S: 0.0030
TRANSITIONS: (C)
Pearlite: 699.4
Bainite: 612.5
Ferrite: 842.8
Martensite:
Start: 434.1
50%: 401.5
90%: 325.9
Grain size : 30 microns
Austenitisation : 880.0 C

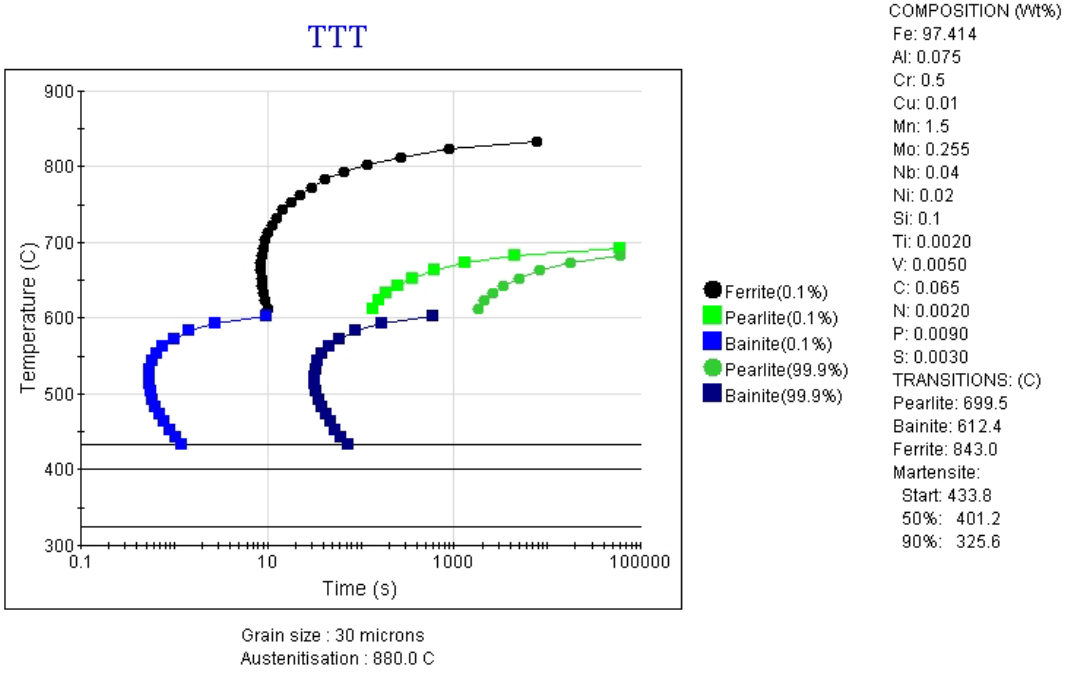
(a)


TTT
Temperature (C)
900
800
700
600
500
400
300
0.1
10
1000
100000
Time (s)
Ferrite(0.1%)
Pearlite(0.1%)
Bainite(0.1%)
Pearlite(99.9%)
Bainite(99.9%)
COMPOSITION (Wt%)
Fe: 97.31
Al: 0.075
Cr: 0.499
Cu: 0.012
Mn: 1.555
Mo: 0.239
Nb: 0.04
Ni: 0.024
Si: 0.107
Ti: 0.0020
V: 0.051
B: 0.0020
C: 0.066
N: 0.0050
P: 0.01
S: 0.0030
TRANSITIONS: (C)
Pearlite: 700.9
Bainite: 610.0
Ferrite: 843.2
Martensite:
Start: 431.8
50%: 399.1
90%: 323.4
Grain size : 30 microns
Austenitisation : 880.0 C

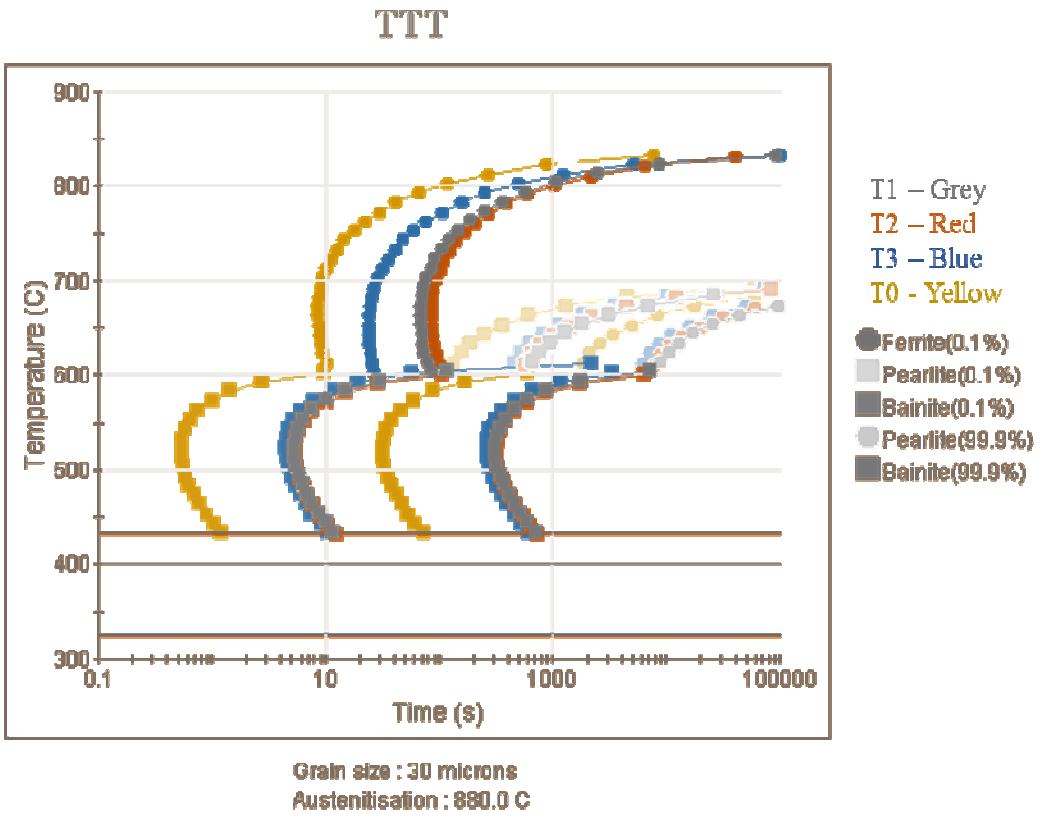
(b)


TTT
Temperature (C)
Time (s)
900
800
700
600
500
400
300
0.1
10
1000
100000
Ferrite(0.1%)
Pearlite(0.1%)
Bainite(0.1%)
Pearlite(99.9%)
Bainite(99.9%)
COMPOSITION (Wt%)
Fe: 97.4641
Al: 0.076
Cr: 0.505
Cu: 0.013
Mn: 1.5
Mo: 0.198
Nb: 0.031
Ni: 0.018
Si: 0.059
Ti: 0.0020
V: 0.046
B: 0.0024
C: 0.071
N: 0.0045
P: 0.0090
S: 0.0010
TRANSITIONS: (C)
Pearlite: 702.5
Bainite: 614.7
Ferrite: 839.6
Martensite:
Start: 433.7
50%: 401.1
90%: 325.5
Grain size : 30 microns
Austenitisation : 880.0 C

(c)

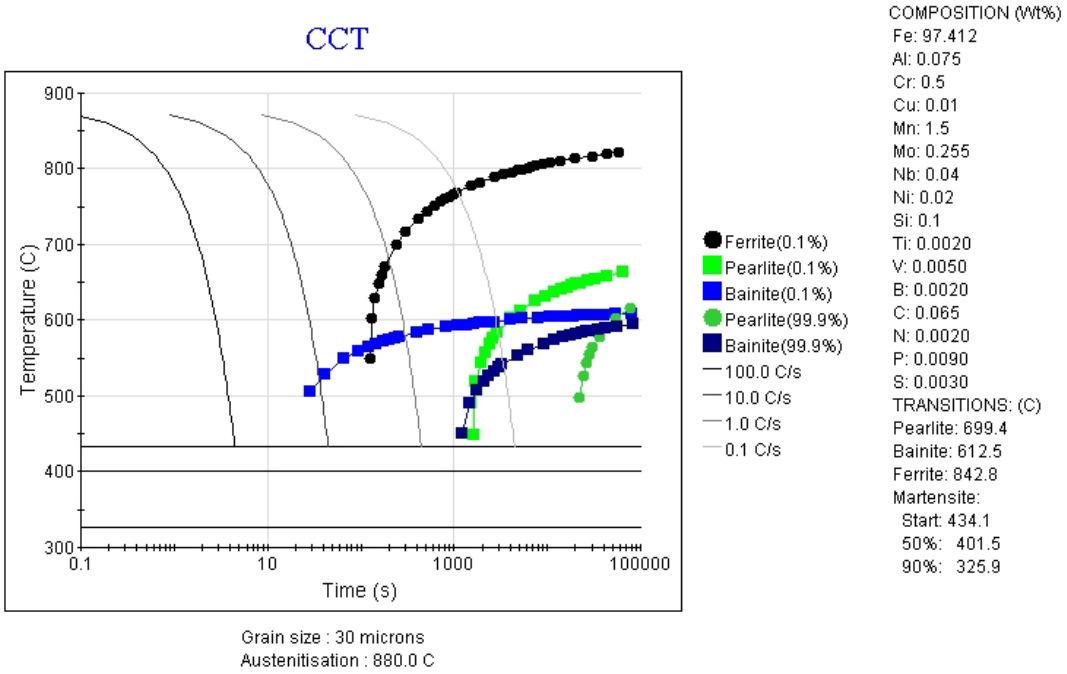

TTT
Temperature (C)
Time (s)
900
800
700
600
500
400
300
0.1
10
1000
100000
Ferrite(0.1%)
Pearlite(0.1%)
Bainite(0.1%)
Pearlite(99.9%)
Bainite(99.9%)
COMPOSITION (Wt%)
Fe: 97.414
Al: 0.075
Cr: 0.5
Cu: 0.01
Mn: 1.5
Mo: 0.255
Nb: 0.04
Ni: 0.02
Si: 0.1
Ti: 0.0020
V: 0.0050
C: 0.065
N: 0.0020
P: 0.0090
S: 0.0030
TRANSITIONS: (C)
Pearlite: 699.5
Bainite: 612.4
Ferrite: 843.0
Martensite:
Start: 433.8
50%: 401.2
90%: 325.6
Grain size : 30 microns
Austenitisation : 880.0 C

(d)

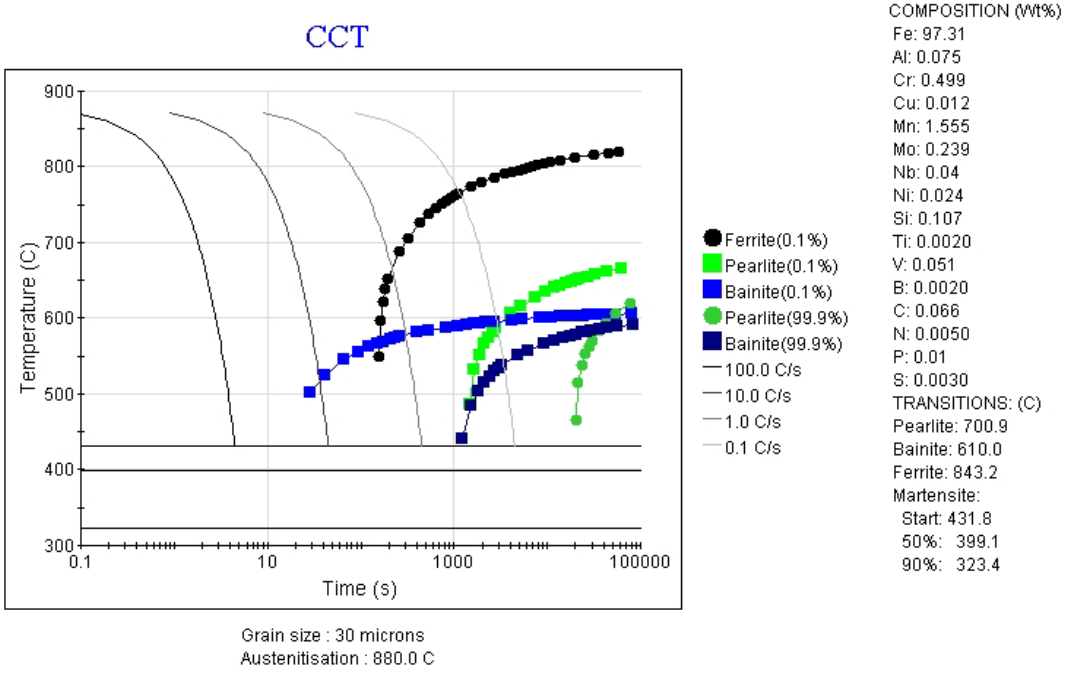


(e)

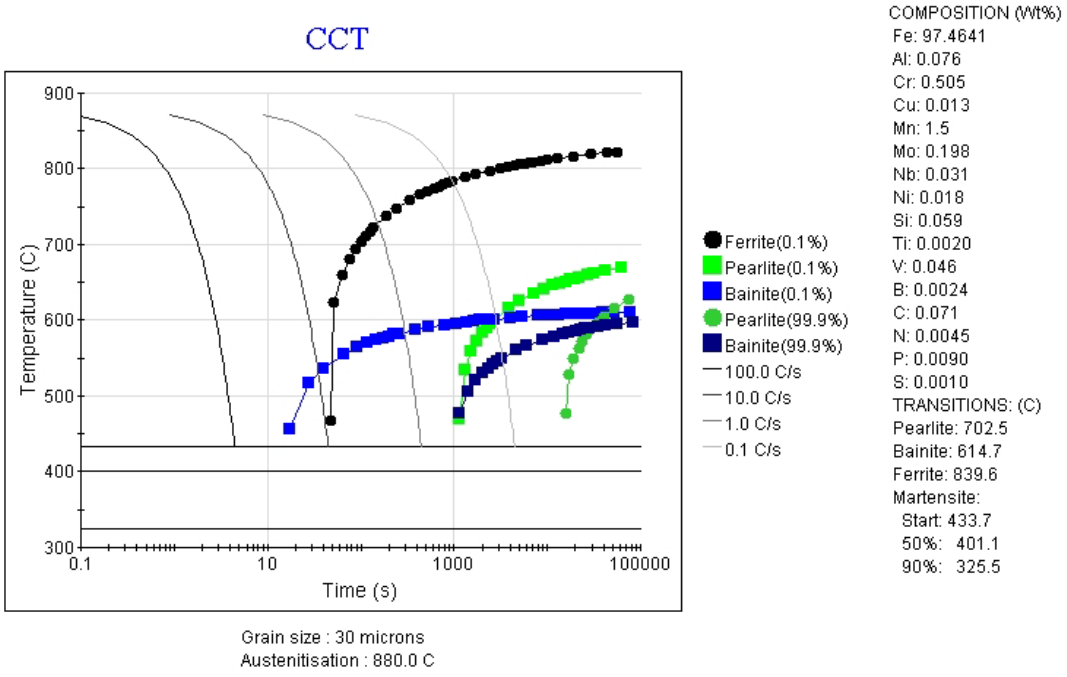
Figure 6.1 TTT diagrams modelled by JMatPro software for (a) T1 steels, (b) T2 steels, (c) T3 steels, (d) T0 composition (T1 chemical without B) and (d) comparison of the 3 trials and T0.


CCT
Temperature (C)
900
800
700
600
500
400
300
0.1
10
1000
100000
Time (s)
Ferrite(0.1%)
Pearlite(0.1%)
Bainite(0.1%)
Pearlite(99.9%)
Bainite(99.9%)
100.0 C/s
10.0 C/s
1.0 C/s
0.1 C/s
COMPOSITION (Wt%)
Fe: 97.412
Al: 0.075
Cr: 0.5
Cu: 0.01
Mn: 1.5
Mo: 0.255
Nb: 0.04
Ni: 0.02
Si: 0.1
Ti: 0.0020
V: 0.0050
B: 0.0020
C: 0.065
N: 0.0020
P: 0.0090
S: 0.0030
TRANSITIONS: (C)
Pearlite: 699.4
Bainite: 612.5
Ferrite: 842.8
Martensite:
Start: 434.1
50%: 401.5
90%: 325.9
Grain size : 30 microns
Austenitisation : 880.0 C

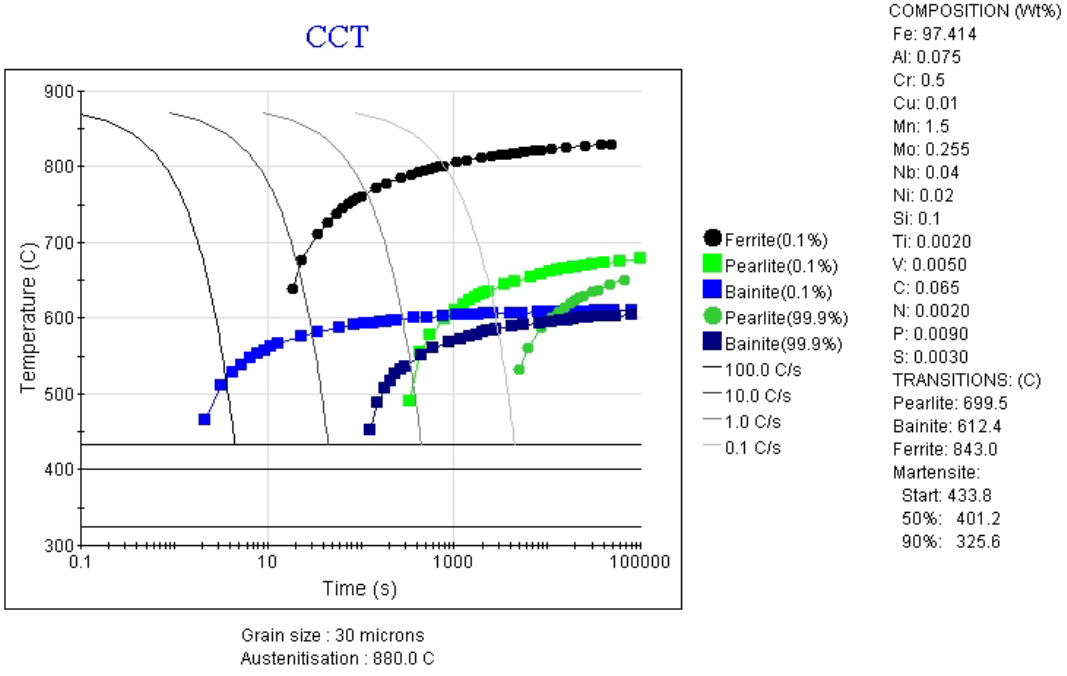
(a)


CCT
Temperature (C)
900
800
700
600
500
400
300
0.1
10
1000
100000
Time (s)
Ferrite(0.1%)
Pearlite(0.1%)
Bainite(0.1%)
Pearlite(99.9%)
Bainite(99.9%)
100.0 C/s
10.0 C/s
1.0 C/s
0.1 C/s
COMPOSITION (Wt%)
Fe: 97.31
Al: 0.075
Cr: 0.499
Cu: 0.012
Mn: 1.555
Mo: 0.239
Nb: 0.04
Ni: 0.024
Si: 0.107
Ti: 0.0020
V: 0.051
B: 0.0020
C: 0.066
N: 0.0050
P: 0.01
S: 0.0030
TRANSITIONS: (C)
Pearlite: 700.9
Bainite: 610.0
Ferrite: 843.2
Martensite:
Start: 431.8
50%: 399.1
90%: 323.4
Grain size : 30 microns
Austenitisation : 880.0 C

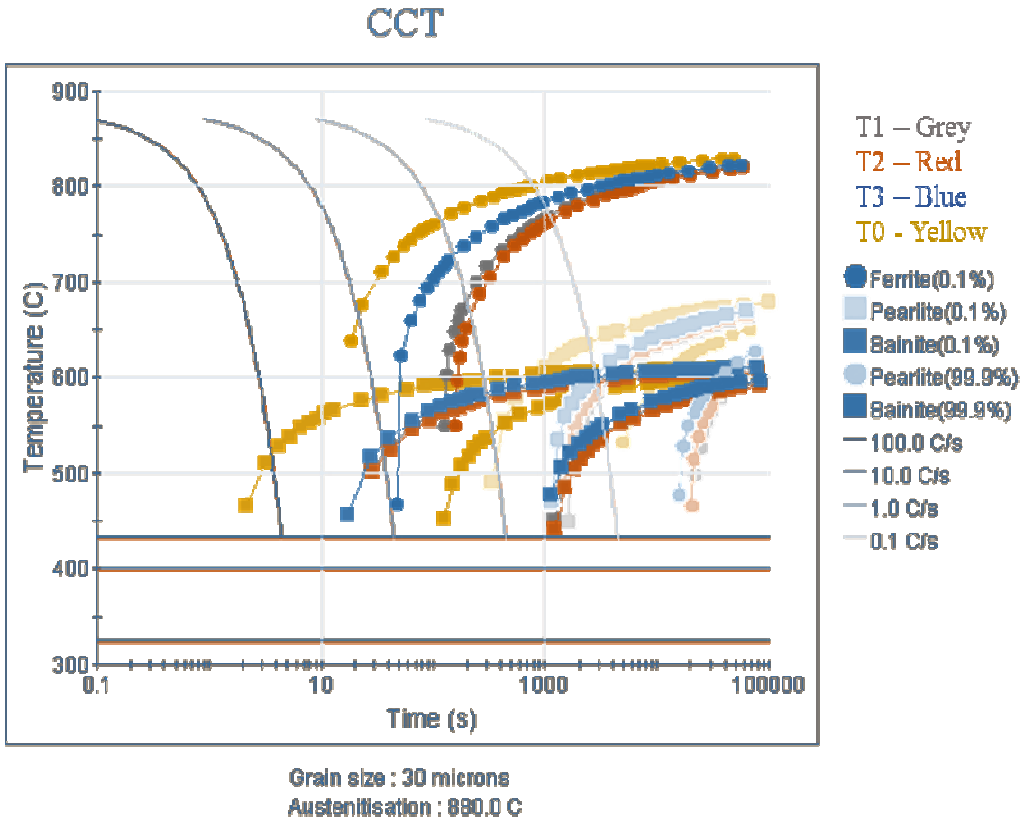
(b)


CCT
Temperature (C)
Time (s)
900
800
700
600
500
400
300
0.1
10
1000
100000
Ferrite(0.1%)
Pearlite(0.1%)
Bainite(0.1%)
Pearlite(99.9%)
Bainite(99.9%)
100.0 C/s
10.0 C/s
1.0 C/s
0.1 C/s
COMPOSITION (Wt%)
Fe: 97.4641
Al: 0.076
Cr: 0.505
Cu: 0.013
Mn: 1.5
Mo: 0.198
Nb: 0.031
Ni: 0.018
Si: 0.059
Ti: 0.0020
V: 0.046
B: 0.0024
C: 0.071
N: 0.0045
P: 0.0090
S: 0.0010
TRANSITIONS: (C)
Pearlite: 702.5
Bainite: 614.7
Ferrite: 839.6
Martensite:
Start: 433.7
50%: 401.1
90%: 325.5
Grain size : 30 microns
Austenitisation : 880.0 C

(c)


CCT
Temperature (C)
Time (s)
900
800
700
600
500
400
300
0.1
10
1000
100000
Ferrite(0.1%)
Pearlite(0.1%)
Bainite(0.1%)
Pearlite(99.9%)
Bainite(99.9%)
100.0 C/s
10.0 C/s
1.0 C/s
0.1 C/s
COMPOSITION (Wt%)
Fe: 97.414
Al: 0.075
Cr: 0.5
Cu: 0.01
Mn: 1.5
Mo: 0.255
Nb: 0.04
Ni: 0.02
Si: 0.1
Ti: 0.0020
V: 0.0050
C: 0.065
N: 0.0020
P: 0.0090
S: 0.0030
TRANSITIONS: (C)
Pearlite: 699.5
Bainite: 612.4
Ferrite: 843.0
Martensite:
Start: 433.8
50%: 401.2
90%: 325.6
Grain size : 30 microns
Austenitisation : 880.0 C

(d)



(e)

Figure 6.2 CCT diagrams modelled by JMatPro software for (a) T1 steels, (b) T2 steels, (c) T3 steels, (d) T0 composition (T1 chemical without B) and (d) comparison of the 3 trials and T0.

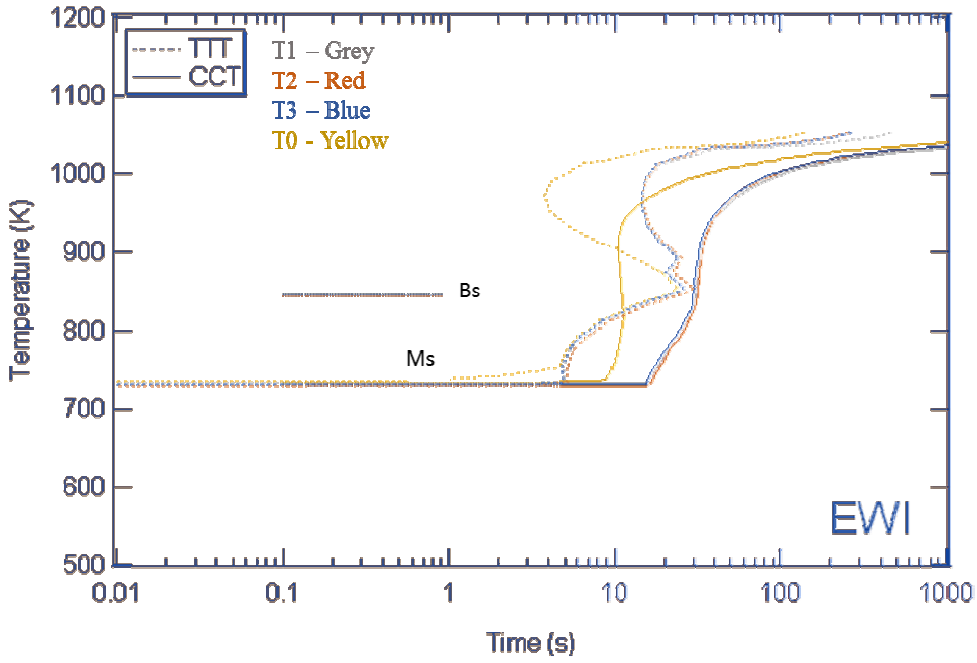


Figure 6.3 TTT / CCT diagrams modelled by EWI online tool (note the temperature is in Kelvin) for T1, T2, T3 and T0 compositions.

In Figures 6.1 and 6.2, the alloying level of each trial has been listed on the right hand side of each graph, together with the calculated bainite starting (Bs) and martensite starting (Ms) temperatures. Figure 6.3 shows both TTT and CCT curves of the four chemical compositions in the same graph, the Bs and Ms lines are also marked on the figure, however no exact numbers were given by the EWI model on Bs and Ms temperatures. Table 6.1 compares the Bs and Ms temperatures generated via modelling and calculated with equations (1) and (2). It can be seen that the Bs and Ms temperatures of the three trials are similar when calculated with the same method, however there are differences from one method to another. For Bs temperature, JMatPro gives closer prediction to equation (1) than the EWI model does, while for Ms temperature the EWI model gives similar prediction to equation (2). The reason for this is unclear.

Table 6.1 Comparison of calculated (equations (1) and (2) from Section 2.3.2.1) and modelled Bs and Ms.

	Bs / °C			Ms / °C		
	Calculated	JMatPro	EWI	Calculated	JMatPro	EWI
T1	620.4	612.5	572	457.5	434.1	457
T2	616.6	610	572	455.6	431.8	457
T3	623.4	614.7	572	455.5	433.7	457
T0	620.4	612.4	572	457.5	433.8	457

Comparing the TTT and CCT curves for the T1 and T0 compositions, JMatPro and EWI modelling results give different effects of B on delaying ferrite transformation. According to the JMatPro results, it seems that the B added into T1 steels delays both austenite – ferrite and austenite – bainite transformations, while bainite transformation is further delayed compared with ferrite transformation. However, on the contrary, the EWI model suggests that about 10 to 20 ppm B addition delays ferrite formation to a much greater extent compared with its effect on bainite formation during continuous cooling, which is more consistent with literature findings (Section 2.3.2.1) (Bhadeshia, 2001, Heller and Nuss, 2005, Anjana Deva, 2011, Lis et al., 2011, Mun et al., 2012, Sung et al., 2012) and the fully bainitic microstructure presence in the investigated samples (Sections 5.2 and 5.3). Therefore the EWI model gives better prediction in terms of boron effect on the TTT / CCT diagrams of current steel. Overall, it is clear that the 20 ppm boron addition to the steels is efficient in increasing hardenability and enabling austenite – bainite transformation during continuous cooling. However, the boron added into the steels needs to be protected so that boron can stay in solution and not forming boron nitride (BN, which is not effective in increasing hardenability of B-added steels), therefore approximately 0.075 wt% Al is added to remove N and protect B.

As mentioned in Section 3.2, the main differences between the 3 trials in chemical composition are associated with Mo and V contents. While T1 has the highest Mo content (0.255 wt%) and almost no V, T2 has similar Mo content (0.239 wt%) but 0.05 wt% V addition, and T3 has reduced Mo content (0.198 wt%) and the same V content compared with T2. There are also some small differences in C content (0.065 wt% and 0.066 wt% for T1 and T2 respectively, while 0.071 wt% for T3). It can be seen from the TTT / CCT diagrams (Figures 6.1 to 6.3) that both models suggest the V addition in T2 results in a slight move of both the TTT and CCT curves towards the right hand side compared with T1 curves, indicating the effect of 0.05 wt% addition V has effect on slightly increasing hardenability, assuming that the V is in solution; while with reduced Mo, the transformation curves of T3 tend to move towards the left hand side compared with T2 and T1, suggesting under the same cooling rate, the cooling curve will tend to cross the lower bainite region earlier for T3 steels than T1 or T2 steels. This is consistent with the microstructure quantification results, comparing steels from T3 and T1 / T2 that coiled at roughly similar temperatures (e.g. T3-2, T1-3 and T2-1), T3 steel has larger amount of lower bainite phase, which is probably as a result of the shifted CCT curve.

In summary, the two models used for TTT / CCT diagram predictions provide some general ideas on the transformation behaviours and the effects of alloying elements (boron, vanadium and molybdenum) on the phase transformation of current samples. Nevertheless, due to limitations in the two models (EWI did not consider the austenite grain size, while JMatPro did not take the deformation of austenite grains prior to phase transformation into account), there are some differences between the two modelling results. To find out more detailed phase transformation behaviours of the investigated

steels, to allow more accurate predictions to be made, experimental phase transformation characterisation was carried out.

6.3 Gleeble simulation and investigation on transformation behaviour

As mentioned in Chapter 3, due to the unavailability of the dilatometer both at the University of Birmingham and Tata Steel R&D centre, the power module of a Gleeble 3500 machine was used as an alternative way to measure the phase transformation behaviour of the investigated materials. In Section 3.6, the Gleeble method was shown to be reliable in measuring phase transformation start and finish points for a rail steel (however only over a limited cooling rate).

Figure 6.4 shows the CCT data points generated via Gleeble simulation for T1, T2 and T3 steels. However, please note that for each data point, a ±3 °C error (at maximum) exists for the temperature value (i.e. y-axis), which is not plotted in Figure 6.4, because the error is too small, and it is hard to spot even if the error bars are plotted on the graph. During Gleeble simulation, four cooling rates have been used, including 2.5 °C/s, 5 °C/s, 7.5 °C/s and 10 °C/s; the measured phase transformation starting and finishing points are marked on the figure, with T1 in red, T2 in blue and T3 in green. Unfortunately, as mentioned in Section 3.6.2, due to the limitation of the technique, the maximum cooling rate which allowed the power-temperature curve to show the full transformation process is 10 °C/s. This means a complete CCT diagram is not available via this method. Nevertheless, it is still possible to determine the transformation behaviour and the effects of alloying elements (such as B, V and Mo) through the diagram, as well as subsequent microstructure investigation and micro-hardness measurements on tested samples.

Figure 6.5 shows the comparison of CCT diagram / data points generated by Gleeble measurements (with highlighted backgrounds in yellow) and modelling results. It can be seen from both Figure 6.5 (a) and (b) that the transformation starting points determined from Gleeble simulation tests (cooling rates between 2.5 °C/s and 10 °C/s) agree well with the JMatPro modelling results and there is reasonable agreement with the EWI model curves, although there appears to be slightly lower transformation start temperatures predicted for the EWI CCT approach compared to JMatPro. However, the transformation finishing points modelled with JMatPro do not match well with experimental results. The reason for such disagreement is not clear yet (but possibly related with the prior austenite grain size input to the model) and could be further investigated in the future as a part of a following project. Nevertheless, the Gleeble results give similar trend of T3 composition results shifting slightly towards top-left side away from T1 and T2 compositions, which is also seen in both modelling results.

In Figures 6.6 and 6.7 the optical and SEM microstructures of T1 at different cooling rates have been presented, respectively. It can be seen that bainitic microstructures have been achieved at all cooling rates, as the etch reveals clear austenite grain boundaries. At low cooling rate such as 2.5 °C/s, the bainite laths are very coarse and the steel forms granular bainite and upper bainite, while with the increase of cooling rate, the bainite laths become finer, and at 10 °C/s, small amount of lower bainite packets can also be identified alongside the granular bainite and upper bainite, as shown in Figures 6.6 (d) and 6.7 (d).

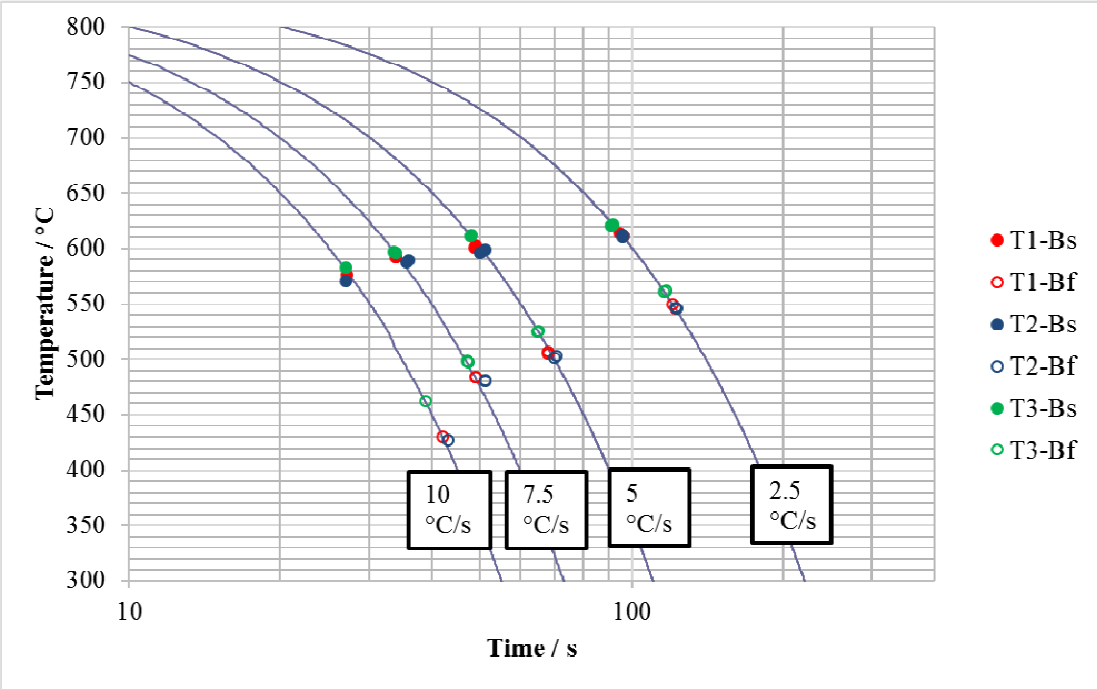
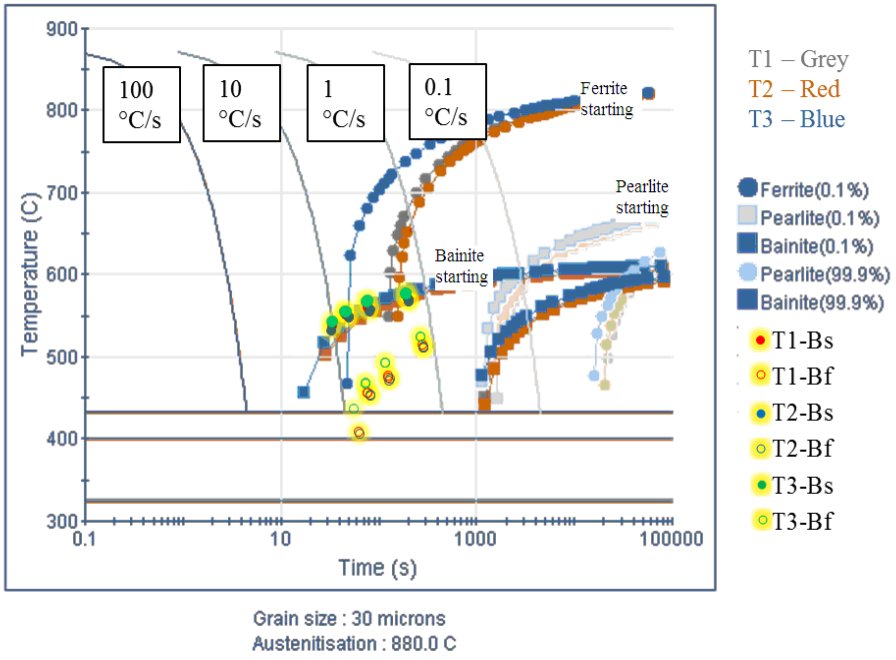
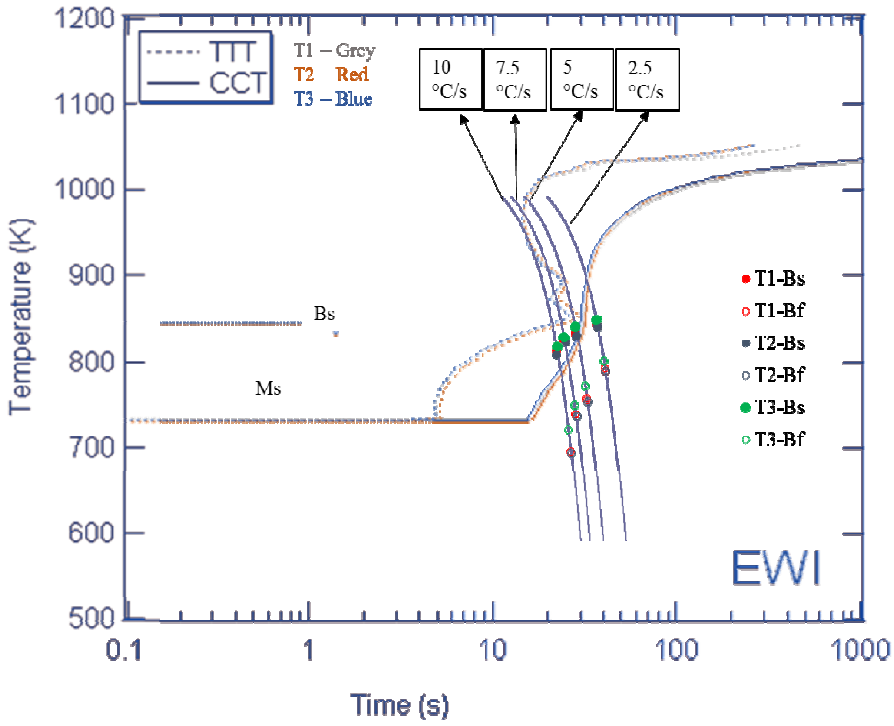


Figure 6.4 CCT diagrams of T1, T2, and T3 measured by Gleeble power-temperature method (T1 data is almost overlapped with T2 data).

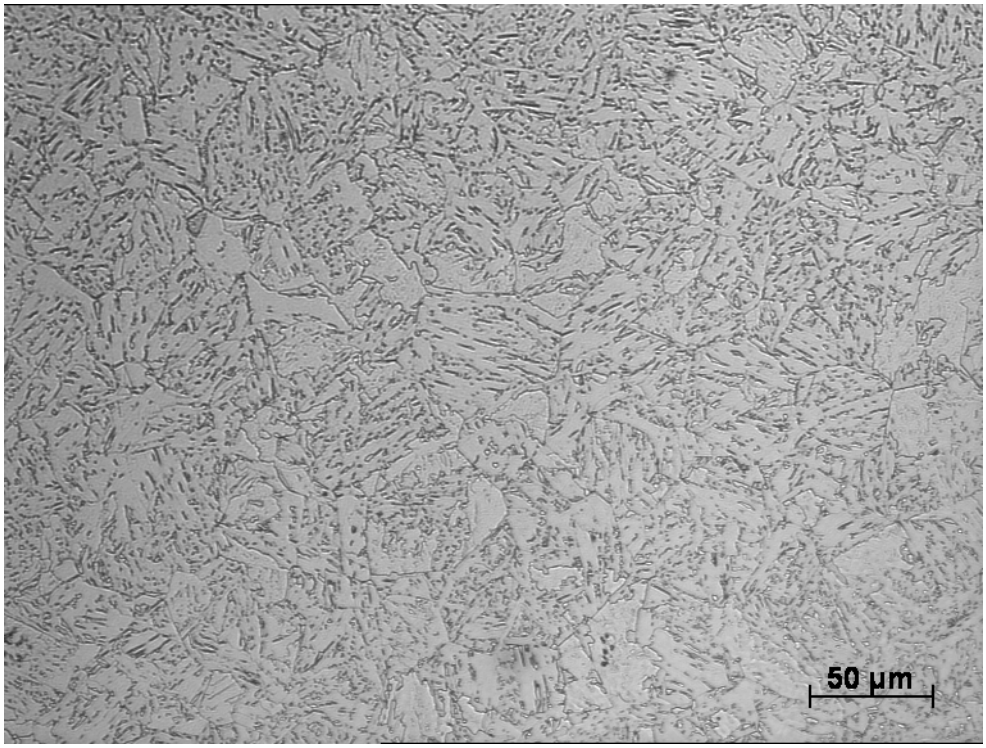


(a)

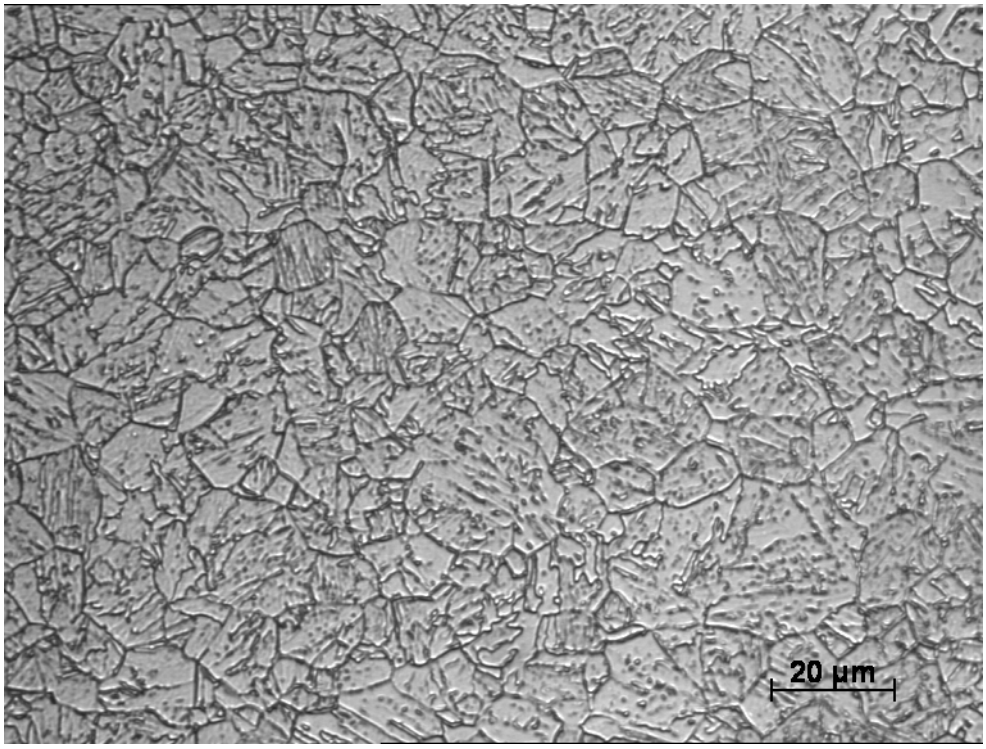


(b)

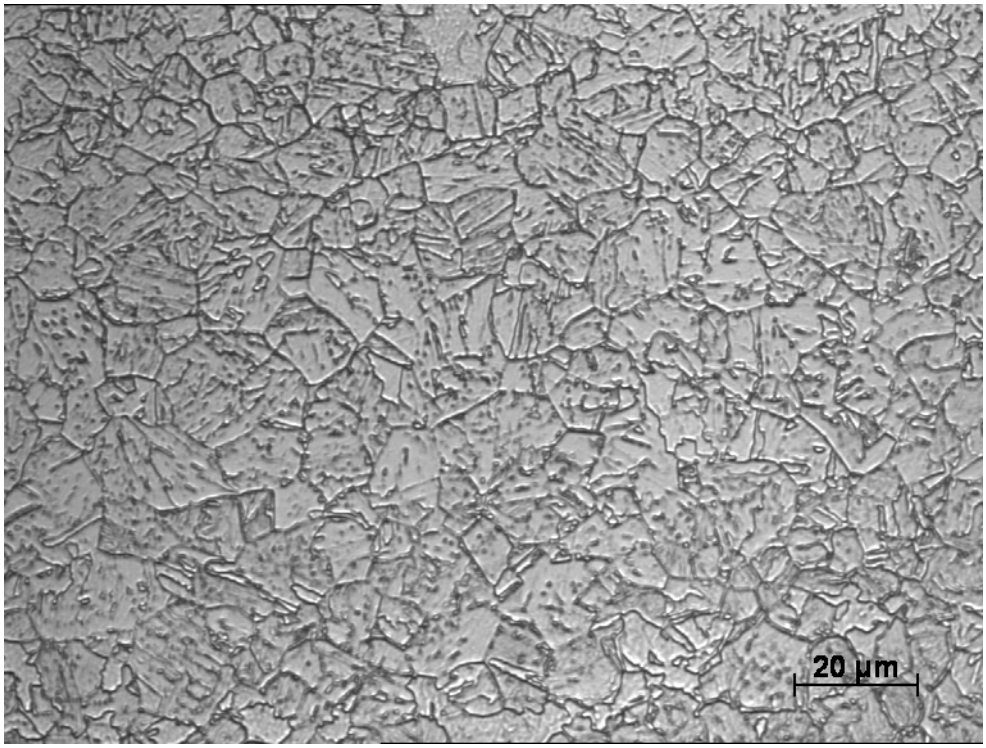
Figure 6.5 Comparison between measured CCT data and modelled results from (a) JMatPro (with the Gleeble measured data points highlighted with a yellow background colour), and (b) EWI..



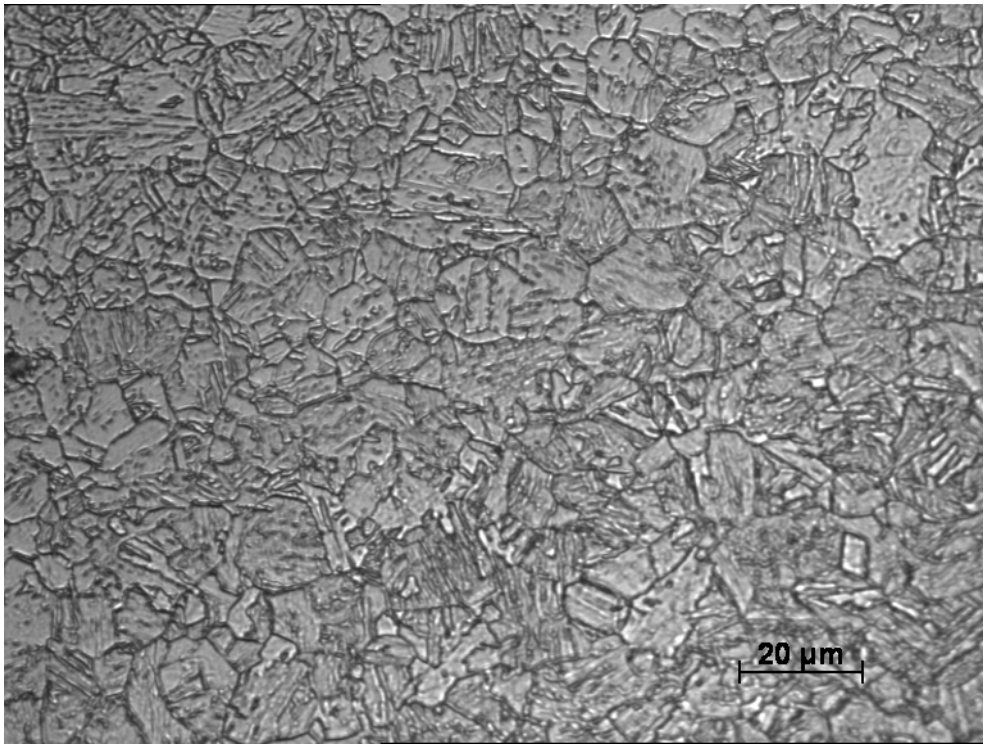
(a)



(b)

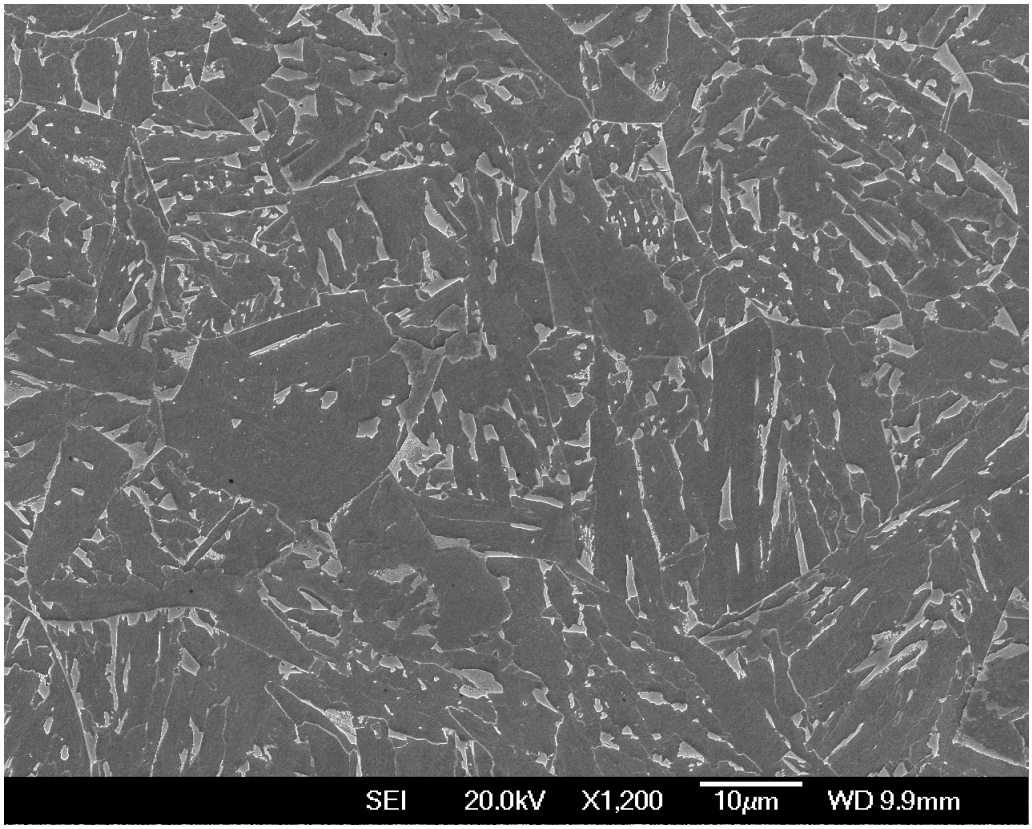


(c)

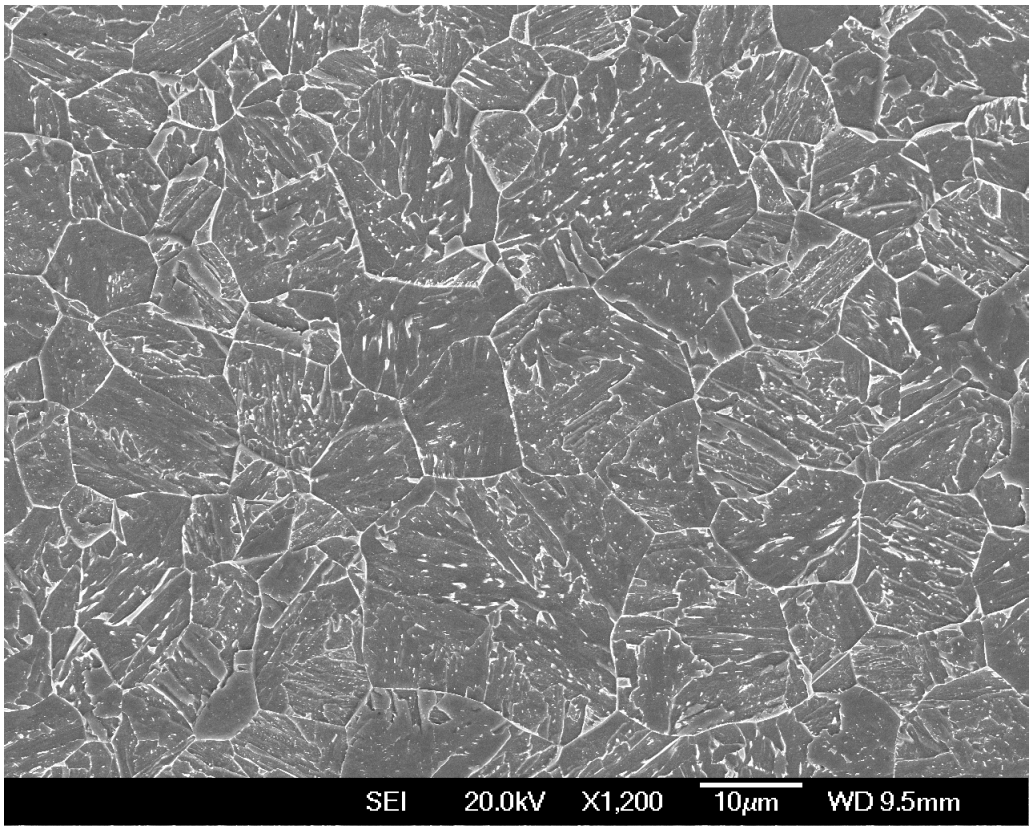


(d)

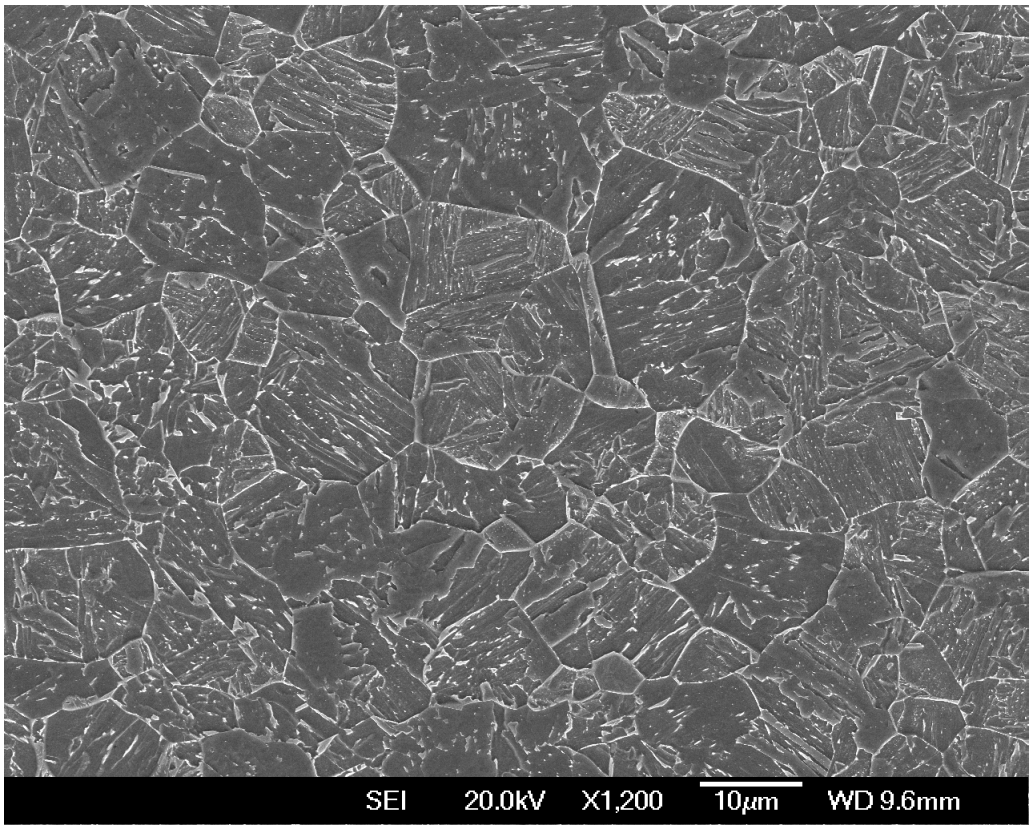
Figure 6.6 Optical images of microstructure achieved at different cooling rates. (a) 2.5 °C/s; (b) 5 °C/s; (c) 7.5 °C/s and (d) 10 °C/s.



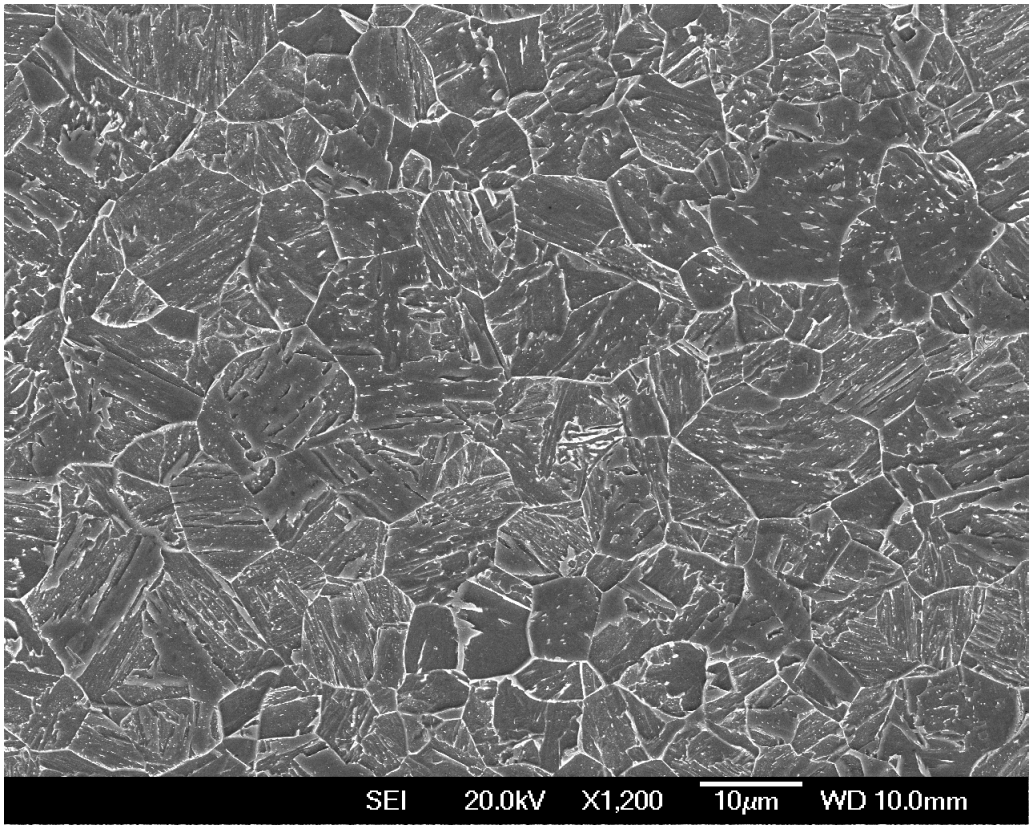
(a)



(b)



(c)



(d)

Figure 6.7 SEM (secondary electron) images of microstructure achieved at different cooling rates. (a) 2.5 °C/s; (b) 5 °C/s; (c) 7.5 °C/s and (d) 10 °C/s.

Table 6.2 Micro-hardness (HV30) results of samples with different cooling rate.

Cooling rate	2.5 °C/s	5 °C/s	7.5 °C/s	10 °C/s
T1	221 ± 3	245 ± 4	289 ± 3	294 ± 5
T2	233 ± 5	258 ± 2	295 ± 4	303 ± 7
T3	228 ± 3	256 ± 5	290 ± 4	300 ± 6

It can be seen from Figure 6.4 that the experimental CCT diagram indicates the Bs temperature of T1, T2 and T3 steels to vary from 612 to 622 °C, which agrees with the prediction made with equation (1) and JMatPro software, Table 6.1. However, no ferrite was found in all cooling rates, while the JMatPro predicted that at about below 5 °C/s cooling rate there would be some ferrite in the final microstructure, which is probably due to the higher austenising temperature of 1000 °C (and therefore larger prior austenite grains) used for Gleeble simulation compared to the predictions (880 °C).

Figure 6.4 also indicates the differences between the CCT curves of the three trials. As shown in the diagram, T1 and T2 curves almost overlap with each other; compared with T1 and T2, the T3 curve is located towards the left hand side, suggesting reduced hardenability of the steel. These differences between each trial are consistent with the predictions given by the JMatPro and EWI models, and confirm the effects of Mo and V in altering the transformation behaviour of the steel. According to literature findings, Mo increases the hardenability of steels via reducing diffusivity of carbon, therefore promotes the transformation from austenite to bainite (rather than ferrite). For this reason, when Mo is reduced from 0.255 wt% in T1 composition to 0.198 wt% in T3 composition, there will be less effect of Mo on reduction of carbon diffusion, therefore the hardenability of T3 is slightly less than T1 and T2 composition (although the carbon content is slightly increased by 0.005 wt% in T3 compared to T1 and T2, and there are 0.05 wt% vanadium addition in T3 compared with T1, the increase in hardenability via these additional carbon and vanadium is not significantly great, as shown in the CCT prediction and measurement results). Although it has been reported that V can increase the hardenability of steel (Heller and Nuss, 2005, Yu, 2006) because V in solution can slow down C diffusion, however it seems from either predicted T1 and T2 CCT or

experimental results that the effect of V addition on changing phase transformation behaviour is not obvious. This is due to the small addition (0.05 wt%) of V in current products, as reported in literature (Xue and Baker, 1995, Zajac et al., 1998, Siwecki et al., 2010, Hutchinson et al., 2014), V(C, N) tends to precipitate between 400 to 600 °C during coiling after continuously cooling, therefore suggesting that vanadium will be in solution before / during austenite – bainite phase transformation to have an effect on hardenability. However, it has been reported in some literatures (Xue and Baker, 1995, Zajac et al., 1998, Siwecki et al., 2010, Hutchinson et al., 2014) that, when tempered or coiled at 600 °C for 1 hour, a small addition of V into steel, e.g. 0.05 – 0.08 wt%, can increase the hardness of a low carbon (0.1 – 0.22 wt% C) steel by 15 – 30 HV via forming V(C, N) nano-precipitation, and therefore yield strength can be increased by 60 – 100 MPa. Unfortunately, this effect in increasing hardness is not observed through Gleeble simulation, but may occur in the industrial coils due to the slow cooling of the steel after coiling. As shown in Table 6.2, when processed under the same cooling rate during Gleeble simulation, the samples of T1 (without V), T2 and T3 (both have 0.05 wt% V) gave generally less than 10 HV difference in hardness, which is probably due to the continuous cooling that was applied during the tests so that VC / V(C, N) did not have enough time to precipitate to strengthen the steel. In comparison, the hardness values of the as-received (coiled) materials (Figure 4.1 and Table 5.2) have shown much more obvious difference (from 30 – 60 HV) between the three trials, which suggests the effect of V in strengthening the bainitic steel after coiling.

6.4 Development on Optimum Coiling Conditions and Alloying Combination

Based on the literature, experimental results and analysis, the chemical composition and coiling condition for the high strength strip steel (grade S700) can be optimised to achieve a good combination of strength and impact toughness (i.e. yield strength above 700 MPa level and ductile-brittle transition temperature below -40 °C), taking into account other product requirements (weldability, ductility, cost) and industrial steel production constraints (coiling temperature, rolling schedule). The constraints are: limited cooling rate between 15 – 30 °C/s on the run-out-table for 12 mm thick products, coiling temperature above 400°C and reductions in expensive alloying elements such as Mo.

According to the results discussed in Sections 4.2 and 5.3 a decreasing coiling temperature often results in a better mixture of microstructure (larger amount of lower bainite) and therefore better combination of hardness (strength) and impact toughness. However, it is not always beneficial to have a very low coiling temperature, for example Hutchinson et al. (2014) reported that the coiling temperature also plays an important role in strengthening bainitic steels through promoting V(C, N) precipitates, seen in strip coiled at about 500 °C. Furthermore, coiling temperatures below 350 °C are also not commercially desirable due to the high cost of intensive water quenching and the lack of accurate coiling temperature control. An additional problem of low coiling temperatures is excessive spring back on uncoiling, which is undesired (Crowther, 2012). Therefore, in this work an aim coiling temperature of above 400 °C was selected, ideally as close to 500 °C as possible.

Besides the coiling temperature, control of austenite grain size and shape is also critical, as this affects the impact toughness via controlling the bainite packet size and hence unit crack path, as discussed in Section 2.2.4 and 2.2.5. The bainite packet size is controlled by the phase balance (formation of mixed granular, upper and lower bainite) and austenite grain size / shape (small austenite grain size and / or pancake shaped prior austenite grains give smaller bainite packet size). Therefore, it is desired to have a smaller prior austenite grain size or heavily deformed prior austenite grains to provide better impact toughness; this can be achieved via a reduction in the finishing rolling temperature (for a constant alloying level), or increasing the Nb content (as mentioned in Section 4.2) to raise T_{NR} (for a constant rolling schedule). However, both methods to alter austenite grain size or shape were not considered in this analysis due to industrial constraints on rolling schedule and a desire not to increases Nb content (due to cost). Therefore, the austenite grain size or shape could not be changed much compared to the current products (T1 – T3).

According to the study on microstructure – mechanical relationships in the current products, it was concluded that a mixed bainitic microstructure, which contains about 10 – 15 % lower bainite, less than 15 % granular bainite and upper bainite, gave the greatest benefit in terms of strength and impact toughness, i.e. balancing the strength and toughness to fulfil the grade requirement and reduce the cost for manufacturing. In terms of generating the desired mechanical properties and microstructure, the micro-alloying level must be controlled to give the appropriate austenite – bainite phase transformation during continuous cooling. As suggested in the previous section, an addition of B is necessary to delay ferrite transformation and increase the hardenability of the steel product. According to the literature and analysis on the current products T1,

T2 and T3, it has been found that 20 ppm B addition is sufficient and effective for achieving this propose. Furthermore, as B is a strong nitride forming element, addition of Al to provide B "protection" is also necessary. According to previous chapters (Section 2.2.3.2), Mo increases hardenability via reducing carbon diffusivity, and it has been suggested in the literature (Kong and Xie, 2006, Han et al., 2008) that 0.2 to 0.4 wt% addition of Mo in low carbon (0.1 wt%) boron-added (approximately 20 ppm) steel is effective to give austenite – bainite transformation (rather than ferrite) and refine the bainitic microstructure as cooling rate increases, for example granular bainite was found to form at cooling rates greater than 0.5 °C/s, and ferritic structures were not found in steels continuously cooled at approximately 10 °C/s or faster. Unfortunately, due to cost control in steel production, it is desirable to reduce the Mo contents compared to the current level (about 0.2 wt%). However, it was concluded that Mo addition is still necessary as it affects hardenability and reduces the coarsening rate of strengthening iron carbides during coiling, therefore a small reduction (to 0.15 wt%) was suggested. Likewise, whilst it is also desirable to reduce the Nb level (currently ≈ 0.03 wt%) due to its cost, Nb has a significant effect on recrystallisation control (Bain and Paxton, 1966, Haensch and Klinkenberg, 2005, Yu, 2006, Feng et al., 2009) it is suggested that it should be maintained at the current level. A higher aim coiling temperature of around 430 – 480 °C (higher than most of products investigated (except T1-1) in this work) was chosen as this is desired for better production control and low cost. Steel T1-1, for which the coiling temperature was 453 °C (close to the aim coiling temperature), did not achieve the required yield strength of 700 MPa (680 MPa in the longitudinal direction for T1-1) and ductile-brittle transition temperature below -40 °C (+7 °C for T1-1), which was found to be because the presence of coarse granular bainite

and lack of fine lower bainite microstructure. Decreasing the Mo content will result in an increase in the Bs temperature (by 4 °C with every 0.05 wt% decrease of Mo according to equation (1)) and slightly reduced hardenability, which means there will be a slightly higher amount of lower bainite formed (due to the increased Bs) when holding at the same coiling temperature (e.g. 400 – 450 °C) compared to current trials, and the hardenability will still be sufficient to avoid ferrite formation at the cooling rates expected.

V addition of the new trial to be kept at 0.05 wt% is suggested to form V(C, N) precipitation during the coiling process, and therefore improve the combination of hardness / strength (via precipitation strengthening) and impact toughness (via promoting lower bainite formation). It has been reported (Xue and Baker, 1995, Zajac et al., 1998, Siwecki et al., 2010, Hutchinson et al., 2014) that in steels containing 0.04 – 0.22 wt% C and 0.05 – 0.2 wt% V, the precipitation of V(C, N) tends to occur at about 450 – 600 °C during coiling, overlapping with the lower bainite transformation starting temperature in low carbon (< 0.1 wt% C) steels. For this reason, the addition of strong carbide forming elements, such as V, which decrease the carbon diffusion rate (Yu, 2006), is thought to be helpful in lower bainite formation. Therefore, when coiled at about 400 – 500 °C, the addition of vanadium will increase the tendency for lower bainite formation, via the effect of V(C, N) formation. For this reason, lower bainite was observed in T3, which has a similar coiling temperature (about 400 °C) and chemical composition except for the addition of V, compared with T1-2 and T1-3. It has been reported that 0.05 wt% V addition can provide approximately 60 – 100 MPa increase in yield strength, since the fine V(C, N) prevent dislocation recovery during the

coiling process (Siwecki et al., 2010) and provide some precipitation strengthening (Xue and Baker, 1995, Zajac et al., 1998).

According to British Standard BS EN 10149-2:2013, for S700 grade steels, the longitudinal (i.e. rolling direction) yield strength should be at least 680 MPa for products with thickness higher than 8 mm (the current products are 12 mm thick strips), and the tensile strength in the longitudinal direction should be within the range 750 – 950 MPa, also, the elongation should be no less than 12 %. Considering that T2 and T3 steels all showed yield strength levels ranging from 750 – 870 MPa (and tensile strength from 840 – 960 MPa) due to the V addition, which is close to the upper limit in the strength level for a S700 grade steel product, it was decided to reduce the C content to a slightly lower level to decrease the yield / tensile strength and increase elongation / impact toughness properties (Bhadeshia and Honeycombe, 2006, Yu, 2006, Yang and Qiang, 2009, Calik et al., 2010).

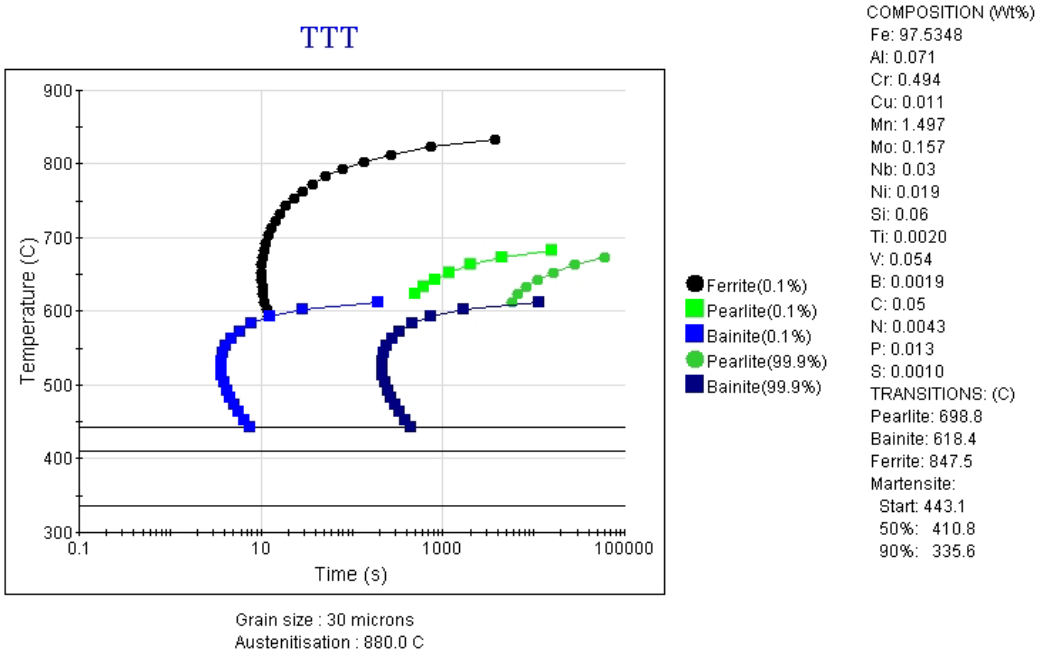
Therefore, for the new trial the suggested coiling temperature was between 430 – 480 °C, and the chemical composition, compared to the previous trial, had a decreased C (from current level of 0.07 wt% to 0.05 wt%) and decreased Mo (from current level of 0.2 wt% to 0.15 wt%) content, therefore the bainite starting temperature is expected to be increased by approximately 10 °C according to equation (1) allowing for a desirable combination of granular, lower and upper bainite to be formed at the higher coiling temperature.

6.5 Validation of suggested combination of chemical composition and coiling process

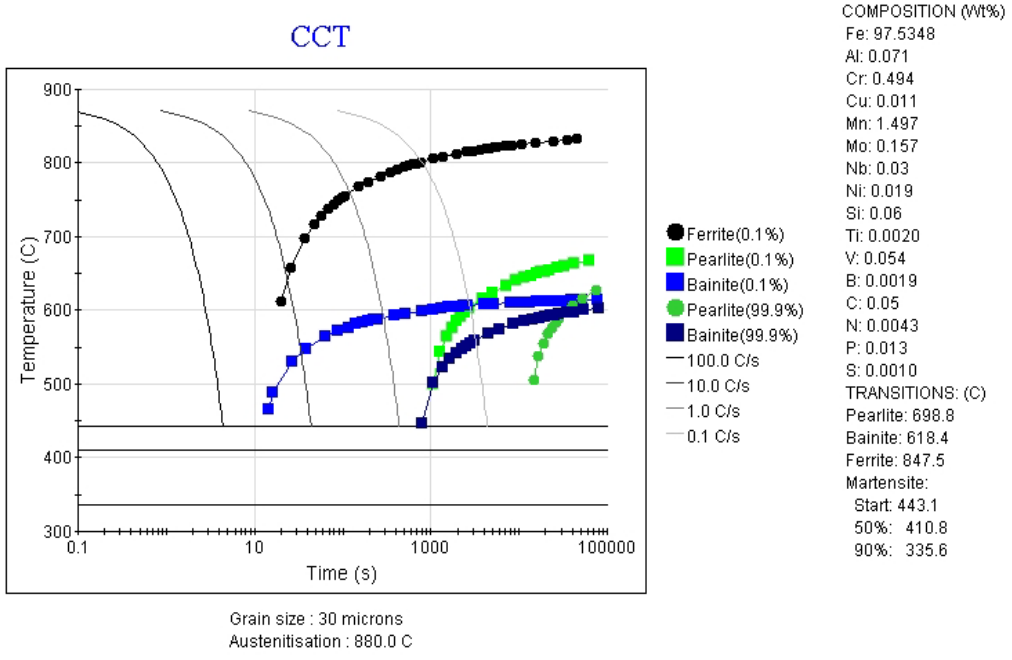
A new production trial, T4, was produced towards the end of this project, and had chemical composition and rolling / coiling parameters close to the suggestions made above (Section 6.4). This trial has been used to consider and validate the approach suggested to optimise properties taking into account industrial constraints. The chemical composition of T4 is shown in Table 6.3, it can be seen that the C has been decreased from about 0.07 wt% to 0.05 wt% (according to private communication with Dr. D. Crowther (2012) from Tata Steel, to slightly reduce yield strength to the level required in the standard, i.e. above 680 MPa, but improve ductility and toughness of products), Mo decreased from about 0.2 wt% to 0.16 wt%, Nb decreased from 0.04 wt% to 0.03 wt%, while other alloying levels remain the same with T3. Figure 6.8 shows the modelled TTT and CCT curves of the T4 composition, and in Figure 6.9 the comparison between modelling results of T4 and previous trials (T1, T2 and T3) is presented.

Table 6.3 Chemical composition of T4 (all in wt %).

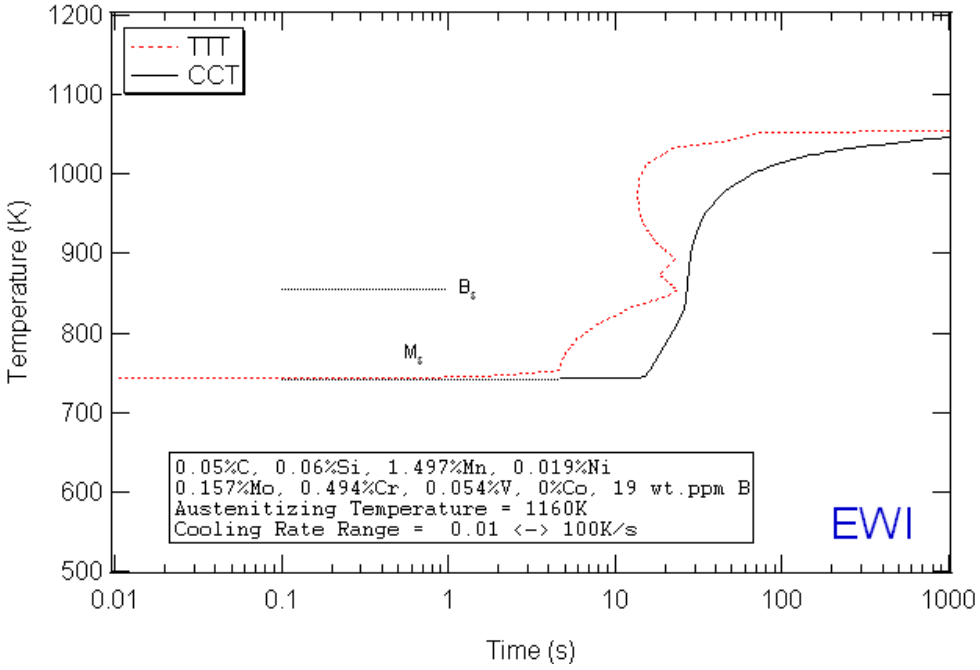
Trial 4	*C*	*Si*	*Mn*	*P*	*S*	*Ni*	*Mo*	*Cr*
	0.05	*0.06*	*1.50*	*0.01*	*0.001*	*0.019*	*0.157*	*0.5*
	Cu	*Al*	*Nb*	*V*	*Ti*	*N*	*B*	-
	0.011	*0.071*	*0.03*	*0.054*	*0.002*	*0.004*	*0.002*	


TTT
Temperature (C)
Time (s)
900
800
700
600
500
400
300
0.1
10
1000
100000
Ferrite(0.1%)
Pearlite(0.1%)
Bainite(0.1%)
Pearlite(99.9%)
Bainite(99.9%)
COMPOSITION (Wt%)
Fe: 97.5348
Al: 0.071
Cr: 0.494
Cu: 0.011
Mn: 1.497
Mo: 0.157
Nb: 0.03
Ni: 0.019
Si: 0.06
Ti: 0.0020
V: 0.054
B: 0.0019
C: 0.05
N: 0.0043
P: 0.013
S: 0.0010
TRANSITIONS: (C)
Pearlite: 698.8
Bainite: 618.4
Ferrite: 847.5
Martensite:
Start: 443.1
50%: 410.8
90%: 335.6
Grain size : 30 microns
Austenitisation : 880.0 C

(a)


CCT
Temperature (C)
Time (s)
900
800
700
600
500
400
300
0.1
10
1000
100000
Ferrite(0.1%)
Pearlite(0.1%)
Bainite(0.1%)
Pearlite(99.9%)
Bainite(99.9%)
100.0 C/s
10.0 C/s
1.0 C/s
0.1 C/s
COMPOSITION (Wt%)
Fe: 97.5348
Al: 0.071
Cr: 0.494
Cu: 0.011
Mn: 1.497
Mo: 0.157
Nb: 0.03
Ni: 0.019
Si: 0.06
Ti: 0.0020
V: 0.054
B: 0.0019
C: 0.05
N: 0.0043
P: 0.013
S: 0.0010
TRANSITIONS: (C)
Pearlite: 698.8
Bainite: 618.4
Ferrite: 847.5
Martensite:
Start: 443.1
50%: 410.8
90%: 335.6
Grain size : 30 microns
Austenitisation : 880.0 C

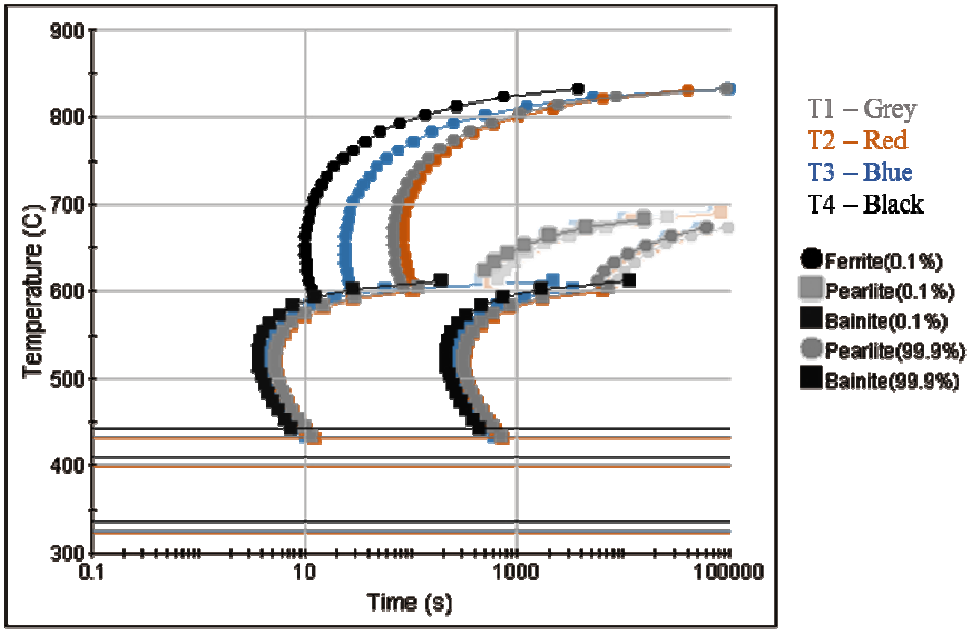
(b)



(c)

Figure 6.8 Modelling of TTT and CCT diagrams of T4 composition. (a) JMatPro TTT result; (b) JMatPro CCT result; and (c) EWI TTT and CCT results.

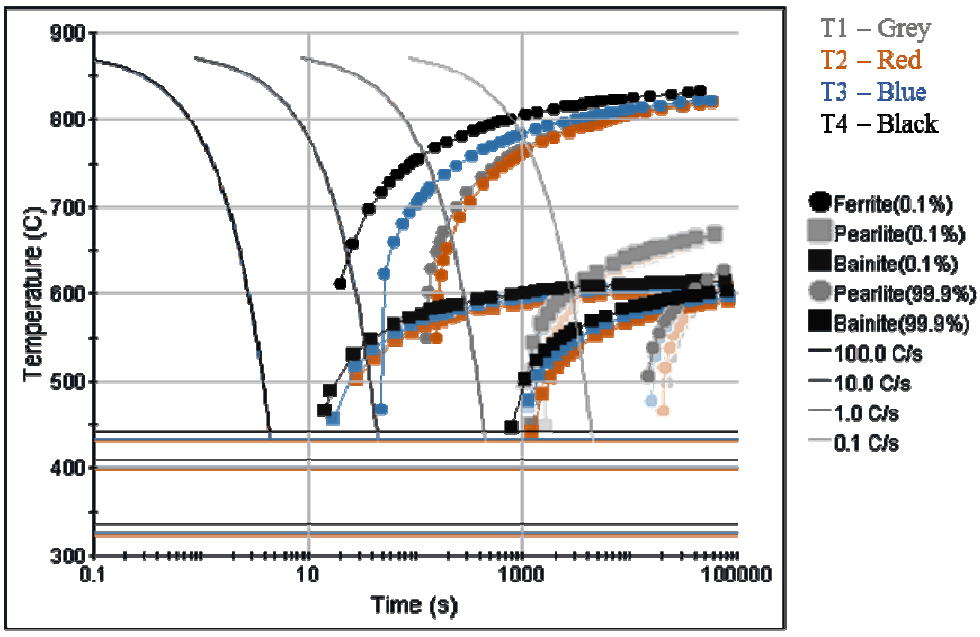
TTT



Grain size : 30 microns
Austenitisation : 880.0 C

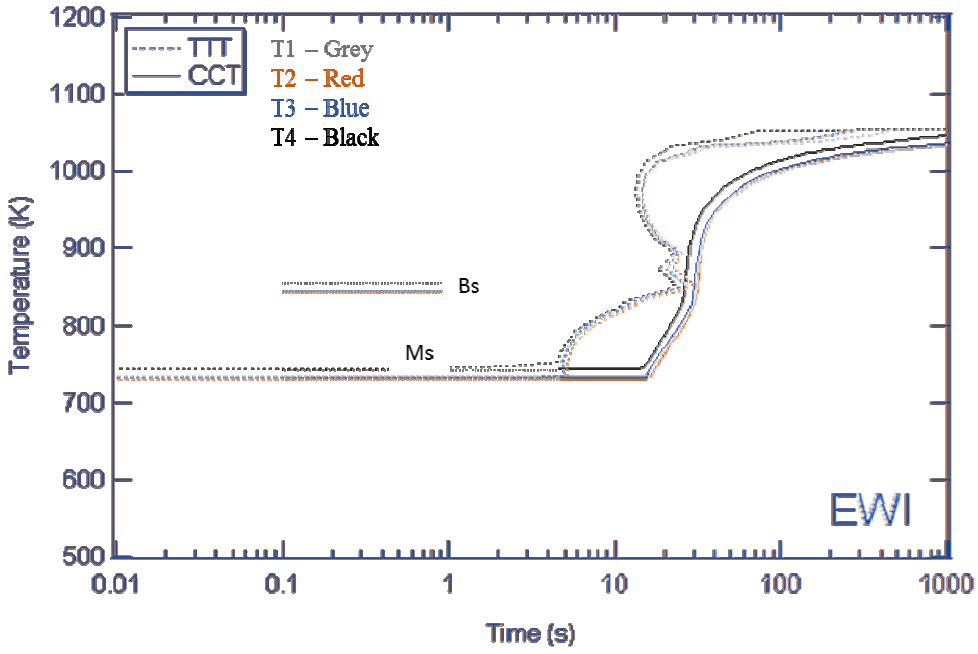
(a)

CCT



Grain size : 30 microns
Austenitisation : 880.0 C

(b)



(c)

Figure 6.9 Comparison of TTT and CCT modelling of T4 with previous trials. (a) JMatPro TTT diagrams; (b) JMatPro CCT diagrams; and (c) EWI TTT and CCT diagrams.

It can be seen from Figures 6.7 and 6.8 that the JMatPro model and EWI model again give different predictions (especially on austenite – ferrite transformation part). However, the TTT and CCT diagrams predicted by both models for T4 show the curves to be slightly shifted towards left hand side (shorter times) compared with the previous trials, and as expected the Bs and Ms temperatures became 6 – 10 °C higher than T1/2/3, which is due to the reduction in C and Mo content. At the same time, according to equations (1) and (2), the reduced C (by 0.02 wt%) and Mo (by 0.04 wt%) contents give a rise in Bs of about 8.9 °C and a rise in Ms of 8.8 °C, which matches with the modelling results.

Gleeble simulation to investigate the transformation behaviour of T4 was also carried out. Figure 6.10 shows the results for the T4 composition and the comparison between

T4 and the previous trials. However, please note again (similar with Figure 6.4) a maximum ±3 °C error exists for the temperature value (i.e. y-axis) of each data point in Figure 6.10, but the error bars were not plotted due to the error is too small, and it is hard to spot even if the error bars are plotted on the graph. As shown in the figure, the change in transformation behaviour for the T4 composition agrees with predictions made by the models, as the transformation starting and finishing points are moved towards left hand side, which is mainly due to the reduced C and Mo content. This shift in the CCT diagram, i.e. with the raise of Bs and Ms while keep the shape of the CCT curve (and therefore the hardenability), could be beneficial for achieving similar bainitic microstructure at a slightly higher coiling temperatures. According to the Bs and Ms predictions (by the two models) and calculation (by equations (1) and (2)), the coiling temperature can accordingly be raised by about 10 °C or more (considering variation during production) compared with T3 series, and the final microstructure of the product would be similar with T3 products. Figure 6.11 gives the comparison between the Gleeble simulation and modelling results of the CCT diagram of T1 to T4 compositions. Similar to Figure 6.5, the experimental measured results determined from Gleeble simulation tests agree well with JMatPro modelling results and show a reasonable agreement with EWI model curves on austenite to bainite transformation starting points; while for transformation finishing points, the experimental work again did not match with JMatPro modelling results. Nevertheless, the Gleeble results show a further shift of the transformation starting points of T4 composition toward top-left side away from T1 – T3 compositions, which is also seen in both modelling results.

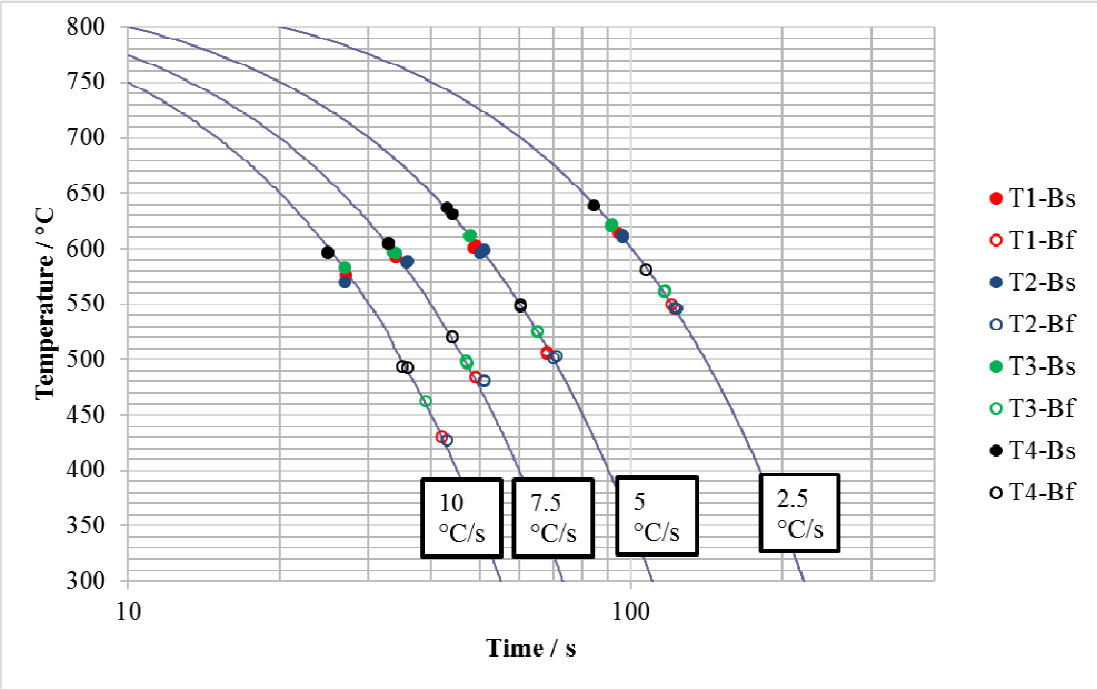
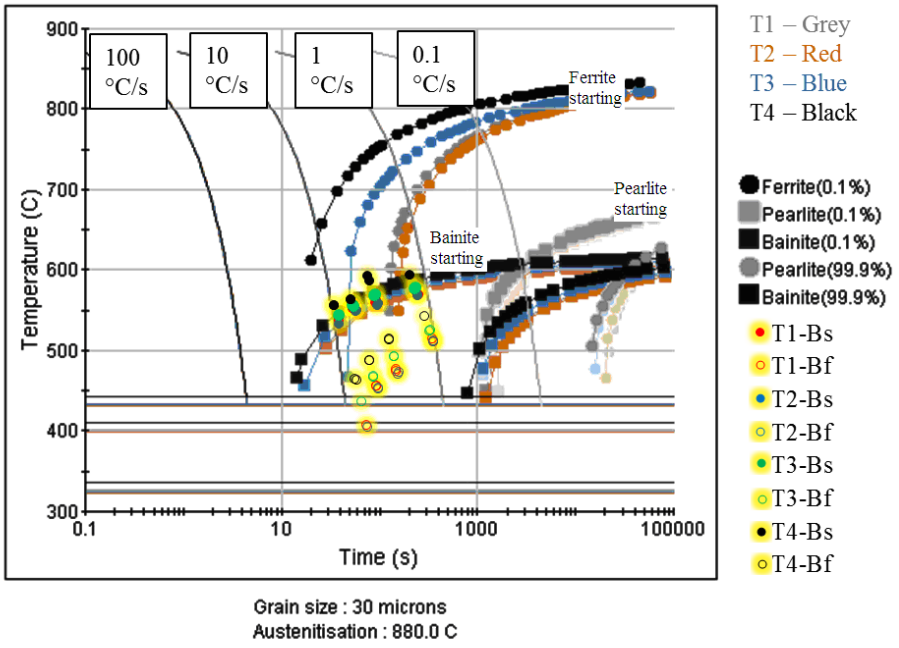
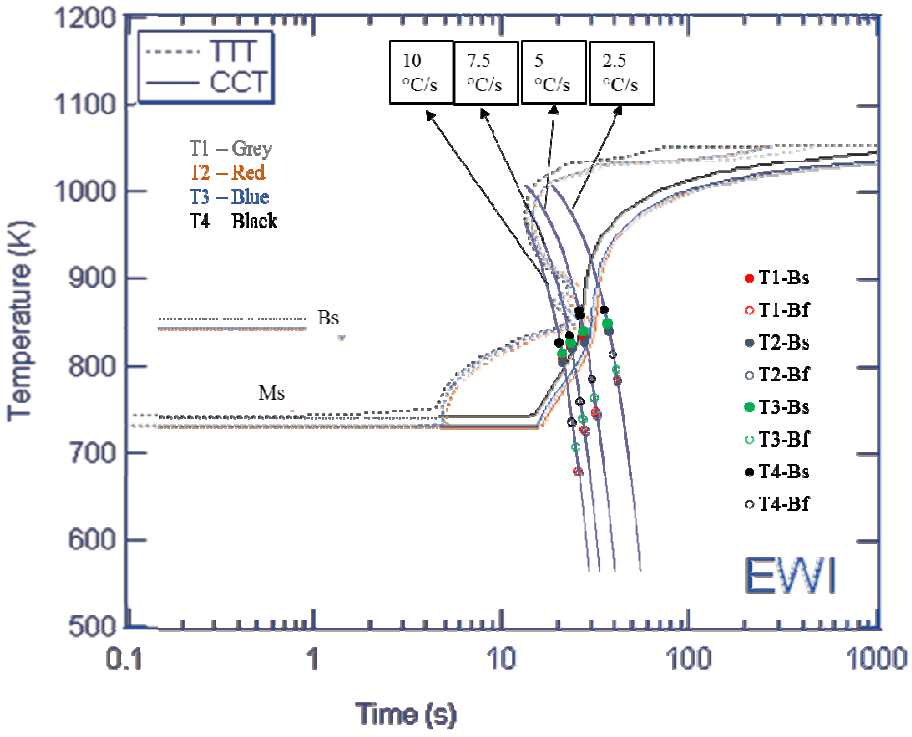


Figure 6.10 Gleeble simulated CCT results for T4 and comparison between the four compositions (note there is a maximum ±3 °C error for each data point on temperature plots).



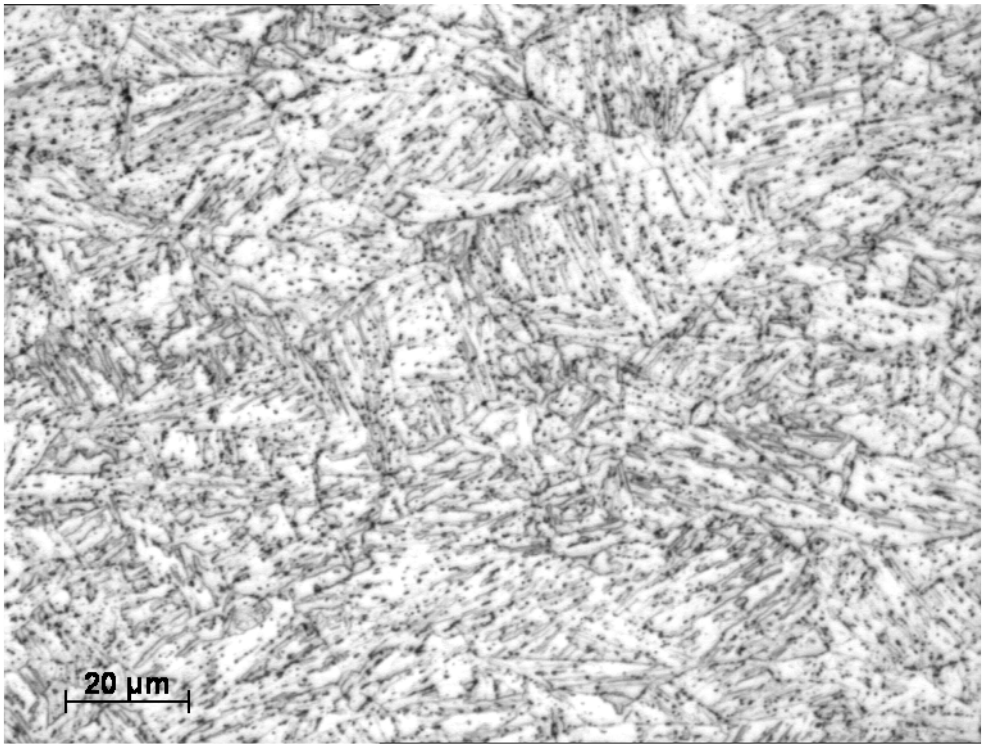
(a)



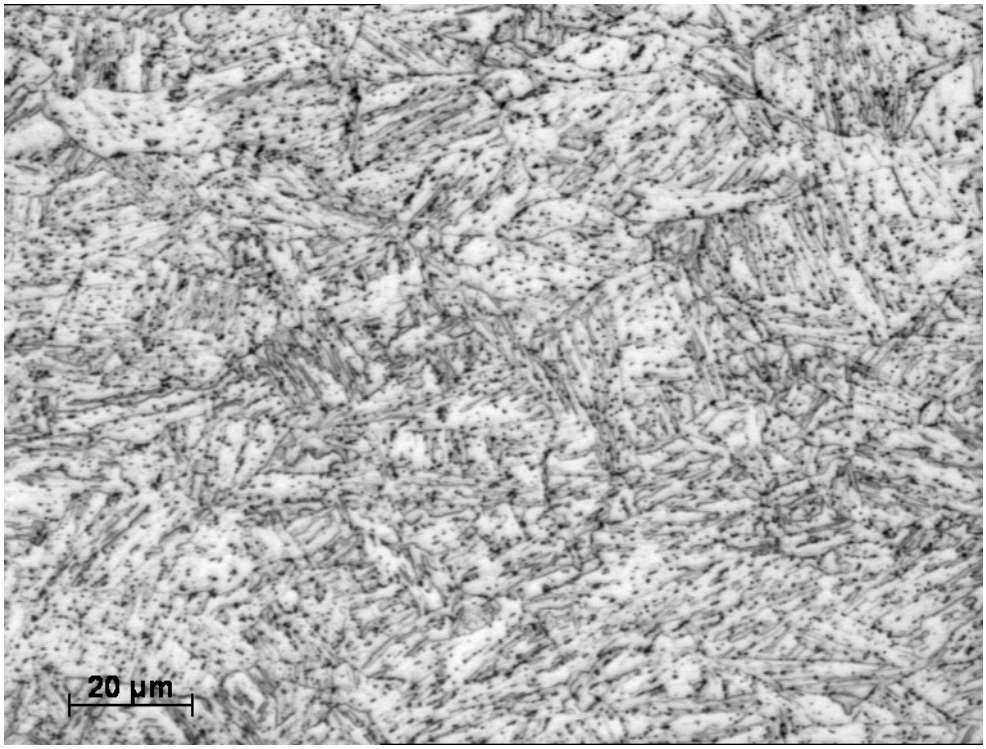
(b)

Figure 6.11 Comparison between measured CCT (including Steels T1 – T4 data) and modelled results from (a) JMatPro (with the Gleeble measured data points highlighted with a yellow background colour), and (b) EWI.

The rolling schedule used for T4 is the same with previous trial T3, two products were hot rolled and coiled, coded as T4-1 and T4-2. For the two products, the coiling temperature is increased to 471 °C for T4-1 and 427 °C for T4-2, i.e. 30 – 70 °C higher than T3 steels. Optical and SEM images of the microstructure are shown in Figures 6.12 and 6.13, respectively. From the images it can be seen that the microstructures of T4-1 and T4-2 are still fully bainitic, however compared with the previous trials the bainitic ferrite lath (especially for upper bainite) is much coarser, which is probably due to the increased coiling temperature. The phase balance quantification was carried using the method mentioned in Section 5.3.1, and the results are presented in Table 6.4, together with T1, T2 and T3 results for comparison.

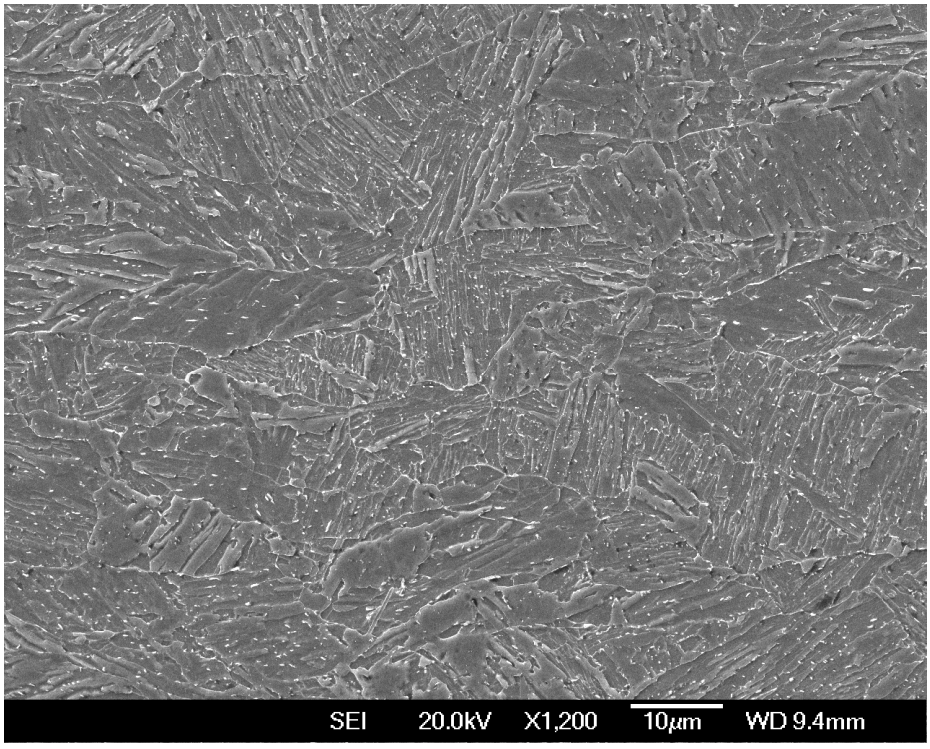


(a)

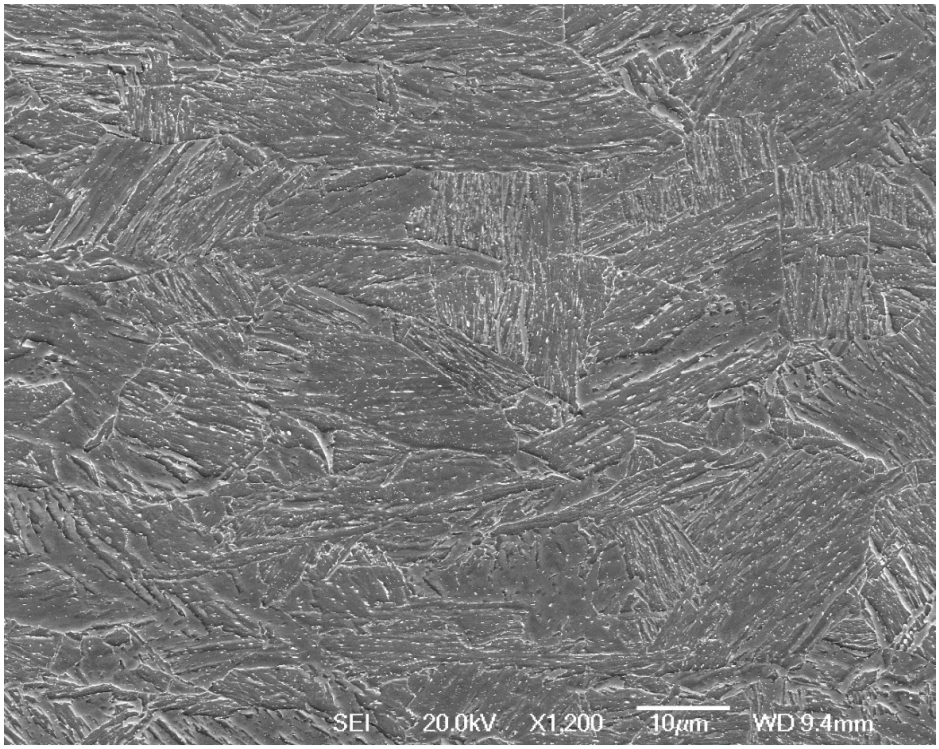


(b)

Figure 6.12 Optical images of the two trial products in T4. (a) T4-1; (b) T4-2.



(a)



(b)

Figure 6.13 SEM (secondary electron) images of the two trial products in T4. (a) T4-1; (b) T4-2.

In Table 6.4 the phase quantification for different bainitic microstructures is presented (T4 steels highlighted in green), compared with the phase balance of the previous samples. It can be seen that due to the high coiling temperature (above 400 °C) the granular bainite is as expected at about 10 to 15 % for both steels; and the lower bainite percentage for T4-1 is 6.5 % while for T4-2 it is 13.2 %. T4-2 was coiled at 427 °C and has a similar lower bainite percentage with T3-2 (12.5 %), which was coiled at a slightly lower temperature of 390 °C, this is also expected as the reduced Mo and C results in raising Bs and therefore it is possible to form lower bainite at coiling temperatures above 400 °C (with the assistance of V), as discussed above.

Table 6.4 Quantification results of phase balance in T4 steels (highlighted in green), and comparison with previous trials (T1 – T3).

	CT / °C	UB	LB	GB
T1-1	453	86.6±0.8%	0.0%	13.4±0.6%
T1-2	411	87.4±0.4%	0.0%	12.6±0.5%
T1-3	393	84.5±0.7%	0.0%	15.5±0.5%
T1-4	290	78.4±1.0%	14.6±0.9%	7.0±0.5%
T2-1	347	88.0±0.5%	8.0±0.5%	4.0±0.3%
T2-2	314	85.0±0.7%	9.0±0.6%	6.0±0.4%
T2-3	253	87.1±0.9%	10.9±0.9%	2.0±0.2%
T3-1	400	76.7±0.8%	10.6±0.6%	12.7±0.6%
T3-2	390	75.0±0.7%	12.5±0.6%	12.5±0.3%
T4-1	471	79.5±0.5%	6.5±0.6%	14.0±0.5%
T4-2	427	77.0±0.9%	13.2±0.8%	9.8±0.4%

The impact toughness and micro-hardness of the two T4 steels were also tested using the exact same method mentioned in Chapter 3, and the 95% confidence interval of the results was also analysed with method mentioned in Section 5.2.2. Figure 6.14 presents the impact transition curves of the two steels from T4 composition. Table 6.5 shows the average micro-hardness values at ¼ thickness position and toughness properties (including DBTT, UCP and BPS) of all trials (again, T4 results are highlighted in green).

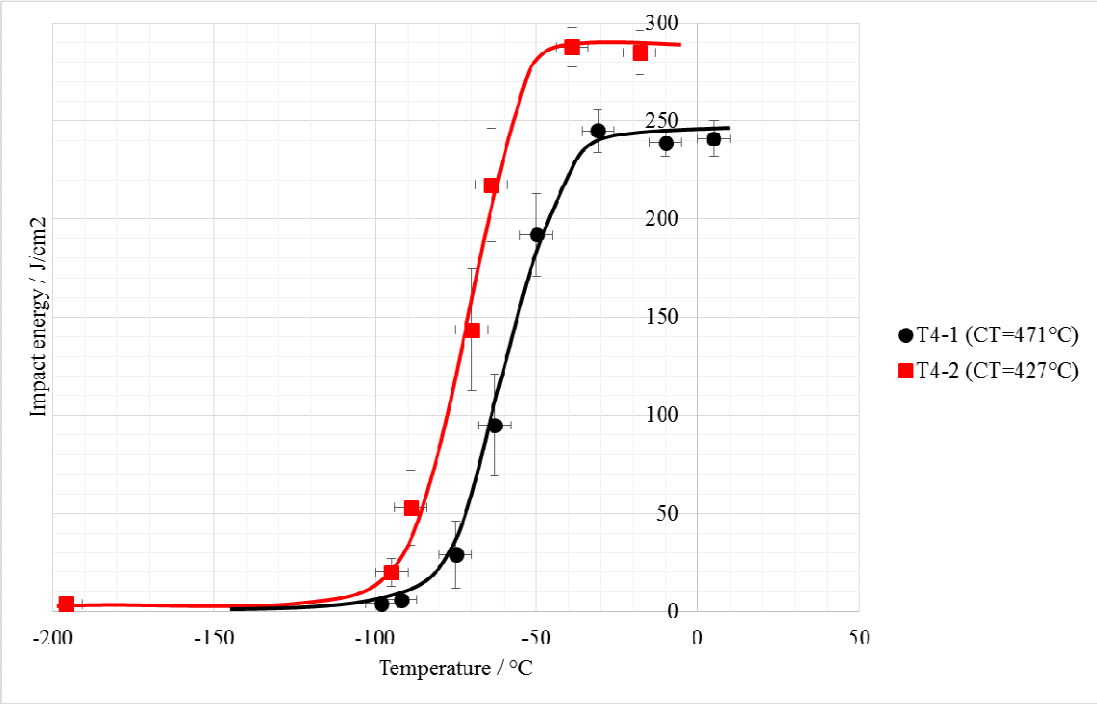


Figure 6.14 Impact transition curves of T4-1 and T4-2.

Table 6.5 Comparison of mechanical properties of all trials.

Trial	T1				T2			T3		T4	
Strip	T1-1	T1-2	T1-3	T1-4	T2-1	T2-2	T2-3	T3-1	T3-2	T4-1	T4-2
CT / °C	453	411	393	290	347	314	253	400	390	471	427
Hardness / HV	271 ± 6	274 ± 2	271 ± 6	300 ± 14	330 ± 9	313 ± 13	359 ± 7	331 ± 8	327 ± 2	308 ± 9	323 ± 17
YS / MPa	764	678	708	755	816	757	838	862	861	778	818
UCP / µm	16.5 ± 3.1	15 ± 2.9	14 ± 2.1	13.5 ± 2.3	12.6 ± 2	13.5 ± 2.6	11 ± 1.4	11 ± 1.6	10.5 ± 2.1	13.3 ± 1.8	10.9 ± 2
BPS / µm	12.1 ± 2.8	11.3 ± 1.9	10 ± 2.1	8.7 ± 1.1	8.1 ± 2	8.8 ± 1.5	6.9 ± 1.1	7.2 ± 1.3	7 ± 1.1	8 ± 1.2	7.2 ± 1
UCP/BPS	1.36 ± 0.4	1.33 ± 0.3	1.4 ± 0.4	1.55 ± 0.3	1.56 ± 0.5	1.53 ± 0.4	1.59 ± 0.3	1.53 ± 0.4	1.5 ± 0.4	1.56 ± 0.3	1.51 ± 0.3
DBTT / °C	+7 ±5	-10 ±7	-28 ±3	-78 ±11	-73 ±13	-60 ±8	-82 ±8	-70 ±5	-90 ±12	-60 ±9	-75 ±12

It can be seen from the Tables 6.4 and 6.5 that the amount of lower bainite of T4 products is increased compared to steels coiled at similar temperature from T1 (T1-1, T1-2, T1-3). When compared with T3 series, the amount of lower bainite of T4-1 is less and T4-2 is similar, this is because that both T4 steels were coiled at higher

temperatures than T3 steels. As a result of increased lower bainite content, both the bainite packet and unit crack path sizes for T4 steels are decreased compared with T1 steels (T1-1, T1-2 and T1-3) coiled at similar temperature, but at similar level when compared with T1-4, T2 and T3 steels due to the similar bainitic phase balance. It can also be seen from Table 6.5 that the UCP/BPS ratios of T4 steels are also about 1.5, which is consistent with previous findings. Compared with previous trials, e.g. T3-1 and T3-2, the hardness value of T4-1 is decreased, and the BPS and UCP have increased, which results in worse toughness and yield strength; while T4-2 presents slightly decreased hardness and similar BPS and UCP size compared with T3 products, and therefore decreased yield strength but similar impact toughness property. This is linked with the coarser bainitic ferrite lath in T4 steels due to higher coiling temperature, and decrease of C and Mo contents in T4 steels. However, the strength and toughness combination of both T4 products are acceptable for an S700 grade (as mentioned by Dr. D. Crowther (Crowther, 2012) as well as in the British Standard which means longitudinal yield strength is above 680 MPa and DBTT lower than -40 °C). Nevertheless, for better strength and impact toughness combination, it is still suggested to go for coiling temperatures no higher than 430 °C (considering there may be ±20 °C difference from one end to another of a hot rolled coil) for this chemical composition.

In summary, the new trial, T4 has proved the proposed effects of adjusting alloying elements and coiling temperature on the final microstructure and mechanical properties. It has been validated that a fully bainitic microstructure mixed with upper bainite, 10 – 15 % lower bainite and less than 10 % granular bainite is still achievable through industrial process, even if the Mo content is reduced to about 1.6 wt% and the coiling temperature is raised to about 430 °C. Also, the microstructure in the final product gives

good combination of strength and toughness. However, when the coiling temperature goes up to about 470 °C, the mechanical properties will become worse than for the lower coiling temperatures due to the presence of more granular bainite and less lower bainite.

CHAPTER 7

CONCLUSIONS AND SUGGESTIONS FOR FUTURE WORK

7.1 Summary and Conclusions

7.1.1 Summary

A good combination of strength and impact toughness is required for strip steel products used in the Lifting and Excavating Sector. In this work, in total four commercial trials (different compositions and coiling temperatures in the range 250 to 480 °C) of 12 mm B-added hot rolled S700 grade steels, which require a minimum yield strength level of 700 MPa and Ductile-Brittle Transition Temperature (DBTT) lower than -40 °C, have been analysed. The first three trials were used to characterise the microstructures, and consider the role of processing conditions (particularly coiling temperature) on its development, and to relate the microstructure to the mechanical properties. This information was then used to design optimum composition and processing, taking into account industrial considerations (cost and rolling mill constraints), to achieve the required strength and improved toughness, which was verified with the fourth trial. The chemical composition of the S700 grade is based on a low carbon low alloy steel with addition of boron, which increases the hardenability of the steel. The initial three trials had similar chemical compositions, but with slightly differences in vanadium and molybdenum additions, and a range of coiling conditions. The microstructures of each

sample were analysed via both optical and Scanning Electron Microscopy (SEM). The main conclusions from the work are as given below:

7.1.2 Conclusions

1. All the samples from the four trials have fully bainitic microstructures, with different fractions of three different types of bainite; upper bainite, granular bainite and lower bainite, which were quantified using SEM images. It was found that the microstructure varies from one trial to another due to differences in chemical composition, with additions of Mo and 0.05 wt% V increasing the amount of lower bainite, and within each trial, where steels coiled at a lower temperature contain larger amounts of lower bainite compared to the ones coiled at higher temperatures. Hot rolling history was found to have effect on prior austenite grain size / shape, the prior austenite grains in steels with a larger initial strain at the first pass of rough rolling were deformed more than those had smaller initial strain at the first pass of rough rolling. Literature model explained the reason for this is the austenite grain size after recrystallisation decreases with the increase of strain, and small austenite grains could therefore appear to be thinner in the normal direction than large grains during rolling passes below non-recrystallisation temperature (T_{NR}) of finishing rolling process.

2. Vicker's hardness measurements and Charpy impact tests were carried out. The results from the hardness test showed good agreement with tensile test strength results provided by Tata Steel Europe; the coefficients to transfer micro-hardness into strength ranged between 2.3 to 2.6 for yield strength and 2.6 to 2.8 for tensile strength for the investigated steels. It has been found that 0.05 wt% addition of vanadium has an effect on increasing hardness by 60 – 100 MPa, considered to be through preventing recovery

(via pinning dislocation) during coiling and precipitation strengthening. The impact properties of the investigated steels vary with microstructure composition, i.e. different bainite phase balance.

3. Lower bainite has beneficial effects on improving both the strength / hardness and impact toughness performance. Steels with 5 – 15 % area fraction of lower bainite perform better than those consisting of upper and granular bainite only, even when coiled at similar temperatures. This is because of the nature of the lower bainite microstructure, which contains fine carbide precipitates inside the bainitic ferrite lath and high dislocation density. The presence of lower bainite also results in a decrease in the average bainite packet size and unit crack path length and therefore results in good resistance to crack propagation and good impact toughness. Granular bainite has detrimental effect on toughness due to its larger crystallographic packet size compared to lower bainite and therefore lower crack propagation resistance.

4. Heat treatments using a Gleeble thermo-mechanical simulator have been used to investigate the phase transformation behaviour from austenite to bainite. The results, in terms of the measured effect of alloying elements on phase transformation behaviour, are comparable with modelling work via both modelling software (JMatPro and EWI model) and literature model (Bs calculation equation), suggesting data from the power module in the Gleeble can be used to observe phase transformation behaviour of steels, however this was only possible at cooling rate lower than 15 °C/s for the steels and set up used, while industrial production may use higher cooling rates between 20 – 40 °C/s for steels with thin thickness gauges such as 6 – 8 mm. CCT / TTT diagrams acquired by both modelling (through software and literature model / equation) and Gleeble

simulation have shown the effects of boron, vanadium and molybdenum on increasing the hardenability of the current steels. The results suggested that 20 ppm addition of boron is beneficial in increasing hardenability, retarding austenite – ferrite transition and promoting the formation of bainite. The addition of 0.05 wt% vanadium tends to increase hardenability of investigated steels slightly, and at the same time increase the strength level of the steel through precipitation strengthening effect. The reduction of molybdenum content by 0.05 wt%, from around 0.25 wt% (T1 composition) to 0.2 wt%, has effects on decreasing hardenability, and at the same time, raise bainite starting temperature (Bs) by around 4 – 5 °C.

5. A new steel composition and processing route was suggested to achieve improved toughness, whilst achieving the required strength for the S700 grade. Consideration of limitations in industrial steel production (requirement to have coiling temperatures above 400 °C) and low cost alloying (within the steel grade) were taken into account. The new steel had lower levels of carbon and molybdenum (to reduce cost), which raised the bainite starting temperature, meaning that sufficient lower bainite was still formed at the desired coiling temperatures of above 400 °C, which provided benefits in achieving good combination of yield strength and impact toughness.

6. This work has shown that the effects of bainitic microstructure and alloying elements, such as boron, vanadium and molybdenum, on altering strength and toughness of low carbon hot rolled coiled strip steels. The knowledge gained from developing an understanding of the relationship between processing and microstructure development, and that microstructure and the mechanical properties, has enabled steel

design for beneficial alloying level, coiling conditions and hence microstructure to satisfy both industrial constraints and requirements for such steel product applications.

7.2 Suggestions for Future Work

1. The steels investigated in this work were industrial products, meaning that alloying and processing design has to cope with industrial constraints such as limitation of cost and variations in the rolling / coiling processes through limits on process control. Through investigation in this work, it has been found that lower bainite is especially beneficial to improve strength and toughness at the same time. Therefore it is important to understand the effect of lower bainite in shaping steel mechanical properties and eliminate undesired microstructures for future products, i.e. investigations on steel with greater lower bainite content, or even completely lower bainite microstructure is desired. Besides, the effect of hot deformation (retained strain for deformation below the recrystallisation stop temperature) on phase transformation is also important for industrial production. Alloying and isothermal holding process design can be achieved by the use of thermal dynamic software such as JMatPro, and simulation can be achieved via a deformation dilatometer or lab-scale casting and rolling process simulation with a Gleeble HDS-V40 Direct Rolling Simulator and dilatometer, which will be available soon in Warwick Manufacturing Group at Warwick University.

2. Tempering and welding of steel products is also critical in application. The effect of tempering, welding and post welding heat treatment (PWHT) is important in shaping mechanical properties. Especially for vanadium added steels, the tempering temperature and time has significant effects on V(C, N) precipitation (Xue and Baker, 1995, Siwecki et al., 2010). Therefore to study effects of vanadium, carbon and nitrogen

content, as well as the temperature and time of tempering, on current S700 grade steels becomes necessary. This could be achieved through using Gleeble heat treatments and software such as ThermoCalc + DICTRA or MatCalc to simulate and model the response of V(C, N) to tempering and effect of welding to microstructure.

3. Lower bainite has shown beneficial effects in achieving good combination of strength and impact toughness for S700 steels with mixed bainitic microstructure. However, when developing steel products that require even higher strength and better impact toughness, the upper bainite and granular bainite become undesirable. The possibility falls on mixed microstructure of lower bainite and martensite / tempered martensite (Abbaszadeh et al., 2012). To achieve such microstructures higher alloying level (such as carbon and molybdenum) than in the investigated products may be necessary, however phase quantification becomes even more important and difficult (due to the fine nature of the microstructure). For example, the fine precipitation in both lower bainite and tempered martensite, means that high resolution scanning electron microscopy and transmission electron microscopy may be needed for further investigation of microstructure and therefore mechanical properties.

REFERENCES

1996-1998. *GLEEBLE 3500/3800 Options Reference Manual 2/98 N320, Chapter: Hot Deformation Options*, Dynamic Systems Inc.

2014. *Gleeble Application Notes: APN024 - Controlling Temperature with the Powangle Variable* [Online]. Dynamic Systems Inc.

AARONSON, H. I., SPANOS, G. & REYNOLDS JR, W. T. 2002. A progress report on the definitions of bainite. *Scripta Materialia,* 47**,** 139-144.

AARONSON, H. I. & WELLS, C. 1956. Sympathetic Nucleation of Ferrite. *Trans. AIME,* 206**,** 1216-1223.

ABAD, R., FERNANDEZ, A. I., LOPEZ, B. & RODRIGUEZ-IBABE, J. M. 2001. Interaction between Recrystallization and Precipitation during Multipass Rolling in a Low Carbon Niobium Microalloyed Steel. *ISIJ International,* 41**,** 1373-1382.

ABBASCHIAN, R., ABBASCHIAN, L. & REED-HILL, R. E. 2009. *Physical Metallurgy Principles,* United States of America, Cengage Learning.

ABBASZADEH, K., SAGHAFIAN, H. & KHEIRANDISH, S. 2012. Effect of Bainite Morphology on Mechanical Properties of the Mixed Bainite-martensite Microstructure in D6AC Steel. *J. Mater. Sci. Technol.,* 28**,** 336-342.

ADAMCZYK, J. 2006. Development of the microalloyed constructional steels. *Journal of Achievements in Materials and Manufacturing Engineering,* 14**,** 9-20.

ANJANA DEVA, B. K. J., N.S. MISHRA 2011. Influence of boron on strain hardening behaviour and ductility of low carbon hot rolled steel. *Materials Science and Engineering A,* 528**,** 7375-7380.

AUSTIN, A. E. & SCHWARTZ, C. M. 1952. Electron-Diffraction Study of Iron Carbides in Bainite and Tempered Martensite. *Proc. ASTM,* 52**,** 592-596.

BAIN, E. C. & PAXTON, H. W. 1966. *Alloying Elements in Steel,* London, American Society for Metals.

BALART, M. J., DAVIS, C. L. & STRANGWOOD, M. 2000. Cleavage initiation in Ti–V–N and V–N microalloyed ferritic–pearlitic forging steels. *Materials Science and Engineering A284***,** 1-13.

BHADESHIA, H. K. D. H. 1980. The Lower Bainite Transformation and the Significance of Carbide Precipitation. *Acta Metallurgica,* 28**,** 1103-1114.

BHADESHIA, H. K. D. H. 1992. *Bainite in Steels: Transformations, Microstructure and Properties,* London, The Institute of Materials.

BHADESHIA, H. K. D. H. 1999. The bainite transformation: unresolved issues. *Materials Science and Engineering A,* 273-275**,** 58-66.

BHADESHIA, H. K. D. H. 2001. *Bainite in Steels,* London, UK, IOM Communications Ltd.

BHADESHIA, H. K. D. H. 2012. *Get TTT and CCT Diagram with Steel Composition* [Online]. Available: http://calculations.ewi.org/vjp/secure/TTTCCTPlots.asp [Accessed 21 Febuary 2012].

BHADESHIA, H. K. D. H. & EDMONDS, D. V. 1979. The Bainite Transformation in a Silicon Steel. *Metallurgical Transactions A,* 10A**,** 895-907.

BHADESHIA, H. K. D. H. & EDMONDS, D. V. 1980. The Mechanism of Bainite Formation in Steels. *Acta Materialia,* 28**,** 1265-1273.

BHADESHIA, H. K. D. H. & HONEYCOMBE, R. W. K. 2006. *Steels: microstructure and properties*, Oxford : Butterworth Heinemann.

BORATTO, F., BARBOSA, R., YUE, S. & JONAS, J. J. Effect of Chemical Composition on Critical Temperature of Microalloyed Steels. THERMEC-88, 1988 Tokyo, Japan. Iron and Steel Institute of Japan, 383-390.

BORGENSTAM, A., HILLERT, M. & □GREN, J. 2009. Metallographic evidence of carbon diffusion in the growth of bainite. *Acta Materialia,* 57**,** 3242-3252.

BROZZO, P., BUZZICHELLI, G., MASCANZONI, A. & MIRABILE, M. 1977. Microstructure and cleavage resistance of low-carbon bainitic steels. *Metal Science***,** 123-129.

CABALLERO, F. G., ROELOFS, H., HASLER, S., CAPDEVILA, C., CHAO, J., CORNIDE, J. & GARCIA-MATEO, C. 2012. Influence of bainite morphology on impact toughness of continuously cooled cementite free bainitic steels. *Materials Science and Technology,* 28**,** 102-95.

CALIK, A., DUZGUN, A., SAHIN, O. & UCAR, N. 2010. Effect of Carbon Content on the Mechanical Properties of Medium Carbon Steels. *Z. Naturforsch,* 65a**,** 468-472.

CHATFIELD, C. 1978. *Statistics for Technology*, Springer-Science+Business Media, B.V.

CROWTHER, D. 2012. *RE: Hot rolled Strip product development.* Type to DU, J.

CROWTHER, D. N., HUSAIN, Z., KRANENDONK, W. & RICHARDSON, A. 2005. 2nd International Conference on Thermomechanical Processing of Steels – TMP 2004. *Ironmaking and Steelmaking,* 32**,** 277-283.

CURRY, D. A. & KNOTT, J. F. 1978. Effects of microstructure on cleavage fracture stress in steel. *Metal Science,* 12**,** 511-514.

DATTA, S., BANERJEE, P. S. & BANERJEE, M. K. 2004. Effect of thermomechanical processing and aging on microstructure and precipitation hardening in low carbon Cu–B steel. *Ironmaking & Steelmaking,* 31**,** 312-318.

DU, J., STRANGWOOD, M. & DAVIS, C. L. 2012. Effect of TiN Particles and Grain Size on the Charpy Impact Transition Temperature in Steels. *Journal of Materials Science and Technology,* 28**,** 878-888.

FAIRCHILD, D. P., HOWDEN, D. G. & CLARK, W. A. T. 2000a. The mechanism of brittle fracture in a microalloyed steel: Part I. Inclusion Induced Cleavage. *Metallurgical and Materials Transactions A,* 31A**,** 641-652.

FAIRCHILD, D. P., HOWDEN, D. G. & CLARK, W. A. T. 2000b. The mechanism of brittle fracture in a microalloyed steel: Part II. Mechanistic modelling. *Metallurgical and Materials Transactions A,* 31A**,** 653-667.

FENG, C., FANG, H.-S., ZHENG, Y.-K. & BAI, B.-Z. 2009. Mn-Series Low-Carbon Air-Cooled Bainitic Steel Containing Niobium of 0.02%. *JOURNAL OF IRON AND STEEL RESEARCH, INTERNATIONAL,* 17**,** 52-58.

FIELDING, L. C. D. 2013. The Bainite Controversy. *Materials Science and Technology,* 29**,** 383-399.

FONDEKAR, M. K., RAO, A. M. & MALLIK, A. K. 1970. Strain Tempering of Bainite. *Metallurgical Transactions,* 1**,** 885-890.

GAO, G. H., ZHANG, H. & BAI, B. Z. 2012. Improved properties of Mn series ultralow carbon steel with ultrafine bainitic structure. *Materials Science and Technology,* 28**,** 829-836.

GRAF, M. K., HILLENBRAND, H. G. & PETERS, P. A. Accelerated Cooling of Plate for High Strength Large DIameter Pipe. Accelerated Cooling of Steels, 1985 Pittsburgh.

GRENINGER, A. B. & TROIANO, A. R. 1940. Crystallography of Austenite Decomposition. *Trans. AIMME,* 140**,** 307-330.

HAENSCH, W. & KLINKENBERG, C. 2005. Low carbon niobium alloyed high strength steel for automotive hot strip. *Ironmaking & Steelmaking,* 32**,** 342-346.

HAGEL, W. C., POUND, G. M. & MEHL, R. F. 1956. Calorimetric Study of the Austenite: Pearlite Transformation. *Acta Metallurgica,* 4**,** 37-46.

HAN, F., HWANG, B., SUH, D.-W., WANG, Z., LEE, D. L. & KIM, S.-J. 2008. Effect of molybdenum and chromium on hardenability of low-carbon boron-added steels. *Metals and Materials International,* 14**,** 667-672.

HAWKINS, M. J. & BARFORD, J. 1972. Experimental Kinetics of Bainite Formation. *Journal of the Iron and Steel Institute,* 210**,** 97-105.

HECKMANN, C. J., ORMSTON, D., GRIMPE, F., HILLENBRAND, H.-G. & JANSEN, J.-P. 2005. Development of low carbon Nb–Ti–B microalloyed steels for high strength large diameter linepipe. *Ironmaking and Steelmaking,* 32**,** 337-341.

HELLER, T. & NUSS, A. 2005. Effect of alloying elements on microstructure and mechanical properties of hot rolled multiphase steels. *Ironmaking & Steelmaking,* 32**,** 303-308.

HILLERT, M., BORGENSTAM, A. & □GREN, J. 2010. Do bainitic and Widmanstätten ferrite grow with different mechanisms? *Scripta Materialia,* 62**,** 75-77.

HIROSHI MATSUDA, H. K. D. H. B. 2004. Kinetics of the Bainite Transformation. *Proc. R. Soc. Lond. A,* 460**,** 1707-1722.

HULTGREN, A. 1947. Isothermal Transformation of Austenite. *Trans. ASM,* 30**,** 915-1005.

HUTCHINSON, B., SIWECKI, T., KOMENDA, J., HAGSTRÖM, J., LAGNEBORG, R., HEDIN, J. E. & GLADH, M. 2014. New vanadium-microalloyed bainitic 700 MPa strip steel product. *Ironmaking & Steelmaking,* 41**,** 1-6.

HWANG, B. & LEE, C. G. 2010. Influence of thermomechanical processing and heat treatments on tensile and Charpy impact properties of B and Cu bearing high-strength low-alloy steels. *Materials Science and Engineering: A,* 527**,** 4341-4346.

HYO KYUNG SUNG, S. Y. S., BYOUNGCHUL HWANG, CHANG GIL LEE, NACK J. KIM, SUNGHAK LEE 2011. Effects of carbon equivalent and cooling rate on tensile and Charpy impact properties of high-strength bainitic steels. *Materials Science and Engineering A,* 530**,** 530-538.

IRVINE, K. J. & PICKERING, F. B. 1957. Low-carbon Bainitic Steels. *Journal. Iron and Steel Institute,* 182**,** 292-309.

IRVINE, K. J. & PICKERING, F. B. 1963. The Impact Properties of Low Carbon Bainitic Steels. *Journal. Iron and Steel Institute,* 20**,** 518-531.

IRVINE, K. J. & PICKERING, F. B. 1965. Physical Properties of Martensite and Bainite. Special Report No.93**,** 110-125.

JANSSON, B., ROLFSON, M., THUVANDER, A., MELANDER, A. & WULLIMANN, C. 1991. Calculation of Microstructure and Hardness of Hot Rolled Steel Bars. *Materials Science and Technology,* 7**,** 118-127.

JOSEFSSON, B. & ANDREN, H. O. 1988. Microstructure of Granular Bainite. *Le Journal de Physique Colloques,* 49**,** C6-293-C6-298.

KAMADA, A., KOSHIZUKA, N. & FUNAKOSHI, T. 1976. Effect of Austensite Grain Size and C Content on the Substructure and Toughness of Tempered Martensite and Bainite. *Trans. ISIJ,* 16**,** 407-416.

KANGYING ZHU, C. O., CÉLINE MUSIK, DIDIER LOISON, THIERRY IUNG 2011. Effect of B and B + Nb on the bainitic transformation in low carbon steels. *Materials Science and Engineering A,* 258**,** 4222-4231.

KERN, A., NIESSEN, T., SCHRIEVER, U. & TSCHERSICH, H. J. 2005. Production and properties of thermomechanically rolled high strength steel plates with minimum yield strengths up to 700 MPa. *Ironmaking & Steelmaking,* 32**,** 331-336.

KONG, J. & XIE, C. 2006. Effect of molybdenum on continuous cooling bainite transformation of low-carbon microalloyed steel. *Materials & Design,* 27**,** 1169-1173.

KREIESEMENT, O. & WEVER, F. 1956. Mechanism of Phase Transformation in Metal. London: Institute of Metals.

KREMNEV, L. S., SVISHCHENKO, V. V. & CHEPRASOV, D. P. 1997. Structure and Mechanism of the Formation of Granular Bainite in Steel 20KhNACh. *Metal Science and Heat Treatment,* 39**,** 367-370.

KRIELAART, G. P. & ZWAAG, S. V. D. 1998. Kinetics of $\gamma \rightarrow \alpha$ Phase Transformation in Fe-Mn Alloys Containing Low Manganese. *Materials Science and Technology,* 14**,** 10-18.

L'ECUYER, J. D., L'ESPERANCE, G., AKBEN, M. G. & BACROIX, B. 1987. Precipitation behavior of a hsla steel containing molybdenum, aluminum and trace amounts of titanium. *Acta Metallurgica,* 35**,** 1149-1158.

LI, C.-M., SOMMER, F. & MITTEMEIJER, E. J. 2002. Characteristics of the $\gamma \rightarrow \alpha$ Transformation in Fe–Mn Alloys. *Materials Science and Engineering A,* 325**,** 307-319.

LI, H.-J., LI, Z.-L., GUO, Y., WANG, Z.-D. & WANG, G.-D. 2013. Development of New Generation Cooling Control System After Rolling in Hot Rolled Strip Based on UFC. *Journal of Iron and Steel Research, International,* 20**,** 29-34.

LINAZA, M. A., ROMERO, J. L., RODRIGUEZ-IBABE, J. M. & URCOLA, J. J. 1995. Cleavage fracture of microalloyed forging steels. *Scripta Metallurgica et Materialia,* 32**,** 395-400.

LIS, J., LIS, A. & KOLAN, C. 2011. INVESTIGATION OF BORON SEGREGATION IN LOW CARBON STEEL. *METALURGIJA,* 50**,** 123-126.

LIU, Y. C., SOMMER, F. & MITTEMEIJER, E. J. 2003. Abnormal austenite–ferrite transformation behaviour in substitutional Fe-based alloys. *Acta Materialia,* 51**,** 507-519.

LONT, M. A. 2000. The Determination of Uncertainties in Charpy Impact Testing. *Standards Measurement & Testing*.

LYMAN, T. & TROIANO, A. R. 1946. Influence of Carbon Content Upon the Transformation in 3 per cent Chromium Steel. *Trans. ASM,* 37**,** 402-448.

MATSUDA, S., INOUE, T. & OGASAWARA, M. 1968. The Fracture of Tempered Martensite. *Trans. Jpn. Inst. Met,* 9**,** 343.

MATSUDA, S., INOUE, T. & OGASAWARA, M. 1972. The Fracture of A Low Carbon Tempered Martensite. *Trans. Jpn. Inst. Met,* 11**,** 36.

MAZANCOVÁ, E., SLAVÍKOVÁ, I., JONŠTA, Z. & MAZANEC, K. Comparison of Microfractographic Behaviour of Acicular Ferrite and Bainite and Hydrogen Cracking Resistance. 11th International Research/Expert Conference, 2007 Tunisia. 283-286.

MEDINA, S. F., RANCEL, L., GÓMEZ, M., CABRERA, J. M. & GUTIERREZ, I. 2014. Microstructural Unit Controlling Cleavage Crack Propagation in High Strength Bainitic Steels. *Key Engineering Materials,* 622-623**,** 846-853.

MIIHKINEN, V. T. T. & EDMONDS, D. V. 1987. Microstructural Examination of Two Experimental High-strength Bainite Low-alloy Steels Containing Silicon. *Materials Science and Technology,* 3**,** 422-431.

MISRA, R. D. K., NATHANI, H., HARTMANN, J. E. & SICILIANO, F. 2005. Microstructural evolution in a new 770MPa hot rolled Nb–Ti microalloyed steel. *Materials Science and Engineering: A,* 394**,** 339-352.

MORRIS, P., BEYNON, J. & RIDAL, K. 2004. Advances in the hot rolling of steels. *Ironmaking and Steelmaking,* 31**,** 8-13.

MORRIS, P. F., JACKSON, M. & RIDAL, K. 2013. Optimising design and performance of engineering components. *Ironmaking & Steelmaking,* 40**,** 243-252.

MORRIS, P. F., MORGAN, P. & RIDAL, K. A. 2012. Metals fit for the twenty-first century: processing for high performance applications. *Ironmaking & Steelmaking,* 39**,** 236-243.

MORRISON, W. B. & ABERNETHY, K. 1990. The Influence of Controlled Levels of Centreline Segregation on the Toughness of Structural Steels. London: British Steel Plc.

MUN, D. J., SHIN, E. J., CHOI, Y. W., LEE, J. S. & KOO, Y. M. 2012. Effects of cooling rate, austenitizing temperature and austenite deformation on the

transformation behavior of high-strength boron steel. *Materials Science and Engineering: A,* 545**,** 214-224.

NAYLOR, J. P. & KRAHE, P. R. 1974. The Effect of the Bainite Packet Size on Toughness. *Metallurgical Transactions A,* 5**,** 1699-1701.

NEMOTO, M. 1974. *High Vlotage Electron Microscopy,* New York, Academic Press.

OBLAK, J. M., GOODENEW, R. H. & HEHEMANN, R. F. 1964. Effect of Alloying Additions on the Lattice Parameter of Austenite. *Trans. AIME,* 230**,** 258-259.

OBLAK, J. M. & HEHEMANN, R. F. Structure and growth of widmanstatten ferrite and bainite. *In:* ARBOR, A., ed. Transformation and Hardenability in Steels, 1967 Michigan. Climax Molybdenum Co, 15-30.

OHMORI, Y. 1971. The Crystallography of the Lower Bainite Transformation in A Plain Carbon Steel. *Trans. ISIJ,* 11**,** 95-101.

OHMORI, Y., OHTANI, H. & KUNITAKE, T. 1974. Tempering of the Bainite and the Bainite Martensite Duplex Structure in a Low-Carbon Low-Alloy Steel. *METAL SCIENCE,* 8**,** 357-366.

P. CIZEK, B. P. W., C.H.J. DAVIES, B.C. MUDDLE, AND P.D. HODGSON 2002. Effect of Composition and Austenite Deformation on the Transformation Characteristics of Low-Carbon and Ultralow-Carbon Microalloyed Steels. *Metallurgical and Materials Transactions A,* 33A**,** 1331-1349.

PAVLINA, E. J. & TYNE, C. J. 2008. Correlation of Yield Strength and Tensile Strength with Hardness for Steels. *Journal of Materials Engineering and Performance,* 17**,** 888-893.

PICKERING, F. B. Mechanism of Bainite Formation in the Low Alloy Steel containing up to 0.40 wt. % Carbon. Transformation and Hardenability in Steels, 1967a Michigen. Climax Molybdenum Co, 109.

PICKERING, F. B. The Structure and Properties of Bainite in Steels. Transformation and Hardenability in Steels, 1967b Michigan. Climax Molybdenum, 109-129.

PORTER, D. 2011. Thermomechanical processing on hot strip and plate mills. *Ironmaking and Steelmaking,* 28**,** 164-169.

PUNCH, R. B. 2014. *Toughness Enhancement of High Strength Low Alloy Strip Steels.* Ph.D., University of Birmingham.

QIAO, Z. X., LIU, Y. C., YU, L. M. & GAO, Z. M. 2009. Formation mechanism of granular bainite in a 30CrNi3MoV steel. *Journal of Alloys and Compounds,* 475**,** 560-564.

RANCEL, L., GÓMEZ, M., MEDINA, S. F. & GUTIERREZ, I. 2011. Measurement of bainite packet size and its influence on cleavage fracture in a medium carbon bainitic steel. *Materials Science and Engineering A,* 530**,** 21-27.

REGER, M., VERO, B., FELDE, I. & KARDOS, I. 2010. The Effect of Heat Treatment on the Stability of Centerline Segregation. *Journal of Mechanical Engineering,* 56**,** 143-149.

REHMAN, M. K. U. 2014. *Modeling the Microstructure Evolution During Hot Deformation of Microalloyed Steels.* Ph.D., McMaster University.

SANDVIK, B. P. J. 1982. The Bainite reaction in Fe-Si-C Alloys: The primary stage. *Metallurgical Transactions A,* 13**,** 777-787.

SHANMUGAM, S., MISRA, R. D. K., MANNERING, T., PANDA, D. & JANSTO, S. G. 2006. Impact toughness and microstructure relationship in niobium- and vanadium-microalloyed steels processed with varied cooling rates to similar yield strength. *Materials Science and Engineering: A,* 437**,** 436-445.

SHOW, B. K., VEERABABU, R., BALAMURALIKRISHNAN, R. & MALAKONDAIAH, G. 2010. Effect of vanadium and titanium modification on the microstructure and mechanical properties of a microalloyed HSLA steel. *Materials Science and Engineering: A,* 527**,** 1595-1604.

SIWECKI, T., ELIASSON, J., LAGNEBORG, R. & HUTCHINSON, B. 2010. Vanadium Microalloyed Bainitic Hot Strip Steels. *ISIJ International,* 50**,** 760-767.

SKOBIR, D. A. 2011. High Strength Low Alloy (HSLA) Steels. *Materials and technology,* 45**,** 295-301.

SMITH, G. M. 1984. *The Microstructure and Yeilding Behaviour of Some Ti Steels.* Ph.D., University of Cambridge.

SMITH, G. V. & MEHL, R. F. 1942. Lattice Relationships in Decomposition of Austenite to Pearlite, Bainite and Martensite. *Trans. AIMME,* 150**,** 211-226.

SRINIVASAN, G. R. & WAYMAN, C. M. 1968. Transmission electron microscope study of the bainite transformation in iron-chromium-carbon alloys. *Acta Materialia,* 16**,** 609-620.

SUNG, H. K., SHIN, S. Y., HWANG, B., LEE, C. G., KIM, N. J. & LEE, S. 2011. Effects of carbon equivalent and cooling rate on tensile and Charpy impact properties of high-strength bainitic steels. *Materials Science and Engineering: A,* 530**,** 530-538.

SUNG, H. K., SHIN, S. Y., HWANG, B., LEE, C. G. & LEE, S. 2012. Effects of B and Cu Addition and Cooling Rate on Microstructure and Mechanical Properties in Low-Carbon, High-Strength Bainitic Steels. *Metallurgical and Materials Transactions A,* 43**,** 3703-3714.

TANAKA, T. 1995. Science and technology of hot rolling process of steel. *Microalloying 95.* Pittsburgh USA: Iron and steel society.

TÓTH, L., ROSSMANITH, H. P. & SIEWERT, T. A. 2002. Historical background and development of the Charpy test. *In:* FRANÇOIS, D. & PINEAU, A. (eds.) *European Structural Integrity Society.* Elsevier.

VERVYNCKT, S., VERBEKEN, K., LOPEZ, B. & JONAS, J. J. 2012. Modern HSLA steels and role of non-recrystallisation temperature. *International Materials Reviews,* 57**,** 187-207.

WANG, X., SHANG, C., YANG, S., HE, X. & LIU, X. 2006. The refinement technology for bainite and its application. *Materials Science and Engineering: A,* 438-440**,** 162-165.

XIAO, B. 2013. *Multipass Laboratory Simulation of Steel Plate Hot Rolling for Improved Productivity.* Ph.D., The University of Sheffield.

XUE, H. & BAKER, T. N. 1995. Mechanical properties of low carbon-vanadium microalloyed quenched and tempered steels vvith aluminium additions. *Materials Science and Technology,* 11**,** 883-892.

YAN, W., SHAN, Y. Y. & YANG, K. 2006. Effect of TiN inclusions on the impact toughness of low-carbon microalloyed steels. *Metallurgical and Materials Transactions a-Physical Metallurgy and Materials Science,* 37A**,** 2147-2158.

YAN, W., SHAN, Y. Y. & YANG, K. 2007. Influence of TiN Inclusions on the Cleavage Fracture Behavior of Low-Carbon Microalloyed Steels. *Metallurgical and Materials Transactions A,* 38**,** 1211-1222.

YANG, W. & QIANG, W. 2009. *Mechanical Behavior of Materials,* Beijing, Chemical Industry Press.

YI, H.-L., DU, L.-X., WANG, G.-D. & LIU, X.-H. 2008. Strengthening Mechanism of a New 700 MPa Hot Rolled High Strength Steel. *Journal of Iron and Steel Research, International,* 15**,** 76-80.

YU, Y. N. 2006. *Foundamental of Materials Science,* Beijing, Higher Education Press.

ZAJAC, S., SIWECKI, T., HUTCHINSON, W. B. & LAGNEBORG, R. 1998. Strengthening Mechanisms in Vanadium Microalloyed Steels Intended for Long Products. *ISIJ international,* 38**,** 1130-1139.

ZHANG, D., SHINTAKU, Y., SUZUKI, S. & KOMIZO, Y.-I. 2012. Effect of cooling rate on phase transformation in the low-carbon boron-treated steel. *Journal of Materials Science,* 47**,** 5524-5528.

ZHANG, L. P. 2000. *Microstructure and Fracture Toughness in the HAZ of a Structural Steel Containing TiN Particles.* PhD, The University of Birmingham.